ISBN 978-3-00-042717-6

Herausgeber (Published by):
Bauhaus-Universität Weimar
F. A. Finger-Institut für Baustoffkunde
Professur Werkstoffe des Bauens
Direktor: Prof. Dr.-Ing. Horst-Michael Ludwig

V.-T.-A. VAN

DISSERTATION

2013

Bauhaus-Universität Weimar

FIB

Characteristics of Rice Husk Ash and Application in Ultra-High Performance Concrete

Viet-Thien-An Van

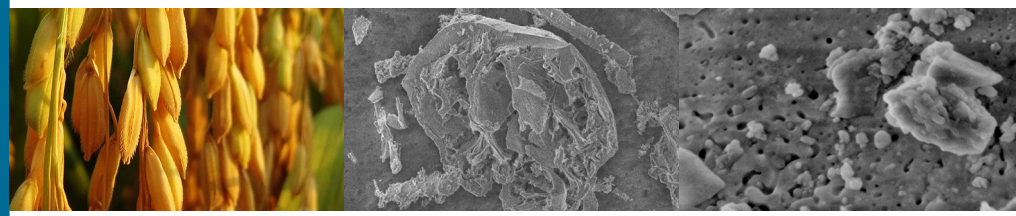

Professur Werkstoffe des Bauens

Charakterisierung von Reisschalenasche und deren Verwendung im Ultrahochfesten Beton

Dissertation

zur Erlangung des akademischen Grades
Doktor-Ingenieur (Dr.-Ing.)

an der Fakultät Bauingenieurwesen
der Bauhaus-Universität Weimar

vorgelegt von

Viet-Thien-An Van

aus Vietnam

Gutachter:

Prof. Dr. –Ing. Horst-Michael Ludwig

Prof. Dr. –Ing. Detlef Heinz

Prof. Dr. H. F. Reinhard Trettin

Die öffentliche Disputation der Arbeit fand am 13.6.2013 in Weimar statt.

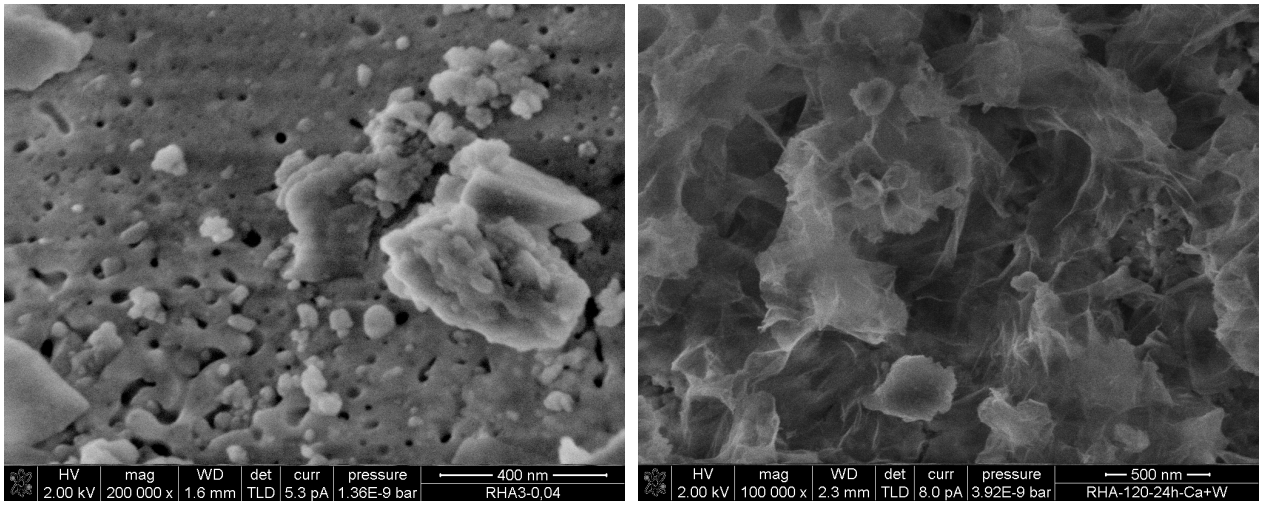

Surface structure of rice husk ash (RHA) particle after grinding with many mesopores and after 24-hour hydration in saturated portlandite solution at 40°C with hydration products.

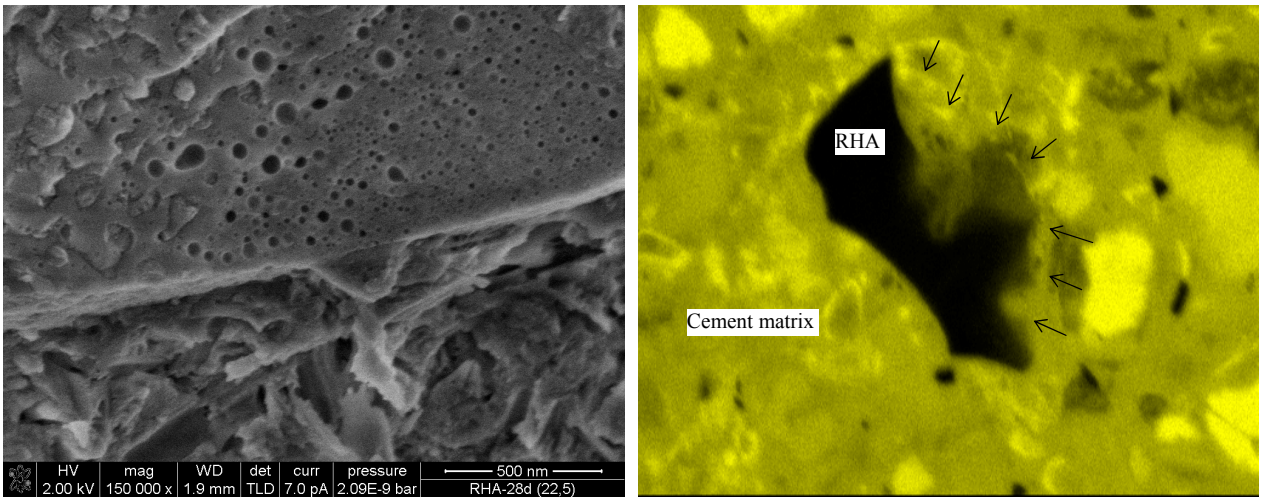

Mesoporous surface structure of RHA particle in UHPC matrix and EDX-Ca-mapping of RHA particle in cement paste at w/b of 0.22. Solid arrows indicate the high Ca^{2+} concentration parts (bright areas) of RHA particle.

ISBN 978-3-00-042717-6

Keywords: Rice husk ash, silica fume, mesoporous structure, pozzolanic reactivity, ultra-high performance concrete.

Herausgeber (Published by):
Bauhaus-Universität Weimar
F.A. Finger-Institut für Baustoffkunde
Professur Werkstoffe des Bauens
Direktor: Prof. Dr. –Ing. Horst-Michael Ludwig

Acknowledgements

This PhD study received the financial supports from Ministry of Education and Training of Vietnam, F.A. Finger- Institute for Building Materials Science (FIB)- Bauhaus University Weimar, and German Academic Exchange Service (DAAD). The supply of superplasticizers from Sika and BASF companies was crucial to this study. The author would like to gratefully acknowledge these supports.

I would like to express my sincere gratitude to my supervisor, Prof. Dr. -Ing. Horst-Michael Ludwig for his useful advice and encouragement during the whole progress of this PhD study. I would also like to thank Prof. Dr. -Ing. habil. Jochen Stark for his encouragement and support on the study of rice husk ash in ultra-high performance concrete.

I owe my deepest gratitude to my co-supervisor, Dr. rer. nat. Christiane Rößler for all her patient guidance, encouragement and kindliness. I am always grateful for her fruitful suggestions and discussions. I am also indebted to Dr. Bùi Danh Đại and Dipl. -Min. Claudia Pfeifer for their invaluable discussions.

I would like to thank all of the staff at FIB, especially to Dr. rer. nat. Bernd Möser, Dr. -Ing. habil. Frank Bellmann, Dipl. -Ing. Thomas Sowoidnich, Dipl. -Ing. Dennys Dressel, Dipl. -Ing. Simone Peters, Dipl. -Ing. Lê Thanh Hà, Dipl. -Ing. (FH) Christian Matthes and others in electron microscopic analysis and cement chemistry group for their technical assistance, discussion and friendship. The contribution of Dipl. -Ing. Alexander Gypser to autogenous shrinkage, internal relative humidity tests, of Dipl. -Ing. Colin Giebson to cyclic climate storage test and of M.Sc. Ulrike Salbach to zeta potential test with their discussions is here acknowledged.

I am grateful to Prof. Dr. -Ing. Bùi Văn Bội and to all my colleagues at Department of Building Materials Technology, National University of Civil Engineering, Vietnam, for all their support and encouragement. A special thank to my friends, M.Sc. Tống Tôn Kiên and M.Sc. Trần Đức Trung who helped me to produce rice husk ash in Vietnam.

Finally, I would like to express my heartfelt gratitude to my parents, parents-in-law, my wife- Phương Thảo, my daughter- Minh Anh as well as other family members. Their love, unwavering support and encouragement help me to overcome all difficulties in completing this PhD study. I know that my debt to them is beyond measure.

Weimar, December 2012 VĂN Viết-Thiên-Ân

Table of Contents

Acknowledgements
Table of Contents
List of Abbreviations
Summary
Zusammenfassung (German Summary)
Tóm Tắt (Vietnamese Summary)
1. Introduction 1
2. Objectives and Research Methodology 3
2.1. Objectives 3
2.2. Research methodology 3
3. Literature Review on Ultra-High Performance Concrete and Rice Husk Ash 5
3.1. Ultra-high performance concrete 5
3.1.1. Introduction 5
3.1.2. Ingredients and composition of UHPC 8
3.1.3. Workability of mixture 12
3.1.4. Treatment regime of UHPC 12
3.1.5. Mechanical properties of UHPC 12
3.1.5.1. Shrinkage 12
3.1.5.2. Compressive strength 13
3.1.5.3. Tensile strength 13
3.1.6. Microchemical and microstructural features of UHPC 14
3.1.7. Durability of UHPC 14
3.1.7.1. Resistance to aggressive solution 14
3.1.7.2. Carbonation 15
3.1.7.3. Freezing and thawing resistance 15
3.1.7.4. Alkali silica reaction 15
3.2. Rice husk ash and using rice husk ash in mortar and concrete 16
3.2.1. Introduction 16
3.2.2. Producing reactive rice husk ash (RHA) 18
3.2.3. Chemical and mineral compositions of RHA 18
3.2.4. Microstructure and specific surface area of RHA 19
3.2.5. Pozzolanic reactivity of RHA 20
3.2.6. The influences of RHA on properties of cementitious system 23
3.2.6.1. Setting time, water demand and workability 23
3.2.6.2. Hydration of Portland cement 23
3.2.6.3. Shrinkage 23
3.2.6.4. Compressive strength 24
3.2.6.5. Microstructure and durability 24
3.2.7. The combination of RHA with other mineral admixture in concrete 25
3.2.8. RHA in producing UHPC 25

3.3. Concluding remarks **26**
4. Experimental Design **29**
4.1. Materials **29**
4.2. Mix design of UHPC **31**
4.3. Mixing, casting and treatment of UHPC **32**
4.4. Experimental methods **33**
4.4.1. RHA ***33***
4.4.1.1. Porous structure *33*
4.4.1.2. Pozzolanic reactivity *33*
4.4.1.3. Zeta potential *35*
4.4.2. RHA as a pozzolanic admixture in UHPC ***35***
4.4.2.1. Workability and compressive strength *35*
4.4.2.2. Shrinkage *36*
4.4.2.3. Self-desiccation *37*
4.4.2.4. Microstructure *37*
4.4.2.5. Durability *38*
5. Results and Discussion **41**
5.1. Porous structure and pozzolanic reactivity of RHA **41**
5.1.1. Effect of grinding time on characteristics of RHA ***41***
5.1.1.1. Mean particle size and specific surface area of RHA *41*
5.1.1.2. Porous structure and morphology of RHA by SEM imaging *42*
5.1.1.3. Pore volume and water absorption *44*
5.1.2. RHA in cementitious system ***45***
5.1.2.1. Influence of RHA on water demand and setting time of cement paste *45*
5.1.2.2. Accelerated pozzolanic strength reactivity index (API) *45*
5.1.2.3. Portlandite content and pozzolanic reactivity of RHA in cement paste *46*
5.1.3. RHA in saturated $Ca(OH)_2$ solution ***47***
5.1.3.1. Electrical conductivity and pH of CH-pozzolan suspension *47*
5.1.3.2. Concentration of pozzolan silica and calcium in CH suspension *50*
5.1.3.3. Evaluation of pozzolanic reaction product of RHA and SF *51*
5.1.4. Zeta potential ***54***
5.1.5. Discussion ***54***
5.1.5.1. Effect of grinding on characteristics of RHA *54*
5.1.5.2. Effect of RHA on cement system *55*
5.1.5.3. Pozzolanic reactivity of RHA in saturated CH solution *56*
5.1.5.4. Evaluation pozzolanic reactivity of high specific surface area pozzolan *58*
5.1.5.5. Charged surface and ions adsorption of pozzolan *59*
5.1.6. Concluding remarks ***60***
5.2. RHA as a pozzolanic admixture in UHPC **61**
5.2.1. Preliminary test of UHPC ***61***
5.2.1.1. Compatibility between different SP and RHA-blended mixture *61*
5.2.1.2. Effect of GGBS, SP dosage, W/F_v and vibration period on properties of UHPC *63*

5.2.1.3. Effect of fineness of RHA on properties of UHPC 64
5.2.2. Optimization of mix proportions of UHPC containing RHA and GGBS **65**
5.2.2.1. Influence of RHA content on properties of UHPC containing RHA 65
5.2.2.2. Synergic effects of RHA, GGBS and SP on properties of UHPC 65
5.2.3. Discussion **75**
5.2.4. Concluding remarks **77**
5.3. Impact of pozzolanic materials and treatment conditions on compressive strength and shrinkage of UHPC **78**
5.3.1. Workability and compressive strength **79**
5.3.1.1. Workability 79
5.3.1.2. Effect of RHA content on compressive strength of UHPC containing GGBS 79
5.3.1.3. Effect of pozzolans and treatment conditions on compressive strength 80
5.3.1.4. Effect of cements and treatment conditions on compressive strength 81
5.3.2. Shrinkage and internal relative humidity of UHPC **82**
5.3.2.1. Autogenous shrinkage 82
5.3.2.2. Autogenous and total shrinkage at different treatment conditions 83
5.3.2.3. Internal relative humidity 85
5.3.3. Discussion **86**
5.3.3.1. Compressive strength 86
5.3.3.2. RHA as an internal curing agent 87
5.3.4. Concluding remarks **88**
5.4. Microstructure and durability of sustainable UHPC **89**
5.4.1. Microstructure of UHPC **89**
5.4.1.1. Portlandite content 89
5.4.1.2. Porosity and water absorption coefficient 90
5.4.1.3. Microstructure of UHPC containing RHA by SEM imaging 92
5.4.2. Durability of UHPC **93**
5.4.2.1. In NH_4NO_3 5M 93
5.4.2.2. In H_2SO_4 pH 2.5 94
5.4.2.3. Alkali silica reaction (ASR) 97
5.4.2.4. In cyclic climate storage (CCS) 100
5.4.3. Discussion **101**
5.4.4. Concluding remarks **103**
6. Conclusions and Further Research **105**
6.1. Conclusions **105**
6.2. Further research **107**
References **109**
Erklärung (German Declaration) **121**
List of Publications **123**
Curriculum Vitae **125**

List of Abbreviations

API	Accelerated pozzolanic strength reactivity index
ASR	Alkali silica reaction
BET	Brunauer-Emmett-Teller
BJH	Barrett-Joyner-Hanlenda
BSE	Backscattered electron
CCS	Cyclic climate storage
CDF	Capillary suction, de-icing agent and freeze-thaw
CIF	Capillary suction, internal damage and freeze-thaw
CH	Calcium hydroxide
C-S-H	Calcium silicate hydrates
DTA-TG	Thermal analysis
EDX	Energy-dispersive X-ray spectroscopy
FA	Fly ash
GGBS	Ground granulated blast-furnace slag
HPC	High performance concrete
l/s	Liquid to solid ratio
L.O.I	Loss on ignition
MIP	Mercury intrusion porosimetry
MK	Metakaolin
MPS	Mean particle size
NanoSEM	Ultra high resolution scanning electron microscopy
QXRD	Quantitative X-ray diffraction
RDM	Relative dynamic modulus
RH	Relative humidity
RHA	Reactive rice husk ash
RPC	Reactive powder concrete
SAP	Super-absorbent polymer
SCC	Self-compacting concrete
SEM	Scanning electron microscopy
SF	Silica fume
SP	Superplasticizer
SSA	Specific surface area
UHPC	Ultra-high performance concrete
w/b	Water to binder ratio
W/F_v	Water to fine material in volume ratio
XRD	X-ray diffraction

Summary

The outstanding mechanical properties and durability of ultra-high performance concrete (UHPC) characterize this new class of concrete. UHPC performance has been studied in previous scientific works as well as on-site. However, UHPC contains a very high content of Portland cement and silica fume (SF) accompanying with a high dosage of superplasticizer (SP) at a very low water to binder ratio (w/b). Thus, from environmental and economic points of view, UHPC offers challenges. To improve the sustainability of UHPC, less expensive and energy intensive materials such as ground granulated blast-furnace slag (GGBS) and fly ash (FA) have been used to partially replace Portland cement. Furthermore, expensive undensified SF may be replaced by a cheaper and more sustainable pozzolanic admixture (i.e. reactive rice husk ash). Using reactive rice husk ash (RHA) in concrete also reduces the impact of rice husk disposal on environment and enhances the income of farmers in developing countries. To appropriately utilize RHA in UHPC, it is important to understand in detail the influences of this renewable pozzolan on properties of fresh and hardened UHPC.

RHA is produced by burning rice husk, an agricultural waste in many developing countries such as Vietnam, China, Thailand and others under suitable conditions. RHA has a very high pozzolanic reactivity comparable with that of SF. The present thesis studies the effects of RHA as a pozzolanic admixture and the combination of RHA and GGBS on properties of UHPC. The ultimate purpose of this study is to replace completely SF and partially Portland cement by RHA and GGBS to achieve sustainable UHPC. To reach this aim, characteristics of RHA in dependence of grinding period, especially its pozzolanic reactivity in saturated $Ca(OH)_2$ solution and in a cementitious system at a very low w/b were assessed. The influences of RHA on compatibility between superplasticizer and binder, workability, compressive strength, shrinkage, internal relative humidity, microstructure and durability of UHPC were also evaluated. Furthermore, synergic effects of RHA and GGBS on the properties of UHPC were investigated to produce more sustainable UHPC. Finally, various heat treatments were applied to study the properties of UHPC under these conditions. All the characteristics of these UHPCs containing RHA were compared to those of mixtures containing SF. These investigations are crucial for gaining a more detailed understanding on how RHA acts as a pozzolanic admixture in UHPC.

The novel and major results and conclusions from the experiments can be summarized as follows:

- Properly burned RHA is a renewable mesoporous amorphous siliceous material with very high amorphous silica content and specific surface area. The pozzolanic reactivity of RHA is strongly affected by its porous structure. It is shown that the porous structure partially collapses during grinding. Because of its mesoporous structure, ground RHA can absorb a high volume of water and allows Ca^{2+} ions to diffuse into internal parts of particle, enhancing its pozzolanic reactivity. RHA acts as both highly reactive pozzolan and water absorbing material in cementitious system. Thus, a continuous hydration of cement and a long lasting pozzolanic reaction of RHA are assured also at low w/b.

- With respect to portlandite consumption, the pozzolanic reactivity of SF is higher than that of RHA in both cementitious system and portlandite solution. The differences in surface structure, alkali content and possible difference in nature of dissolved Si (i.e. Si-OH groups) between RHA and SF result in distinct differences in their Ca^{2+} ion adsorption as well as dissolution-precipitation processes in saturated portlandite suspension at 40°C. In the portlandite-pozzolan suspensions of RHA and SF, C-S-H phases can be observed as products of the pozzolanic reaction after 6 hours of hydration. In this study, it is proposed that the electrical conductivity reduction rate [mS/cm·min] of the portlandite-pozzolan suspension between 30 and 210 min can be used to compare well the pozzolanic reactivity of RHA ground for different periods of time and SF.
- UHPC can be produced by using RHA to completely replace SF. With a sufficient water content (i.e. water to fine material in volume ratio of 0.55), RHA-blended UHPC possesses a flowability and compressive strength comparable with those of SF-blended UHPC at the same water content and SP dosage. For compressive strength development of UHPC containing RHA, pozzolanic reactivity of RHA is not the most important parameter. Rather the microstructural effects such as mesoporous structure and fineness of RHA can be considered as the important strength determining parameters.
- Highly water absorbing RHA acts also as an internal curing agent in UHPC. The decrease in the internal relative humidity and thus self-desiccation of UHPC is reduced by the presence of RHA. Hence, it was shown that the addition of RHA strongly reduces autogenous shrinkage of UHPC. With small particle size, high water absorption and high pozzolanic reactivity, RHA is considered as an advanced pozzolanic internal curing material. It serves very well for both homogeneous internal water reservoir distribution and dense microstructure in UHPC. However, the RHA-modified UHPC possesses the increased total porosity, water absorption coefficient and $Ca(OH)_2$ content, thus leading to an increased drying shrinkage and slightly lower durability in aggressive solutions compared to the SF-modified UHPC. If this can be improved by variation in SP type or content in order to lower the w/b of UHPC containing RHA should be the subject of further studies.
- The combined utilization of GGBS and RHA or SF in UHPC production enhances the workability, reduces the total porosity, water absorption coefficient, shrinkage, and thus improves compressive strength and durability of UHPC.
- Heat treatment accelerates and enhances the Portland cement clinker and RHA hydration in the very low w/b matrix. But the final compressive strength of the heat treated UHPCs containing RHA is similar to the RHA-modified UHPC treated at 20°C. After 48 hour treatment at 65°C or 90°C, autogenous shrinkage of the mixtures containing RHA almost ceases. Compressive strength, shrinkage and durability of the 65°C treated samples are slightly better than those of the 90°C treated samples. In terms of economical and technical aspects, the 65°C treatment instead of the 90°C treatment should be used for accelerating early (7-day) compressive strength. Finally, it can be stated that using RHA as a pozzolanic admixture in UHPC production is sustainable.

Zusammenfassung (German Summary)

Die sehr guten mechanischen Eigenschaften und die hohe Dauerhaftigkeit von Ultra-Hochfestem Beton (engl.: Ultra-High Performance Concrete- UHPC) beschreibt eine neue Klasse von Betonen und ist Gegenstand zahlreicher Forschungen in vielfältigen Anwendungsgebieten. Aufgrund des hohen Anteils an Zement und Silikastaub (engl.: Silica fume- SF) sowie hohen Dosierungen von Fließmittel (engl.: Superplasticizer- SP) und des sehr niedrigen Wasser-Zement-Wertes (W/Z-Wert) besteht die Frage, inwiefern ökologische und wirtschaftliche Potentiale von UHPC ausgeschöpft sind. Um die Nachhaltigkeit von UHPC zu verbessern werden günstigere und weniger energieintensive Materialien wie zum Beispiel Hüttensand (engl.: Ground Granulated Blast-furnace Slag- GGBS) und Flugasche (engl.: Fly Ash- FA) eingesetzt, welche den Zement teilweise ersetzen. Weiterhin sollte der mangelhafte und kostenintensive hochfeine Silikastaub durch günstigere puzzolanische Betonzusatzstoffe (wie zum Beispiel Reisschalenasche) ersetzt werden. Die Verwendung von Reisschalenasche (engl.: Rice Husk Ash- RHA) in Beton ersetzt darüber hinaus die problematische Entsorgung der Asche und schont so die Umwelt. In Entwicklungsländern kann so außerdem die wirtschaftliche Situation von Reisbauern verbessert werden. Um RHA in UHPC fachgerecht einsetzen zu können, ist es wichtig, den Einfluss dieses erneuerbaren Puzzolans auf die Frisch- und Festbetoneigenschaften im Detail zu verstehen.

Bei der Verbrennung von Reisschalen, einem landwirtschaftlichen Abfallprodukt in vielen Entwicklungsstaaten wie zum Beispiel Vietnam, China und Thailand, entsteht RHA. Der Verbrennungsvorgang, d.h. Temperatur, Dauer und Kühl- und Aufheizrate sollte kontrolliert werden. Die RHA hat eine sehr hohe puzzolanische Reaktivität, vergleichbar mit der von SF. Im Rahmen der vorliegenden Dissertation werden die Effekte von RHA als ein zementärer Zusatzstoff auf Frisch- und Festbetoneigenschaften (auch in Kombination mit GGBS) von UHPC untersucht. Am Ende der Untersuchungen sollte es möglich sein SF komplett durch RHA und Zement teilweise durch GGBS zu ersetzen, um so nachhaltigen UHPC herzustellen. Um dieses Ziel zu erreichen, wurden RHA mit unterschiedlichen Feinheiten hinsichtlich ihrer puzzolanischen Reaktivität in gesättigter $Ca(OH)_2$-Lösung und in zementösen Systemen mit niedrigem w/z-Wert untersucht. Der Einfluss von RHA auf die Kompatibilität zwischen Fließmittel und Binder, Verarbeitbarkeit, Druckfestigkeit, Schwinden, interne relative Feuchte, Mikrostruktur und Dauerhaftigkeit waren Gegenstand der Untersuchungen. Um eine höhere Nachhaltigkeit von UHPC zu erzielen, wurden auch Synergie-Effekte zwischen RHA und GGBS untersucht. Schlussendlich wurden die Eigenschaften von UHPC in Abhängigkeit einer Warmbehandlung mit unterschiedlichen Randbedingungen erforscht. Alle UHPC mit RHA wurden mit denen verglichen, die nur SF enthielten. Diese Untersuchungen sind ausschlaggebend für das genaue Verständnis, wie RHA als Zusatzstoff in UHPC wirkt.

Die neuen und bedeutenden Resultate und Schlussfolgerungen dieser Arbeit können wie folgt zusammengefasst werden:

- RHA ist ein erneuerbares, mesoporöses, amorphes, silikatisches Material mit einem sehr hohen Gehalt an amorpher Kieselsäure und einer typischen großen spezifischen Oberfläche. Die puzzolanische Reaktivität wird sehr stark von der spezifischen Oberfläche und der porösen Struktur beeinflusst. Aufgrund der porösen Struktur kann die RHA Wasser innerhalb der Zementmatrix absorbieren und erlaubt Calcium-Ionen weit in die inneren Bereiche der Partikel zu diffundieren. Das verbessert die puzzolanische Reaktivität der RHA. Die RHA ist also auf der einen Seite ein hoch puzzolanischer Stoff und auf der anderen Seite ein wasserabsorbierendes Material innerhalb des zementösen Systems. Aus diesem Grund ist eine kontinuierliche Hydratation des Zements und eine lang dauernde puzzolanische Reaktion der RHA gewährleistet.
- Sowohl in der Zementmatrix als auch in der $Ca(OH)_2$-Lösung ist die puzzolanische Reaktivität in Form von $Ca(OH)_2$-Verbrauch für SF höher als von RHA. Die Unterschiede hinsichtlich der Oberflächenstruktur, des Alkaligehaltes und der chemischen Natur der Kieselsäure in RHA und SF verändern die Calciumadsorption und den Lösungs-Fällungs-Mechanismus des amorphen SiO_2 deutlich in der $Ca(OH)_2$-Lösung bei 40°C. Als ein Produkt der puzzolanischen Reaktion innerhalb der CH-Puzzolan-Suspensionen können nach 6 Stunden C-S-H Phasen beobachtet werden. In dieser Arbeit wurde erfolgreich die Reduktionsrate der elektrischen Leitfähigkeit [mS/cm·min] an CH-Puzzolan Suspensionen (Wasser/Puzzolan-Verhältnis 40, 40°C) zwischen 30 und 210 min Hydratation angewandt, um die puzzolanischen Reaktivität zu evaluieren. Der Test ist insbesondere bei dem Vergleich der puzzolanischen Reaktivität von unterschiedlich adsorbierenden Puzzolanen wie RHA und SF zielführend.
- In UHPC kann SF vollständig durch RHA ersetzt werden. Bei ausreichendem Wassergehalt besitzt UHPC mit RHA vergleichbare Verarbeitbarkeits- und Festigkeitseigenschaften wie UHPC mit SF. Für die Festigkeitsentwicklung in zementösen Systemen ist die puzzolanische Reaktivität nicht der einzige wichtige Einflussparameter sondern auch mikrostrukturelle Effekte wie die Porenstruktur und Einbindung der RHA in die zementöse Matrix. Wesentlicher festigkeitsbeeinflussender Parameter der RHA ist die Mahlfeinheit.
- RHA besitzt aufgrund ihrer porösen Struktur eine hohe Wasseraufnahmefähigkeit. Infolgedessen wirkt sie im Beton als ein inneres Nachbehandlungsmittel. Die Abnahme der inneren relativen Feuchte in UHPC wird durch RHA vermindert und das autogene Schwinden dadurch stark abgeschwächt. Aufgrund der Kombination von kleiner Partikelgröße, hoher puzzolanischen Reaktivität, hohem Wasserspeichervermögens und seiner mesoporösen Mikrostruktur ist RHA für die Anwendung im ultra-dichten UHPC ein geeignetes Mittel für die innere Nachbehandlung. UHPC mit Reisschalenasche besitzt eine höhere absolute Porosität und einen höheren Wasserabsorptionskoeffizient. Deshalb besitzt dieser Beton ein größeres Trocknungsschwinden und eine geringere Dauerhaftigkeit in aggressiven Umgebungen als UHPC mit SF.
- Das Zusammenwirken von RHA und GGBS verbessert die Verarbeitungseigenschaften und erhöht die Druckfestigkeit von UHPC. Darüber hinaus werden der

Wasserabsorptionskoeffizient und die absolute Porosität gesenkt was insgesamt zu einer Verbesserung der Dauerhaftigkeit von UHPC mit RHA führt.

- Die Warmbehandlung beschleunigt und fördert die Zementhydratation und die puzzolanische Reaktivität von RHA im Zementstein mit sehr niedrigen W/Z-Werten. Jedoch hat die Warmbehandlung keinen Einfluss auf die Endfestigkeit von UHPC mit Reisschalenasche. Nach 48 Stunden bei 65°C bzw. 90°C ist kein autogenes Schwinden mehr feststellbar. Jedoch weisen die Proben der 65°C-Lagerung ein etwas geringeres Schwinden, höhere Druckfestigkeiten und Dauerhaftigkeit auf als jene Proben, die bei 90°C gelagert wurden. Auch aus wirtschaftlichen und technischen Gründen sollte deshalb die 48h-Warmebehandlung (falls nötig) bei 65°C erfolgen. Zusammenfassend bleibt festzustellen, dass es sich bei RHA um einen anwendbaren, nachhaltigen Zusatzstoff für UHPC handelt.

Tóm Tắt (Vietnamese Summary)

Với các tính chất cơ lý và độ bền cực cao, bê tông chất lượng siêu cao (Ultra-High Performance Concrete- UHPC) là một phân hạng bê tông mới sử dụng chất kết dính xi măng. UHPC đã và đang được nhiều nhà nghiên cứu và ứng dụng quan tâm phát triển trong gần hai thập niên qua. UHPC cần có cường độ nén lớn hơn 150 MPa ở tuổi 28 ngày trong điều kiện dưỡng hộ thường. Để đạt được các tính năng siêu cao, UHPC được chế tạo với hàm lượng lớn xi măng, muội silic và phụ gia siêu dẻo ở tỷ lệ nước/chất kết dính (N/CKD) rất thấp. Chính vì vậy, UHPC có giá thành cao hơn nhiều so với bê tông chất lượng cao hiện hành, đặc biệt với giá bán ngày càng cao của muội silic. Đồng thời, do sử dụng với hàm lượng lớn xi măng, tính thân thiện với môi trường của loại bê tông này cũng được đặt ra. Việc sử dụng các loại vật liệu từ các nguồn phụ phẩm như xỉ lò cao, tro bay để thay thế từng phần xi măng và muội silic trong UHPC là một trong những vấn đề được quan tâm nghiên cứu nhằm giảm giá thành, tăng tính thân thiện với môi trường cho loại bê tông này. Tro trấu hoạt tính, với chế độ đốt hợp lý, có hoạt tính pozzolan rất cao. Nó có khả năng thay thế muội silic và một phần xi măng nhằm giảm giá thành cho bê tông, bảo vệ môi trường và tăng thu nhập cho nông dân. Để sử dụng một cách hợp lý tro trấu trong loại vật liệu chất lượng cực cao này, ảnh hưởng của tro trấu đến các tính chất của hỗn hợp bê tông và bê tông đã đóng rắn cần được nghiên cứu chi tiết.

Mục tiêu của đề tài nghiên cứu này là sử dụng tro trấu hoạt tính và sự kết hợp tro trấu-xỉ lò cao nhằm thay thế hoàn toàn muội silic và một phần xi măng trong UHPC. Để đạt được mục tiêu này, đề tài đã tiến hành các nghiên cứu thực nghiệm về các đặc tính của tro trấu ở các thời gian nghiền khác nhau qua các tính chất về độ nghiền mịn, tỷ diện tích bề mặt, thể tích rỗng, khả năng hút nước, khả năng hoạt tính của tro trấu trong dung dịch nước vôi bão hòa ở 40°C và trong hệ chất kết dính xi măng, đặc biệt là ở tỷ lệ N/CKD = 0.22. Kết quả của những nghiên cứu này giúp giải thích rõ vai trò của tro trấu trong hệ chất kết dính xi măng. Với UHPC, ảnh hưởng của tro trấu đến tính tương hợp giữa phụ gia siêu dẻo và chất kết dính, tính công tác, cường độ nén, tính co ngót, sự suy giảm độ ẩm tương đối- sự tự khô trong bê tông, vi cấu trúc và độ bền của UHPC đã được thí nghiệm. Sự ảnh hưởng của việc phối hợp giữa tro trấu và xỉ lò cao đến các tính chất của UHPC cũng đã được nghiên cứu một cách chi tiết. Hơn nữa, hai chế độ dưỡng hộ nhiệt đã được áp dụng nhằm so sánh ảnh hưởng của chúng đến các tính chất của bê tông sử dụng tro trấu. Tất cả các tính chất của UHPC sử dụng tro trấu đều được so sánh một cách tương ứng với các tính chất của hỗn hợp bê tông sử dụng muội silic. Những nghiên cứu này giúp hiểu rõ hơn vai trò của tro trấu như là loại phụ gia khoáng hoạt tính trong UHPC.

Những kết quả và nhận định mới từ các nghiên cứu của đề tài này được tóm tắt như sau:

- Tro trấu được đốt ở chế độ đốt hợp lý là một loại vật liệu cấu trúc rỗng xốp có tỷ diện tích bề mặt và hàm lượng SiO_2 vô định hình rất cao. Vi cấu trúc của hạt tro trấu trong quá trình nghiền mịn lần đầu tiên được nghiên cứu bởi thiết bị chụp ảnh vi cấu trúc có độ phân giải cực cao (NanoSEM). Cấu trúc rỗng xốp bị phá vỡ một phần trong quá trình nghiền sẽ ảnh hưởng mạnh đến khả năng hoạt tính pozzolan của tro trấu. Với cấu trúc

xốp rỗng, tro trấu có khả năng hút một lượng nước trong bê tông. Điều này cho phép Ca^{2+} ion thẩm thấu vào bên trong hạt tro trấu nhằm tăng độ hoạt tính của nó. Tro trấu đóng vai trò đồng thời như vật liệu có độ hoạt tính pozzolan cao và là tác nhân dưỡng hộ trong cho bê tông. Vì thế, quá trình thủy hóa của xi măng và tro trấu trong UHPC được duy trì ở tuổi dài ngày.

- Về phương diện phản ứng với $Ca(OH)_2$, muội silic có độ hoạt tính cao hơn tro trấu ở cả trong hệ chất kết dính xi măng và dung dịch vôi bão hòa. Sự khác nhau về cấu trúc hạt, hàm lượng kiềm và đặc tính của silica giữa tro trấu và muội silic tạo nên sự khác biệt về khả năng hấp phụ Ca^{2+} ion, quá trình hòa tan của SiO_2 hoạt tính và kết tủa của sản phẩm thủy hóa trong dung dịch vôi bảo hòa giữa hai loại vật liệu này. Sản phẩm thủy hóa C-S-H đã được phát hiện sau 6 giờ thủy hóa giữa tro trấu hoặc muội silic với dung dịch vôi bão hòa ở 40°C. Tốc độ suy giảm mức độ dẫn điện của dung dịch vôi-pozzolan trong khoảng thời gian từ 30 đến 210 phút là một tiêu chuẩn mới được đề xuất bởi đề tài này nhằm đánh giá đúng khả năng hoạt tính pozzolan giữa các loại vật liệu có tính hấp phụ khác nhau mà cụ thể là tro trấu và muội silic.
- Có thể sử dụng tro trấu để thay thế hoàn toàn muội silic trong sản xuất UHPC. Với cùng lượng dùng nước và phụ gia siêu dẻo, hỗn hợp UHPC sử dụng tro trấu có tính công tác và cường độ rất tốt, tương đương với bê tông chứa muội silic. Đặc tính về cấu trúc rỗng và độ nghiền mịn là những yếu tố chính ảnh hưởng đến cường độ của bê tông chứ không phải là hoạt tính pozzolan của tro trấu.
- Tro trấu còn là một loại vật liệu dưỡng hộ bên trong. Tro trấu hút một lượng nước tự do ban đầu để nâng cao cường độ của hỗn hợp bê tông, đặc biệt là ở tuổi sớm và tiếp tục cung cấp nước trở lại cho quá trình thủy hóa của xi măng và tro trấu. Đồng thời nó làm chậm lại quá trình suy giảm độ ẩm bên trong- sự tự khô của UHPC. Điều này tạo cho tính tự co ngót của UHPC có chứa tro trấu được cải thiện rõ rệt so với UHPC có chứa muội silic. Kết hợp giữa kích thước hạt bé và độ hoạt tính pozzolan cao, tro trấu có đồng thời ưu điểm cho sự phân bố nguồn nước dưỡng hộ bên trong và vi cấu trúc của UHPC. Tuy nhiên, độ rỗng và tính hút nước của UHPC có chứa tro trấu lại cao hơn hỗn hợp chứa muội silic. Nó làm tăng độ co ngót khô và làm giảm độ bền của UHPC có chứa tro trấu. Việc liệu có thể tăng cường độ bền, giảm độ co ngót khô bằng cách thay đổi hàm lượng hoặc loại phụ gia siêu dẻo nhằm hạ thấp N/CKD của UHPC sử dụng tro trấu sẽ là đối tượng nghiên cứu của các nghiên cứu sau này.
- Sự phối hợp giữa tro trấu hoặc muội silic với xỉ lò cao cải thiện rõ rệt tính công tác, cường độ, tính co ngót, độ rỗng, độ hút nước và độ bền của UHPC.
- Dưỡng hộ nhiệt thúc đẩy quá trình thủy hóa của xi măng và tro trấu trong UHPC. Tuy nhiên, cường độ ở tuổi dài ngày của mẫu dưỡng hộ thường lại tốt hơn so với mẫu dưỡng hộ nhiệt. Sau 2 ngày dưỡng hộ nhiệt ở 65 hoặc 90°C, sự tự co ngót của UHPC gần như kết thúc. Cường độ, độ tự co ngót và độ bền của mẫu dưỡng hộ ở 65°C có phần tốt hơn so với mẫu dưỡng hộ ở 90°C. Vì vậy, về phương diện kinh tế và kỹ thuật, khi dưỡng hộ nhiệt là cần thiết thì dưỡng hộ ở nhiệt độ trung bình (65°C) nên được áp dụng thay vì dưỡng hộ ở 90°C nhằm đẩy nhanh cường độ ở tuổi sớm của UHPC. Có thể kết luận rằng việc sử dụng tro trấu trong sản xuất UHPC là tiết kiệm và bảo vệ môi trường sinh thái.

1. Introduction

Innovations in modern concrete technology and the development of new superplasticizers facilitate new properties of concrete that have never before been obtained. Concrete design is now made from the macroscopic scale to the microscopic scale. Ultra-high performance concrete (UHPC) is a new class of concrete that has gained a strong interest in research and application in recent years [1-5]. UHPC, also called reactive powder concrete (RPC), was first developed in the early 1990s in France and Canada [6, 7]. UHPC commonly consists of a high amount of Portland cement, silica fume (SF) with fine grained aggregates and steel fibers for reinforcement. UHPC possesses a very low water to binder ratio (w/b) with the addition of a high superplasticizer (SP) dosage [6, 8, 9]. Hence, UHPC achieves compressive strength between 150 and up to 800 MPa, modulus of elasticity of 50-60 MPa, high flexural strength and very high durability [1, 6, 10-12].

UHPC is produced by using the advantages of SP and pozzolanic admixtures. SP dosage in UHPC is almost at the saturation dosage in order to obtain the highest workability of concrete at a very low w/b. In addition, pozzolanic admixtures are always used in UHPC to enhance the microstructure, density, and thus compressive strength and durability of UHPC. Pozzolanic admixtures are selected for UHPC to optimize particle size distribution of materials as well, thereby increasing the packing density, reducing the voids and hence increasing the amount of excess water of the binder paste. This can improve both rheology and microstructure of cement matrix and concrete. Undensified SF is widely used as a pozzolanic admixture in UHPC. The optimal dosage of SF is about 20-30 wt.-% of cement to improve the filler effect of SF in UHPC [6, 8, 13, 14]. With the high content of cement (up to over 1000 kg/m^3) and SF (about 200 kg/m^3), UHPC not only is concerned about the heat of hydration, shrinkage and microcracking of the matrix, but it also is not environmentally friendly and is too expensive. Partial replacement of Portland cement and expensive SF by increasing the use of binary or ternary cement blends would result in a more sustainable UHPC. Many studies focused on the partial substitution of cement and SF by other environmentally friendly, low-cost cementitious materials such as fly ash (FA) [15-20], ground granulated blast-furnace slag (GGBS) [16-27] and metakaolin (MK) [15, 28].

Reactive rice husk ash is produced by burning rice husk, an agricultural waste, under suitable conditions. The term “RHA” exclusively refers to reactive rice husk ash in this thesis. Properly burned RHA is a very porous, soft material, and hence it can be easily ground. RHA has a high content of amorphous silica and a high specific surface area determined by nitrogen adsorption, above 85 wt.-% and about 60 m^2/g, in some cases more than 200 m^2/g, respectively. Therefore, RHA has a very high pozzolanic reactivity comparable with SF [29-36]. It is reported that the use of RHA in concrete leads to a noticeable increase in compressive strength, sulfate resistance, a significant reduction of rapid chloride penetrability and autogenous shrinkage of normal and high performance concretes [34-56]. Another advantage of RHA is that it improves properties of fresh concrete, especially the high tendency to

segregation and bleeding as observed in self-compacting concrete and lightweight aggregate concrete [36, 37, 54]. RHA can also be a good pozzolanic admixture to produce UHPC without significant change in compressive strength [57-60]. However, due to the high specific surface area, porous structure of particles and irregular particle shape, RHA has a higher water demand than cement, and hence it needs a higher SP dosage to maintain the workability of mixture [35, 36, 54, 58-61].

According to Foods and Agriculture Organization (FAO) [62], the annual production of rice paddies in the world is about 700 million tons. It is estimated that the husk content of paddy is generally about 20 wt.-% and the rice husk on combustion yields about 20 wt.-% of ash [36, 63]. Therefore, about 140 million tons of rice husk are annually disposed. That is causing large environmental problems in rice producing countries like Vietnam, China, Thailand, etc. About 28 million tons of RHA as a renewable siliceous material can be potentially produced. Using RHA also increases the income of farmers in developing countries. Moreover, the huge demand of SF in the concrete industry all over the world induces the shortage and increases the price. The use of RHA to replace SF in concrete is thus desirable to decrease the overall material cost of concrete, especially with the high SF content of UHPC. Hence, using RHA in concrete not only improves the certain properties of concrete, but also enhances both environmental relief and economic benefits.

On the other hand, when GGBS partially replaces cement, workability of UHPC significantly improves with GGBS content. Compressive strength above 150 MPa is obtained when up to 75 wt.-% cement is replaced by GGBS [20, 22, 26]. In addition, the incorporation of RHA with other pozzolan, e.g. SF or FA improves workability, compressive strength and durability of mortar and concrete [43, 51, 61, 64, 65]. The self-compacting concrete (SCC) using a quaternary binder containing FA, GGBS and RHA has similar properties for both fresh and hardened concrete compared to the mixture containing FA, GGBS and SF [42]. The combination of a less reactive pozzolan, such as GGBS, with a more reactive one, i.e. RHA, produces synergic physical and chemical effects in ternary concrete mixtures. These effects are higher when the pozzolan content is optimized and the w/b is low [46]. Therefore, the combination of RHA and GGBS may be the perspective idea to improve properties of fresh and hardened UHPC. Thus, the current thesis studies on the effects of RHA and the combination of RHA and GGBS on UHPC's properties. This thesis will contribute to making the application of RHA as a pozzolanic admixture in UHPC production successful and in obtaining more sustainable UHPC.

2. Objectives and Research Methodology

2.1. Objectives

Despite the fact that many studies on characteristics and contributions of RHA in concrete have been reported, most of them have been applied on normal and high performance concretes [30]. The information of using RHA for UHPC production is scarce [60]. For a better understanding of performance of RHA in UHPC, fundamental knowledge about its interaction and reaction with other constituents which affect both fresh and hardened concrete is crucial. The specific objectives of the present study are followed:

- Characteristics of RHA and pozzolanic reactivity of RHA in portlandite solution and cementitious systems, especially at a very low w/b of 0.22;
- Influence of RHA, the synergic effects of RHA, GGBS and SP on workability and compressive strength of UHPC to choose the suitable materials and mix proportions which can produce sustainable UHPC by using normal mixers;
- Measuring the following properties of UHPCs containing RHA in dependence of different treatment conditions: compressive strength, shrinkage, internal relative humidity, microstructure and durability. In this way, UHPCs containing RHA and SF are compared.

2.2. Research methodology

The experimental studies can be divided into two main parts. The characteristics of RHA and pozzolanic reactivity of RHA in portlandite solution as well as in cementitious systems are studied. The aim is to understand in more detail the effects of RHA on cement hydration systems, especially at a very low w/b of 0.22. The second part focuses on the influences of RHA alone as well as in the combination with GGBS on workability, compressive strength, shrinkage, internal relative humidity, microstructure and durability of UHPCs at varying treatment conditions.

In the first part, an ultra-high resolution scanning electron microscope (FE-SEM, NanoSEM, FEI) was applied to capture the porous surface structure and morphology of RHA particles during grinding. Mean particle size (MPS), specific surface area (SSA), pore volume and water absorption capacity of RHA samples in dependence of grinding period were measured. Accelerated pozzolanic strength reactivity index of pozzolan with Portland cement, calcium hydroxide content in cement pastes, electrical conductivity of portlandite-pozzolan suspension, and solubility of silicon and calcium consumption in portlandite solution were conducted to evaluate the pozzolanic reactivity of RHA ground for different periods of time. Results were compared with SF. The products of the pozzolanic reaction between portlandite solution and RHA or SF was identified by SEM and quantified by thermogravimetric analysis (DTA-TG).

In the second part, mini-cone slump flow and compressive strength tests were carried out to study the influences of SP, RHA grinding, RHA content and the synergic effects of RHA, GGBS and SP on the properties of UHPC. The combined mixture-process model was applied to interpret the synergic effects of RHA, GGBS and SP on slump flow and compressive strength of UHPC through 3D response surface and contour plots (Design-Expert 8 software). Optimized UHPC mixtures containing RHA, respectively, GGBS and RHA were selected. Sealed and free stored samples were utilized to measure autogenous and drying shrinkages of the UHPCs. Additionally, the internal relative humidity of sealed samples was also measured during hydration by relative humidity sensors to evaluate if due to high water absorption capacity, RHA may act as an internal curing agent against self-desiccation in the UHPC. For microstructural and durability aspects, tests of the total porosity, pore size distribution, water absorption coefficient, $Ca(OH)_2$ content, aggressive solution resistance, alkali silica reaction and cyclic climate storage were conducted on the samples. SEM of Backscattered Electrons (BSE) together with Energy Dispersive X-ray (EDX) spectroscopy was applied to capture the microstructure of the UHPC containing RHA before and after the durability tests. All these properties of the UHPCs containing RHA were compared with those of UHPCs containing SF at three different treatment conditions (20, 65 and 90°C).

3. Literature Review on Ultra-High Performance Concrete and Rice Husk Ash

3.1. Ultra-high performance concrete

3.1.1. Introduction

Ultra-high performance concrete (UHPC) obtains compressive strength over 150 MPa and advanced durability properties. It is considered as a new type of cementitious building material (Figure 3.1 and Figure 3.2) [1, 60, 66, 67]. UHPC is emerging as an interesting subject in research and application [4, 5]. The main objectives are not only improving compressive strength, ductility, microstructure and durability of concrete, but also enhancing workability, cost efficiency and sustainability [5].

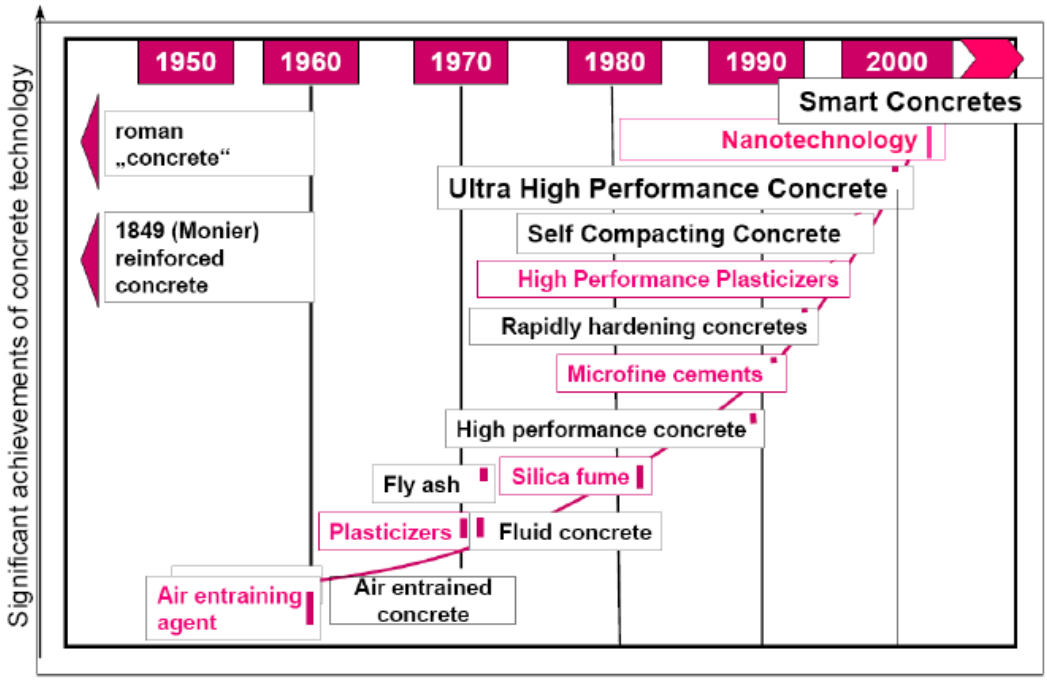

Figure 3.1. Significant development in concrete technology in the last 40 years [60, 66].

To optimize the strength and ductility/toughness in such a way to approach the structural properties of steel, new kinds of cementitious materials (Figure 3.2) are currently being developed, such as [67, 68]:

- SIFCON (Slurry Infiltrated Fiber CONcrete).
- DSP (Densified with Small Particle systems).
- RPC (Reactive Powder Concrete) or UHPC (Ultra-High Performance Concrete).
- BSI (Béton Spécial Industriel- Special Industry Concrete).
- MDF (Macro-Defect-Free) cement.

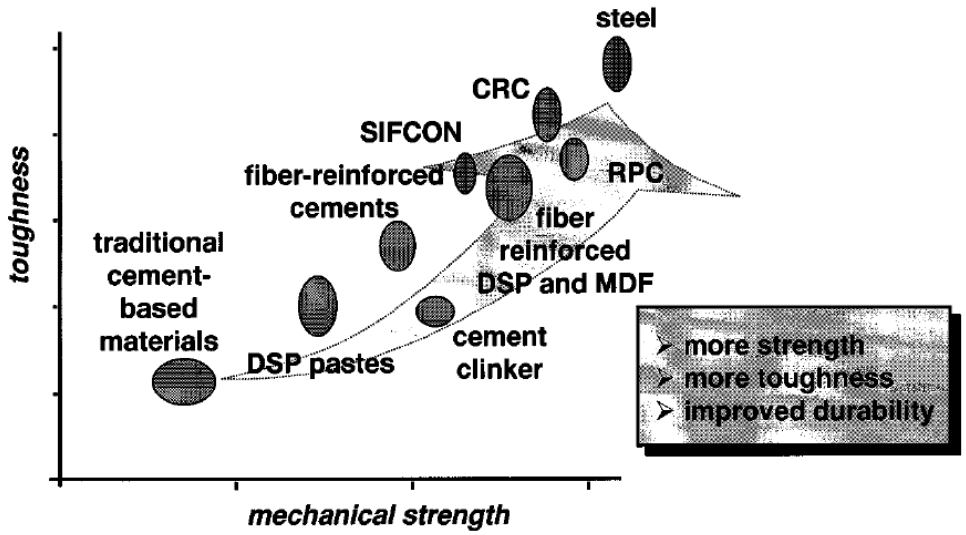

Figure 3.2. Trends of cement-based materials [67, 68].

Development of these materials is possible due to [68]:

- The introduction of new reinforcement systems;
- The study of fiber-matrix interface and consequent optimization of adhesive properties;
- The development of high-performance cementitious matrices which possess greatly improved microstructural properties in terms of compressive strength and durability;
- The innovation in processing techniques (including controlling chemical reactions) which allow us to obtain materials with surprisingly high toughness and low porosity.

A typical UHPC which presents improved compressive strength and durability is produced by the application of the following basic principles [1, 6]:

- Enhancement of concrete homogeneity by elimination of coarse aggregates;
- Enhancement of compacted density by optimization of particle size distribution of fines and aggregates and application of pressure before and during setting;
- Enhancement of the microstructure by the pozzolanic reaction and post-set heat-treating;
- Maintaining mixing and casting procedures as close as possible to existing practice;
- Enhancement of ductility by incorporation of steel fibers.

Application of the first four principles produces a concrete with very high compressive strength, but its ductility is not improved compared to normal concrete. The addition of fibers improves compressive strength, tensile strength and ductility of UHPC. Application of pressure and post-set heat-treating enhances the performance of concrete. With these principles, concrete exhibits compressive strength over 150 MPa with normal temperature treatment, about 200-250 MPa with post-set heat treatment at 90°C, 450-650 MPa by the use of a high volume of steel fibers, high temperature treatments, pressurization of the fresh material during setting and hardening, and up to 800 MPa with steel aggregates (Table 3.1) [6, 69].

Table 3.1. UHPC mix proportions and properties of concretes [69]

N^0	Content	Unit	UHPC200	UHPC800
1	Portland cement	[kg/m^3]	950	980
2	Silica fume	[kg/m^3]	237	225
3	Crushed quartz	[kg/m^3]	-	382
4	Silica sand	[kg/m^3]	997	490
5	13 mm steel fibers	[kg/m^3]	146	-
6	3 mm stainless steel fibers	[kg/m^3]	-	617
7	Superplasticizer (solid content)	[kg/m^3]	17	18
8	Total water	[kg/m^3]	180	186
9	Water/(Cement + Silica fume)	-	0.15	0.14
10	Pressurization during setting	[MPa]	-	60
11	Temperature treatment	[°C]	90	250
12	Compressive strength	[MPa]	194-203	422-520
13	Static Young's modulus in linear range, E_c	[GPa]	62-66	63-74
14	Dynamic Young's modulus, E_{dyn}	[GPa]	59-61	32-36
15	Static Poisson's ratio	-	0.22-0.24	0.19-0.28

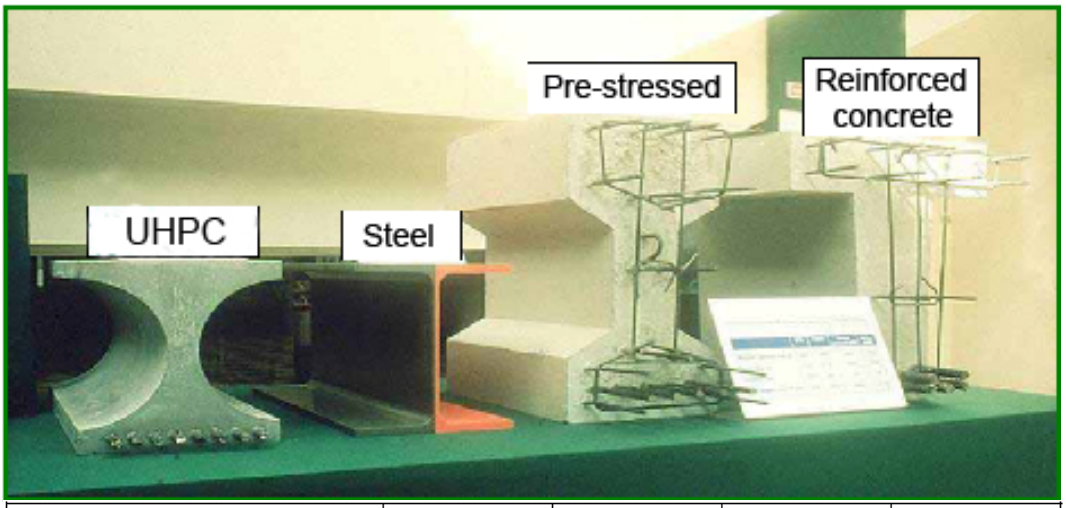

Material	UHPC	Steel	Pre-stressed concrete	Reinforced concrete
Height of cross section [mm]	360	360	700	700
Weight [kg/m]	141	110	466	528

Figure 3.3. UHPC, steel, pre-stressed and reinforced concrete beams with equal loading capacity [70].

With high content of Portland cement, SF and SP, the manufacture of UHPC is much more expensive than that of high performance concrete (HPC). Furthermore, a high content of cement clinker makes UHPC not really sustainable, especially with respect to CO_2 emission. However, the increased mechanical properties of UHPC allow us to decrease the cross-section of concrete structures while maintaining similar or longer spans of structures (Figure 3.3) [70]. Due to reduced cross section of UHPC structure, sustainability is enhanced by increasing the efficiency of using concrete and structure. The advantage of UHPC is the improved durability of this concrete against freeze-thaw deterioration, corrosion of steel and chemical attack (Table 3.2) [10]. The improved durability of UHPC leads to a lower repair and

maintenance cost of construction. In addition, longer lifetime of structures made of UHPC will minimize the impact on the environment. Even when UHPC requires increased cement clinker content than normal and high performance concretes, the amount of cement used in a lifetime of an UHPC structure may be less than the amount of cement used for several lifetimes of a normal or high performance concrete structure. Hence, the price of concrete is now not the cost of 1 m^3 concrete but rather the cost of 1 MPa or 1 year of life cycle of a structure. It is necessary to take into account the final cost of UHPC and above all, of the produced constructions.

Table 3.2. Characteristic durability values for normal concrete, HPC, and UHPC [10]

Indicator	Unit	Normal concrete C 35	HPC C 100/115	UHPC > C 150
Total porosity (by MIP)	[vol.-%]	app. 15	app. 8	4-6
Capillary pore	[vol.-%]	app. 8	app. 5	1.5-2.0
Nitrogen permeability	[m^2]	10^{-16}	10^{-17}	$< 10^{-18}$
Chloride-ion intrusion 6h quick-migration test	[mm]	23	8	1
Carbonation depth, after 3 years, 20°C, 65% humidity	[mm]	7	4	1.5
Freeze-salt-resistance after 28 cycles	[g/m^2]	< 1500 air entrained	150 air entrained	20-50 water, heat cured
Water absorption factor		60	11	1

3.1.2. Ingredients and composition of UHPC

Cement

Theoretically, a Portland cement or other cements can be used to produce UHPC. It is well known that the amount of cement used in concrete does not only influence its strength and durability but rather the w/b, especially in case of HPC and UHPC [71]. In UHPC, less than 40 wt.-% cement has hydrated after two years [27]. Unhydrated clinker is still in the matrix, and thus acts as aggregates. The compatibility between cement and SP is important to select cement for UHPC production to maximize water reduction efficiency. Thus, cement with low C_3A content is used to reduce SP demand, to increase fluidity and thus the packing density of UHPC [6, 72, 73]. As for particle size, a high Blaine specific surface is not necessary because it increases water demand of cement. The fineness of cement should be between 0.30 and 0.45 m^2/g for designing UHPC [74].

The volume of paste (i.e. the volume of water and fine materials ≤ 0.125 mm) in UHPC is about 50-60 vol.-% which is about 15-20 vol.-% more than the void volume of non-compacted aggregates (particle size > 0.125 mm) [6, 23]. Depending on water content, the partial replacement of cement by fine materials and used aggregates, Portland cement content in UHPC ranges between about 600 and 1000 kg/m^3 concrete [5, 6, 8, 11, 23, 75, 76].

Pozzolanic admixture

The water demand to produce a workable concrete mixture is a key factor in producing UHPC. Many ongoing studies concentrate on the development of new blended binder

systems by using different pozzolanic admixtures. The aim is to decrease the amount of water and cement clinker content, and at the same time to improve the quality of concrete.

Silica fume: Silica fume (SF) is an industrial waste which is generated by the production of silicon or alloys containing silicon. SF is a highly reactive pozzolanic material, normally with more than 85 wt.-% amorphous silica. The particles are spherical and extremely fine (0.1-0.3µm). It has become the first choice of pozzolanic admixture in the concrete industry. SF products are offered as undensified or densified powder or as slurry. Because it is aimed to achieve a proper dispersion of SF in UHPC, undensified SF powder is used. The SF slurry should not be used because the quantity of water in the slurry may exceed the total quantity of water required for UHPC.

SF used in UHPC has three main functions: 1) to fill the voids between particles to achieve a high packing density; 2) to improve the rheological properties by lubrication effects resulting from small and perfect spherical particles; and 3) to produce secondary hydration products by consumption of portlandite (the pozzolanic reaction). Hence, SF strongly influences properties of concrete [72, 77-79]. In a curtain Portland cement concrete with water cement ratio of 0.5, about 18.3% SF, referred to the weight of cement, is enough to totally consume $Ca(OH)_2$ that is released from cement hydration [80]. However, the optimal content of SF in UHPC is normally about 20-30 wt.-% of cement to improve the filler effect [6, 8, 13, 14, 23].

Ground granulated blast-furnace slag: Ground granulated blast-furnace slag (GGBS) is a latent hydraulic material [81]. GGBS is a by-product of the steel industry and always cheaper than Portland cement. When GGBS partially replaces cement, it enhances some properties of concrete, such as workability, heat release and durability. Furthermore, the use of GGBS to partially replace cement makes concrete more environmentally.

The partial replacement of cement by GGBS increases the degree of Portland cement clinker hydration and reduces portlandite content by decreased cement content in UHPC. It also enhances the degree of SF hydration (shown by relative portlandite consumption) [27]. GGBS also decreases the very high autogenous shrinkage of UHPC [82].

In UHPC, partial replacement of cement by GGBS improves workability and reduces superplasticizer demand [20, 22, 25]. After 28 days of hydration, compressive strength of UHPC with 15 vol.-% [20] or about 20-35 wt.-% [23, 25] GGBS replacing cement is similar or even higher than that of the reference mixture. The higher GGBS content will reduce the 28 day compressive strength of UHPC (both normal curing and heat treatments) [20, 23, 25]. Increasing fineness of GGBS leads to a reduction in slump flow and a higher compressive strength of UHPC compared to coarse GGBS [22]. By heat treatment, UHPC containing 75 vol.-% [20] or 60 wt.-% [25] GGBS replacing cement can reach the strength over 200 MPa.

Fly ash: The effects of fly ash (FA) as partial replacement of Portland cement, SF or complete replacement of quartz powder on properties of UHPC were investigated [18, 20, 23, 26]. When FA partially replaces Portland cement, workability of the UHPC increases but its compressive strength decreases. When quartz powder is completely replaced by FA, workability of the UHPC dramatically decreases with coarse FA and is constant with finer ones. The mixture containing fine FA to partially replace SF needs higher SP dosage and

possesses slower compressive strength development in water at 20°C compared to the mixture containing SF. With heat treatment, the strength of UHPC containing up to 50 wt-% FA replacing cement (cement + SF + FA) can reach that of reference mixture (cement + SF). Compressive strength of UHPC without SF (cement + FA) under heat treatment can obtain over 200 MPa.

Metakaolin and rice husk ash: Metakaolin (MK) and rice husk ash (RHA) are highly reactive pozzolanic materials. The substitution of SF by MK can produce UHPC with similar mechanical performance to the SF-modified UHPC [28]. RHA can also be a good substitute for SF in UHPC because of the known effect of improved autogenous shrinkage and compressive strength [58, 60, 83]. However, due to the high specific surface area, porous structure, irregular particle shape and coarse grain size, UHPC containing these pozzolans needs higher water content or/and SP dosage to maintain the workability. Their mixing processes are also longer and more difficult than that of the mixture containing SF [28, 58, 60].

Aggregate

The paste volume in UHPC (water + fine materials ≤ 0.125 mm) is about 15-20 vol.-% more than the void volume of non-compacted aggregates [6, 23]. The paste's shrinkage is blocked locally around each aggregate particle and in the cement matrix. In order to enhance the homogeneity between cement matrix and aggregate, the maximum particle size of aggregate normally reduces to about 600 μm [6]. Quartz sand is usually used in UHPC because it possesses hard characteristics, low water surface absorption, good particle shape and excellent interface with cement matrix. Quartz sand is readily available and is a low cost material [6]. Some different aggregates such as natural sand, recycled glass cullet, bauxite and granite aggregates could be also used for UHPC [25, 84].

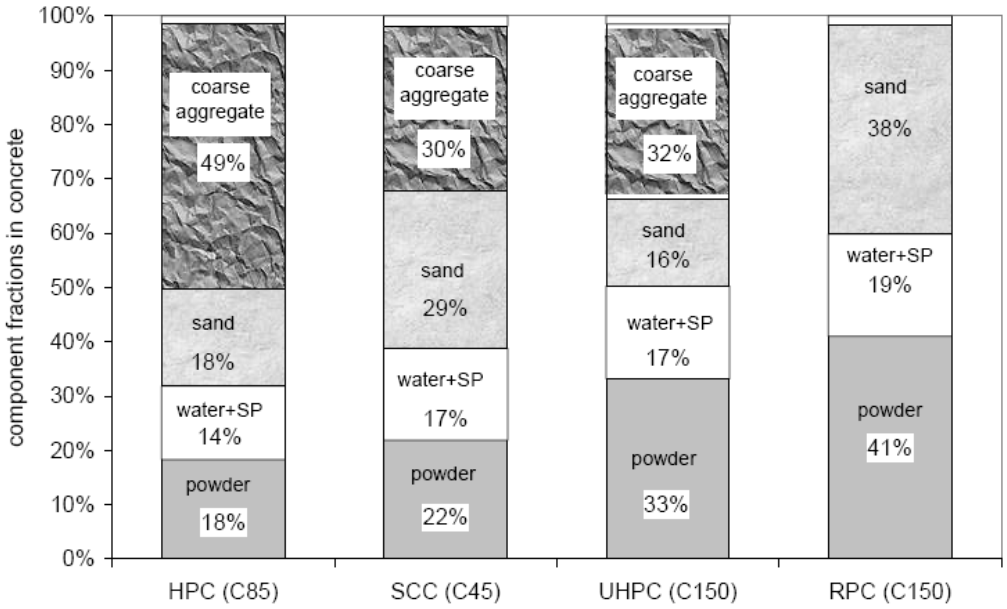

Figure 3.4. Component volume fractions in HPC, SCC and UHPC [75].

The fine particle size of aggregate induces increased surface area, and hence it needs more volume of cementitious paste to envelope the surface. Therefore, a higher paste volume in UHPC comparing with HPC and SCC is needed to meet a sufficient workability (Figure

3.4) [75]. Cement content in UHPC is often from 600 up to 1000 kg/m^3 which results in some disadvantages of the concrete, e.g. not sustainable, high heat of hydration and high autogenous shrinkage. In order to reduce the volume of cementitious paste, some researchers [11, 75, 85] tried to use coarse aggregate to produce UHPC. The utilization of coarse aggregate (8 mm or 16 mm) not only decreases cementitious paste volume (Figure 3.4), but also changes mixing process, shrinkage and mechanical properties of UHPC [75].

Filler

Packing density of granular mixture is an important parameter to reduce its water demand, i.e. the minimum volume of water that must be added to obtain sufficient flowability of the mixture. Besides cement and cementitious materials, filler powder is added into the granular mixture. The aim is to optimize particle size distribution of UHPC mixture to enhance the packing density of the granular mixture [6, 8, 11]. Because of low water demand, good particle shape, excellent interface with cement matrix and reactivity during high temperature treatment, crushed crystalline quartz powder is used as filler in UHPC [6]. Some different particle size quartz powders can be used depending on the requirement of packing density of mixture [8, 11].

Fiber

UHPC which has a very high compacted density with optimized particle size distribution and a very low w/b obtains a very high compressive strength. But its ductility is not improved from that of normal concrete. The inclusion of fibers improves not only tensile strength but also compressive strength [11]. Because of the use of fine aggregates, high homogeneity, good flowability and high ductility, UHPC normally uses small-size fibers with 3 to 13 mm in length and 0.15 to 0.2 mm in diameter. The fiber content is varied about 1 up to 8 vol.-% of mixture [6, 11, 23, 86]. Fibers can be made of steel or organic material. UHPC incorporating with carbon fibers is only used for the special durability requirement. Polymer fibers are utilized to mainly enhance the fire resistance of UHPC [11].

Water

Water used in concrete is required to hydrate cement and other cementitious materials as well as to produce workability of the mixture. Normally, there is an amount of free water in concrete which does not react with the cementitious materials. This free water is detrimental to properties of hardened concrete. The w/b used in UHPC varies from 0.15 to about 0.25 to produce both the sufficient workability and the lowest porosity of hardened concrete. This water content in UHPC is not enough to hydrate all the cement.

Superplasticizer

In order to reduce the excess water in UHPC, the low w/b usually does not provide sufficient workability to the mixture. SP is the obligatory ingredient to enhance workability of UHPC. SP dosage in UHPC is almost at the saturation dosage in order to obtain the highest workability of concrete at a very low w/b. Thanks to new generations of SP which provide very high water reduction efficiency. The compatibility between SP and mixture is governed by SP [87-89], cement [73, 89, 90] and mineral admixture [91-93].

3.1.3. Workability of mixture

Apart from some laboratory experiments in which UHPC has mini-cone slump flow below 250 mm. Normally, UHPC requires high workability, i.e. more than 250 mm with mini-cone slump flow test or 550 mm with normal slump cone flow test [11]. Hence, UHPC can almost obtain the workability of self-compacting concrete. The air content in UHPC should be as low as possible. The high slump flow is necessary in most of the cases because of the high viscosity and thus the difficult compaction of UHPC.

3.1.4. Treatment regime of UHPC

Normal and heat treatments can be conducted on UHPC. At normal treatment, UHPC still obtains advanced strength and durability characteristics compared to HPC. Heat treatment is required to reach the highest strength of concrete in a short time. It also substantially reduces delayed shrinkage and creep. Heat treatment must be carried out only after the concrete has set in order to avoid any risk of delayed ettringite formation (DEF) [12]. Temperature treatment (approximately 60-90°C) significantly accelerates the hydration of clinker and the pozzolanic reaction of pozzolan at an early age. But at extended periods, the hydration almost stops due to the lack of water in UHPC [94-96]. Gerlicher et al. [27] indicated that heat treatment enhances strongly portlandite reaction of SF, especially in high GGBS content mixture. However, the hydration degree of heat treated cement and GGBS is lower than that with normal treatment after 28 days and 2 years of hydration. With 90°C heat treatment, quartz powder does not react even after 2 years [27]. The high degree of the pozzolanic reaction modifies the chemical composition of the hydrated products at high temperature treatment (up to 400°C) by reducing further their CaO/SiO_2 and H_2O/CaO ratios. Heat treatment also changes the matrix heterogeneity, the interfacial transition zone between hydrated and non-hydrated products and even forms crystal products [78, 95, 97-99].

3.1.5. Mechanical properties of UHPC

3.1.5.1. Shrinkage

Total shrinkage of concrete includes autogenous shrinkage and drying shrinkage. Until setting, autogenous shrinkage is equivalent to chemical shrinkage. Afterwards, chemical shrinkage is restrained by the skeleton formed by hydration products. Concrete begins to appear air void networks and the relative humidity (RH) in the pores decreases during cement hydration. That is called self-desiccation. Drying shrinkage is caused by the loss of water to environment. Both self-desiccation and drying shrinkage reduce the RH in matrix which results in the increased capillary pressure to create shrinkage of concrete [81, 100, 101].

UHPC possesses a very high total shrinkage value. Because of very high Portland cement clinker and SF content, very low w/b, inherently fine pore structure and extremely dense matrix, autogenous shrinkage of UHPC is significantly higher than drying shrinkage [102]. The results of experiments on two samples of one UHPC mixture (w/b = 0.14) containing steel fibers in Figure 3.5 show that the internal RH strongly decreases and autogenous shrinkage significantly increases in UHPC at early ages [103]. Hence, the major part of autogenous

shrinkage of UHPC is related to self-desiccation [103-106]. Because UHPC has a very low w/b, this concrete almost completely self-desiccates between casting and heat treatment. Thus, UHPC exhibits non post-heated treatment shrinkage [11, 105].

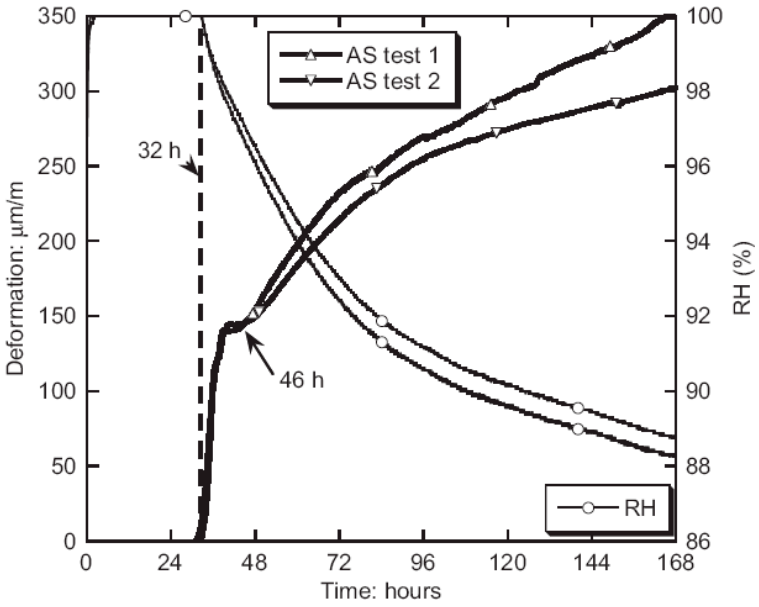

Figure 3.5. Curves zeroed at the beginning of autogenous shrinkage and RH of UHPC containing steel fibers [103].

Autogenous shrinkage is particularly problematic in UHPC. When cement is partially replaced by GGBS, autogenous shrinkage is reduced but it is still very high [82]. The addition of shrinkage reducing admixture or expansive admixture mitigates autogenous shrinkage of UHPC [107, 108]. Internal curing agent, i.e. super-absorbent polymer (SAP) or pre-saturated lightweight aggregate (LWA) is commonly used in UHPC to mitigate autogenous shrinkage. Internal curing agent particles release their absorbed water to delay the internal relative humidity decrease, and hence to mitigate autogenous shrinkage at an early age [20, 101, 102, 107, 109-111]. However, it has a negative effect on pore structure of cement matrix and thus on properties of concrete with a high content of SAP or entrained water, especially in UHPC. The mixture with SAP has higher volume of gel pores in comparison to the mixture without SAP. SAP also increases the pore volume due to the volume reduction of coarse SAP particles (up to 500 µm) causing a split or gap between matrix and polymer particles [20, 111].

3.1.5.2. Compressive strength

Compressive strength of UHPC is high because of optimized particle size distribution, low w/b, low porosity and high portlandite consumption by the pozzolanic reaction (especially under heat treatment). According to the state-of-the-art-report on Ultra-High-Performance Concrete (DAfStB UHPC) and the interim recommendations for ultra-high performance fiber-reinforced concretes (AFGC-SETRA) cited in the reports of Schmidt et al. [1] and Resplendino [12], compressive strength of UHPC exceeds 150 MPa and can obtain 250 MPa. Application of special aggregates and production procedures, compressive strength of UHPC can possibly attain up to 800 MPa [6, 69].

3.1.5.3. Tensile strength

Compressive strength of UHPC exceeds that of normal concrete. However, the tensile strength of UHPC without fibers is similar to that of normal concrete. To improve the ductility/toughness in such a way to approach the structural properties of steel, small-size steel fibers are normally added into UHPC. Hence, the tensile strength of ultra-high performance fiber reinforced concrete (UHPFRC) is strongly enhanced [11, 24, 112, 113].

3.1.6. Microchemical and microstructural features of UHPC

In UHPC, the high content of SF and heat treatment create a favorable environment for the pozzolanic reaction. Therefore, portlandite content in UHPC is low. Due to very low porosity of UHPC, the crystal growth of hydrates is restricted, leading to a very dense intergrowth of C-S-H phases [114]. High density of the C-S-H matrix and low CH content strongly reduce the thickness of the interfacial transition zone between aggregate particles or fibers and binder matrix [99, 115]. The heat treatment (up to 400°C) modifies the chemical composition of the hydrated products by reducing their CaO/SiO_2 and H_2O/CaO ratios due to the pozzolanic reaction [78, 98]. It even leads to formation of crystals, i.e. tobermorite, xonotline [95, 97-99].

The pore size distribution and total porosity strongly influence not only strength but also durability of concrete. Induced by very low water dosage and increased filler content, packing density of UHPC is high, i.e. the total and capillary porosity is significantly lower than those of normal or high performance concretes (by mercury intrusion porosimetry, Figure 3.6) [116]. By increasing the treatment temperature (up to 200°C), the pozzolanic reaction causes the pore refinement in pozzolan-blended matrix. Therefore, the gel and capillary porosity is reduced [117, 118]. Due to low capillary porosity of UHPC, the permeability and water absorption are very low. Thus, UHPC is regarded as highly durable [116, 118, 119].

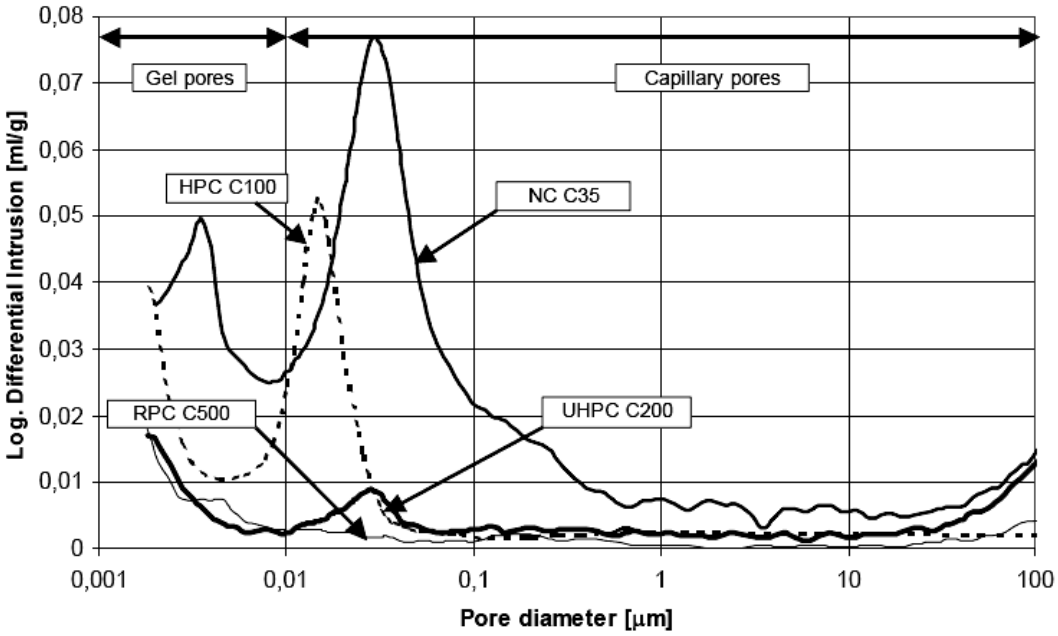

Figure 3.6. Pore size distribution in different concretes by mercury intrusion porosimetry [116].

3.1.7. Durability of UHPC

3.1.7.1. Resistance to aggressive solution

Franke et al. [119, 120] investigated the durability of different UHPCs with regard to leaching in sulfuric and lactic acid as well as in ammonia solution. The results showed that after 8000 hours and 12000 hours in aggressive solutions, the durability of UHPC was very high compared with that of a reference mortar with cement-sand ratio of 0.33 and water-cement

ratio of 0.45. The penetration of chloride into UHPC (ASTM C1202 and AASHTO T259-80) is extremely low [121, 122].

3.1.7.2. Carbonation

The kinetic of carbonation is significantly related to the density of matrix and the remaining portlandite content in the matrix. UHPC matrix possesses a very dense, disconnected pore structure and a low portlandite content. Hence, carbonation is harmless in UHPC **[10]**.

3.1.7.3. Freezing and thawing resistance

Despite containing a very low air void content, UHPC exhibits very high freeze/thaw deterioration resistance [121-124]. Bonneau et al. [121] found that 100% of the relative dynamic modulus (RDM) of UHPC retains after 300 cycles of the capillary suction, internal damage and freeze-thaw (CIF) test. Graybeal et al. [122] conducted the ASTM C666-03 (procedure A-CIF test) to measure the RDM and mass change of UHPC with different treatments during 690 cycles. The results showed that mass of all the samples increases during testing. The RDM of the heat treated samples slightly decreases, but it increases clearly in the normally treated sample.

The very high freeze/thaw resistance of UHPC is also documented in the presence of deicing salts. During the capillary suction, de-icing agent and freeze-thaw (CDF) test, the surface scaling and moisture uptake of UHPC is accelerated compared with the CIF test. However, there is no internal damage (i.e. the decrease in the RMD) in UHPC with both fine and coarse aggregate. Scaling values of the samples are below 600 g/m^2 after 112 freeze-thawing cycles [125]. Investigations by Thomas et al. [126] on UHPC under marine environment showed that the condition of samples was excellent with very low loss of compressive strength and minor chloride penetration after 5-15 years with approximately 100 freeze-thaw cycles per year.

3.1.7.4. Alkali silica reaction

The research of Graybeal [122] indicated that alkali silica reaction (ASR) would not be a problem to UHPC containing SF. The expansion of UHPC samples is far below the threshold of the ASR test according to ASTM C1260-01 ("Standard Test Method for Potential Alkali Reactivity of Aggregates. Mortar-Bar Method") [127].

Durability of UHPC under the influence of the accelerated Mid-European climate conditions was tested by cyclic climate storage (CCS) developed at the F.A. Finger for Building Materials Science (FIB), Bauhaus-University Weimar, Germany [114]. This test is especially suitable to evaluate the deterioration of concrete by ASR [128-130]. The results indicated that the expansion of all the investigated UHPC samples is very low compared with that of a normal concrete sample using a reactive aggregate. However, ASR has been locally observed in UHPC microstructure because of insufficient dispersion of SF. But it had no macroscopic effect on durability [114].

3.2. Rice husk ash and using rice husk ash in mortar and concrete

3.2.1. Introduction

When rice grains are produced from rice paddies, a huge amount of rice husks is left as by-product. Rice paddy consists of about 72 wt.-% rice, 5-8 wt.-% bran and 15.3-24.6 wt.-% husk. The bulk density of rice husks ranges from 83 to 160 kg/m³ leading to a large volume of waste material [36, 131-133]. Rice husk is composed of organic and inorganic matters. The chemical components of dry husk are 39-42 wt.-% carbon, 30-34 wt.-% oxygen, 5 wt.-% hydrogen, 0.6 wt.-% nitrogen and 16-23 wt.-% inorganic elements [132, 134]. The organic matters consist of cellulose, lignin, pentosans and a small amount of protein and vitamins. The inorganic components (of ash) are major silica and the following oxides: CaO, MgO, Fe_2O_3, Al_2O_3, Na_2O, K_2O and MnO_2 (Table 3.3 and Table 3.6) [36].

The structure of rice husk from the outer surface to the inner surface includes outer epidermis, layers of fibers, vascular bundles, parenchyma cells and inner epidermis. Most of silica is contained in the outer epidermal cells, particularly in the dome-shaped protrusions (Figure 3.7) [36, 135]. The nature of silica in rice husk is amorphous and namely opaline silica [136, 137]. Because of the tough, woody, abrasive nature of husk, its insolubility in water, low nutritive properties, resistance to weathering, low bulk density and high ash content, the use or disposal of rice husk is difficult. Apart from a small amount of rice husk used as a low-grade fuel by farming families or in small electric plants, most of rice husk is considered as waste, dumped or burned in the open. It pollutes soil, water and air.

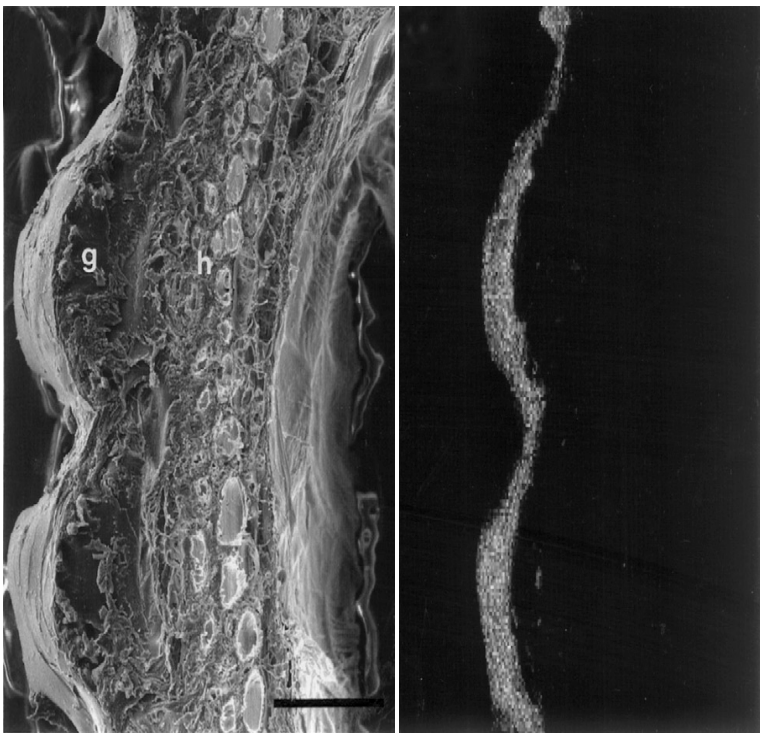

Figure 3.7. FE-SEM view (left, bar = 25 µm) and X-ray Si-mapping (right) on cross section of husk [130].

Table 3.3. Chemical composition of rice husk [36]

N⁰	Constituents [wt.-%]	Rice husks	
		Vietnam	Tanzania
1	Pentosans	1.9 – 2.1	17.5 – 18.0
2	Hemicellulose	20.5 – 20.9	20.5 – 21.9
3	Cellulose	41.0 – 41.9	25.8 – 26.5
4	Lignin	18.1 – 18.6	11.5 – 11.6
5	Mineral component	16.5 – 17.4	23.2 – 23.5

The organic matters in rice husk will be decomposed during combustion, and the residue obtained is ash. Silica content of the ash is about 90-98 wt.-% in completely burned samples [36, 138, 139]. The differences in geographical conditions, climate, types of paddy, soil chemistry and fertilizers used to cultivate rice plant will influence the husk content of paddy, the ash content of husk and the chemical constituents of ash. Generally, 20 wt.-% is considered to be an acceptable average value of husk content of paddy and ash content of husk. This means that one ton of rice paddy will produce about 200 kg of husk and approximately 40 kg of ash [63]. The world yield of rice paddies is about 700 million tons (Table 3.4) [62]. Most of these are produced in developing countries. It means that about 140 million tons of rice husk are annually disposed and about 28 million tons of reactive rice husk ash (RHA) can be potentially burned from rice husk. Like many other countries, rice is cultivated in all parts of Vietnam. The rice paddy production of Vietnam is about 40 million tons. Therefore, 1.6 million tons of RHA as a renewable source of reactive siliceous material can be potentially obtained (Table 3.4).

Table 3.4. World rice paddy, potential husk and ash production [million tons] [62]

N^0	Country	Rice paddy production in years		Potential husk	Potential ash
		2009	2010		
1	China	196.7	197.2	39.4	7.9
2	India	133.7	120.6	24.1	4.8
3	Indonesia	64.4	66.4	13.3	2.7
4	Bangladesh	47.7	49.4	9.9	2.0
5	Vietnam	40.0	40.0	8.0	1.6
6	Thailand	32.1	31.6	6.3	1.3
7	Rest of the world	170.2	166.8	33.4	6.6
8	World total	684.8	672.0	134.4	26.9

Table 3.5. Ash and silica content of ash of various plants [56]

N^0	Plant	Part of plant	Ash [%]	Silica [%]
1	Rice husk	Grain sheath	22.1	93.0
2	Wheat	Leaf sheath	10.5	90.5
3	Sorghum	Leaf sheath epidermis	12.5	88.7
4	Rice straw	Stem	14.6	82.0
5	Breadfruit tree	Stem	8.6	81.8
6	Bagasse	-	14.7	73.0
7	Corn	Leaf blade	12.1	64.3
8	Bamboo	Nodes (inner portion)	1.5	57.4
9	Sunflower	Leaf and stem	11.5	25.3
10	Lantana	Leaf and stem	11.2	23.3

Among the agricultural wastes, rice husk has very high ash content. The ash has very high silica content (Table 3.5) [56]. Rice husk ash is highly porous, lightweight. These induce a material with high specific surface area and high melting point. Rice husk ash is useful for many industrial applications [140-146]. Two main applications of rice husk ash are insulator in the steel industry and pozzolan in the cement and concrete industry. Rice husk ash used in the

steel industry is usually crystalline which is easily burned in many boilers or furnaces. The cement and concrete industry requires amorphous and low carbon ash which is burned under a suitable combustion to ensure a consistent quality of ash.

3.2.2. Producing reactive rice husk ash (RHA)

The alkaline extraction method can produce high purity amorphous silica from rice husk ash. It involves a large number of steps and therefore takes a long time to process (1-2 days) with the use of various types of chemicals. This results in a very expensive product [147, 148]. Other methods to obtain RHA are based on combustion. They range from open-heap uncontrolled burning conditions to specially designed incinerators with controlled conditions [35, 36, 149, 150]. Sugita [150] invented a batch method and a continuous method of producing RHA. The burning process is controlled in the continuous method but uncontrolled in the batch method. Bui [36] also used a drum type incinerator with uncontrolled combustion, but the obtained RHA has a high pozzolanic reactivity. Rice husk is also pre-treated by acid to leach out cellulose, hemicelluloses, lignin and alkalis before burning in furnaces to improve the quality of RHA [151-153].

3.2.3. Chemical and mineral compositions of RHA

Chemical composition of RHA is affected not only by geographical conditions, types of paddy, soil chemistry, climate and fertilizers used to cultivate rice plant, but also by pre-treatment and combustion process of rice husk. Among these, the pre-treatment and combustion process pose a significant influence on the quality of RHA. RHA mainly contains silica and minor amounts of other metallic oxides. The silica content of RHA is in the range of 85 to 95 wt.-%. The major impurities in RHA are carbon and alkali oxides (Table 3.6) [36, 131]. The significant amount of alkalis in rice husk melts at low temperature and carbon entrapped in this melt cannot be oxidized. Hence, acid leaching is used to remove most of alkalis in rice husk before burning. The received RHA has a high silica content, high specific surface area and very low content of carbon and of other metallic impurities [34, 151-154].

Table 3.6. Chemical composition of RHA from various locations [131]

Constituents	Weight [%]						
	Malaysia	Brazil	Vietnam	India	Iraq	USA	Canada
SiO_2	93.10	92.90	86.90	90.70	86.80	94.50	87.20
Al_2O_3	0.21	0.1	0.84	0.40	0.40	Trace	0.15
Fe_2O_3	0.21	0.43	0.73	0.40	0.19	Trace	0.16
CaO	0.41	1.03	1.40	0.40	1.40	0.25	0.55
MgO	1.59	0.35	0.57	0.5	0.37	0.23	0.35
K_2O	2.31	0.72	2.46	2.20	3.84	1.10	3.68
Na_2O	*	0.02	0.11	0.10	1.15	0.78	1.12
SO_3	*	0.10	*	0.10	1.54	1.13	0.24
L.O.I	2.36	*	5.14	4.80	3.30	*	8.55

*- Not reported; L.O.I- Loss on ignition

The reactivity of RHA as a pozzolanic material mainly depends on the amorphous/crystalline ratio and porous structure of RHA [155]. Silica inherently exists in amorphous form in rice husk [136, 156]. During combustion of rice husk, the structural transformation of silica from amorphous to different crystalline phases can occur. Generally, burning at 500-700°C with suitable burning time is favored to produce amorphous silica from rice husk [29-32, 152, 157, 158].

3.2.4. Microstructure and specific surface area of RHA

Rice husk is made up of a silica skeleton and a cellulose-lignin matrix. Isothermal heating at a minimum of 402°C is required for the destruction of organic matters from rice husk to produce silica. On combustion, the cellulose-lignin matrix burns away, leaving a porous silica skeleton with a high surface area (Figure 3.8) [60, 135, 159].

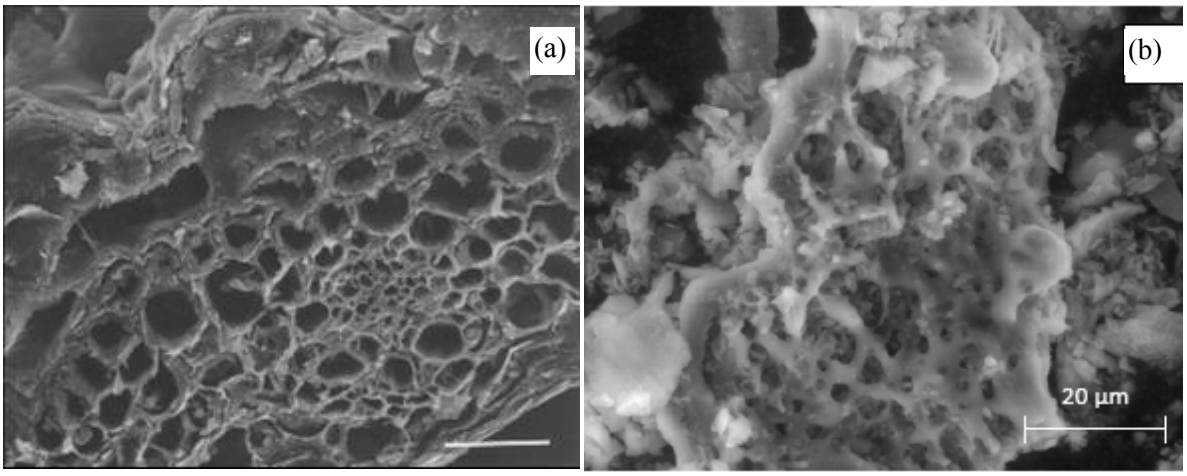

Figure 3.8. a) Internal structure through view of cross section of rice husk, bar = 20µm [135]; b) porous surface structure of RHA particle [60].

Table 3.7. Pore distribution and pore volume of RHA obtained from different conditions [160]

Tempera -ture, °C	Conditions	Pore distribution [%]			BET-SSA [cm^2/g]	Pore volume [cm^3/g]
		Macropores	Mesopores	Micropores		
		> 50 nm	2-50 nm	< 2 nm		
500	untreated	25.00	55.51	19.49	142	0.31
550		20.41	53.77	25.82	164	0.32
800		59.71	40.29	0.00	9.24	0.09
600	1 N HCl	12.60	46.84	40.56	270	0.37
700		15.81	48.40	35.79	311	0.43
700	3 N HCl	26.79	38.99	34.22	251	0.39
800	1 N HCl	23.55	46.31	30.14	257	0.34
900		27.22	44.30	28.47	145	0.29

The very high specific surface area (SSA) of RHA is significantly governed by the porous structure of RHA particles. The porous surface structure of RHA evaluated by the Brunauer-Emmett-Teller (BET) method to determine the BET-SSA and the Barrett-Joyner-Hanlenda (BJH) method to calculate the pore size distribution, pore volume and mean section diameter shows that RHA is a mesoporous material [141, 160, 161]. When rice husk is pre-treated by acid leaching, the micropore volume increases, meanwhile the macropore and mesopore volumes

reduce. Acid leaching also increases total pore volume and BET-SSA of RHA (Table 3.7) [153, 160, 162]. The heating rate and temperature of burning also strongly affect the total pore volume and BET-SSA of RHA (Table 3.7 to Table 3.9) [32, 160, 163].

Table 3.8. BET-SSA and pore volume of RHA burned at 700°C in 2 hours with different heating rates [32]

	Rate of heating [°C /min]	BET-SSA [m^2/g]	Pore volume [cm^3/g]
1	1	11.53	0.0071
2	2	10.44	0.0062
3	3	7.61	0.0039
4	5	9.30	0.0054
5	7	18.99	0.0084
6	10	50.20	0.0245

Table 3.9. BET-SSA of differently ground RHA and SF and variation in electrical conductivity of CH-pozzolan suspensions from 0 to 2 min at 40°C [163]

Sample	Grinding period [min]	BET-SSA [m^2/g]	Variation in electrical conductivity [mS/cm]
RHA-600°C	10	19.74	1.35
	40	21.61	1.63
	80	14.92	1.16
RHA-700°C	10	10.69	0.54
	40	11.25	0.70
	80	10.52	0.63
RHA-800°C	10	8.92	0.45
	40	9.49	0.56
	80	8.15	0.56
Silica fume A	-	13.65	1.01
Silica fume B	-	21.22	1.83
Silica fume C	-	24.06	1.65
Silica fume D	-	19.37	1.62
Silica fume E	-	23.00	1.46

During grinding, different changing trends in the SSA of RHA are observed at different degree of grinding [36, 53, 60, 163]. The collapse of the porous structure of RHA particles generally reduces the BET-SSA of the sample. The increase in the SSA of RHA sample at intermediate grinding periods is also observed (Table 3.9) [36, 60, 163]. In contrast, Cordeiro et al. [53] showed that the SSA of RHA decreases firstly and then increases. The decrease and increase of the SSA of RHA during grinding are not clearly interpreted and the porous structure of finely ground RHA particle has not yet been shown by images.

3.2.5. Pozzolanic reactivity of RHA

RHA produced by a proper combustion possesses a large amount of amorphous silica and a high BET-SSA. During the hardening process, the pozzolanic reaction consumes CH and increases the amount of C-S-H in cement matrix containing RHA [158, 164]. Thus, RHA enhances compressive strength and improves durability of cement mortar or

concrete [33-39, 41-56, 165]. Current methodologies used for evaluation and classification of pozzolanic material are based on determination of chemical or physical effects of pozzolan. Some specific methods on how to investigate reactivity of pozzolan with high content of amorphous silica and high BET-SSA such as SF and RHA are:

Mehta [166] proposed a method to estimate the "silica activity index". The "silica activity index" is determined by the percentage of pozzolan dissolved by boiling in 0.5M sodium hydroxide during 3 min. RHA samples obtained a "silica activity index" from 50 to 85 in his report. Payá, J., et al. [167] used a rapid analytical method to determine the dissolving amorphous silica fraction of pozzolan in glycerol solution.

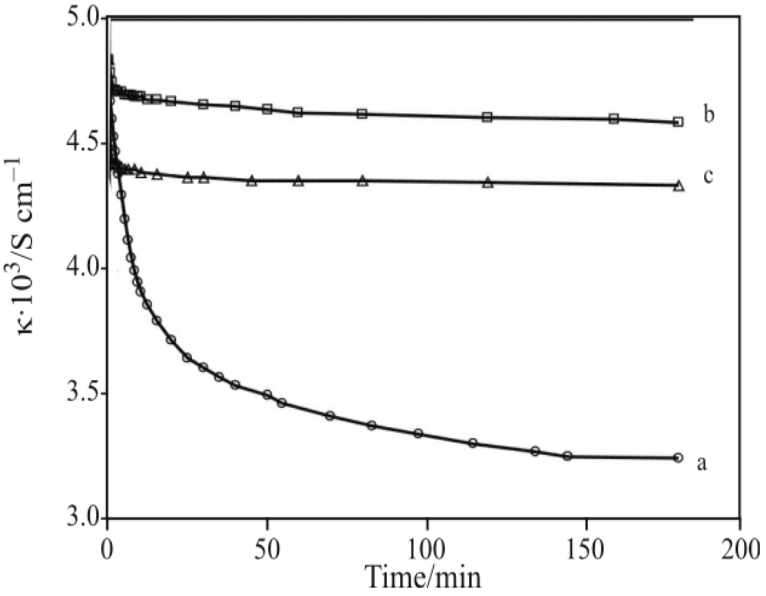

Figure 3.9. Kinetic curves of adsorption of H_2SeO_3 out of aqueous solution at 25°C on: a) γ-Al_2O_3; b) black RHA; c) white RHA [161].

Table 3.10. Characteristics of the porous structure of the samples in Figure 3.9 [161]

Sample	BET-SSA [m^2/g]	Pore volume [ml/g]	Pore radius [nm]
Black RHA	96	0.185	3.6
White RHA	126	0.208	8.9
γ-Al_2O_3	162	0.534	6.5

The reaction between $Ca(OH)_2$ and RHA has been the subject of previous investigations [158, 163, 164, 168, 169]. Amorphous silica in RHA reacts with Ca^{2+} and OH^- ions to form $Ca_{1.5}Si_{1.0}O_{3.5}$ xH_2O. These C-S-H phases are observed after 12 days of hydration of RHA in saturated CH solution at 40°C [164]. The method of Luxan et al. [170] is commonly used as a rapid method to evaluate the pozzolanic reactivity of RHA and SF. In this method, the pozzolanic reactivity is evaluated by measuring the variation in electrical conductivity of saturated $Ca(OH)_2$ solution at 40°C before and after 2 minutes of pozzolan addition. It is reported that pre-treatment, burning and grinding of RHA induce large differences in the electrical conductivity of CH-RHA suspensions [29, 34, 163]. It is known that the electrical conductivity of CH-pozzolan suspension is affected not only by amorphous SiO_2 content but also by BET-SSA as well as the soluble oxide content of pozzolan [155, 163, 171, 172]. RHA with high BET-SSA and low amorphous SiO_2 content induces a similar electrical conductivity as RHA with low BET-SSA and high amorphous SiO_2 content [155]. Cizer et al. [172] and Sugita et al. [163] assumed that a change in the SSA by grinding leads to a changed variation in the electrical conductivity of CH-RHA suspension (Table 3.9). The variation in electrical conductivity of saturated CH solution with certain RHA in Feng's study [34] is even about 3

times higher than that of SF in Table 3.9. It means that according to the classification of Luxan's method [170], the pozzolanic reactivity of RHA is very high, i.e. significantly higher than that of SF.

On the other hand, adsorption of metal ions of porous RHA from solution rises sharply during the initial 30 minutes. The ion adsorption capacity of RHA depends on its BET-SSA, pore volume and porous structure (Table 3.10 and Figure 3.9) [141, 161]. Hence, it is questionable whether the variation in electrical conductivity after 2 minutes of hydration proposed by Luxan et al. [170] represents well the full pozzolanic reactivity of the pozzolan. It may not be appropriate for comparing the pozzolanic reactivity of pozzolans such as RHA and SF with large differences in the adsorption ability.

The pozzolanic reactivity of RHA is also evaluated through determining the content of $Ca(OH)_2$ in hardened cement paste by thermal or X-ray diffraction analysis. After 3 days of hydration, the amount of CH in a cement paste containing 30 wt.-% RHA at w/b of 0.55 begins to decrease. The CH content reaches nearly zero at the age of 91 days, whereas it continuously increases in the control paste [164]. CH content in cement paste containing RHA is normally higher than in cement paste containing SF [33, 48, 57]. This indicates that the pozzolanic reactivity of SF is higher than that of RHA in cement matrix.

The effect of RHA on compressive strength of mortar and concrete has to be discussed under the following aspects: due to the increased BET-SSA of RHA, the w/b has to be increased in the presence of RHA to obtain a given workability. Thus, compressive strength may decrease in the presence of RHA (increased porosity due to higher w/b) [173-175]. If workability is maintained by SP-addition, it is possible to increase compressive strength in the presence of RHA [39, 175]. Different RHA and water content in the mixture also induce different effects of RHA on compressive strength [174, 175]. To evaluate the effect of a high specific surface pozzolanic material on compressive strength of Portland cement, ASTM C1240-05 [176] ("Standard Specification for Silica Fume Used in Cementitious Mixture") estimates the accelerated pozzolanic strength reactivity index. Thereby, for application of SF, the SP dosage is varied to maintain the workability of the test mortar containing SF at the constant w/b and heat treatment [176]. This standard is also suitable for evaluating the pozzolanic reactivity of RHA. But until now, to the knowledge of the author, there is no study on the pozzolanic reactivity of RHA using this published standard.

It is important to note that the ground RHA particle size is about 25-50 times larger than that of SF. The high BET-SSA of RHA results from the high porosity [63, 160]. Thus, the pozzolanic reaction process of porous RHA may be different from that of SF in CH solution or in cementitious matrix, especially in very dense matrix of UHPC. Hence, the effect of grinding and porous structure of RHA on its pozzolanic reactivity in CH solution and cementitious systems is one of the main objectives of the present PhD study. Pozzolanic reactivity of RHA is evaluated by different methods and compared with SF and pozzolan-free references.

3.2.6. The influences of RHA on properties of cementitious system

3.2.6.1. Setting time, water demand and workability

RHA increases the standard consistency (water demand) of cement paste [47, 177, 178]. The setting times of cement paste increase with increasing RHA content [177]. Meanwhile, Ganesan et al. [47] reported that the increase in RHA content initially increases and then decreases the initial setting time. The final setting time is reduced. But Rostovsky et al. [178] concluded that setting times of cement paste decreases with increased RHA content. These contradictory results might be due to the differences in the particle size, SSA and pozzolanic reactivity of different RHA.

For constant RHA content, increasing the SSA of RHA results in an increased SP or water demand of concrete [49]. The more RHA partially replaces cement, the more the water demand or the higher the dosage of SP is needed to maintain a given workability [33, 35, 36, 163, 165, 179]. All of previously investigated RHA mortars and concretes possess a w/b higher than 0.3. Similar conclusions about the effect of particle size and content of RHA on workability of UHPC mixture at w/b of 0.18 are also shown by Nguyen et al. [58]. The effect of RHA addition on workability or SP demand of mortars and concretes with w/b from 0.18 to 0.3 has not yet been published.

3.2.6.2. Hydration of Portland cement

Feng et al. [34] found that during 12 h hydration of plain and cement pastes containing 30 wt.-% of good quality RHA samples or of a quartz powder, percentage of heat release of the pastes containing RHA is increased compared with that of the plain or cement paste containing quartz powder. The RHA shortens the induction period of hydration and increases the second maximum of the exothermic curve. Furthermore, the CH content in the cement paste containing 10 wt.-% RHA after 3 days of hydration is slightly higher than that in the cement paste containing 10 wt.-% quartz powder. It means that the hydration of clinker cement in the presence of the highly reactive rice husk ash is accelerated, and hence, it produces more CH content in the RHA-blended cement paste at the early age. After 7 days of hydration, the CH content in the cement paste containing RHA is lower than that of the paste containing quartz powder [34]. The increased degree of clinker cement hydration in the RHA-blended matrix after a long hydration period compared with that in the reference or SF-blended matrices was observed by analysis of backscattered electron images [48, 57].

3.2.6.3. Shrinkage

Studies on the effect of RHA on shrinkage of concrete are still not detailed. De Sensale et al. [44] investigated the effect of partial replacement of Portland cement by amorphous and partially crystalline RHA on autogenous shrinkage of cement paste at w/b of 0.30. The results showed that the RHA clearly decreases autogenous shrinkage of the sample. The higher the RHA content, the more the effectiveness in mitigating autogenous shrinkage. The same conclusion was given with autogenous shrinkage of SCC [56] or UHPC [60, 83] containing RHA. However, Habeeb et al. [49] stated that fine RHA results in an increased autogenous shrinkage

of sample, even higher than that of a control sample. Thus, the effect of RHA on self-desiccation, autogenous and total shrinkage of UHPC is investigated in great detail in the present study.

3.2.6.4. Compressive strength

Many studies assumed that up to 30 wt.-% cement replaced by RHA can increase compressive strength of cement mortar or concrete. Compressive strength of concrete continuously develops with hydration time for all the dosages of RHA [34-39, 45-47, 180-183]. Investigations of Bui et al. [39] indicated that for w/b of 0.30 and 0.34, compressive strength of the concretes with 10, 15 and 20 wt.-% RHA replacing cement is always higher than that of the reference mixture (from 3 to 91 d of hydration). The increase in RHA content (in range of 10, 15 and 20 wt.-%) results in the increased compressive strength of concrete. The effect of RHA on compressive strength also depends on particle size distribution (i.e. packing density) and w/b of mixture [39]. Compressive strength of mixture containing a good quality RHA is even higher than that of mixture containing SF at the ages of 28 and 56 days [35]. In some cases, compressive strength of RHA-blended sample is enhanced not only at older ages but even on the 1st day of hydration [35, 39, 157]. This may be explained by the acceleration of cement hydration by RHA at early age [34]. In UHPC, RHA can also be a good pozzolanic admixture to produce UHPC without significant change in compressive strength compared with that of mixture containing SF [57-60].

3.2.6.5. Microstructure and durability

Due to its high pozzolanic reactivity, increasing RHA content in a cement matrix results in the decrease of portlandite content and leads to the refinement of the pore structure [60, 165, 177]. In coarse aggregate concretes, RHA reduces the thickness of the interfacial transition zone (ITZ) between aggregate and cement matrix [48]. Hence, the water absorption and aggressive solution resistance (chloride penetration, sulfate attack) of RHA-modified concretes are improved [33, 35, 38, 41, 51, 179, 184, 185].

While RHA has a positive influence on the microstructure, chloride or sulfate resistance and mechanical properties of concrete, there are some concerns about the alkali silica reaction (ASR) in RHA-blended mixtures due to the fairly high alkali content which inherently exists with the high amorphous silica content in RHA. Hasparyk et al. [186] tested the expansive behavior of mortar bars as specified in ASTM C1260 [127] and concluded that it is possible to significantly reduce the mortar-bar expansion for both reactive quartzite and basalt aggregates by using up to 15 wt.-% either SF or RHA replacing cement. After 14 days in NaOH 1M at 80°C, the specimens containing 12 or 15 wt.-% RHA had expansion levels lower than the prescribed limit. Mehta et al. [185] also had the same conclusion for the improvement of ASR resistance of RHA for mixtures using reactive aggregate. On the other hand, Ramezanianpor et al. [187] reported that an optimum amount of RHA seems to be between 7 and 10 wt.-% to control ASR of reactive aggregates. Increasing the amount of RHA can cause an increase in the expansion. Hence, the ASR risk of UHPC containing high volume content of RHA is carefully considered in the present PhD study.

3.2.7. The combination of RHA with other mineral admixture in concrete

Due to the simple technology of production, low cost, enhancement of strength, durability and sustainability of concrete, utilization of blended binder with high volume of FA or GGBS is expected to increase [188, 189]. However, the compressive strength development of these concretes is slow at early ages. The combination of a less reactive pozzolan, such as FA, GGBS with a more reactive one, such as RHA, SF results in synergic physical and chemical effects [43, 51, 64, 65, 190]. Incorporation of RHA with other fine pozzolan such as SF, FA and GGBS improves rheological performance of concrete (moderate plastic viscosity and low yield stress) [42, 61]. When RHA and FA are combined, the early and long term compressive strength are improved [61]. Using blended binder can strongly improve the durability of concrete as well [42, 190]. These effects are higher when pozzolan content is optimized and the w/b is low [46].

As a result, the combination of RHA and GGBS for production of UHPC may possess a valuable perspective. This idea is followed by investigations in the present PhD study. Thus, the synergic effects of RHA, GGBS and SP on workability and compressive strength of UHPC are discussed. The influences of RHA and GGBS on compressive strength, shrinkage and durability of UHPC under different treatment conditions are also assessed.

3.2.8. RHA in producing UHPC

Nguyen's investigations [57-60, 83] indicated that RHA can be used to totally replace SF in UHPC production. At w/b of 0.18 and normal treatment, compressive strength of UHPC containing 20 wt.-% of RHA (5.6 μm mean particle size) partial replacement cement is comparable with that of UHPC containing SF in hydration periods between 3 and 91 days. The parking density of UHPC containing SF exceeds that of UHPC containing RHA. SP dosage in UHPC containing RHA is significantly higher than that in UHPC containing SF to maintain a given mini-cone flow value of 210-230 mm. Decreasing mean particle size of RHA or the combination of RHA and SF improves the packing density, compressive strength of RHA-blended UHPC. RHA-blended UHPC possesses a significantly lower autogenous shrinkage compared to reference UHPC (without pozzolan) or SF-blended UHPC. For hydration and microstructure of UHPC by SEM, the addition of RHA increases the degree of cement hydration in UHPC matrix at later ages [57, 60]. During 28 days of hydration, the degree of cement hydration in SF-blended UHPC exceeds that in RHA-blended UHPC, but it is comparable after 91 days of hydration. SF induces increased portlandite consumption (by DTA-TG) and stronger pore refinement (by MIP) in UHPC than RHA.

The packing density of granular mixture is a main factor in the design of blended Portland cement binders for HPC [39, 191] and UHPC [14]. The increase in compressive strength of crystalline RHA-blended concrete is observed due to the filler effect [192]. Reducing the mean particle size of RHA induces the increased packing density and hence compressive strength [39, 60]. However, Mehta [63] has argued that grinding RHA to a high fineness should be avoided because its high pozzolanic reactivity derives mainly from the high internal surface

area of the particles. In addition, the porous structure of RHA particles may absorb an amount of free water in RHA-blended Portland cement mixture to improve compressive strength. The absorbed water in the porous structure may allow Ca^{2+} ions to diffuse into internal parts of RHA particles to enhance the pozzolanic reactivity. The absorbing RHA may play as a kind of internal curing agent which strongly decreases autogenous shrinkage of UHPC [60]. And the degree of cement hydration is enhanced in RHA-blended Portland cement sample compared with that in reference or SF-blended Portland cement sample after long periods of curing by analysis of backscattered electron images [48, 57].

Therefore, the synergic effects of physical and chemical factors of porous RHA particles on properties of RHA-blended Portland cement matrix should be considered. The effect of porous structure of RHA particles on water absorption capacity and pozzolanic reactivity of RHA and hence on characteristics of very low water content cementitious system needs more detailed investigations, particularly in comparison with those of SF. Thus, the characteristics of RHA ground for different periods of time and SF is considered by different tests in the following study. The internal curing effect of porous RHA on autogenous shrinkage needs to be proven by a study on the effect of the RHA addition on the change in the internal relative humidity in UHPC during hydration. For a safe and economical application of RHA, in the present thesis, it is necessary to investigate the effects of RHA alone and in the combination with GGBS on workability, long term compressive strength and durability of UHPC.

3.3. Concluding remarks

UHPC is a new class of concrete which possesses many advantages in mechanical and durability properties. However, the high amount of cement and silica fume content causes the high autogenous shrinkage, high cost of material and low sustainability of UHPC. Using renewable, cheap and less energy intensive pozzolanic admixtures to partially replace cement and SF in producing UHPC is the appropriate trend for research and application.

Rice husk is one of the major wastes in agricultural countries all over the world. The rice husk disposal is causing soil, water and air pollutions. Properly burned RHA is a highly reactive pozzolanic admixture in concrete production. Utilization of RHA in the concrete industry will improve quality of concrete, decrease the cost of concrete by reducing the dosage of SF and cement. It diminishes carbon oxide emission from cement production. It also increases the income of farmers in developing countries. Hence, using RHA in concrete production is sustainable.

Variation of pozzolanic reactivity of RHA and SF is a result of differences in their porous structure, particle size, chemical and mineral compositions. Thus, pozzolanic reactivity of RHA ground for different periods of time and SF should be compared by different methodologies and discussed under the synergic effects of physical and chemical factors. The aim is to explain in detail the behavior of RHA in concrete, especially in a very dense matrix of UHPC.

For UHPC with a very low w/b value and a high workability, the role of SP is important. Cementitious materials and characteristics of SP strongly affect their compatibility which is necessary for a good workability, strength development and final compressive strength.

GGBS, the latent hydraulic cementitious material improves workability or decreases SP demand of UHPC. It also enhances the long term compressive strength and durability of concrete. Meanwhile, RHA possesses a very high pozzolanic reactivity but it needs a high water or SP dosage. Combination of the less reactive, less water demanding GGBS with the more reactive, more water demanding RHA may improve properties of both fresh and hardened concrete. Discussion of the advantages and disadvantages of combining GGBS and RHA for UHPC production is one main concern of the present thesis.

Evaluation of the pozzolanic reactivity of porous RHA needs more detailed investigations. The influence of different types and dosages of SP on workability and compressive strength of RHA-blended UHPC is important. Studies on the effects of RHA and the combination of RHA and GGBS on properties of UHPC such as workability, compressive strength, shrinkage and durability under various treatment conditions are crucial to apply RHA and GGBS as pozzolanic admixtures in UHPC successfully. These are the main topics discussed in the following thesis. The global aim is to propose an environmentally friendly and economical UHPC. As a result, sustainable and durable UHPC can be proposed for further production. Particularly, it helps promote the production and application of UHPC in Vietnam where SF is totally imported and RHA is available.

On the aims and approaches of the thesis, used materials, UHPC production and methods of experiments are present in Chapter 4. Chapter 5 includes all results and discussion. Characteristics and pozzolanic reactivity of RHA ground for different periods of time compared to those of SF are discussed in Section 5.1. Section 5.2 provides the effects of different superplasticizers, pozzolanic admixtures, water to fine material in volume ratios (W/F_v), superplasticizer dosages and vibration period on slump flow, air content and compressive strength of UHPC. With these preliminary tests, the type of superplasticizer, the suitable water to fine material in volume ratio, the composition of UHPC and the suitable fineness of RHA are chosen to produce economical UHPC without SF by using normal mixers. These preliminary results also help to choose the variable constraints for optimization of UHPC mixture containing RHA, GGBS and SP by using the combined mixture-process model (Design-Expert 8 software). With 3D response surface and contour plots, the synergic effects of RHA, GGBS and SP on flowability and compressive strength of UHPC are also clearly interpreted in Section 5.2. In Section 5.3 and 5.4, the behaviors of the designed UHPC containing RHA or SF, GGBS-RHA or GGBS-SF under different treatment conditions are discussed by results of compressive strength, shrinkages, internal relative humidity, microstructure and durability of the concretes. Finally, general and specific conclusions in Chapter 6 are drawn from the results of this PhD study.

4. Experimental Design

4.1. Materials

A large quantity of reactive rice husk ash (RHA) was produced by burning local rice husk in Vietnam in a simple prototype incinerator under uncontrolled combustion conditions. The incinerator is modified and developed from the batch method of producing RHA which was invented by Shuichi Sugita [150]. Details of the incinerator are shown in Figure 4.1. The volume of the incinerator is about 1.2-1.5 m^3. It can produce about 20-25 kg of RHA in a single batch. Fire is set from the bottom of the chimney with a small amount of waste paper or wood. The husks burn themselves when they catch the fire.

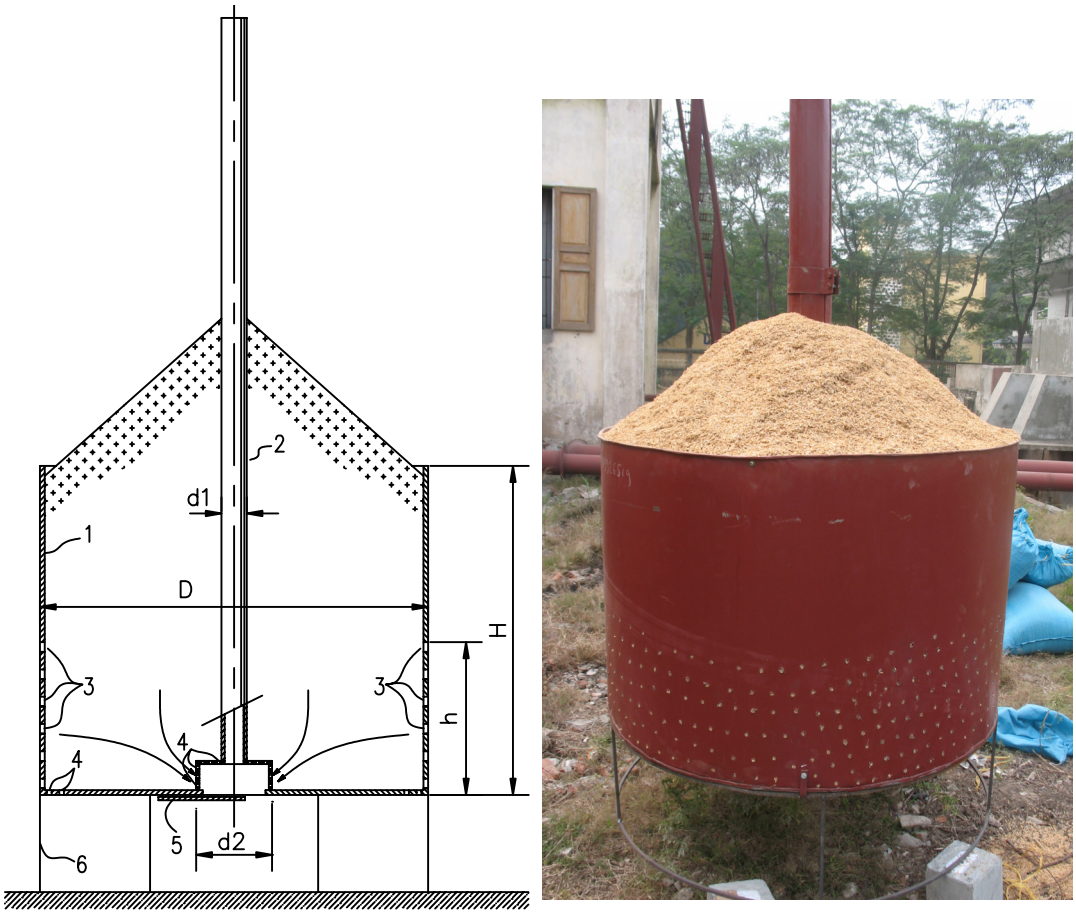

Figure 4.1. Modified incinerator developed from the Sugita's batch method: 1) drum; 2) chimney; 3,4) holes; 5) adjusting door; 6) steel frame.

The obtained RHA has high silica and low carbon contents (Table 4.1). By the quantitative X-ray diffraction (QXRD) analysis (Figure 4.2), it shows that this RHA mainly consists of a large quantity of amorphous material with 97.4 wt.-% amorphous, 2 wt.-% quartz, and 0.6 wt.-% calcite. Hence, the obtained RHA is an amorphous siliceous material. The RHA was ground in a lab ball mill with diameter of 270 mm, length of 400 mm and rotation speed of 67 rpm for 15, 30, 45… 540 minutes. In each batch, the internal volume was partially filled with 21 kg steel balls (balls with 7 kg of 12.5 mm, 8.4 kg of 22 mm and 5.6 kg of 28 mm

diameter) and 1 kg RHA. Sample designation indicates grinding time in minute, i.e. RHA-15, RHA-30 and so on.

Table 4.1. Chemical composition of cementitious materials

	SiO_2	Fe_2O_3	Al_2O_3	CaO	Na_2O	Na_2O_{eq}	MgO	SO_3	L.O.I
CEM-De [wt.-%]	21.6	5.1	3.7	64.3	0.17	0.41	0.6	2.4	0.9
CEM-Vn [wt.-%]	21.4	3.2	6.2	63.4	0.2	0.72	1.2	1.7	1.0
SF [wt.-%]	96.0	0.0	0.1	0.6	0.20	0.65	0.2	0.4	1.2
RHA [wt.-%]	87.4	0.3	0.4	0.9	0.04	2.27	0.6	0.4	4.6
GGBS [wt.-%]	37.8	0.5	8.0	39.7	0.38	0.87	10.8	0.1	0.2

Na_2O_{eq}- Equivalent sodium oxide = $Na_2O + 0.658K_2O$
L.O.I- Loss on ignition

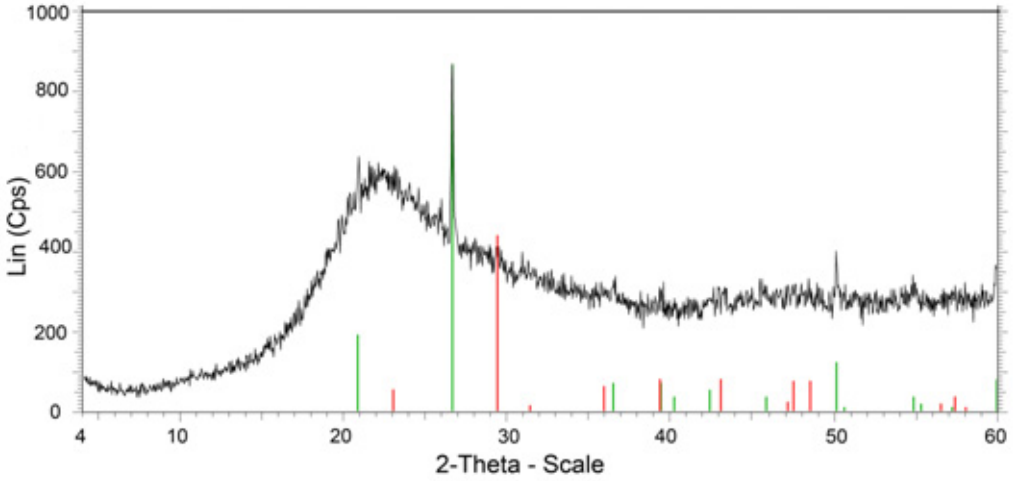

Figure 4.2. XRD pattern of RHA.

Besides RHA, two kinds of ordinary Portland cement, an undensified powder of SF and a ground granulated blast-furnace slag (GGBS) as cementitious materials were used. One cement sample (CEM-De) was CEM I 52.5 R-HS/NA conforming to DIN EN 1164-10 which was a product in Germany. The other namely CEM-Vn was produced in Vietnam. CEM-Vn was only utilized for compressive strength test in order to ascertain the possibility of using commercial Portland cement and RHA to produce UHPC in Vietnam. CEM-Vn was CEM I 42.5 N conforming to DIN EN 197-1. Chemical, mineral and physical properties of the materials are shown in Table 4.1 to Table 4.4. CEM-De possesses higher C_3S, C_4AF contents but lower C_2S, C_3A contents than CEM-Vn (calculated by the Bogue equations, Table 4.2). CEM-De is finer than CEM-Vn (Table 4.3).

Saturated calcium hydroxide solution at 40°C was utilized to evaluate the pozzolanic reactivity of RHA and SF. Standard sand (DIN EN 196-1) has been used to fabricate mortar specimens for determining the accelerated pozzolanic strength reactivity index of RHA and SF in Section 5.1. Quartz powder and quartz sand (Table 4.3) were filler and aggregate in UHPC, respectively. Steel fibers with a length of 9 mm and a diameter of 0.15 mm were introduced into mixtures only for producing prisms to measure compressive strength of UHPC in Section 5.3.

Table 4.2. Mineral composition of cements (calculated by the Bogue equations)

Cement	Unit	C_3S	C_2S	C_3A	C_4AF
CEM-De	wt.-%	55.7	19.9	1.2	15.5
CEM-Vn	wt.-%	42.3	29.5	11.0	9.7

Table 4.3. Physical properties of materials

	CEM-De	CEM-Vn	SF	RHA-120	GGBS	Quartz powder	Quartz sand
Density [g/cm^3]	3.2	3.17	2.3	2.19	2.91	2.64	2.64
Blaine (BET) SSA [m^2/g]	0.462	0.386	(21.05)	(52.28)	0.670	0.438	-
Mean particle size [μm]	9.15	14.22	0.31	7.41	2.93	14.6	174.5
n- The RRSB slope	0.756	0.792	1.911	1.262	0.754	0.869	2.321
x'- The location parameter of RRSB [μm]	13.51	20.52	0.36	10.46	5.53	20.66	383.78

RHA-120- RHA sample was ground for 120 min
RRSB- Rosin, Rammler, Sperling and Bennett

Table 4.4. Compressive strength of cements

Cement	CEM-De			CEM-Vn		
Age	2 d	7 d	28 d	2 d	7 d	28 d
Compressive strength [MPa]	32.4	49.8	62.2	18.9	42.2	55.2

Superplasticizer polycarboxylate ether was added to adjust the flow of mortar or concrete mixtures. To study the compatibility between superplasticizer and UHPC containing RHA, six different superplasticizers (SP1-SP6) have been used. Solid content of the superplasticizers is given in Table 4.5.

Table 4.5. Solid content of superplasticizers

Superplasticizer	SP1	SP2	SP3	SP4	SP5	SP6
Solid content [wt.-%]	20	29.3	35	25	30	40
Application	Ready mix	Precast	Ready mix	Ready mix	Ready mix	Ready mix

4.2. Mix design of UHPC

UHPC mixture can be considered to have two main parts which are aggregate particles and paste. Based on the results of previous studies [6, 8, 24], the paste volume of UHPC was chosen 15% higher than the void volume of non-compacted quartz sand. The void index of non-compacted quartz sand was 46%, so the paste had a volume of 61% of UHPC. Quartz powder volume was 20% of fine materials (i.e. cement, pozzolans and quartz powder) for all mixtures. Pozzolans partially replaced cement in volume. In SF-modified mixtures, volume of RHA was replaced by volume of SF. Superplasticizer dosage was given as dry weight referred to the amount of cementitious materials (i.e. cement and pozzolans). When 1 vol.-% of steel fibers was added to mixture, the volume of quartz sand was replaced by the volume of fibers. Typical mix proportions of UHPC mixtures are given in Table 4.6. The ratio W/F_v is volume of water to volume of the fine materials.

Table 4.6. Typical mix proportions of UHPC mixtures

UHPC mixtures	Cement	Quartz Sand	Quartz Powder	RHA	GGBS	Total water	w/b	W/F_v
	[kg/m^3]							
Ref	1007.5	1029.6	207.8	-	-	216.5	0.215	0.55
15%RHA	856.4			103.4			0.226	
22.5%RHA	780.8			155.1			0.231	
15%RHA-10%GGBS	755.6			103.4	91.6		0.228	
15%RHA-20%GGBS	654.9			103.4	183.2		0.230	
22.5%RHA-20%GGBS	579.3			155.1			0.236	
15%RHA	884.9		214.7	106.9	-	203.3	0.205	0.50
15%RHA-10%GGBS	780.8				94.7		0.207	

4.3. Mixing, casting and treatment of UHPC

UHPCs were mixed in a Hobart mixer (5 litters) at 140 rpm with a total mixing time of 15 minutes based on the sequence shown in Figure 4.3. High volume mixtures for cyclic climate storage test were mixed in a Pemat ZK30 mixer (Figure 4.4). For durability tests, Teflon was used to prepare specimen moulds to prevent the inhibition of the penetration of water and aggressive agents into specimens. Samples were cast without or with vibration for 30 seconds and were kept in moulds at 20°C, 95% relative humidity (RH) for 48h. After demoulding, three kinds of treatment conditions were applied: Treatment 1- 20°C and 100% RH until testing; Treatment 2- 65°C and 100% RH for 48h; Treatment 3- 90°C and 100% RH for 48h. Samples of Treatment 2 and Treatment 3 were stored afterwards at 20°C and 65% RH until examination.

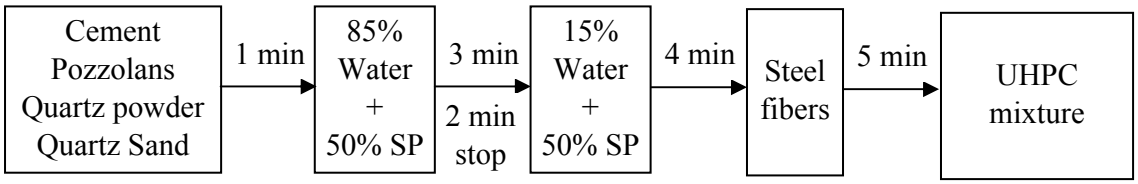

Figure 4.3. Mixing procedure.

Figure 4.4. UHPC containing RHA after mixing in a Pemat ZK30 mixer.

4.4. Experimental methods

4.4.1. RHA

4.4.1.1. Porous structure

The X-ray diffraction diagram (XRD) of RHA sample in Figure 4.2 was recorded at the measurement range between 6-70° 2θ (D5000, Bruker). The quantitative phase analysis (Rietveld) has been done with RHA samples without and with 20 wt.-% zincite as the internal standard (TOPAS 4.2, Bruker AXS, Germany). The RHA samples ground for different periods of time were used to investigate the influence of grinding periods on mean particle size (MPS), specific surface area (SSA), pore volume and water absorption capacity. The MPS of samples was measured by laser diffraction (LS 230, Beckman Coulter). The BET-SSA of SF and RHA was determined by the Brunauer-Emmett-Teller (BET) method (ASAP 2000, Micromeritics). The pore volume and pore size in RHA were measured by the Barrett-Joyner-Hanlenda (BJH) method (SA 3100, Beckman Coulter). To determine the water absorption capacity of SF and RHA, the samples were exposed to 97.5% relative humidity (RH) at 20°C until constant weight. The samples were weighted before and after drying at 110°C. The 97.5% RH condition was created by using saturated K_2SO_4 solution at 20°C [193].

4.4.1.2. Pozzolanic reactivity

The water demand (standard consistency) and setting time of plain (Ref) and cement pastes containing 10 wt.-% RHA or SF were measured by a Vicat apparatus according to DIN EN 196-3. The modified ASTM C1240-05 ("Standard Specification for Silica Fume Used in Cementitious Mixture") [176] was conducted for determining the accelerated pozzolanic strength reactivity index (API) of SF and RHA with Portland cement. The reference mortar (Ref) contained cement and a standard sand (DIN EN 196-1) in the ratio 1 : 2.75. The water to binder ratio amounted 0.484. In the test mixture, Portland cement was partially replaced by 10 wt.-% pozzolan. The flow of the mortars was tested as specified in DIN EN 1015-3. The flow of all the test mixtures deviated no more than ±5 mm for that of the reference mixture. A superplasticizer has been used to adjust the flow of the test mixtures. Mortar bars of 40 × 40 × 160 mm^3 size were cast and tested compressive strength in accordance to DIN EN 196-1. The mortar bars were kept in moulds at 20°C and 95% RH for 24 hours. After demoulding, the samples were placed in airtight containers and stored at 65°C for six days. Compressive strength of mortars was tested after 7 days of hydration. For one mixture, six specimens were tested. The API is determined as follows:

$$API = \frac{A}{B} \times 100\% \tag{4.1}$$

where:

API- accelerated pozzolanic strength reactivity index of pozzolan

A- mean compressive strength of mortar containing pozzolan

B- mean compressive strength of reference mortar

Plain (Ref) sample and cement paste samples containing 10 wt.-% of RHA or SF were produced to evaluate the $Ca(OH)_2$ consumption and thus pozzolanic reactivity of RHA and SF. Water to binder ratio (w/b) of 0.484, 0.3 and 0.22 were applied for the paste experiments. The SP dosage for the pastes at w/b of 0.484 was the same as in the mortars determining the accelerated pozzolanic strength reactivity index (API) of SF and RHA. For the pastes at w/b of 0.3 and 0.22, the SP dosage was 0.6 wt.-% (dry mass). The samples were kept in moulds at 20°C and 95% RH for 24 hours. After demoulding, these samples were divided into two groups: one was placed under the heat treatment according to ASTM C1240-05 followed by storage at 20°C and 65% RH. The other was immersed in water at 20°C until testing. The portlandite (CH) content of the binder pastes after 7 and 91 days of hydration was calculated from the results of the thermal analysis (DTA-TG). The second derivative of DTA was used for identification of the onset of weight loss [194, 195]. For thermal analysis, the samples were ground to a grain size ≤ 63 µm after stopping hydration by isopropanol addition and drying at 40°C until constant weight. The DTA-TG (SDT Q600, TA Instruments) test was conducted in nitrogen atmosphere at a heating rate of 10 °K/min and a nitrogen flow of 100 ml/min.

The electrical conductivity and pH of 200 ml saturated portlandite (CH) solution at 40°C before and after the addition of 5.0 g pozzolan (i.e. RHA ground for different periods of time or SF) were recorded by a dual pH/conductivity meter (S47 SevenMulti, Mettler Toledo) up to 360 min of hydration. To evaluate the effect of water soluble components in the pozzolans on the electrical conductivity of CH-pozzolan suspensions, the electrical conductivity of water-pozzolan suspensions at 40°C was also measured. The pozzolan suspensions have a liquid to solid ratio (l/s) of 40 [170]. These CH-pozzolan or water-pozzolan suspensions were stirred at 350 rpm. Water at 40°C controlled by a thermostatic bath (heating and cooling) was pumped to maintain the temperature of the suspension in a 250 ml two-layer vessel.

Approximately 5 ml of the CH-pozzolan suspensions was taken 2, 5, 10…90 minutes after the addition of the pozzolan. Aqueous phases of the suspensions have been filtered (0.22 µm filter) and acidified (5 M HNO_3). Si, Ca, K, Na concentrations of the solution were measured by an inductively coupled plasma optical emission spectrometry (ICP-OES ACTIVA-M, HORIBA Jobin Yvon).

The DTA-TG was also carried out to compare the hydration of CH-RHA suspension and CH-SF suspension. Therefore, the CH-pozzolan suspensions were filtered after 6 and 24 hours and the residues were removed from free water by isopropanol addition followed by drying at 40°C until constant weight. Relative weight loss of the hydrated and unhydrated pozzolans was calculated for the heating periods from 25 to 250°C and from 250 to 1000°C by TG analysis. Additionally, the relative weight loss of the unhydrated pozzolans was subtracted from the relative weight loss of the hydrated pozzolans yielding the corrected relative weight loss of the hydrated pozzolans at the different heating periods.

An ultra high resolution scanning electron microscope (Nova NanoSEM 230, FEI) was applied to capture the pore structure and morphology of RHA particles before and after grinding. Furthermore, microstructure of the residues of the CH-RHA suspension and CH-SF suspension after 6 and 24 hours of hydration was qualitatively compared by the scanning electron microscopy. Backscattered electron (BSE) imaging in combination with energy

dispersive X-ray (EDX) spectroscopy was carried out on polished section of hydrated cement paste containing RHA (w/b = 0.22) to investigate the distribution of calcium and RHA particles.

4.4.1.3. Zeta potential

The development of a net charge at the particle surface affects the distribution of ions in the surrounding interfacial region resulting in an increased concentration of counter ions (ion of opposite charge to that of the particle) close to the surface. Thus, an electrical double layer exists between the solid particles and the liquid phase. The potential that exists at this boundary (slipping plane) is known as the zeta potential [196]. Electrokinetic properties of material suspensions determined by zeta potential measurement can be used to evaluate the ion adsorption of pozzolan particles [93]. The potential measured in mV at the slipping plane distance from the particle surface (zeta potential) is also useful for understanding and predicting interactions between particles in suspension or in blended cement paste [196].

Zeta potential of RHA and SF suspensions was measured over 120 min at 25°C using Model DT-1200 Acoustic and Electro-acoustic Spectrometer (Dispersion Technology Inc., USA). The pozzolan suspensions had a liquid to solid ratio of 40. At first, pH of the distilled water-SF suspension was adjusted to the pH value of the distilled water-RHA suspension (i.e. pH is about 9.5) by addition of KOH 0.1 mol/l. To prove that Ca^{2+} ions in solution will be adsorbed on surface particles, zeta potential was measured during amounts of Ca^{2+} ions were stepwise titrated (by TA 20^{plus}- SI Analytics) to the pozzolan suspensions. The variation in zeta potential before and after Ca^{2+} ion addition to get the equilibrium condition can be considered as the potential Ca^{2+} ion adsorption ability of the pozzolans. Ca^{2+} ions were provided by $CaCl_2$ 0.15 mol/l.

4.4.2. RHA as a pozzolanic admixture in UHPC

4.4.2.1. Workability and compressive strength

After mixing, mini-cone slump flow of UHPC mixtures was tested. The mini-cone slump flow values (two diameter values) were measured after further 2 minutes without stroking (Figure 4.5). The slump flow was also determined after 15 and 45 minutes of mixing to evaluate the loss of workability of UHPC mixtures with different SP. Three minutes before these moments, UHPCs were remixed for 2 minutes and then tested the

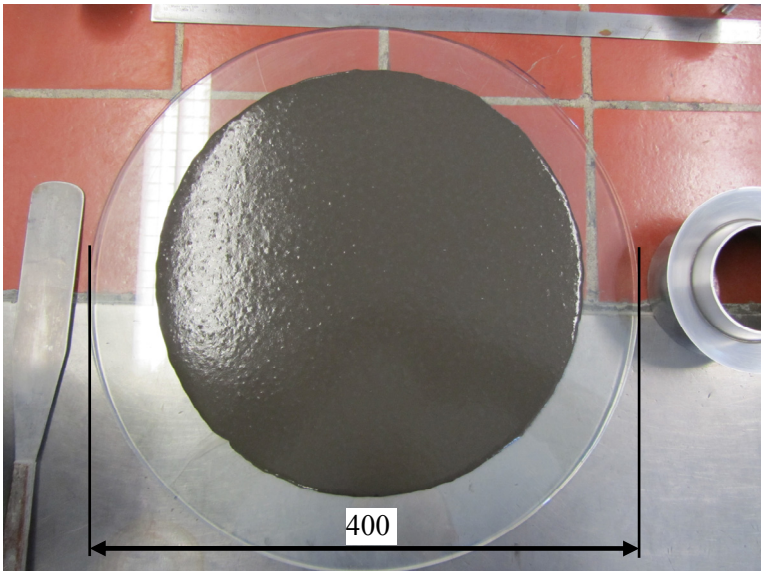

Figure 4.5. Mini-cone slump flow test of UHPC containing RHA.

slump flow. The air content of UHPCs was determined as specified in DIN EN 1015-7. Compressive strength of UHPCs was tested on 40 × 40 × 160 mm^3 sized samples in accordance to DIN EN 196-1.

Concrete is a multivariate system and normally needs more than one important objective function. The classical methods for optimizing mixture proportions are trial and error, or changing one ingredient and studying the effect of the ingredient on the response. It is inefficient and costly. Also, this workflow will often not provide the most economical mixture. Standard response surface designs, such as factorial designs or central composite design are used for optimizing concrete mixtures in which the n mixture components have to be reduced to n-1 independent factors by taking the ratio of two components [197]. However, changing the proportion of one ingredient immediately influences the proportion of others because the mix proportions are limited to sum to 100%. Moreover, some processing factors have strong effect on responses. Hence, different methods are required for selecting an appropriate experimental design and analyzing final results for all variables. The combined mixture-process model is appropriate for these problems [197-199]. In this model, each mixture component can be varied dependently of other mixture components. But each process variable must be varied independently of other process variables and of mixture components. Hence, the user can evaluate all dependent mixture components and independent process variables such as mixing time, vibration period and SP dosage… of concrete mixture. The combined mixture-process model with Design-Expert 8 software was conducted to interpret the synergic effects of RHA, GGBS and SP on mini-cone slump flow and compressive strength of UHPC.

4.4.2.2. Shrinkage

For autogenous shrinkage of UHPCs, an experiment setup as shown in Figure 4.6 has been used to measure the length change and temperature of three 40 × 40 × 250 mm^3 sized samples up to 28 days of hydration. The moveable plate and mould at the ends of samples were fixed in UHPC by fixed plugs. Plastic plate and paraffin wax have been used to avoid any moisture exchange between concrete and environment during the examination. The concrete temperature and length change as well as room temperature were recorded every 6 minutes by temperature sensors and linear variable differential transformers (LVDT). Distinctly, the volume change by the hydration of binder starts by contacting between cementitious materials and water. The linear method described in Figure 4.6 is only carried out after the mixture has set [200]. The zeroed time selection as considered at the beginning of autogenous shrinkage is important and also different in the literature [103, 107, 201]. In this study, the zeroed time is selected when the temperature of concrete mixture is highest.

The long term autogenous shrinkage and total shrinkage of UHPCs under the three treatment conditions were measured on three 40 × 40 × 160 mm^3 sized bars as specified in DIN 52450. The long term autogenous shrinkage of UHPCs was measured on sealed samples with an aluminum foil from 2 days of hydration. For the long term total shrinkage of UHPCs, free samples were cured in water under the three treatment conditions and then exposed to 20°C and 65% RH from 5th day after casting.

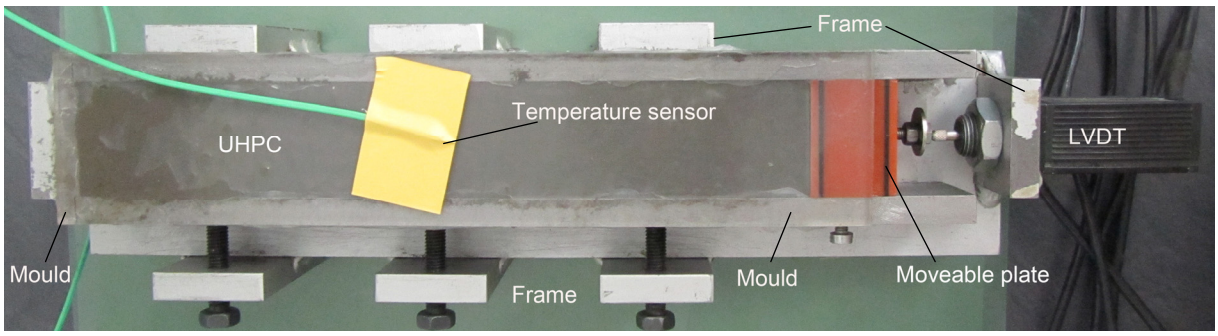

Figure 4.6. Setup of the measurement of temperature and autogenous shrinkage of UHPC.

4.4.2.3. Self-desiccation

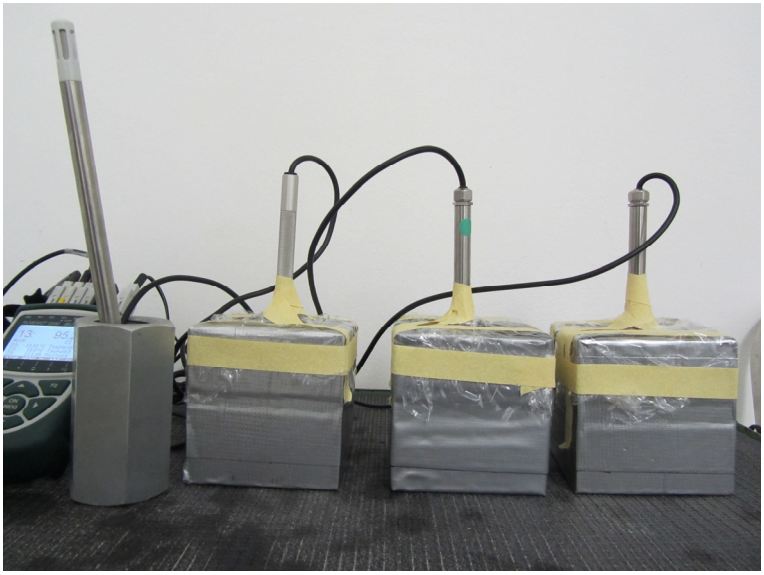

Figure 4.7. Test of internal relative humidity in UHPC.

To illustrate self-desiccation in UHPCs, the internal relative humidity (RH) in UHPCs was measured during hydration. A hole with diameter of 20 mm and 60 mm in depth was created on 100 × 100 × 100 mm^3 sized sample by a free surface steel bar to ensure the free moisture exchange between the concrete matrix and the environment within the hole. After demoulding, the samples were immediately sealed with an aluminum foil. The internal RH in the hole during hydration of UHPC was recorded hourly by a RH sensor. Rubber ring and plastic foil were also used as the setup for the RH sensor to avoid any moisture exchange between the environment in the hole and the external environment during testing. For one mixture, two samples were measured (Figure 4.7).

4.4.2.4. Microstructure

Portlandite content

Portlandite content in binder matrix (cement, pozzolans and water) of UHPCs was calculated from DTA-TG results and the proportions of UHPC mixtures. Sample preparation and DTA-TG testing of UHPC are the same as that of cement paste in Section 4.4.1.2.

Porosity

Total porosity of UHPCs was calculated from the results of bulk density and specific density of UHPCs at the age of 28 days. The bulk density was determined by the dipping in water and weighing method. For the specific density and DTA-TG test, UHPC was ground to a grain size ≤ 63 µm after free water remove by isopropanol addition and drying at 40°C until constant weight. A helium pycnometer (AccuPyc 1330, Micromeritics) was conducted to measure the specific density of the sample.

Mercury intrusion porosimetry (MIP- Micromeritics, Autopore IV 9500) was conducted on UHPC samples with the pressure up to 230 MPa. The sample was reduced to small grains of 3-5 mm (about 10 g), removed from free water by isopropanol addition and afterwards dried at 40°C until constant weight. Based on the consumed mercury amount during the intrusion process and the respective pressure, the pore size radius distribution between 0.003 to 230 µm in UHPC was determined.

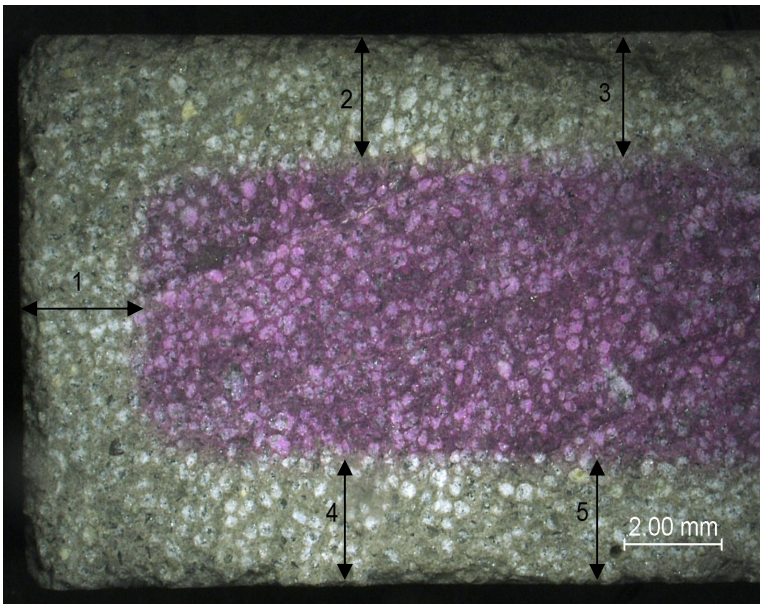

Figure 4.8. Measurement of corrosion depth by phenolphthalein and a digital microscope.

Water absorption

The capillary water absorption was tested on three UHPC cube specimens (a = 40mm) at the age of 28 days by gravimetric weighing as specified in DIN EN ISO 15148:2003 ("Hygrothermal Performance of Building Materials and Products- Determination of Water Absorption Coefficient by Partial Immersion) [202]. The specimens were dried at 105°C for 24 hours before testing. The samples were immersed about 3-5 mm in water and were weighted over time up to 24 hours to measure water absorption coefficient (W_{24}, $kg/m^2.h^{0.5}$).

4.4.2.5. Durability

Chemical resistance

Sulfuric acid (H_2SO_4) pH= 2.5 and ammonium nitrate (NH_4NO_3) 5 M were applied to investigate the deterioration of UHPCs in the aggressive solutions. At the age of 28 days at Treatment 1, and 7 days at Treatment 2 and Treatment 3, three and a half UHPC bars ($10 \times 40 \times 160$ mm^3) for each mixture were immersed in the solution at 20°C. The volume of the solution and concrete ratio was 4. The pH of the sulfuric acid solution was measured weekly by a pH meter (inoLab pH 720, WTW) and a calculated volume of H_2SO_4 pH = 1 was added to remain the pH of the solution. The sulfuric acid solution was renewed every two months during the examination. The NH_4NO_3 solution was not changed during the test. Weight and length change of 3 specimens in the sulfuric acid solution and weight change of 3 specimens in the NH_4NO_3 solution were measured in dependence of time. Additionally, the corrosion depth of the samples in the NH_4NO_3 solution was measured by an acid-base indicator (phenolphthalein) and a digital microscope (VHX 600 II, Keyence). Corrosion depth value is the mean value of five measurements on a 10 × 40 mm cross section sample which was sawed from the half of UHPC bar (Figure 4.8).

Alkali silica reaction (ASR)

The modified German Alkali Guidelines ("Vorbeugende Maßnahmen gegen schädigende Alkalireaktion im Beton (Alkali-Richtlinie)") [203] or ASTM C1260-05 ("Standard test method for potential alkali reactivity of aggregates (mortar-bar method)") [127]) was used to investigate the alkali silica reaction (ASR) of UHPCs. The standard test method requires demoulding the mortar bars at 24 hours, storing the bars in water bath containers and placing the containers in an oven at 80°C for a period of 24 hours. Thereafter, the samples are immersed in NaOH 1M at 80°C with the volume of solution to concrete ratio of 4. Due to the long setting time of UHPCs, samples were tested after 48 hours in form. Weight and length of three 40 × 40 × 160 mm^3 sized specimens were recorded before and after 14 days, respectively, 28 days, immersed in NaOH 1M at 80°C. To evaluate the effect of differently autogenous shrinkage of UHPCs on the length change value, the weight and length change of the samples (40 × 40 × 160 mm^3) were also recorded after 1, 15 and 29 days in water at 80°C. Therefore, the corrected length change of the samples by the NaOH solution was calculated. Additionally, five 10 × 40 × 160 mm^3 sized bars have been tested to evaluate the effect of different specimen dimensions on the results of this ASR test. The length of all samples was measured at 80°C within 20 seconds by the equipment as specified in DIN 52450.

Durability of UHPCs without external aggressive agents under the accelerated conditions was investigated. UHPC specimens (100 × 100 × 400 mm^3) at the age of 7 days were exposed to stimulating Mid-European climate conditions by means of cyclic climate storage (CCS). The test method was developed at the F. A. Finger Institute for Building Materials Science (FIB, Bauhaus University Weimar, Germany). One cycle of the CCS lasts 21 days with 4 days drying at 60°C and RH < 10%, 14 days moisturizing at 45°C and 100% RH and 3 days of freeze-thaw conditions between +20°C and –20°C according to the CIF test (Figure 4.9). More detailed information of this method can be found elsewhere [128, 130, 204]. This test is especially suitable for considering ASR problems of concrete [114, 128-130]. The expansion threshold value of sample for the CCS test without deicer solution (i.e. with water) is 0.4 mm/m after 6 cycles.

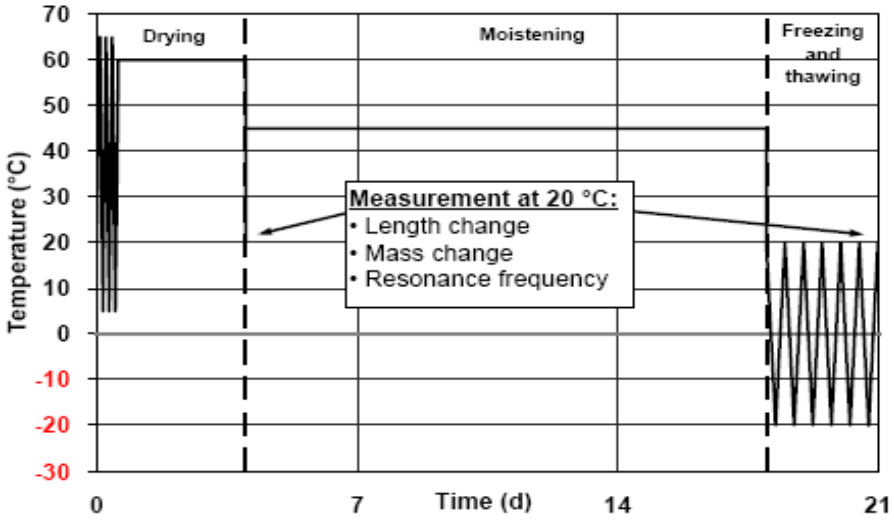

Figure 4.9. Scheme of cyclic climate storage (one cycle).

The ultra high resolution scanning electron microscope (NanoSEM) was applied to see the microstructure of UHPC containing RHA before and after the durability tests. Backscattered electron (BSE) imaging in combination with energy dispersive X-ray (EDX) spectroscopy was conducted on polished sections. UHPCs previously immersed in H_2SO_4 of pH 2.5 were investigated to identify the ingress of sulfate into cement matrix.

5. Results and Discussion

5.1. Porous structure and pozzolanic reactivity of RHA

5.1.1. Effect of grinding time on characteristics of RHA

5.1.1.1. Mean particle size and specific surface area of RHA

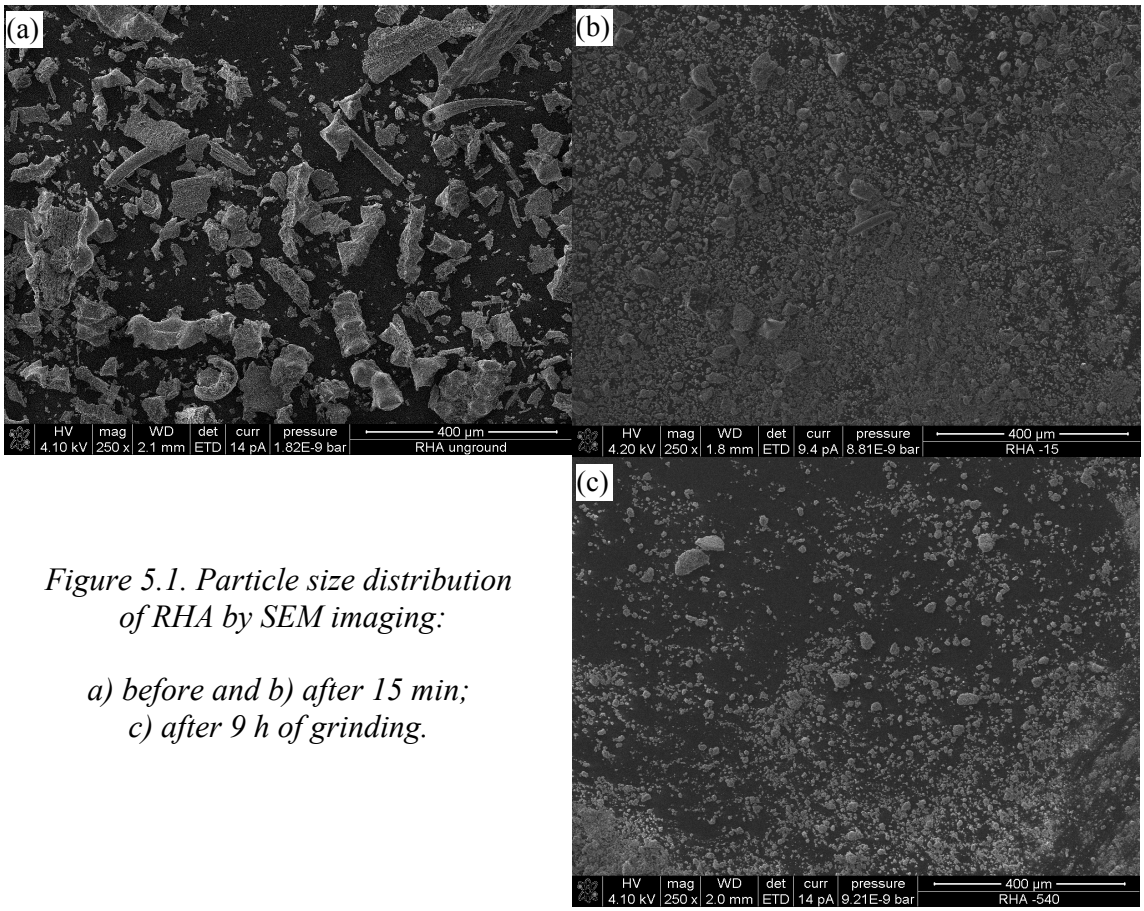

Figure 5.1. Particle size distribution of RHA by SEM imaging:

a) before and b) after 15 min;
c) after 9 h of grinding.

Results in Figure 5.1, Figure 5.2, Figure 5.3 and Table 5.1 illustrate that the mean particle size (MPS) of RHA clearly decreases with increasing grinding time. Before grinding, coarse RHA particles with irregular shapes are found (Figure 5.1a). After 15 min of grinding, the sample still has many coarse particles, i.e. about 100 µm (Figure 5.1b and Figure 5.2). During the first hour of grinding, the MPS of RHA declines

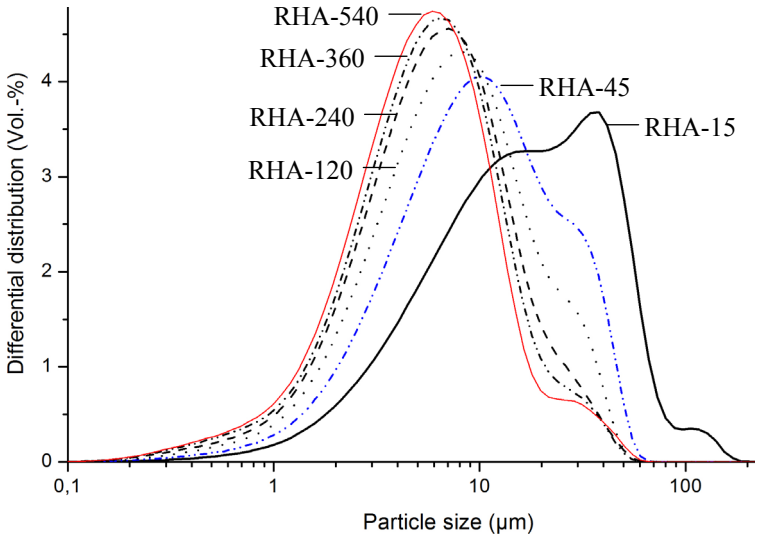

Figure 5.2. Particle size distribution of RHA samples.

dramatically from 95.0 µm to 8.0 µm, the BET-SSA decreases from 62 m^2/g to 57 m^2/g, respectively. There is a slight increase in the BET-SSA of the samples at 30, 45 and 90 min of grinding. Thereafter, when the MPS of RHA sample declines from about 8 µm (RHA-90) to about 6 µm (RHA-360), the BET-SSA strongly reduces from 57 m^2/g to 44 m^2/g, respectively. After grinding for six hours, minor decreases in both the MPS and BET-SSA of RHA are observed (Figure 5.3 and Table 5.1). The increase in the BET-SSA of RHA sample during an intermediate grinding period was also observed in the investigations of Bui [36], Nguyen [60] and Sugita et al. [163].

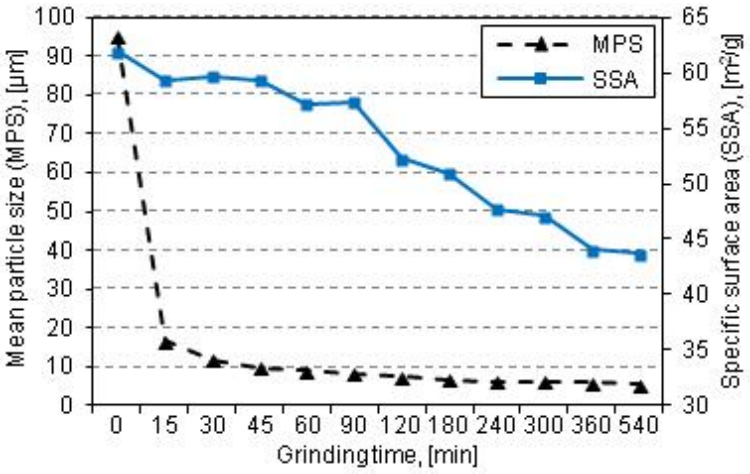

Figure 5.3. MPS and BET-SSA of RHA in dependence of grinding time.

Table 5.1. Influence of grinding time on MPS and BET-SSA of RHA

Sample	RHA-0	RHA-15	RHA-30	RHA-45	RHA-60	RHA-90	RHA-120	RHA-180	RHA-240	RHA-300	RHA-360	RHA-540
Time [min]	0	15	30	45	60	90	120	180	240	300	360	540
MPS [µm]	94.99	16.51	11.54	9.65	8.82	7.94	7.41	6.62	6.22	5.93	5.78	5.34
SSA [m^2/g]	61.97	59.33	59.69	59.42	57.26	57.40	52.28	50.98	47.78	47.11	44.02	43.69

5.1.1.2. Porous structure and morphology of RHA by SEM imaging

By NanoSEM imaging, macropores (section diameters from 50 nm) and mesopores (section diameters of 2 to 50 nm) are clearly visible in the unground RHA (Figure 5.4). The amount of mesopores increases from the outside to the inside of the RHA shell (Figure 5.4b).

Figure 5.5 displays the microstructure of RHA after 15 min of grinding. The macropores of RHA are filled with many finely ground RHA particles (Figure 5.5a). Due to grinding, many large RHA particles are fractured, thus the macropores collapse and particle size is reduced (Figure 5.1b). Fractured surfaces of RHA particles give access to many mesopores (Figure 5.5b). After 9 h of grinding, large RHA particles and thus macropores are virtually absent (Figure 5.1c and Figure 5.6). Nanoscaled RHA particles form agglomerates (Figure 5.6a). Mesopores with section diameters of 2 to 50 nm are observed on RHA particle surface (Figure 5.6b). Application of an ultra high resolution SEM (Nova NanoSEM 230, FEI) allows us to show for the first time the mesoporous structure of ground RHA particles (Figure 5.5b and Figure 5.6b), which before was just theoretically calculated from results of BET-SSA or BJH [141, 160, 161].

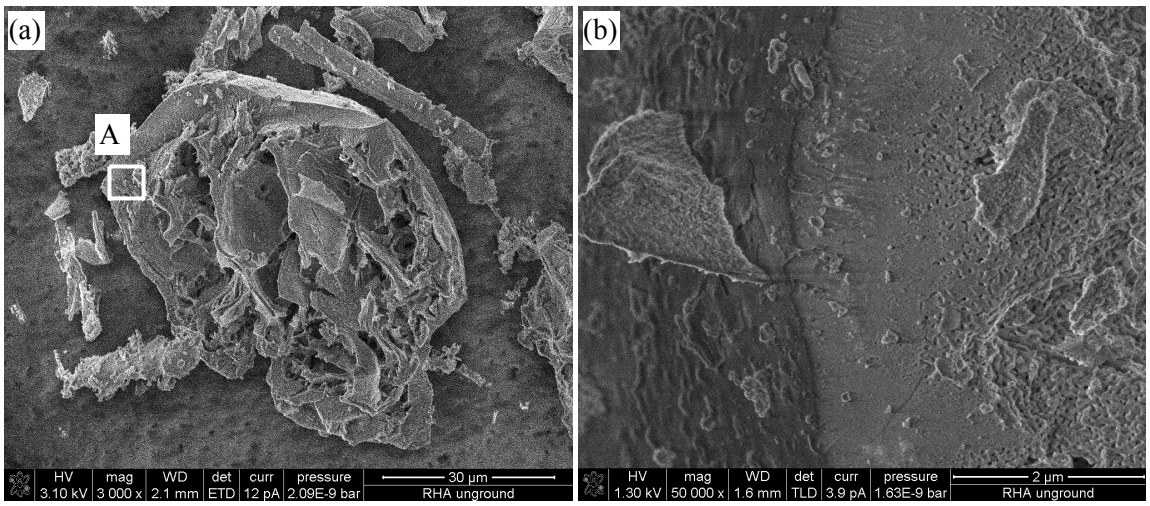

Figure 5.4. Surface structure and morphology of RHA particle before grinding: a) RHA particle at low magnification, showing macropores; b) enlarged image of area A in Figure 5.4a showing increasing amount of mesopores (from left to right side of image).

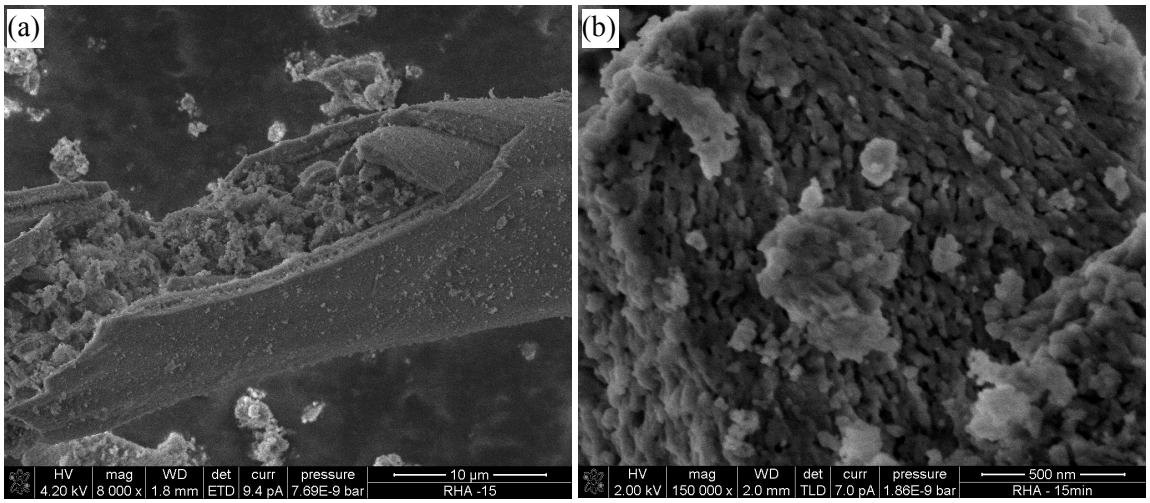

Figure 5.5. Surface structure and morphology of RHA particle after 15 min of grinding: a) RHA particle of low magnification, macropores are filled by finely ground particles; b) mesopores on finely ground RHA particle.

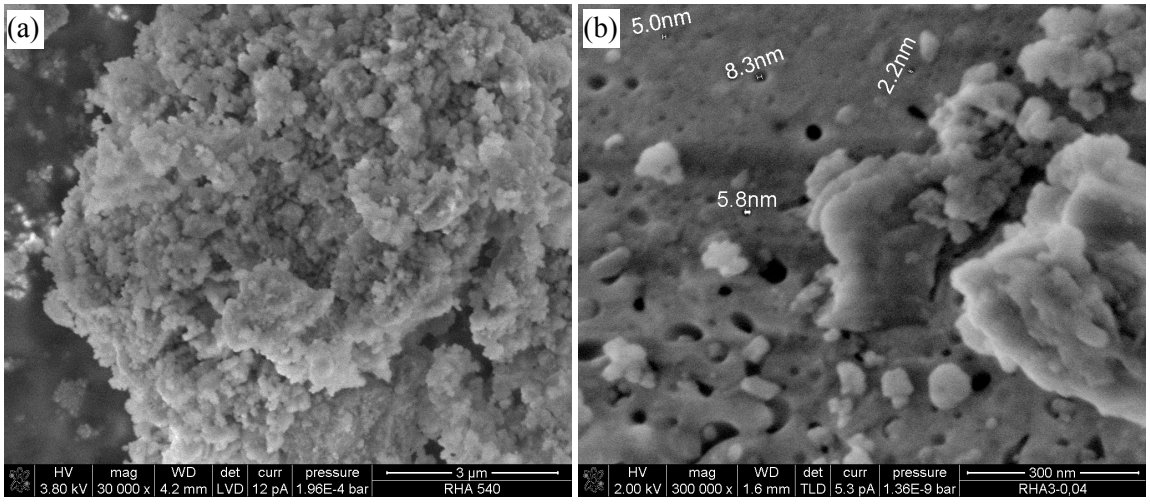

Figure 5.6. Microstructure and morphology of RHA after 9 h of grinding: a) agglomerates of nanoscaled RHA particles; b) surface of RHA particle with mesopores.

5.1.1.3. Pore volume and water absorption

Results of pore volume derived from BJH measurements and of water absorption are shown in Table 5.2. The effect of grinding time on the pore volume and on the water absorption capacity of RHA is somewhat similar to that on the BET-SSA in Figure 5.3 and Table 5.1. Generally, as the BET-SSA of RHA decreases with grinding time, also the pore volume and the water absorption decrease. Similar to the BET-SSA of RHA, there is a slight increase in the pore volume from RHA-15 to RHA-30 and RHA-45 (compare Table 5.1 and Table 5.2). The mean water absorption capacity of RHA in dependence of grinding time is 0.18 ml/g. It is approximately 0.11 ml/g higher than that of SF. The calculated pore volume of RHA from the BJH measurement is of the same magnitude as the difference in the water absorption of RHA and SF, i.e. 0.12 cm^3/g and 0.11 ml/g (Table 5.2). The pore size distribution in RHA particles is mainly from about 2 to 50 nm and the mean pore size of RHA is about 30 nm. Thus, one can conclude that this RHA is a mesoporous material which has significantly high SSA, pore volume and water absorption capacity compare to SF. The variations in BET-SSA and pore volume of RHA are mainly influenced by the collapse of pore volume, new open pores and particle size reduction as shown in Figure 5.7.

Table 5.2. Pore volume of RHA determined by BJH method and water absorption of RHA and SF.

Sample	Grinding time	MPS value	Pore volume	Water absorption
	[min]	[µm]	[cm^3/g]	[ml/g]
RHA- 0	0	94.99	0.1273	-
RHA- 15	15	16.51	0.1134	0.183
RHA- 30	30	11.54	0.1266	-
RHA- 45	45	9.65	0.1351	0.176
RHA- 120	120	7.41	0.1164	0.180
RHA- 540	540	5.34	0.1106	0.168
SF	-	0.30	-	0.073

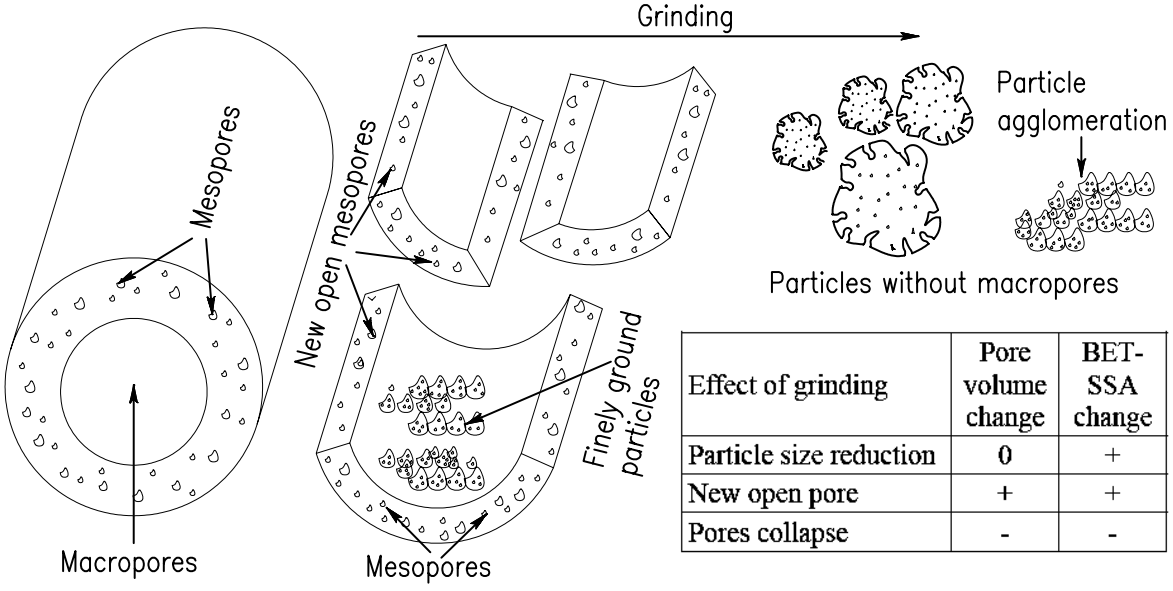

Effect of grinding	Pore volume change	BET-SSA change
Particle size reduction	0	+
New open pore	+	+
Pores collapse	-	-

Figure 5.7. Different stages of RHA particles and its effect on pore volume and BET-SSA during grinding process.

5.1.2. RHA in cementitious system

5.1.2.1. Influence of RHA on water demand and setting time of cement paste

Results of water demand (the standard consistency) and setting time measurements of plain (Ref) and cement pastes containing 10 wt.-% RHA, respectively, SF, are presented in Figure 5.8. The results show that the pozzolans clearly increase the water demand of the cement paste. The water demand of the SF-blended paste is higher than that of the RHA-blended pastes despite its lower BET-SSA (compare Table 4.3 and Table 5.1). The higher the SSA of RHA, the more the water demand of the paste (Figure 5.8). The effect of RHA on the setting time of the cement paste is insignificant. SF decreases the setting time of the cement paste, even though the paste containing SF possesses significantly higher water content (Figure 5.8).

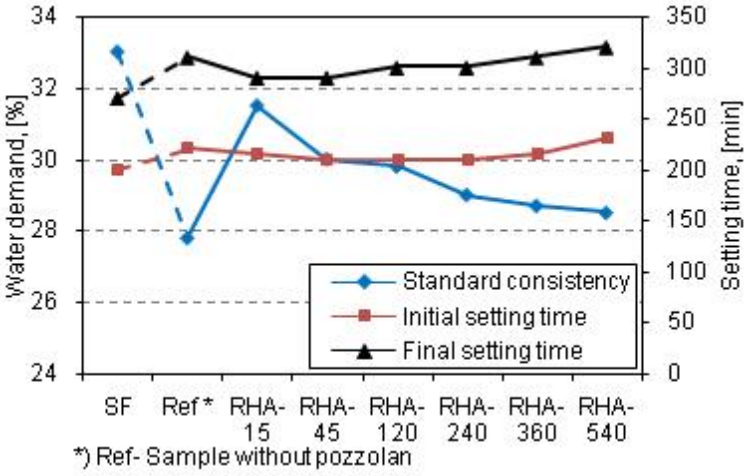

Figure 5.8. Effect of pozzolans on water demand and setting time of cement paste.

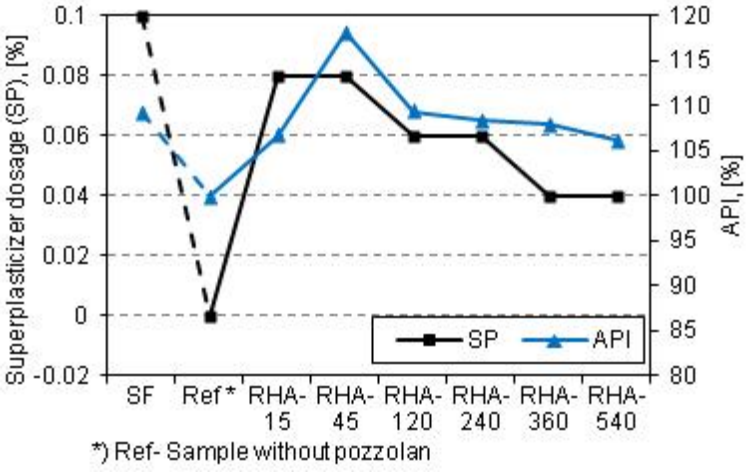

Figure 5.9. SP demand and API of RHA and SF.

5.1.2.2. Accelerated pozzolanic strength reactivity index (API)

Portland cement mortars containing 10 wt.-% pozzolan at w/b of 0.484 were hydrated for 7 days with 6 day heat treatment (at 65°C) to determine the API [176]. The API of RHA ground for different periods of time was compared with the API of SF. The results are shown in Figure 5.9. Additionally, superplasticizer dosage (dry mass) necessary to maintain the given flow is presented (Figure 5.9). The results show that the SP dosage decreases to maintain the given flow value of the mortar containing RHA ground for a longer period of time. The mortar containing SF needs the highest SP dosage to achieve the given workability of the reference mortar. The reference mortar has compressive strength of 59.6 MPa. The API of all the pozzolans exceeds 105%. This is the minimum API required for application of SF in cementitious mixtures [176]. The RHA ground for 45 minutes has the highest API. The API and the BET-SSA of RHA decrease for grinding periods from 45 to 540 minutes. RHA-15 and RHA-45 have almost the same BET-SSA (Table 5.1), but the API of the corresponding RHA are 106.7% and 118.1%, respectively. The API of 120 minute ground RHA is similar to

that of SF. Thus, it can be concluded that the API of RHA is increased by properly chosen grinding period.

5.1.2.3. Portlandite content and pozzolanic reactivity of RHA in cement paste

Because the mortar containing RHA-120 had the same compressive strength as the mortar containing SF, RHA-120 was selected to produce cement pastes to evaluate the $Ca(OH)_2$ consumption and thus the pozzolanic reaction of RHA in different water binder ratio matrices. The $Ca(OH)_2$ contents in the cement pastes calculated from DTA-TG measurement are given in Figure 5.10. To estimate the accuracy of sample preparation and of DTA/TG measurement, the standard deviation of $Ca(OH)_2$ content of five differently prepared samples from the paste containing 10% RHA at w/b of 0.3 is given by an error bar in Figure 5.10c.

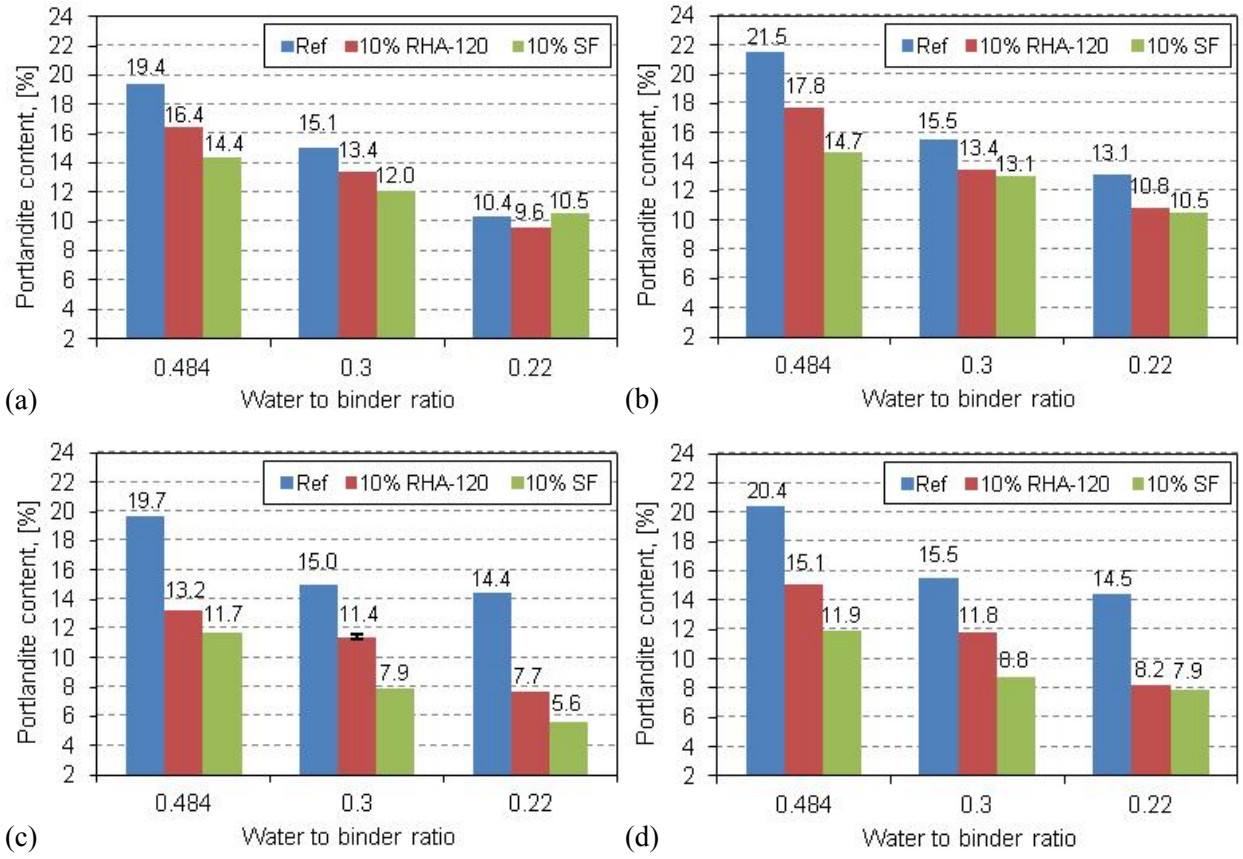

Figure 5.10. CH content of cement pastes determined by DTA-TG analysis in dependence of w/b, pozzolan addition, storage conditions and hydration periods: a) 7 d and b) 91 d hydration with water storage; c) 7 d and d) 91 d hydration heat treatment (Ref- cement paste without pozzolan; 10% RHA-120- cement paste containing 10% RHA-120 and 10%SF- cement paste containing 10% SF partially replacing cement).

Generally, the CH content of the samples decreases with the reduction of w/b and increases over time. The CH consumption and thus pozzolanic reactivity of SF exceeds the CH consumption of RHA, especially at high water content or heat treatment. The heat treatment strongly accelerates the CH consumption of both RHA and SF. This confirms previous findings that showed the increased reactivity of pozzolan under heat treatment [94, 96].

For the samples at w/b of 0.22, the CH content of the reference sample after 91 days of water storage (Figure 5.10b) is lower than that of the heat treated reference sample at the age of 7

days (Figure 5.10c). The CH content of the heat treated reference paste is similar between 7 and 91 days (Figure 5.10c and d). No significant influence of the heat treatment on the CH content is found for the reference pastes at the increased w/b. This indicates that the cement hydration of the reference sample at w/b of 0.22 is accelerated but also almost stopped after 6 days of the heat curing. However, the CH content of the heat treated pastes containing RHA or SF at w/b of 0.22 increases between the ages of 7 and 91 days. The increase in the CH content of the heat treated paste containing SF exceeds that of the heat treated paste containing RHA (Figure 5.10c and d).

Figure 5.11 shows BSE-SEM and EDX-mapping images of a polished sample of the heat treated cement paste containing RHA at w/b of 0.22 after 91 days of hydration. It can be seen that RHA is embedded very tightly into the cement matrix. RHA particles have bright and dark areas on the cross section (Figure 5.11). Combining this finding with previously seen distribution of mesopores (Figure 5.4b) and the phase mapping derived from EDX mapping in Figure 5.11b, it becomes obvious that there is a Ca concentration gradient over the RHA grains indicating a transport of calcium ions from matrix into RHA. This indicates that mesopores are filled with calcium and the pozzolanic reaction enters the RHA particle through the mesopores. Therefore, some parts of the interfacial transition zone (ITZ) between RHA particle and the matrix are deleted (Solid arrows in Figure 5.11). Pozzolanic reactivity of RHA is strongly related to its mesoporous structure.

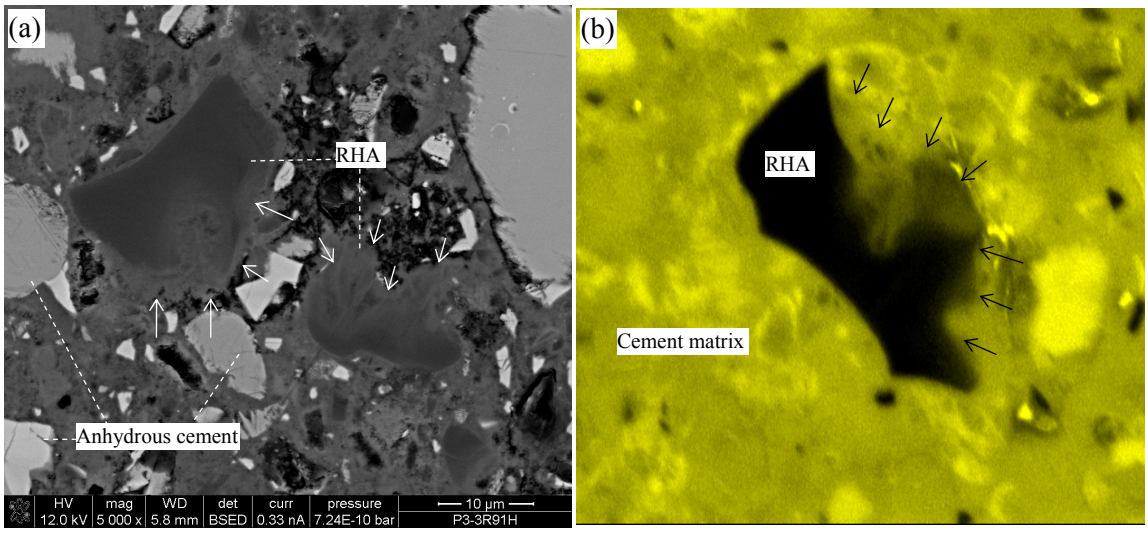

Figure 5.11. a) BSE-SEM image and b) EDX-Ca-mapping of RHA particle in heat treated cement paste at w/b of 0.22 after 91 d hydration. Solid arrows indicate the high Ca^{2+} concentration parts (bright areas) of RHA particle.

5.1.3. RHA in saturated $Ca(OH)_2$ solution

5.1.3.1. Electrical conductivity and pH of CH-pozzolan suspension

The pH and electrical conductivity curves of CH-pozzolan suspensions with SF and RHA at three different grinding stages up to 360 minutes of hydration are shown in Figure 5.12 and Figure 5.13, respectively. The variation in the electrical conductivity of all the CH-pozzolan suspensions from 0 to 2 minutes and from 0 to 360 minutes is presented in Figure 5.14.

During the initial 255 min, the pH and electrical conductivity values of the CH-SF suspension are higher than those of the CH-RHA suspensions. At hydration periods later than 300 min, the effect is reversed (Figure 5.12 and Figure 5.13). The decrease in the electrical conductivity of all the CH-RHA suspensions from 0 to 2 minutes is about 2.4 mS/cm. At the same time, the decrease in the electrical conductivity of the CH-SF suspension is much smaller than that of the CH-RHA suspensions (Figure 5.14). Hence, according to the classification of Luxan's method [170], the RHA has a very high pozzolanic reactivity, i.e. significantly higher than that of SF. However, the decrease in the electrical conductivity of the CH-SF suspension exceeds that of the CH-RHA suspensions after 6 hours (Figure 5.14). This indicates that the CH consumption by SF exceeds that of RHA at the long terms.

When the effect of SSA of the pozzolans on the decrease in the electrical conductivity of the CH-pozzolan suspensions at different periods is considered, it reveals that the high decrease in the electrical conductivity of the CH-RHA suspensions from 0 to 2 min may result from the high SSA of RHA (i.e. adsorption of Ca ions). The effect of the difference in SSA of RHA on the decrease in the electrical conductivity of the CH-RHA suspensions from 0 to 2 min

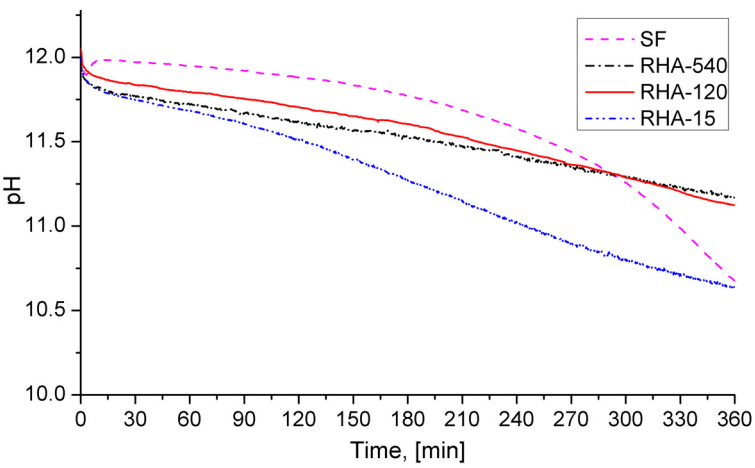

Figure 5.12. pH over time of CH-pozzolan suspensions with l/s = 40 at 40°C.

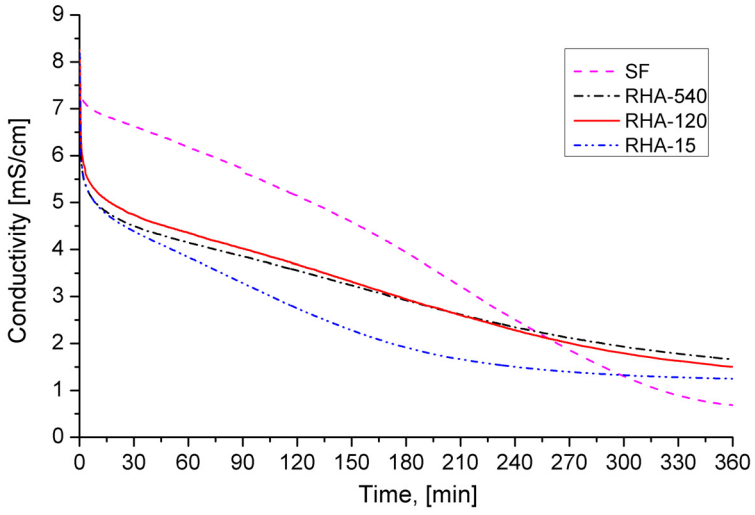

Figure 5.13. Electrical conductivity over time of CH-pozzolan suspensions with l/s = 40 at 40°C.

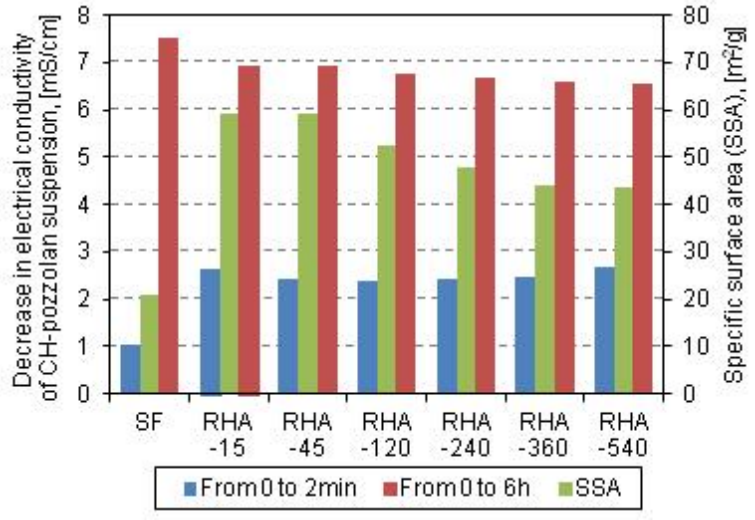

Figure 5.14. SSA of pozzolans and decrease in electrical conductivity of CH-pozzolan suspensions from 0 to 2 min respectively 6 h (l/s = 40 at 40°C).

is unclear. From 0 to 360 minutes, the higher the SSA of RHA, the more it decreases in the electrical conductivity of the CH-RHA suspension (Figure 5.14).

Results of the electrical conductivity measurement of the water-pozzolan suspensions at l/s of 40 and 40°C are shown in Figure 5.15. As expected, the electrical conductivity value in water is much lower than in saturated CH solution. Measuring electrical conductivity in the H_2O suspensions indicates the dissolution behavior of the pozzolan. Clearly, SF dissolves ions much less than RHA. The main reason might be the higher alkali content and SSA of RHA.

In order to eliminate the effect of water soluble components of the pozzolans on the electrical conductivity results measured in the presence of CH, the values of the electrical conductivity of the water-pozzolan suspensions were subtracted from the electrical conductivity values in the CH-pozzolan suspensions. Corrected values are shown in Figure 5.16. Hence, the corrected electrical conductivity curves in Figure 5.16 present the absolute loss in the electrical conductivity due to the $Ca(OH)_2$ consumption by the pozzolan. Comparing Figure 5.13 and Figure 5.16, there is no appreciable difference in the slope of electrical conductivity curves of the CH-pozzolan suspensions. This indicates that dissolved alkali

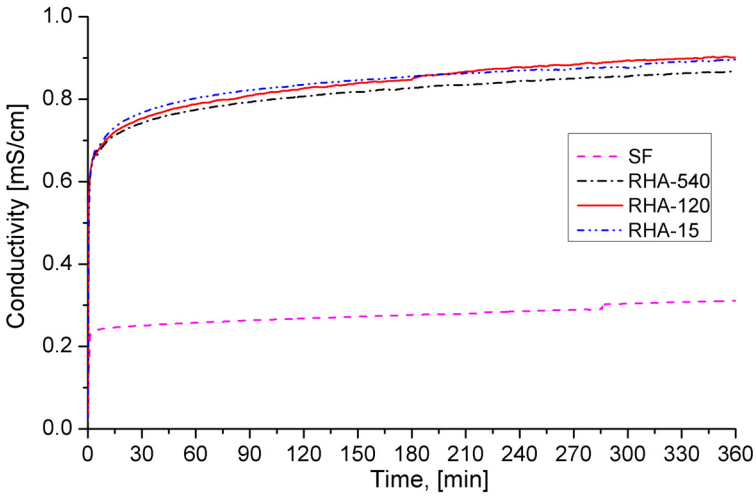

Figure 5.15. Electrical conductivity over time of water-pozzolan suspensions at l/s = 40 and 40°C.

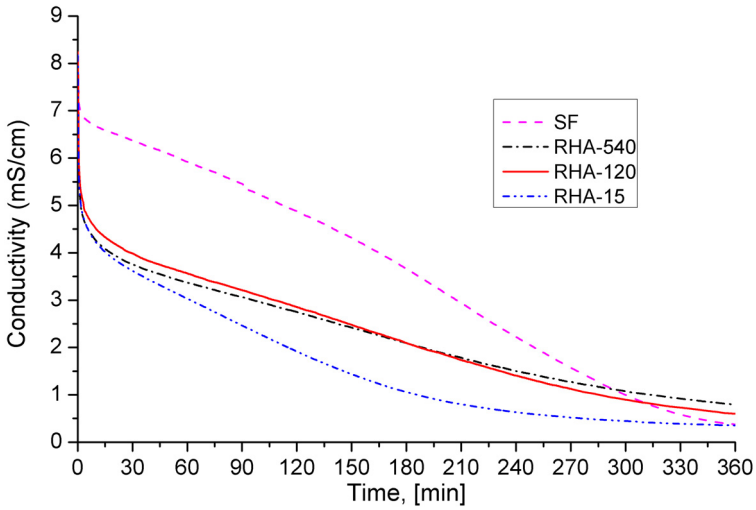

Figure 5.16. Corrected electrical conductivity over time of CH-pozzolan suspensions with l/s = 40 at 40°C.

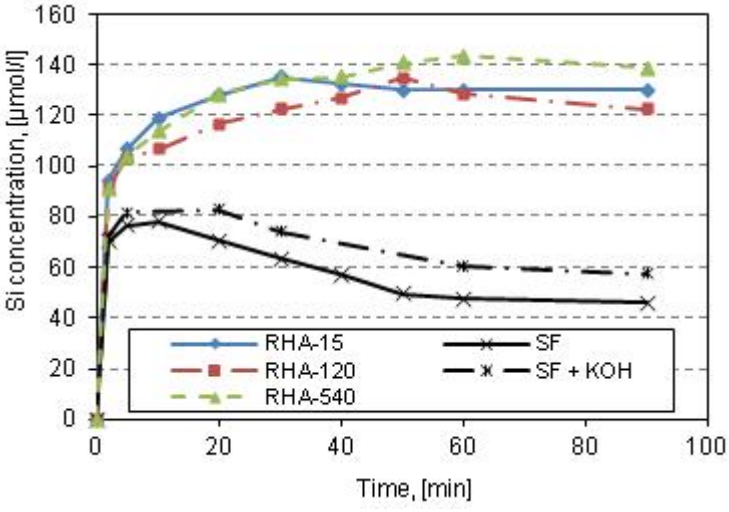

Figure 5.17. Silicon concentration over time in CH-pozzolan suspensions with l/s = 40 at 40°C.

content of the pozzolans strongly increases the decrease in the electrical conductivity before and after the pozzolan addition, but not the electrical conductivity reduction rate during hydration.

5.1.3.2. Concentration of pozzolan silica and calcium in CH suspension

Results in Figure 5.17 and Figure 5.18 show silicon and calcium ion concentrations in the aqueous phase of the CH-pozzolan suspensions (with l/s of 40 at 40°C). The results indicate that the Si concentration of the aqueous phase in the CH-RHA suspensions exceeds that of the CH-SF suspension. The maximum Si concentration in the CH-SF suspension is measured after about 10 minutes. The increase and decrease in Si concentration is accelerated in the SF-suspension compared to the RHA-suspensions (Figure 5.17). Calcium ion concentration strongly decreases during the initial 20 minutes in the RHA-suspensions and within 10 minutes in the SF-suspension. Thereafter, the rate of Ca ion concentration reduction in these suspensions is almost stable. Calcium ion concentration in the CH-SF suspension is always higher than that of the CH-RHA suspensions (Figure 5.18).

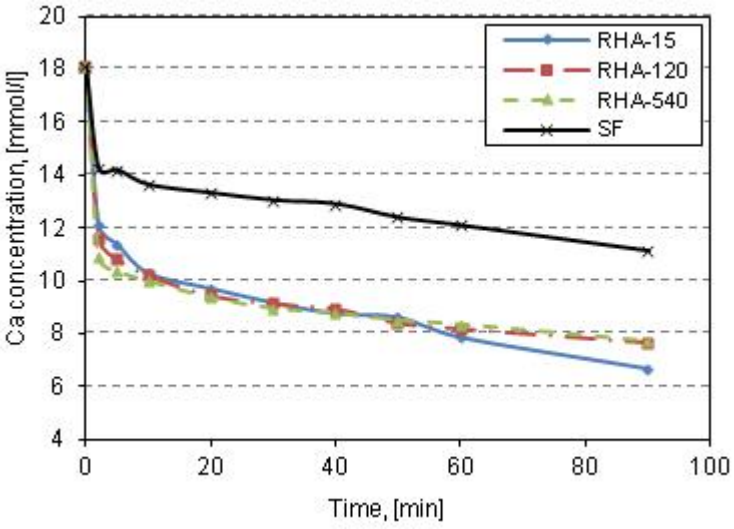

Figure 5.18. Calcium concentration over time in CH-pozzolan suspensions with l/s = 40 at 40°C.

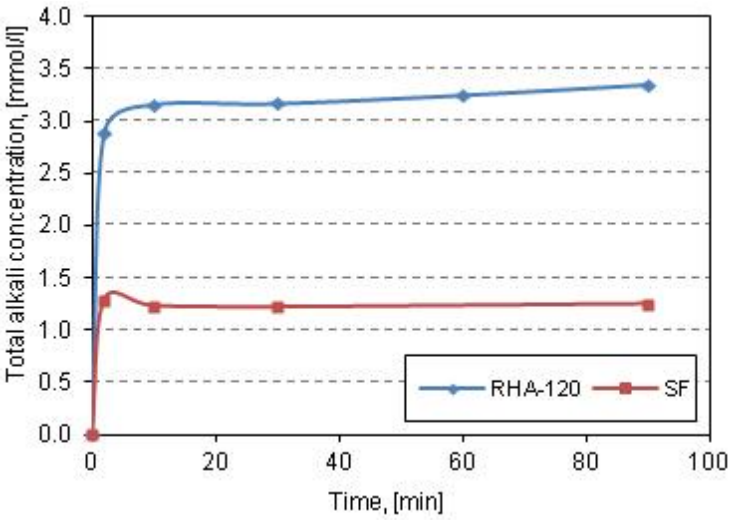

Figure 5.19. Total alkali concentration over time in CH-pozzolan suspensions with l/s = 40 at 40°C.

The total alkali concentration is 1.25 mmol/l in the SF-suspension and is about 3.35 mmol/l in the RHA-120-suspension at 90 min of hydration. The total alkali concentration in the CH-pozzolan suspensions only slightly changes during 90 min of hydration (Figure 5.19). To investigate the effect of increased alkali content in the suspension on the solubility of the pozzolan, 2.10 mmol/l KOH was added to the SF-suspension. Thus, the alkali content in the SF-suspension is adjusted to the alkali level of the RHA-suspensions. As expected, the increase in alkali content increases the Si concentration in the aqueous phase of the CH-SF+KOH suspension (Figure 5.17). This indicates that the high alkali content of RHA is one of important parameters which increase the solubility of silica in the CH-RHA suspensions.

5.1.3.3. Evaluation of pozzolanic reaction product of RHA and SF

SEM images in Figure 5.20a, b and Figure 5.21a, b display that the product of the pozzolanic reaction of RHA or SF is formed after 6 hours in the CH-pozzolan suspensions. The hydrate phases of the pozzolanic reaction in the CH-pozzolan suspensions can be described as foils that form a network, i.e. enclose and connect particles (Figure 5.20 and Figure 5.21). From 6 to 24 hours of hydration, the amount of the hydrates in the RHA-suspension clearly increases (compare Figure 5.20a, b and Figure 5.20c, d). Meanwhile, it is difficult to identify the difference in the amount of the pozzolanic reaction products that forms between 6 and 24 hour hydration of the SF sample (compare Figure 5.21a, b and Figure 5.21c, d).

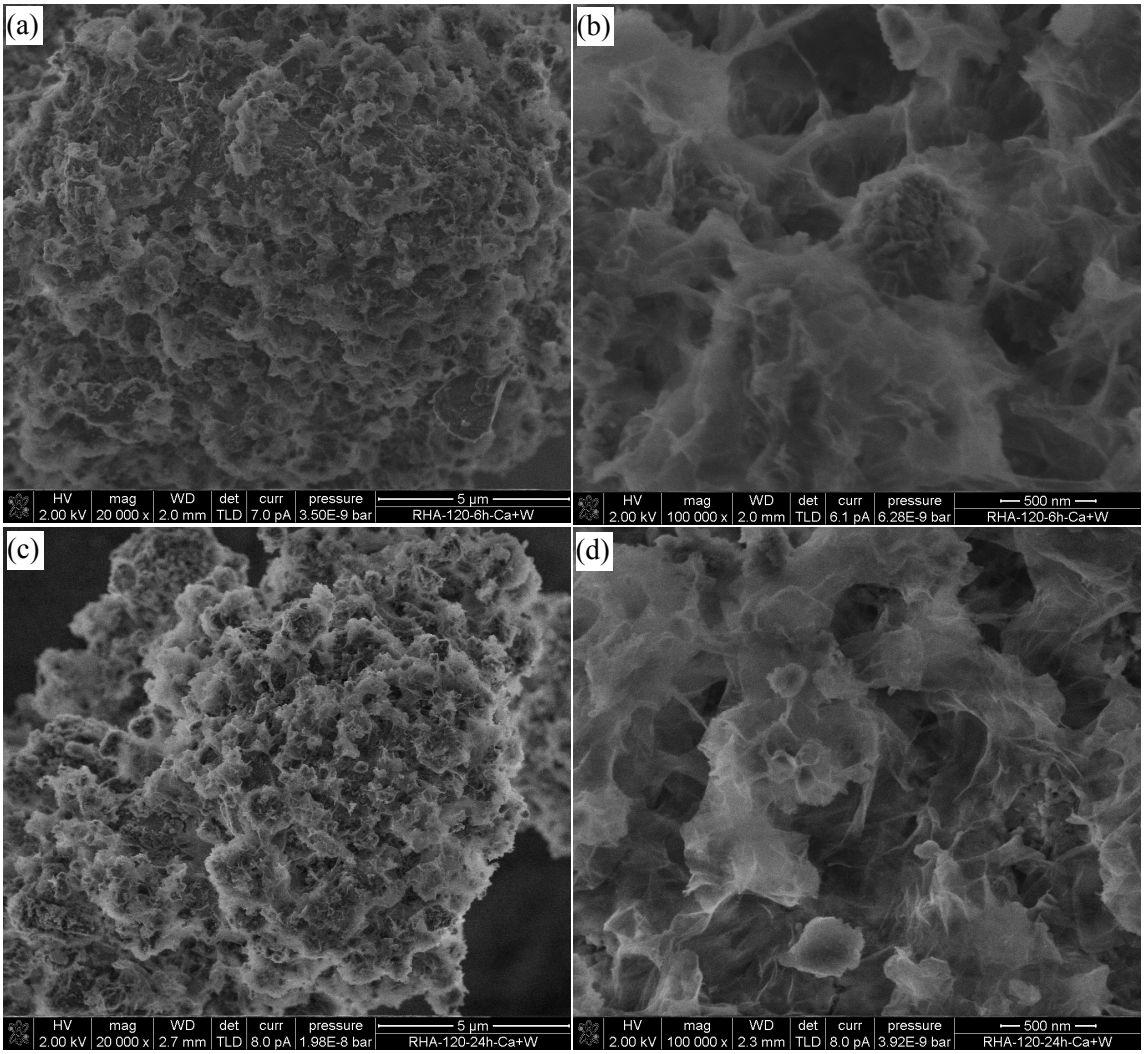

Figure 5.20. SEM images of RHA-120 hydrated in CH solution (l/s = 40 at 40°C) after: a) and b) 6 h; c) and d) 24 h showing foil-like C-S-H phases that envelop RHA particles.

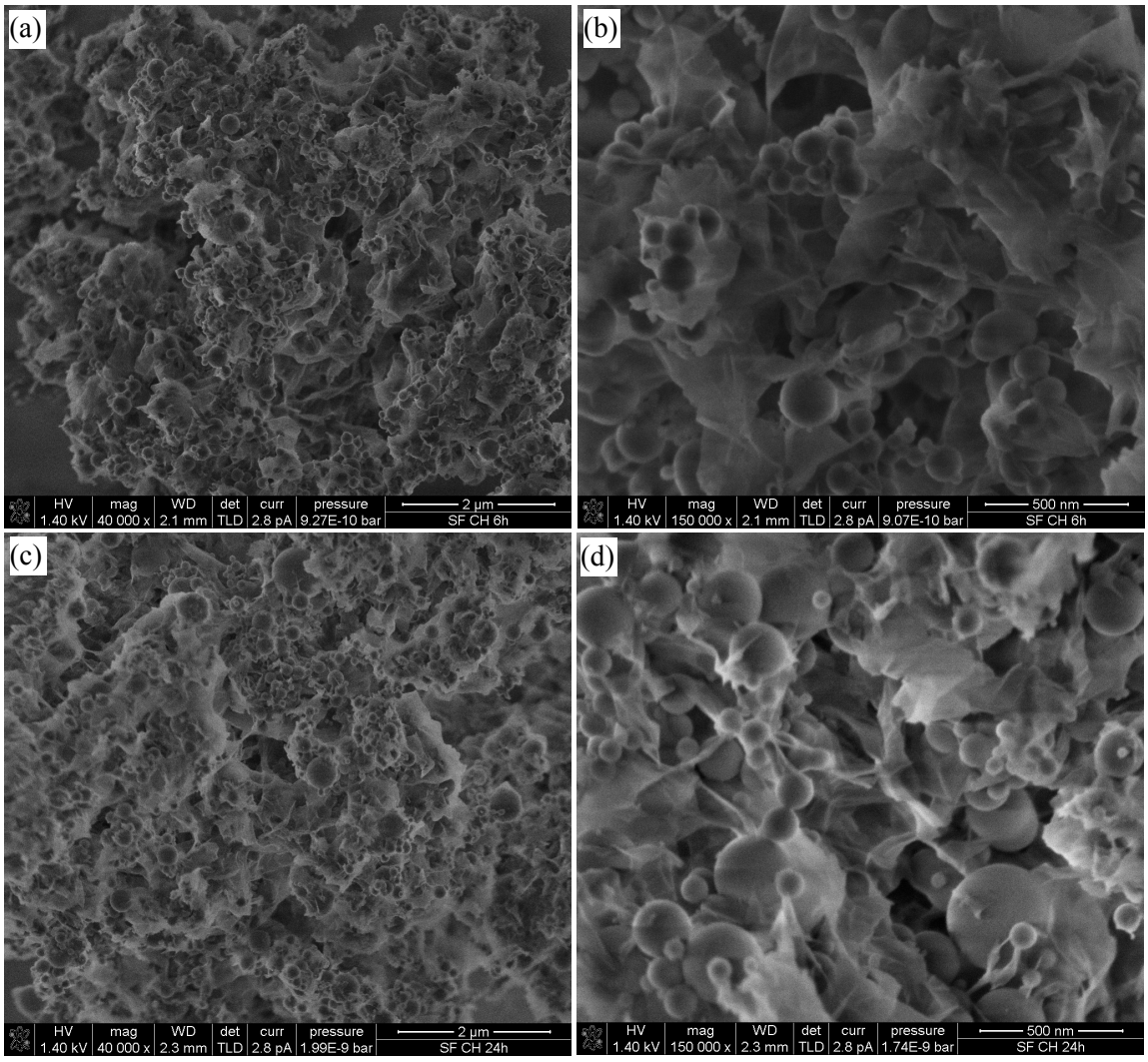

Figure 5.21. SEM images of SF hydrated in CH solution (l/s = 40 at 40°C) after: a) and b) 6 h; c) and d) 24 h showing foil-like hydration products on spherical SF particles.

The amount of hydrated phases was further quantified by thermal analysis (DTA-TG). The results of DTA-TG on the unhydrated and 6 h, respectively, 24 h hydrated pozzolans are shown from Figure 5.22 to Figure 5.24.

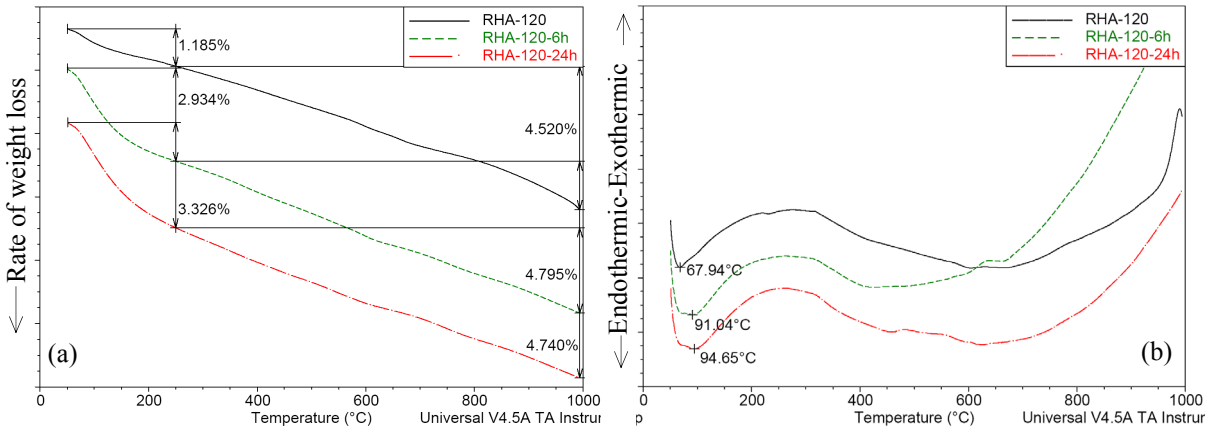

Figure 5.22. a) Weight loss and b) heat flow (DTA-TG) of unhydrated, respectively, RHA-120-6h and RHA-120-24h in CH solution (l/s = 40 at 40°C).

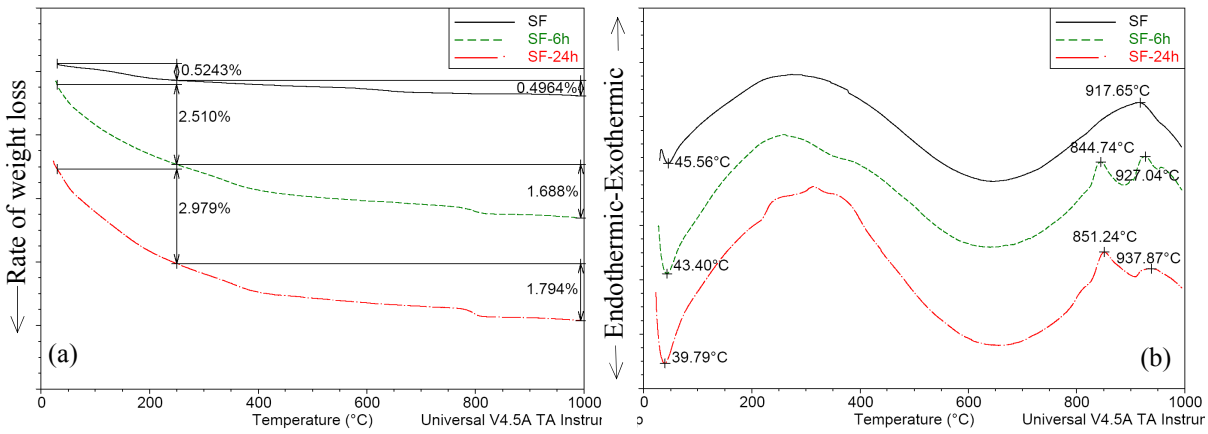

Figure 5.23. a) Weight loss and b) heat flow (DTA-TG) of Unhydrated, respectively, SF-6h and SF-24h in CH solution (l/s = 40 at 40°C).

Comparing the relative weight loss of SF and RHA in Figure 5.24a reveals that the relative weight loss of RHA always exceeds that of SF. The relative weight loss of the unhydrated RHA and SF occurs in the temperature range from 25 to 250°C by the removal of physically adsorbed water and from 250 to 1000°C by the continuous silanol group condensation and some elemental decompositions [137]. For RHA, comparing the relative weight loss of the unhydrated and hydrated RHA in the temperature range from 250 to 1000°C shows that the hydrated samples possess no significant increase in the weight loss (Figure 5.24a and b). Variations in the corrected relative weight loss of RHA are only obvious in the temperature range from 25 to 250°C (Figure 5.24b). This indicates that hydration products in the CH-RHA suspension as shown by SEM imaging in Figure 5.20 contain only weakly bound water. Comparing the corrected relative

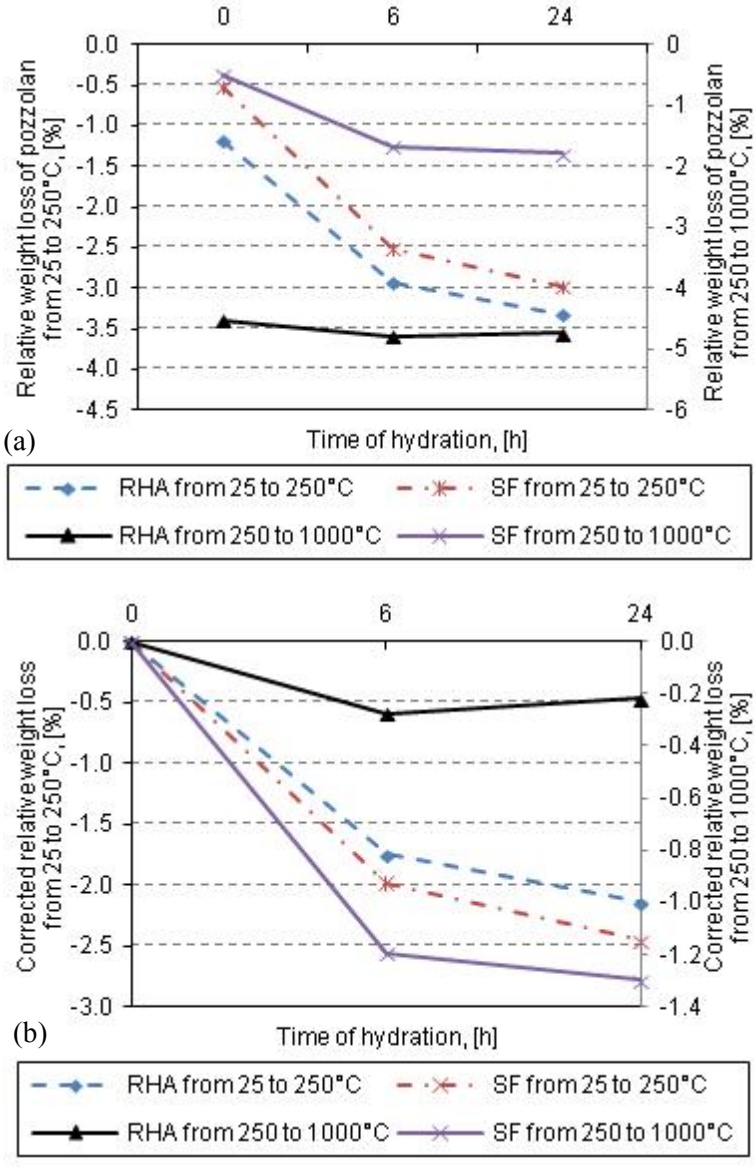

Figure 5.24. a) Relative weight loss and b) corrected relative weight loss from 25 to 250°C and from 250 to 1000°C of pozzolans in dependence with time of hydration (l/s = 40 at 40°C).

weight loss of RHA and SF from 25 to 250°C (Figure 5.24b) shows that the content of hydrated bound water, i.e. the degree of hydration of SF exceeds that of RHA.

Looking at the heat flow curves of RHA and SF in Figure 5.22b and Figure 5.23b, one can deduce clearly that no portlandite is contained in the hydrated samples. This indicates that the ratio of pozzolan to CH at the beginning is too high to induce portlandite precipitation.

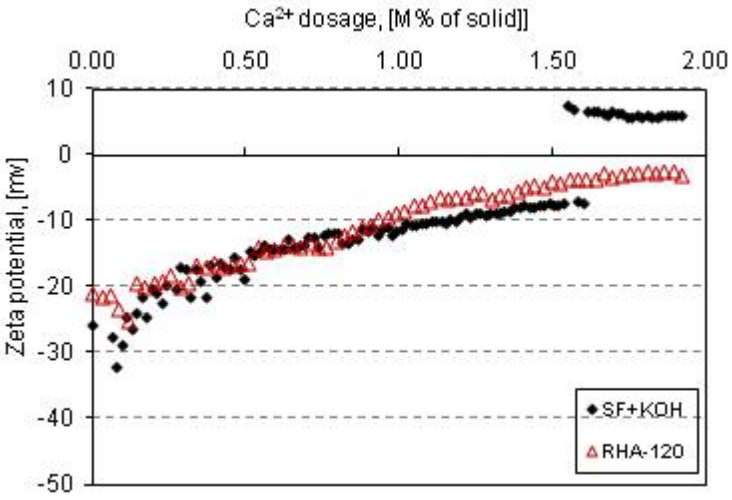

Figure 5.25. Zeta potential of pozzolan-water suspensions at pH about 9.5 with increasing Ca^{2+} ion concentration.

5.1.4. Zeta potential

The development of zeta potential of water-pozzolan suspensions at pH about 9.5 and 25°C with the increasing Ca^{2+} ion concentration is shown in Figure 5.25. The results show that the initial zeta potential of the water-pozzolan suspensions is a negative value. The initial zeta potential value is about -25 mV with the RHA-120 suspension and about -30 mV with the SF suspension. The increasing Ca^{2+} ion concentration clearly increases zeta potential of the suspensions until it reaches a stable state, which is characterized by the saturated adsorption of Ca^{2+} ion onto the particle surface. The equilibrium zeta potential value of the Ca^{2+} ion added suspension containing RHA is about -1.9 mV. There is no significant difference in zeta potential development between the suspension containing SF and the suspension containing RHA when the Ca^{2+} ion concentration increases up to about 1.6% referred to the weight of the pozzolan. Surprisingly, zeta potential of the suspension containing SF jumps from about -7 mV to +7 mV to get the equilibrium condition at the Ca^{2+} ion dosage about 1.6% (Figure 5.25). The reason of this sudden change is unclear. Plank et al. [91] measured the development of zeta potential of a SF-suspension at pH of 12.2, liquid to solid ratio of 5 during the increase of the Ca^{2+} ion concentration. The results showed that zeta potential of the SF suspension gradually increases from about -20 mV to +6 mV. The saturated adsorbed amount of Ca^{2+} (the equilibrium condition) is also about 1.6 to 2%.

5.1.5. Discussion

5.1.5.1. Effect of grinding on characteristics of RHA

The investigated RHA burned in the simple prototype incinerator has a very high amorphous silica content (Table 4.1 and Figure 4.2). The results by the BJH method test show that the pore size distribution in RHA particles is mainly from about 2 to 50 nm and the mean pore size of RHA is about 30 nm. This finding is confirmed by SEM images which show pore

diameter in range of 2-50 nm (Figure 5.6). That means this RHA is a kind of mesoporous amorphous siliceous material [205, 206].

During grinding, the mean particle size of RHA decreases (Figure 5.1, Figure 5.2 and Figure 5.3) involving the collapse of the porous structure of RHA particles. SEM imaging reveals macropores filled by small particles at intermediate grinding periods (Figure 5.5a). According to the BET and BJH methods, the BET-SSA and pore volume are affected by open pore volume and open pore structure of material [207]. Thus, the collapse of the macroporous structure and the filling of macropores will generally result in a reduction of open pore volume (Table 5.2) and a decrease in the BET-SSA (Figure 5.3 and Table 5.1) during grinding of RHA. However, fracturing of RHA particles also gives access to previously closed mesopores (Figure 5.4 to Figure 5.7). This effect can lead to the observed small increase of BET-SSA (Figure 5.3 and Table 5.1) and pore volume (Table 5.2) at the intermediate grinding stops (RHA-30 and RHA-45). Therefore, the general effects of grinding process on the SSA and pore volume of RHA can be displayed in Figure 5.7. The combination of enhancing (+) and reducing (-) effects (Figure 5.7) induces an increase or decrease of pore volume and BET-SSA of RHA at intermediate grinding periods. Thus, the different SSA changes during grinding in previous studies [36, 53, 60, 163] and in this study may result from the different porous structure of RHA samples.

5.1.5.2. Effect of RHA on cement system

The coarse RHA possesses a rough surface, high pore volume and therefore high BET-SSA and water absorption capacity. The coarse RHA decreases the packing density of granular mixture [39, 60]. Thus, addition of coarse RHA requires increased w/b and/or SP dosage to obtain the desired workability of the paste (Figure 5.8) or mortar (Figure 5.9). Furthermore, decreasing the BET-SSA of RHA by grinding will decrease the Ca^{2+} consumption in CH solution (Figure 5.14 and results of previous studies [53, 163]). In the present study, it was shown that the API and thus compressive strength is maximized for RHA at the intermediate grinding period (i.e. RHA-45, Figure 5.9). RHA-15 and RHA-45 have very similar BET-SSA values, but their MPS are 16.5 µm and 9.7 µm, respectively. The reason for the lower API/compressive strength of the mortar containing RHA-15 might be due to the presence of large RHA particles (Figure 5.2).

The CH consumption results indicate the pozzolanic reactivity of SF exceeds that of RHA-120 (Figure 5.10 and Figure 5.14). With super fine particles, SF induces the higher packing density of the granular mixture compared to RHA [60]. However, compressive strength of the mortar containing RHA-120 is comparable with that of the mortar containing SF (Figure 5.9). Therefore, it can be assumed that besides CH consumption, the API is strongly affected by the following parameters: 1) Water absorption capacity; 2) MPS- particle packing density. For RHA, due to its highly porous structure, water absorption is an important strength influencing parameter because it reduces the effective w/b and increases the pozzolanic reactivity. Because the porous structure of RHA stores water, RHA may partly play the role of an internal curing agent. This will be proven by test of the internal relative humidity in matrix containing RHA during hydration in Section 5.3.2.

All cement pastes containing pozzolanic admixtures reveal a slightly increased CH content after 7 to 91 days of hydration (Figure 5.10). This may be due to the limited content of the pozzolanic admixtures (i.e. 10 wt.-%). Thus, the uptake of CH released by cement clinker hydration is always incomplete. The results of CH content in the pastes containing pozzolan confirm previous findings that showed the increased reactivity of pozzolan under heat treatment [94, 96].

On the other hand, the cement hydration ceases in the reference heat treated paste at w/b of 0.22 after 7 days (Figure 5.10c and d). The results in Figure 5.10c and d also reveal that the addition of RHA or SF prolongs the hydration of cement in the heat treated paste at w/b of 0.22. The rate of the CH formation by cement hydration in this heat treated paste containing RHA is comparable to the CH consumption by the pozzolanic reaction. Contrary, in the heat treated paste containing SF, the formation of CH exceeds the consumption by the pozzolanic reaction. Based on the increased degree of cement hydration in RHA-blended matrices [48, 57], if the degree of cement hydration is at least similar in the RHA and SF-blended Portland cement pastes at the very low w/b and heat treatment, the pozzolanic reaction in the paste containing RHA continues longer than that in the cement paste containing SF under similar conditions. Pfeifer et al. [96] also observed that there is only a minor increase in the degree of SF hydration in the SF-blended Portland cement paste in UHPC subjected to heat treatment.

The importance of mesoporous structure of RHA on the pozzolanic reactivity is also evidenced by BSE imaging and EDX-mapping (Figure 5.11). The mesoporous structure of RHA particles absorbs free water and as a consequence it renders possible that calcium ions diffuse into internal parts of RHA particles. This facilitates the hydration products of the pozzolanic reaction to intergrow intensely with the cement matrix. Figure 5.11 indicates that the RHA particles are well-embedded in the cement matrix. A sharp boundary between RHA particle and the matrix is not observed on porous surface parts because of the gradual transition of Ca concentration from cement matrix into RHA particle (Figure 5.11b).

Therefore, the mesoporous structure of RHA provides several benefits: 1) The free water in the cement paste is reduced; 2) absorbed water is available for further cement hydration [48, 57]; 3) pozzolanic reactivity of RHA is increased; 4) compressive strength of the mortar is enhanced.

5.1.5.3. Pozzolanic reactivity of RHA in saturated CH solution

The variation in the electrical conductivity of the saturated CH solution after pozzolan addition mainly correlates with the pH value development and the decrease in Ca^{2+} concentration in the CH-pozzolan suspension. Due to the mesoporous structure, RHA particles strongly adsorb Ca^{2+} and OH^- during the initial hydration period (< 30 minutes, Figure 5.13, Figure 5.16 and Figure 5.18). It is similar to the known RHA adsorption characteristics for Cd(II), Ni(II) and Zn(II) [141] or $HSeO_3^-$ [161] ions from aqueous solution. Moreover, the Si concentration curves in the CH-SF and CH-RHA suspensions (l/s = 40, Figure 5.17) are similar to that of tricalcium silicate (C_3S) in water at l/s of 50 [208] or l/s of 500 [209]. Generally, hydration reactions of C_3S are regarded as dissolution-precipitation processes. For pozzolan, dissolution is known to be slow. It needs a certain time to dissolve

ions and to reach supersaturated and equilibrium conditions (Figure 5.17). Therefore, one has to argue whether the variation in the electrical conductivity before and after 2 minutes of hydration represents well the full pozzolanic reactivity of the pozzolan. The variation in the electrical conductivity during the first 2 min of hydration/dissolution is strongly affected by SSA and adsorptive capacity of the pozzolan (Figure 5.13, Figure 5.14 and Figure 5.16). Furthermore, because of the very high absorbing characteristics and water soluble alkalis of RHA, the corrected electrical conductivity of RHA still exceeds that of SF after 300 minutes of hydration. Thus, results of the present study point out that the electrical conductivity of the aqueous suspensions should be measured up to 360 minutes for evaluation of pozzolanic reactivity of the pozzolans. Then, it is possible to compare the pozzolanic reactivity of the different pozzolans.

Increased alkali content and thus pH value increases the amount of dissolved Si in the CH-SF+KOH suspension (Figure 5.17). Also, Si concentration in the system $CaO\text{-}SiO_2\text{-}NaOH\text{-}H_2O$ exceeds that in the system $CaO\text{-}SiO_2\text{-}H_2O$ [210]. However, for similar alkali content in the aqueous phase of the pozzolan suspensions, the Si concentration in the CH-RHA suspensions is still significantly higher than that in the CH-SF+KOH suspension (Figure 5.17). It was shown that the SSA of RHA is about 2-3 times higher than that of SF (Figure 5.14). The dissolution of silica is strongly influenced by surface structure of particles because the surface plays an important role influencing the binding or release of protons at Si-OH surface groups [211]. Hence, the solubility of silica is not only governed by alkali/pH concentration but also by the surface area of RHA particles.

After 60 and 90 min of hydration, the Si concentrations in the CH-SF suspension are almost similar (Figure 5.17). The Si concentration in the CH-RHA suspensions after 180 min hydration were also measured. A slight decrease in Si concentration in the RHA suspensions compared to after 90 min hydration was observed. Adding KOH to the CH-SF suspension increases pH value and the amount of dissolved Si in the CH-SF+KOH suspension. However, the Si concentrations in the CH-RHA suspensions are still significantly higher than that in the CH-SF+KOH suspension during the hydration time (Figure 5.17). With the different Si concentrations at both the highest concentration and after 90 min hydration of RHA and SF, the possible differences in pozzolanic reactivity of RHA and SF can be discussed herein based on the dynamic equilibrium between dissolution of reactant and precipitation of products:

1) If the solubility of precipitated products of RHA or SF is the same (the same Si concentration at the equilibrium), the equilibrium of the RHA-suspensions does not obtain after 90 min of hydration. The precipitation of products is hindered in RHA-suspensions compared with in SF-suspension. Hence, the amount of the reaction products formed during the pozzolanic reaction of the RHA samples is lower than that of the SF samples (Figure 5.24b) despite the very high supersaturated concentration of Si in the RHA-suspensions.

2) If the CH-pozzolan suspensions can be considered to be a local equilibrium after 90 min hydration (the Si concentration insignificantly reduces thereafter) with respect to the dissolution/precipitation, the equilibrium concentrations in the suspensions are different

(Figure 5.17). Hence, the solubility of precipitation products in the CH-RHA suspensions is higher than in the CH-SF suspension. Comparing with the highest Si concentration (supersaturated concentration), it is indicated that the driving force for precipitation of products in the CH-SF suspension is stronger than that in the CH-RHA suspensions [212, 213]. Hence, it also results in the higher amount of the reaction products formed during the pozzolanic reaction of the SF sample compared with that of the RHA sample (Figure 5.24b).

It can be seen that with both the discussed possibilities, the precipitation process of reaction products mainly controls the pozzolanic reaction between the pozzolan and portlandite, i.e. the precipitation of SF-suspension is more quickly and stronger than that of RHA-suspensions. Furthermore, the high absorption and alkali content of RHA strongly decrease the initial Ca^{2+} concentration in the suspension (Figure 5.18) which also affects the precipitation of the hydration products. It can be assumed that the differences in the SSA, alkali content and possible difference in nature of dissolved Si (Si-OH groups) between RHA and SF in portlandite solution will make dissolution and precipitation processes in the CH-pozzolan suspensions different. In this study, the precipitation and thus the pozzolanic reactivity of SF exceeds that of RHA in portlandite solution within 24 hours of hydration. It needs further study on the reasons of the difference in the precipitation of products and in the long term pozzolanic reactivity between RHA and SF in portlandite solution.

The heat flow (DTA) curves of the hydrated RHA samples are only different with that of the hydrated SF samples within the temperature range of 850-950°C (Figure 5.22b and Figure 5.23b). Combining this finding with the hydration products of the pozzolanic reaction observed by SEM investigation (Figure 5.20 and Figure 5.21) and the similar in chemical composition of RHA and SF (Table 4.1) it can be assumed that the pozzolanic reaction product of RHA or SF and CH is similar and can be described as a kind of C-S-H.

5.1.5.4. Evaluation pozzolanic reactivity of high specific surface area pozzolan

By comparing results of the present study it becomes obvious that different criterions to evaluate reactivity of pozzolans in different systems generate some contradictory results and conclusions. RHA and SF are characterized by a high amorphous silica content, high SSA, but different absorption and adsorption capacities. The correlation between results of compressive strength of mortar (Figure 5.9), portlandite content in cement pastes (Figure 5.10) and results of the calcium reduction rate, the electrical conductivity reduction rate [mS/cm·min] in the CH-pozzolan suspensions up to 210 min of hydration is herein discussed. Calculated Ca ion reduction rate and rate of reduction of the electrical conductivity are shown in Figure 5.26.

Obviously, from 30 to 90 min, the electrical conductivity reduction rate correlates with the Ca reduction rate in the CH-pozzolan suspensions (Figure 5.26). As discussed, the precipitation of the pozzolanic reaction in the CH-SF suspension is higher than that in the CH-RHA suspensions. As a result, the rate of reduction of the electrical conductivity of the CH-SF suspension from 30 to 210 min exceeds that of the CH-RHA suspensions (Figure 5.26), and hence the decrease in the electrical conductivity of the CH-SF suspension from 0 to 360 min exceeds that of the CH-RHA suspensions (Figure 5.14). Also, it was shown that the

pozzolanic reaction product content (i.e. the corrected relative weight loss) in the CH-SF suspension exceeds that of the CH-RHA suspension (Figure 5.24b). This means that the portlandite consumption capacity or pozzolanic reactivity of SF in the portlandite solution is higher than that of RHA. This result is in good agreement with the CH consumption of RHA and SF in cement pastes at the early age or high w/b (Figure 5.10). On the other hand, compressive strength of the mortars containing RHA is comparable or even higher than that of the SF mortar (Figure 5.9). Thus, it is once again shown that compressive strength of the RHA-modified mortars is governed not only by the CH consumption (i.e. degree of pozzolan hydration) but rather by the microstructural effects of the mesoporous RHA particles.

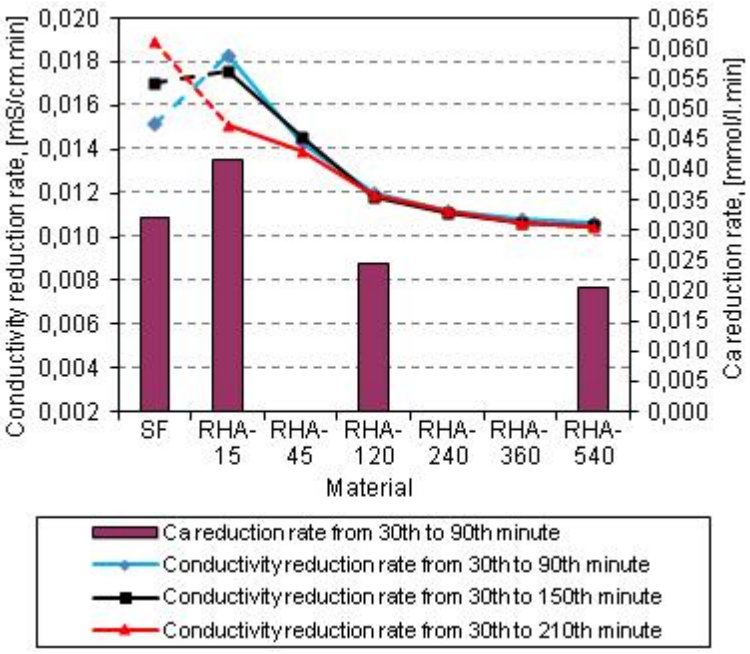

Figure 5.26. Electrical conductivity reduction rate and calcium concentration reduction rate of CH-pozzolan suspensions with l/s = 40 at 40°C.

The higher the SSA of RHA, the more the accelerated pozzolanic strength reactivity index (API) of RHA (i.e. compressive strength of the mortar containing RHA (Figure 5.9)) and the higher the electrical conductivity reduction rate of the CH-RHA suspension (Figure 5.26). Furthermore, the slope of the electrical conductivity curves shown in Figure 5.13 and Figure 5.16 does not significantly change. Electrical conductivity measurement (Figure 5.13, Figure 5.16 and Figure 5.26) revealed that pozzolanic reactivity of RHA exceeds that of SF at early period of hydration but the finding is reversed at extended periods of hydration. It is important to choose the suitable time to compare the pozzolanic reactivity between RHA and SF both characterized by huge specific surface area but different porous surface structure. To evaluate the effects of different grinding time of RHA on pozzolanic reactivity, the electrical conductivity reduction rate [mS/cm·min] from 30 to 90 min of the CH-RHA suspensions is suitable. The electrical conductivity reduction rate for hydration period from 30 to 210 min is a good criterion for comparing the pozzolanic reactivity of RHA and SF in this study.

5.1.5.5. Charged surface and ions adsorption of pozzolan

The initial zeta potential of the pozzolan suspensions (Figure 5.25) shows that both RHA and SF possess initially a negative surface charge which results from alkaline environment , i.e. OH^- groups present at the surface of SiO_2 in the solution [91]. The increase in the zeta potential value during the addition of Ca^{2+} ions indicates the adsorption of Ca^{2+} ions on the surface of pozzolan particles. It should be noted that zeta potential represents an electrical potential at a certain slipping plane around particles (the outer surface). However, RHA with its

mesoporous structure adsorbs Ca^{2+} ions not only on the outer surface but mainly on the inner surface which may not affect zeta potential value. RHA actually consumes significantly higher Ca^{2+} ions in solution than SF (Figure 5.18). Thus, the zeta potential measurements indicate that the totally different particle size and surface structure of pozzolans, i.e. RHA and SF mainly dictate their Ca adsorption behavior.

Furthermore, the electric potential measured in mV at the slipping plane distance from the particle surface (zeta potential) is also useful for understanding and predicting interactions between particles in suspension or in blended cement paste. The final zeta potential values in Figure 5.25 indicate that at alkaline pH and the given Ca concentration, SF possesses a positive electric potential but RHA has a negative electric potential at the slipping plane. Normally, cement particles and cement hydrates possess a positive electric potential which strongly adsorb superplasticizer. The different electric potential of RHA and SF may result in the differences in the adsorption of superplasticizer on particle surface [91], in particle dispersion effect (attractive or repulsive), in rheology [196] and hence in water/SP demand or workability of pozzolan-blended cement mixtures. It needs further detailed studies and discussion.

5.1.6. Concluding remarks

The following conclusions can be drawn from the results of the study in this section:

- The RHA burned in the simple incinerator is a mesoporous amorphous siliceous material. In general, the change of BET-SSA and pore volume of RHA during grinding results from the combination of the effects of crushing (particle size reduction), access to new open pores and the collapse of porous structure. The BET-SSA, pore volume and water absorption capacity of RHA is significantly higher than that of SF.
- With the mesoporous structure, ground RHA can absorb more water on internal and external surfaces which allows Ca^{2+} ions to diffuse into internal parts of particles. Thus, a continuous hydration of cement and a long lasting pozzolanic reaction of RHA are assured. It is shown that up to 91days even after the heat treatment, the pozzolanic reaction of RHA proceeds.
- In cementitious system, there is an optimum grinding time/fineness of RHA to produce the maximum compressive strength. SF possesses a higher water demand compared to RHA. With a suitable grinding time (i.e. RHA-45), the API of RHA exceeds that of SF in this study.
- At cement pastes (w/b = 0.484), the pozzolanic reactivity measured by CH consumption of SF exceeds that of RHA-120. The pozzolanic reactivity of SF in portlandite solution exceeds that of all RHA samples as shown by the electrical conductivity and the pozzolanic reaction product content of the CH-pozzolan suspension. Nevertheless, compressive strength of the RHA-120 and SF mortar at w/b 0.484 is almost the same. The API of RHA-45 even exceeds that of SF. This indicates that the pozzolanic reactivity is not the most important parameter for the compressive strength development. Rather the

microstructural effects such as the mesoporous structure and particle size of RHA can be considered as the important strength determining parameter.

- In portlandite solution, the mesoporous structure of RHA induces an increased Ca^{2+} adsorption capacity compared to SF, especially during the initial 30 min. The alkali content of the pozzolans significantly affects the variation in the electrical conductivity before and after the pozzolan addition, but not the electrical conductivity reduction rate.
- The pozzolanic reaction of RHA or SF in saturated $Ca(OH)_2$ solution at 40°C is a dissolution-precipitation process. In the saturated CH suspension, the Si concentration in aqueous phase of the suspension containing RHA exceeds that of the suspension containing SF. It was also shown that the Si concentration in the CH-pozzolan suspension depends not only on the alkali content of the suspension but to a larger extent on the SSA of the pozzolan.
- Pozzolanic reaction product with a microstructure comparable to C-S-H has been observed after 6 hours in the CH-RHA or CH-SF suspensions. The electrical conductivity reduction rate [mS/cm·min] in the CH-SF suspension from 30 to 210 min is higher than that in the CH-RHA suspensions. The amount of hydrate phases as determined by thermal analysis in the CH-SF suspension exceeds that of the CH-RHA suspension. This indicates that pozzolanic reactivity of SF is higher than that of RHA.
- The higher the SSA of RHA, the more the conductivity reduction rate in the CH-RHA suspension and the higher the compressive strength of the RHA-modified mortar.
- For evaluating the pozzolanic reactivity of RHA, measuring variation in the electrical conductivity after 2 minutes in the CH-pozzolan suspension is not appropriate. The reason lies in the high ion adsorption of RHA and the slow dissolution process involved. Thus, for the evaluation of the pozzolanic reactivity of RHA and SF, the electrical conductivity reduction rate [mS/cm·min] between 30 and 210 min is shown in this study to be an appropriate criterion.
- Different zeta potential of RHA and SF suspensions should be studied in detail by further studies to evaluate their surface chemistry which may affect superplasticizer adsorption and rheology of mineral-blended suspensions.

5.2. RHA as a pozzolanic admixture in UHPC

5.2.1. Preliminary test of UHPC

5.2.1.1. Compatibility between different SP and RHA-blended mixture

The compatibility between SP and UHPC containing RHA was assessed through the slump flow, loss of workability and compressive strength of UHPC-15%RHA at $W/F_v = 0.55$ (Table 4.6). The aim is to choose the best SP out of six different SP (Table 4.5). The best SP should allow the UHPC containing RHA to get the highest slump flow and compressive strength, and to have an acceptable loss of workability over a period of 45 minutes after mixing. The mixture used a saturation dosage of SP and samples were cast without vibration. The

saturation dosage of SP is the dosage of SP which begins to provide the highest mini-cone slump flow to the UHPC after mixing. RHA is RHA-540 (Table 5.1).

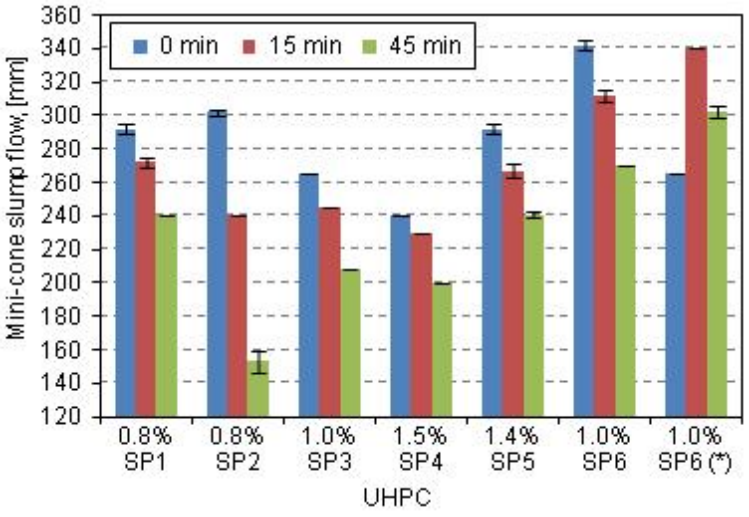

(*)- UHPC-15%SF

Figure 5.27. Flowability after mixing of UHPC-15% RHA with different superplasticizers at the saturation dosage.

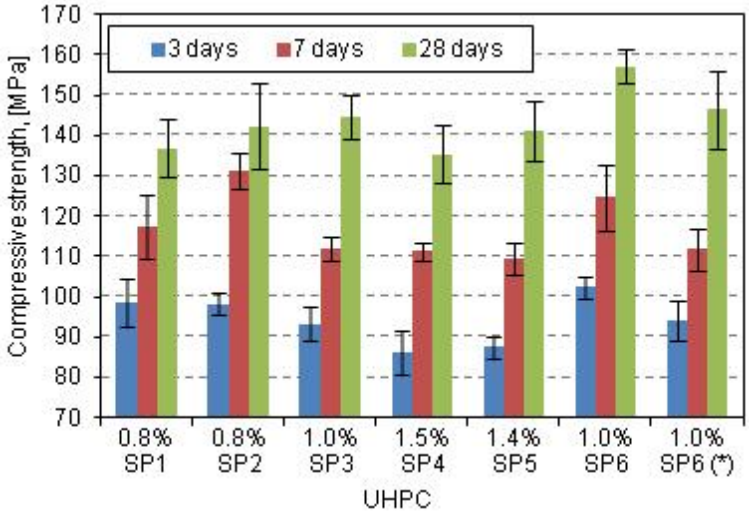

(*)- UHPC-15%SF

Figure 5.28. Compressive strength of UHPC-15% RHA with different superplasticizers.

Results in Figure 5.27 show that different SP obviously possess different saturation dosages and induce various slump flow values for the UHPC containing RHA. The mixture with SP6 has the highest flowability. SP4 possesses the lowest water reduction efficiency (i.e. the lowest flowability of the mixture). The saturation dosages of SP1 and SP5 are 0.8% and 1.4%, respectively. But the slump flow values of these mixtures at respective hydration periods are similar (Figure 5.27). All these mixtures decrease slump flow over a period of 45 minutes after mixing. In particular, flowability of the mixture containing SP2 significantly decreases after 45 min. Comparing the workability of the mixtures containing RHA or SF at 1% SP6 (Figure 5.27), the slump flow of UHPC-15%RHA obtains the maximum value after mixing, and then reduces constantly with time. Meanwhile, the slump flow of UHPC-15%SF initially increases during 15 min after mixing and then decreases (Figure 5.27).

Figure 5.28 displays the development of compressive strength of the UHPCs in dependence of SP-type from 3 to 28 days of hydration. Accompanying with the quick loss of workability (Figure 5.27), compressive strength of the UHPC using SP2 strongly develops at 7 days. The UHPC containing SP3, SP4 or SP5 possesses a low 3 d compressive strength. Although SP1 and SP5 produce the same workability for the UHPC at the saturation dosages (Figure 5.27), compressive strength of the UHPC containing SP1 is higher at the early ages but is similar at the age of 28 days compared with that of the mixture containing SP5 (Figure 5.28). SP6 enhances the strength of UHPC-15%RHA at all the ages of 3, 7 and 28 days compared to the other SP (except at 7 days of the mixture containing SP2). The strength of UHPC-15%RHA-

1%SP6 is slightly higher than that of UHPC-15%SF-1%SP6 at all the ages (Figure 5.28). SP6 provides the highest slump flow and compressive strength of UHPC-15%RHA at both 3 and 28 days of hydration. Hence, SP6 is the best SP and thus is chosen for following investigations.

5.2.1.2. Effect of GGBS, SP dosage, W/F$_v$ and vibration period on properties of UHPC

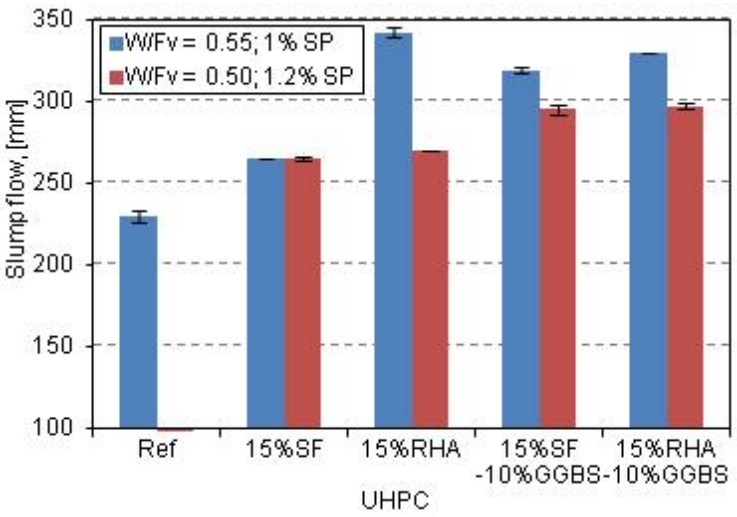

Figure 5.29. Effect of mineral admixture and water content on workability of UHPC.

At first, the combination between GGBS and RHA-540, respectively, SF, was tested to investigate the effect of GGBS and of water content on workability of UHPCs (Figure 5.29). The superplasticizer SP6 was applied for the mixtures. The test was examined at W/F$_v$ of 0.55 and 0.50 with an SP dosage of 1.0 and 1.2%, respectively. Flowability, air content and compressive strength of UHPCs containing RHA were evaluated in more detail in dependence of superplasticizer dosages, W/F$_v$ and vibration period to obtain the highest compressive strength of UHPC (Table 5.3). Mix proportions of the UHPCs can be found in Table 4.6. Slump flow and air content were examined after mixing.

Results in Figure 5.29 show that all of the UHPCs containing pozzolanic admixtures have a better workability than the reference mixtures (Ref). The reference mixtures are difficult to mix. At W/F$_v$ of 0.55 and 1.0% SP, the reference mixture quickly loses its flowability during 15 minutes after mixing. At W/F$_v$ of 0.50 and 1.2% SP, the reference mixture has no slump flow after mixing. The slump flow values of the RHA-blended mixtures exceed that of the SF-blended mixtures, respectively (Figure 5.29). When W/F$_v$ decreases from 0.55 to 0.50 and SP increases from 1.0 to 1.2%, the slump flow of UHPC-15%RHA dramatically decreases from 342 to 270 mm, while the flowability of UHPC-15%SF does not change. GGBS clearly enhances the slump flow of UHPC-15%SF. The combination of GGBS with RHA slightly decreases the slump flow of the mixture containing RHA at the high W/F$_v$ but improves the flowability for the low W/F$_v$ mixture (Figure 5.29).

Results in Table 5.3 indicate that the slump flow of the UHPCs containing RHA slightly decreases if the SP dosage is above the saturation dosage. GGBS also decreases the flowability of both mixtures at W/F$_v$ = 0.55 and 1.0 or 1.2% SP. If W/F$_v$ is reduced, the saturation dosage of SP of the mixture increases. Thus, the slump flow of the RHA-GGBS-blended UHPC at W/F$_v$ of 0.50 increases when the SP dosage increases (Table 5.3). The air content in the mixtures is strongly affected by W/F$_v$, SP content, mineral admixture and vibration. The lower the W/F$_v$, the less the workability and the more the air content in the mixture. Increasing the dosage of SP also results in the increased air content and hence the decreased compressive strength. GGBS improves the mixing behavior of the RHA-blended UHPC. After 30 seconds of vibration, the air content of the UHPCs containing RHA at W/F$_v$

of 0.55 is strongly decreased. At the lower W/F_v, the UHPCs need a suitable casting procedure to reduce the air content and hence to increase compressive strength of concrete. With W/F_v of 0.55, 1% SP and 30 sec vibration, the UHPCs containing RHA (without steel fibers) obtain a compressive strength over 160 MPa after 28 days of hydration at the normal treatment (Table 5.3).

Table 5.3. Effect of GGBS, SP, water content and vibration on properties of RHA-UHPC

UHPC		15%RHA		15%RHA-10%GGBS		15%RHA-10%GGBS	
W/F_v		0.55	0.55	0.55	0.55	0.50	0.50
SP [%]		1.0	1.2	1.0	1.2	1.0	1.2
Slump flow [mm]		342 (2.8)	332 (0)	330 (0)	322 (1.4)	285 (1.4)	297 (1.4)
Air content [%]	a	3.0	3.9	3.3	3.5	4.1	5.2
	b	1.3	1.9	1.1	1.5	3.0	3.4
Compressive strength at 28d [MPa]	a	157.2 (4.4)	136.6 (8.4)	138.8 (5.9)	152.4 (5.3)	150.0 (6.6)	133.4 (4.3)
	b	162.6 (2.1)	157.2 (6.5)	169.4 (6.0)	155.9 (5.5)	164.6 (4.1)	142.2 (4.8)

a- without vibration; b- with 30 sec vibration
The number in parentheses is the standard deviation of the test results.

5.2.1.3. Effect of fineness of RHA on properties of UHPC

The mean particle size of RHA-540 used in the previous experiments is very fine. It needs high energy and suitable equipment to grind RHA (Table 5.1). Furthermore, the investigations in Section 5.1 assumed that there is an optimum grinding time/fineness of RHA to provide the highest compressive strength for the mortar (Figure 5.9). Thus, RHA at five different grinding periods (i.e. RHA-540, RHA-360, RHA-240, RHA-120 and RHA-45) were used to produce UHPC-15%RHA-10%GGBS (Table 4.6) at W/F_v of 0.55 and 1% SP. The effect of RHA ground for different periods of time on the slump flow and compressive strength of UHPC was examined. Concrete samples were cast with 30 sec vibration. These investigations allow us to select the suitable grinding period of RHA to produce economical UHPC.

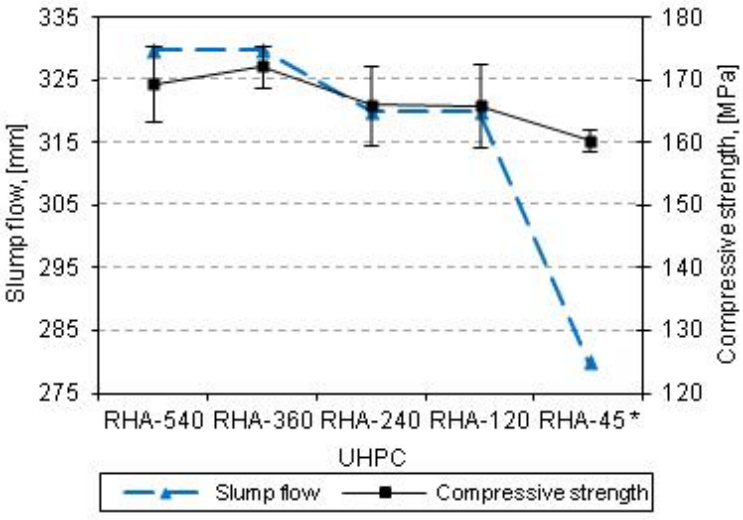

**- Mixing time is 20 minutes*

Figure 5.30. Effect of different RHA on slump flow and compressive strength of RHA-GGBS-blended UHPC.

Results in Figure 5.30 show that the UHPC containing RHA-45 needs a longer mixing time to get a fluid mixture. It has the lowest slump flow and compressive strength. All the other RHA samples are suitable for producing UHPC with a slump flow over 300 mm and a compressive strength over 165 MPa. The standard deviation of all slump flow measurements

is below 3 mm. The variation in workability and compressive strength of these UHPCs are insignificant (except slump flow of the mixture containing RHA-45, Figure 5.30). Thus, RHA-120 will be used to produce economical UHPC in further studies.

5.2.2. Optimization of mix proportions of UHPC containing RHA and GGBS

5.2.2.1. Influence of RHA content on properties of UHPC containing RHA

The slump flow and compressive strength of UHPC at 1% SP, W/F_v of 0.55 and different RHA contents are presented in Figure 5.31. GGBS was not used in these mixtures. Obviously, when the RHA content increases, the flowability of UHPC increases initially and then decreases. The standard deviation of all slump flow measurements is below 3 mm. The same effect is observed for RHA content on 28 d compressive strength (Figure 5.31). The slump flow and compressive strength of UHPC-15%RHA and UHPC-22.5%RHA are equal. When 1 vol.-% of steel fibers was used, 28 d compressive strength of both the UHPCs obtained 169.5 MPa with the same normal treatment condition. Therefore, 22.5 vol.-% RHA to partially replace cement can be considered as the optimal content in UHPC containing RHA.

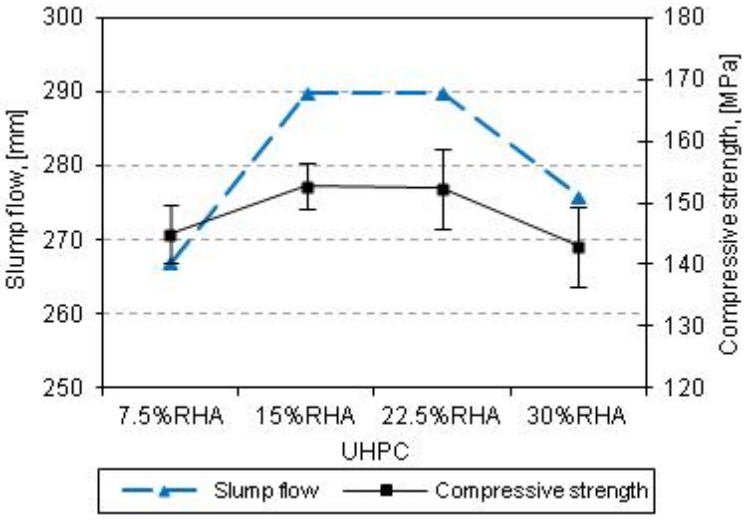

Figure 5.31. Effect of RHA-120 content on slump flow and compressive strength of RHA-blended UHPC.

5.2.2.2. Synergic effects of RHA, GGBS and SP on properties of UHPC

Design of combined mixture-process model

The total volume of the cementitious materials (i.e. cement, GGBS and RHA), the volume of the other components of UHPC at W/F_v of 0.55 as well as the mixing procedure, casting, treatment condition and test methods are kept in constant for all of the mixtures in this investigation. The pozzolans (GGBS and RHA) partially replace cement in volume. Because SP dosage is as dry weight referred to the amount of the cementitious materials and the change of SP dosage is very small, the change of SP dosage is ignored in calculation of mix proportions. Hence, the SP dosage (process variable: D) is independent with the cementitious material content (the component variables: A, B, C). It is a three-component mixture with one process variable experiment [197]. Based on the results of the preliminary tests in Section 5.2.1, the range of the process variable, $0.8\% \leq D \leq 1.2\%$ is selected. The mixture constraints for the binder components (A, B, C) are also chosen:

$$A + B + C = 100\%$$

$$47.5 \text{ vol.-\%} \leq \text{A-Cement} \leq 82.5 \text{ vol.-\%}$$

$$7.5 \text{ vol.-\%} \leq \text{B-RHA} \leq 22.5 \text{ vol.-\%}$$

$$10 \text{ vol.-\%} \leq \text{C-GGBS} \leq 30 \text{ vol.-\%}$$

The D-optimal design with a combined mixture-process model is chosen. It is assumed that combined quadratic × quadratic models would be satisfactory to represent the effects of the mixture components and the process variable on flowability (R_1) and compressive strength (R_2) responses. The complete combined quadratic × quadratic model has 18 parameters (Equation 5.1). The experiment plan which is designed by the D-optimal of the Design-Expert 8 software has 28 runs including 23 points at three levels of the process variable (0.8, 1.0 and 1.2%) with 5 replicated runs to provide an estimate of pure error, and 5 points at D = 0.9 and 1.1% to estimate the lack of fit (Figure 5.32 and Table 5.4). The typical mix proportions of mixtures at W/F_v of 0.55 can be found in Table 4.6. The complete combined quadratic × quadratic model of three-component mixture with one process variable is:

$$R = f(A, B, C, D) = \beta_1 A + \beta_2 B + \beta_3 C + \beta_{12} AB + \beta_{13} AC + \beta_{23} BC + \alpha_{11} AD + \alpha_{21} BD + \alpha_{31} AD + \alpha_{121} ABD + \alpha_{131} ACD + \alpha_{231} BCD + \delta_{111} AD^2 + \delta_{211} BD^2 + \delta_{311} CD^2 + \delta_{1211} ABD^2 + \delta_{1311} ACD^2 + \delta_{2311} BCD^2 \quad (5.1)$$

where: β_1, β_2, β_3 are the linear coefficients; β_{12}, β_{13}, β_{23} are the interactions of the mixture components; α_{11}, α_{21}, α_{31}, α_{121}, α_{131}, α_{231} are the interactions of the mixture components and the linear process variable; and δ_{111}, δ_{211}, δ_{311}, δ_{1211}, δ_{1311}, δ_{2311} are the interactions of the mixture components and the quadratic process variable.

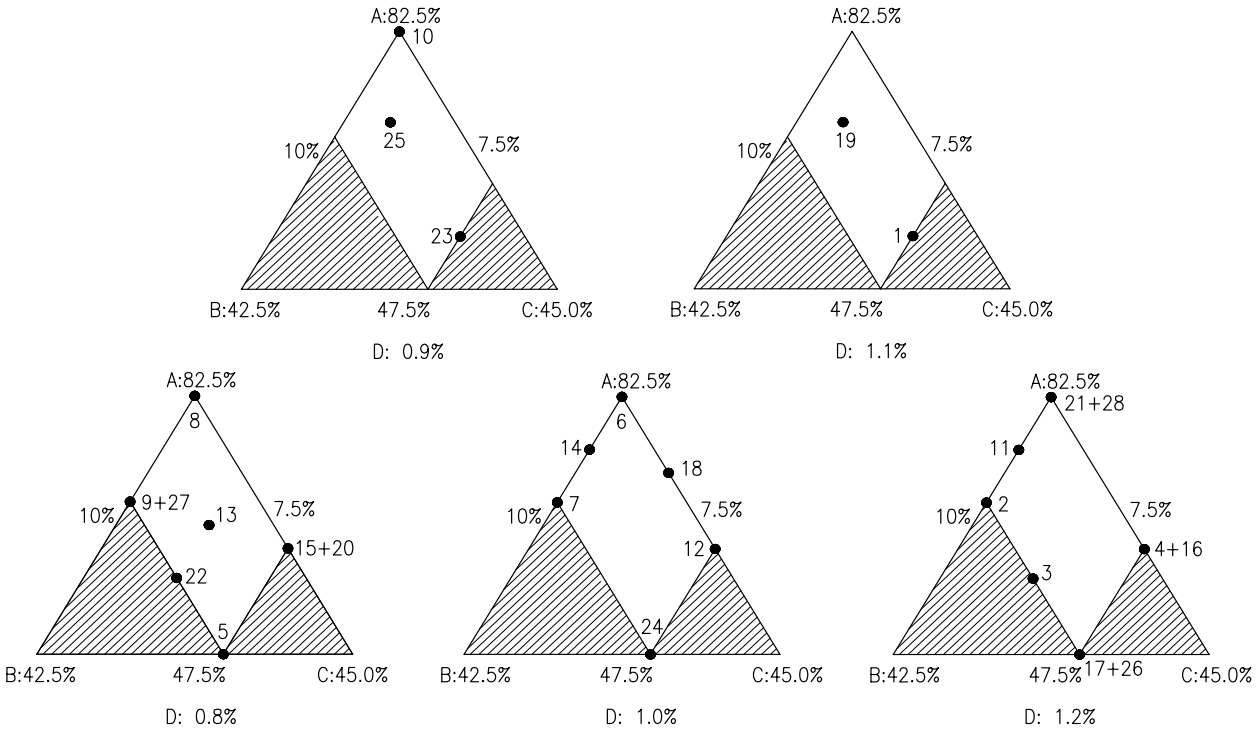

Figure 5.32. Twenty-eight-run D-optimal design. Points with a (+) indicate replicates.

Table 5.4. Twenty-eight-run D-optimal design with data

Run	Cement A [%]	RHA-120 B [%]	GGBS C [%]	SP D [%]	Experimental		Predicted		Ratio	
					R_1 [mm]	R_2 [MPa]	R_1* [mm]	R_2* [MPa]	R_1*/R_1	R_2*/R_2
1	55.0	15.0	30.0	1.1	347	159.9	347.1	158.9	1.0004	0.9934
2	67.5	22.5	10.0	1.2	324	149.4	324.6	149.5	1.0018	1.0004
3	57.5	22.5	20.0	1.2	336	152.3	335.0	151.9	0.9969	0.9973
4	62.5	7.5	30.0	1.2	341	156.8	339.5	155.5	0.9955	0.9918
5	47.5	22.5	30.0	0.8	343	154.2	342.4	154.0	0.9981	0.9989
6	82.5	7.5	10.0	1.0	321	158.7	318.6	158.6	0.9927	0.9996
7	67.5	22.5	10.0	1.0	316	161.5	316.7	161.3	1.0021	0.9987
8	82.5	7.5	10.0	0.8	295	158.3	294.4	158.3	0.9978	1.0000
9	67.5	22.5	10.0	0.8	306	154.8	303.7	155.3	0.9923	1.0030
10	82.5	7.5	10.0	0.9	307	159.8	310.0	160.0	1.0097	1.0011
11	75.0	15.0	10.0	1.2	320	155.8	318.8	155.7	0.9964	0.9992
12	62.5	7.5	30.0	1.0	349	156.8	347.6	157.3	0.9959	1.0032
13	65.0	15.0	20.0	0.8	338	165.2	339.2	165.3	1.0037	1.0005
14	75.0	15.0	10.0	1.0	320	164.6	320.3	164.5	1.0008	0.9991
15	62.5	7.5	30.0	0.8	351	161.2	349.8	161.1	0.9965	0.9991
16	62.5	7.5	30.0	1.2	338	154.4	339.5	155.5	1.0044	1.0092
17	47.5	22.5	30.0	1.2	346	141.0	348.7	142.0	1.0079	1.0073
18	72.5	7.5	20.0	1.0	329	155.1	330.6	154.5	1.0048	0.9963
19	70.0	15.0	15.0	1.1	323	159.0	325.1	160.3	1.0065	1.0084
20	62.5	7.5	30.0	0.8	349	161.0	349.8	161.1	1.0022	1.0003
21	82.5	7.5	10.0	1.2	314	150.0	315.2	147.0	1.0039	0.9803
22	57.5	22.5	20.0	0.8	330	157.0	330.3	157.1	1.0010	1.0009
23	55.0	15.0	30.0	0.9	351	162.1	353.3	162.3	1.0066	1.0014
24	47.5	22.5	30.0	1.0	349	155.3	348.3	155.5	0.9981	1.0014
25	70.0	15.0	15.0	0.9	331	162.7	326.1	162.4	0.9852	0.9979
26	47.5	22.5	30.0	1.2	351	142.7	348.7	142.0	0.9935	0.9953
27	67.5	22.5	10.0	0.8	301	155.7	303.7	155.3	1.0088	0.9972
28	82.5	7.5	10.0	1.2	316	144.2	315.2	147.0	0.9975	1.0197

Statistical analysis

The 28 designed mixtures of UHPC in Figure 5.32 and Table 5.4 were mixed and tested the slump flow and 28 d compressive strength. The 28-designed run data is analyzed by Design-Expert 8. The first step in the analysis is to identify a suitable model. Even though the design selected combined quadratic × quadratic models, other models may be suggested by the software to have a better fitness for the experimental data. With the input data, the fit summary of the combined mixture-process model suggests the combined quadratic × quadratic models against other models, e.g. quadratic × linear, quadratic × cubic… for both of the responses. Thus, the models chosen to design the experiment plan for the responses are good.

The complete models are as follows:

R_1 (flowability) = - 11.54A - 66.55B - 76.76C + 1.21AB + 1.54AC + 1.68BC + 26.72AD + 98.73BD + 154.33CD - 1.85ABD - 2.90ACD - 2.75BCD - 12.12AD^2 - 32.59BD^2 - 71.62CD^2 + 0.70ABD^2 + 1.34ACD^2 + 1.10BCD^2 (5.2)

R_2 (strength) = - 7.22A - 72.13B - 105.33C + 0.90AB + 1.81AC + 2.34BC + 18.43AD + 141.45BD + 222.87CD - 1.72ABD - 3.79ACD - 4.69BCD - 9.67AD^2 - 73.05BD^2 - 113.89CD^2 + 0.90ABD^2 + 1.94ACD^2 + 2.38BCD^2 (5.3)

Table 5.5. ANOVA for the complete combined quadratic × quadratic model of the workability response

Source	Sum of squares	df	Mean square	F value	p-value Prob > F	
Model	7499.22	17	441.13	47.62	< 0.0001	Significant
Linear mixture	*6387.42*	*2*	*3193.71*	*344.77*	*< 0.0001*	
AB	*12.19*	*1*	*12.19*	*1.32*	*0.2779*	
AC	*7.11*	*1*	*7.11*	*0.77*	*0.4015*	
AD	*319.27*	*1*	*319.27*	*34.47*	*0.0002*	
BC	*3.15*	*1*	*3.15*	*0.34*	*0.5726*	
BD	*65.47*	*1*	*65.47*	*7.07*	*0.0240*	
CD	*2.67*	*1*	*2.67*	*0.29*	*0.6034*	
ABD	*50.10*	*1*	*50.10*	*5.41*	*0.0424*	
ACD	*32.80*	*1*	*32.80*	*3.54*	*0.0893*	
BCD	*64.70*	*1*	*64.70*	*6.98*	*0.0246*	
AD^2	*173.72*	*1*	*173.72*	*18.75*	*0.0015*	
BD^2	*0.16*	*1*	*0.16*	*0.018*	*0.8972*	
CD^2	*10.00*	*1*	*10.00*	*1.08*	*0.3233*	
ABD^2	*1.41*	*1*	*1.41*	*0.15*	*0.7048*	
ACD^2	*17.77*	*1*	*17.77*	*1.92*	*0.1962*	
BCD^2	*2.81*	*1*	*2.81*	*0.30*	*0.5940*	
Residual	92.63	10	9.26			
Lack of fit	*59.13*	*5*	*11.83*	*1.77*	*0.2740*	*Not significant*
Pure error	*33.50*	*5*	*6.70*		SD	3.04
Corrected total	7591.86	27			Mean	330.07
R-Squared	0.9878	Adj R-Squared		0.9671	CV %	0.92
Pred R-Squared	0.8206	Adeq Precision		24.161	PRESS	1362.10

With: df- degrees of freedom; SD- standard deviation; CV- cofficient of variation; Adj- adjusted; Pred- predicted; Adeq- adequate; A- cement; B- RHA; C- GGBS; D- SP.

The adequacy of the complete regression models (Equations 5.2 and 5.3) is assessed by using some standards. Firstly, the analysis of variance (ANOVA) is used to check the significance of the models. Both of the models are significant. Their lacks of fit are not significant (Table 5.5 and Table 5.6). The adjusted R-squared and the predicted R-squared are 0.9671, respectively, 0.8206 with the slump flow response (Table 5.5), and are 0.9301, respectively, 0.8204 with the compressive strength response (Table 5.6). Hence, these models are adequate. Some of the coefficients in the complete models (Equations 5.2 and 5.3) are insignificant and could be eliminated (i.e. values of "Prob > F", less than 0.05, in Table 5.5

and Table 5.6, indicate the model terms are significant). In this case, there is no advantage to the reduced models because the adjusted R-squared is only slightly changed. Moreover, the interactions should not be removed in the combined mixture-process model, especially with the combined quadratic × quadratic model [197, 214]. Therefore, the complete models in Equations 5.2 and 5.3 should be used. Several techniques in the diagnostic tool of the Design-Expert 8 software have been also used to check the model's adequacy (Figure 5.33 and Figure 5.34). The predicted data calculated from Equations 5.2 and 5.3 and the ratio between predicted and experimental data are also given in Table 5.4. These indicate that the fitness of the complete models is adequate and these models can be used for further navigations.

Table 5.6. ANOVA for the complete combined quadratic × quadratic model of the compressive strength response

Source	Sum of squares	df	Mean square	F value	p-value Prob > F	
Model	994.12	17	58.48	22.12	< 0.0001	Significant
Linear mixture	*69.05*	*2*	*34.52*	*13.06*	*0.0016*	
AB	*36.36*	*1*	*36.36*	*13.75*	*0.0040*	
AC	*13.08*	*1*	*13.08*	*4.95*	*0.0503*	
AD	*93.56*	*1*	*93.56*	*35.39*	*0.0001*	
BC	*3.27*	*1*	*3.27*	*1.24*	*0.2918*	
BD	*1.28*	*1*	*1.28*	*0.48*	*0.5028*	
CD	*5.86*	*1*	*5.86*	*2.22*	*0.1675*	
ABD	*1.52*	*1*	*1.52*	*0.57*	*0.4661*	
ACD	*5.37*	*1*	*5.37*	*2.03*	*0.1846*	
BCD	*1.11*	*1*	*1.11*	*0.42*	*0.5312*	
AD^2	*32.11*	*1*	*32.11*	*12.15*	*0.0059*	
BD^2	*4.95*	*1*	*4.95*	*1.87*	*0.2013*	
CD^2	*22.93*	*1*	*22.93*	*8.67*	*0.0147*	
ABD^2	*2.36*	*1*	*2.36*	*0.89*	*0.3666*	
ACD^2	*37.46*	*1*	*37.46*	*14.17*	*0.0037*	
BCD^2	*13.17*	*1*	*13.17*	*4.98*	*0.0497*	
Residual	26.43	10	2.64			
Lack of fit	*4.10*	*5*	*0.82*	*0.18*	*0.9569*	*Not significant*
Pure error	*22.34*	*5*	*4.47*		SD	1.63
Corrected total	7591.86	27			Mean	156.04
R-Squared	0.9741	Adj R-Squared		0.9301	CV %	1.04
Pred R-Squared	0.8204	Adeq Precision		17.838	PRESS	183.24

With: df- degrees of freedom; SD- standard deviation; CV- cofficient of variation; Adj- adjusted; Pred- predicted; Adeq- adequate; A- cement; B- RHA; C- GGBS; D- SP.

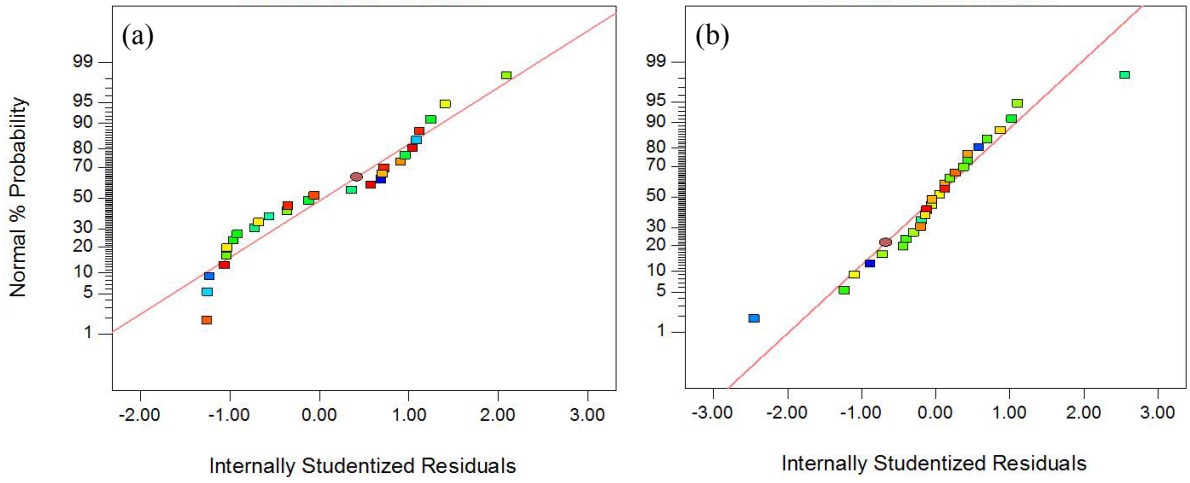

Figure 5.33. Normal plot of residuals: a) the workability response; b) the compressive strength response.

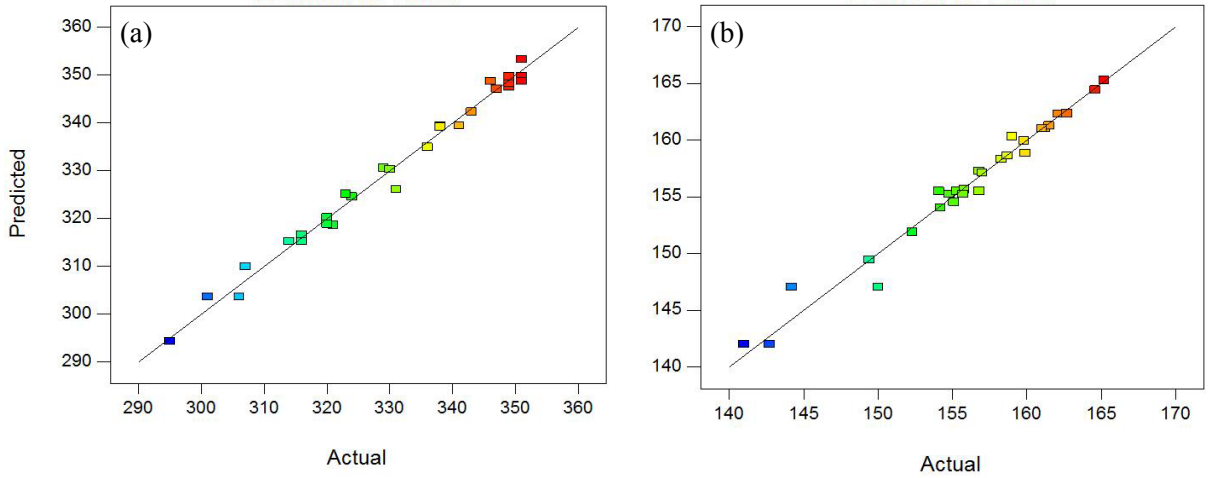

Figure 5.34. Predicted versus actual results: a) the workability response; b) the compressive strength response.

Influence of cementitious materials and SP dosage on the flowability of UHPC

To interpret the influence of the cementitious materials and the SP dosage on the mini-cone slump flow of UHPC, 3D response surface and contour plots of the workability response in dependence of the variables at three levels of SP dosage or at three different contents of GGBS have been produced (Figure 5.35 and Figure 5.36).

Results in Figure 5.35 show that increasing the GGBS content strongly improves the workability of UHPC at all levels of RHA content and SP dosage. At the low SP dosages (Figure 5.35a, b), the flowability of UHPC initially increases and then decreases when the RHA content increases. It is similar to the effect of the RHA content on the workability of UHPC containing RHA at 1.0% SP (Figure 5.31). The effect of the RHA content on the workability of RHA-GGBS-blended UHPC (Figure 5.35) is minor compared with RHA-blended UHPC (Figure 5.31). However, at the high SP dosage (1.2%, Figure 5.35c), increasing the RHA content slightly increases the slump flow of UHPC. The impact of the different cementitious materials on the flowability of UHPC at different dosages of SP is illustrated by how the shape and the pace of the contours change (Figure 5.35).

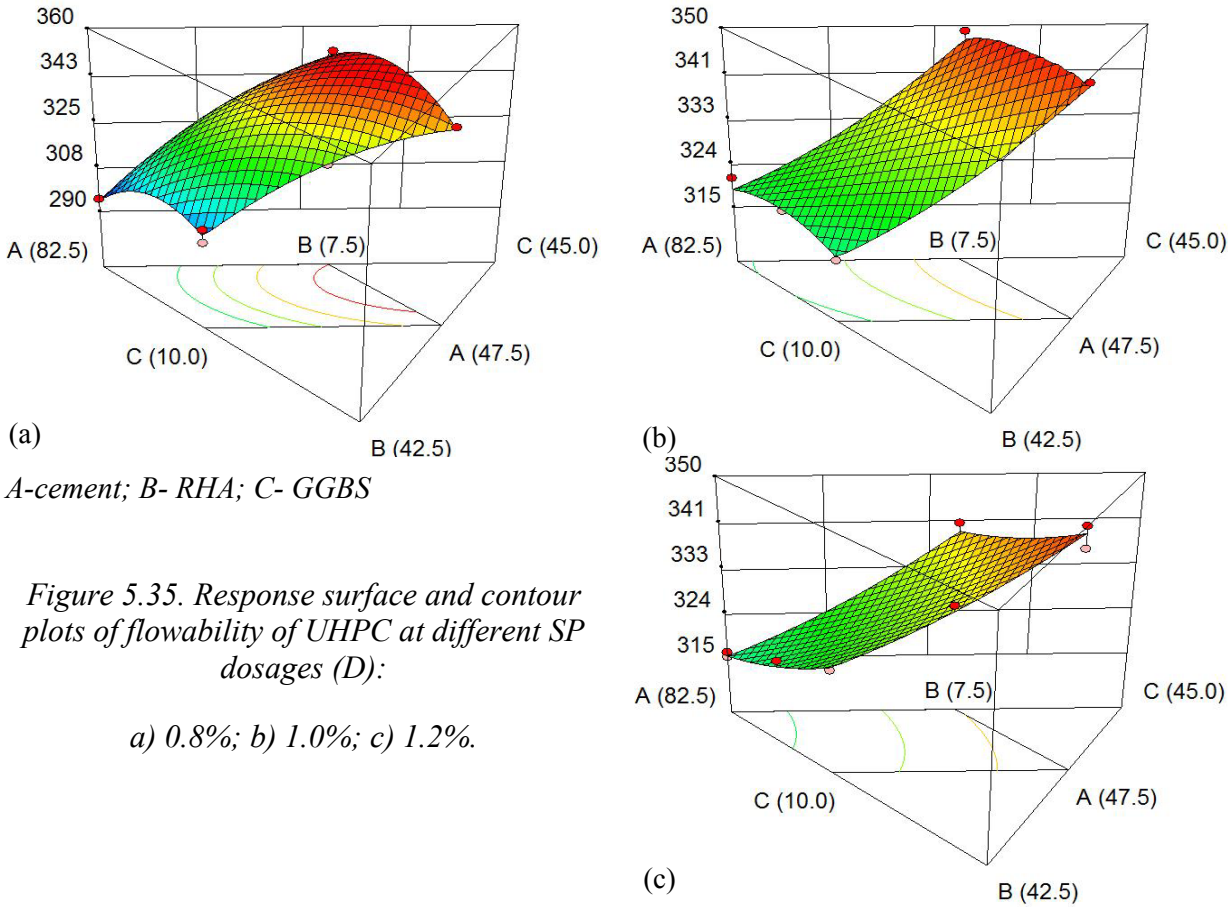

A-cement; B- RHA; C- GGBS

Figure 5.35. Response surface and contour plots of flowability of UHPC at different SP dosages (D):

a) 0.8%; b) 1.0%; c) 1.2%.

The effect of SP dosage on the flowability of UHPC is mainly influenced by the content of GGBS and RHA to partially replace cement (Figure 5.36). At the low GGBS and RHA content (Figure 5.36a), the flowability of UHPC increases initially and then decreases when the SP dosage increases. At the increased RHA contents, increasing the amount of SP results in the improved workability of UHPC. At the higher contents of GGBS (Figure 5.36b, c), increasing the SP dosage still improves the workability of UHPC containing high RHA content. However, increasing SP dosage constantly decreases the flowability of UHPC containing lower RHA content. These results assume that GGBS decreases and RHA increases the saturation dosage of SP in UHPC. The slump flow of UHPC reduces when the SP dosage is higher than the saturation dosage. This is consistent with the flowability results in the preliminary tests (Table 5.3). With the aim to obtain the maximum slump flow of UHPC, it needs adjusting the variables to a high content of GGBS as well as a low dosage of SP in combination with a moderate content of RHA (Figure 5.36c).

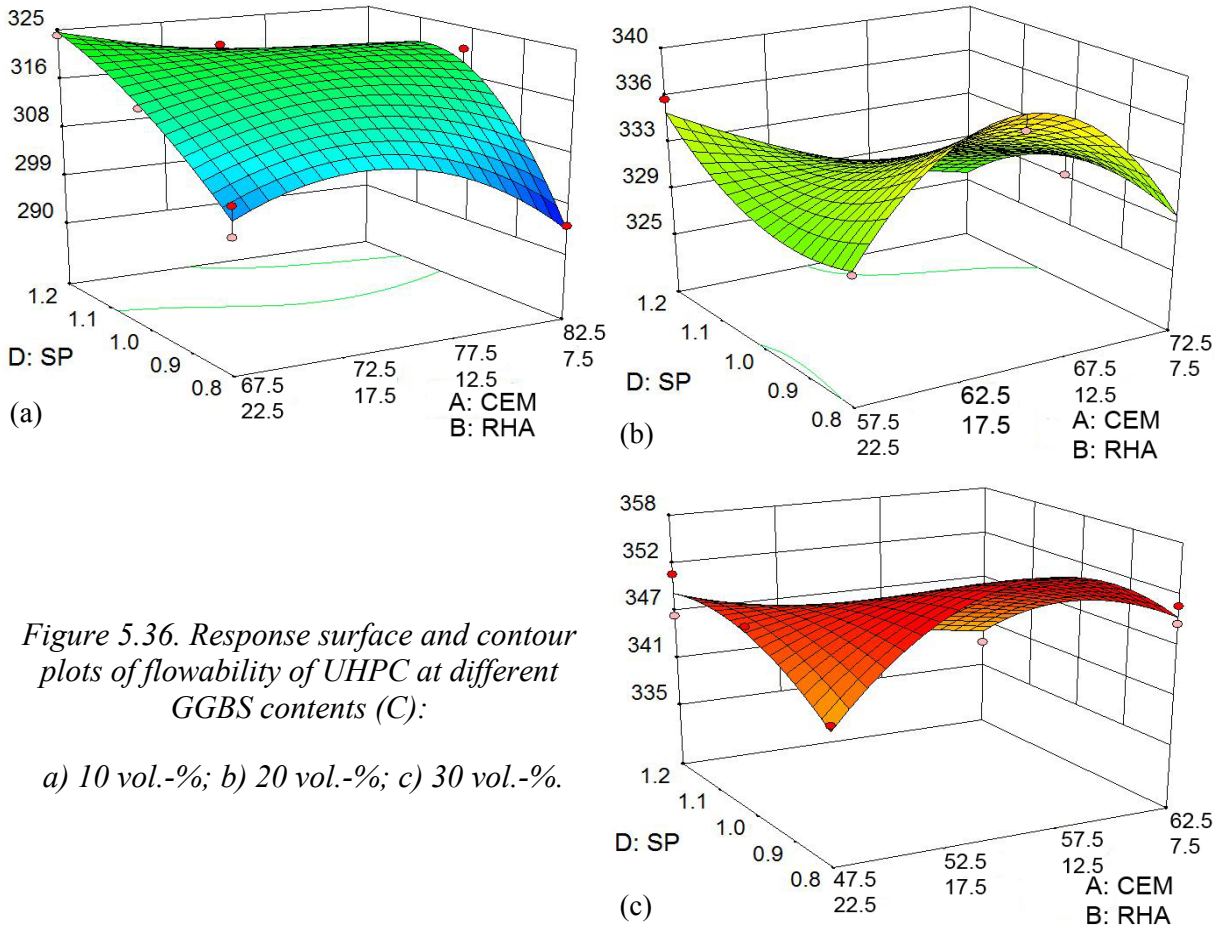

Figure 5.36. Response surface and contour plots of flowability of UHPC at different GGBS contents (C):

a) 10 vol.-%; b) 20 vol.-%; c) 30 vol.-%.

Influence of cementitious materials and SP dosage on compressive strength of UHPC

Similar to the workability response, 3D response surface and contour plots of the compressive strength response versus the variables at three levels of SP dosage or at three different contents of GGBS are also presented (Figure 5.37 and Figure 5.38).

Results in Figure 5.37 illustrate that there is an optimized content of RHA which enables UHPC containing GGBS to obtain the highest compressive strength. This result is consistent with the effect of RHA content on compressive strength of UHPC containing RHA in Figure 5.31. The effect of GGBS content on compressive strength is mainly governed by SP dosage and vice versa. At the SP dosage of 0.8% and 1.2% (Figure 5.37a, c), increasing the amount of GGBS initially increases and then decreases compressive strength. This change is contrary at the SP dosage of 1% (Figure 5.37b). The reason for the difference in the effect of GGBS content on compressive strength of UHPC at 1% SP is unclear.

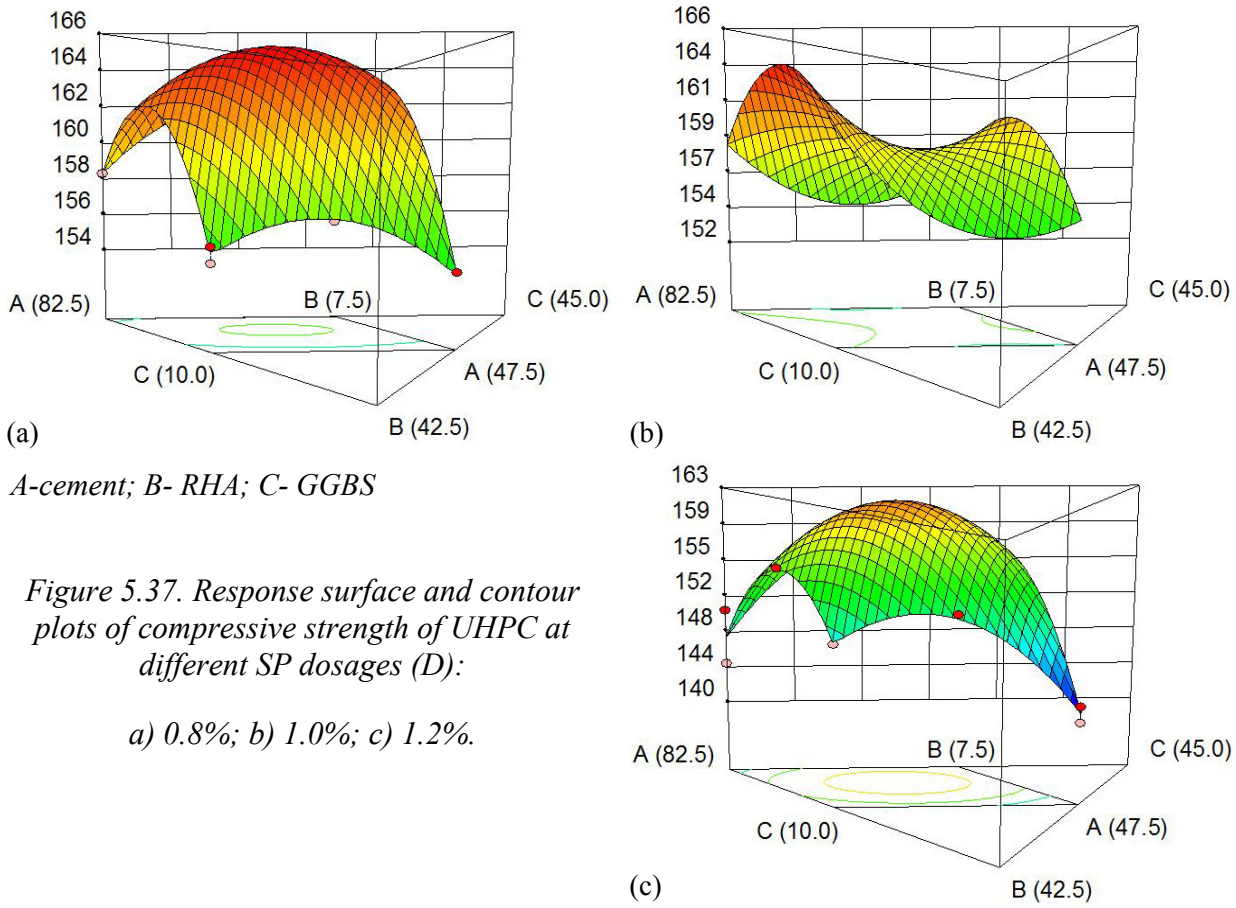

A-cement; B- RHA; C- GGBS

Figure 5.37. Response surface and contour plots of compressive strength of UHPC at different SP dosages (D):

a) 0.8%; b) 1.0%; c) 1.2%.

It is shown in Figure 5.38 that the effect of SP dosage on compressive strength of UHPC is affected by GGBS and RHA content to partially replace cement. At the low GGBS content (Figure 5.38a), for all contents of RHA, increasing the amount of SP initially increases compressive strength and then decreases. When the GGBS content is higher (Figure 5.38b, c), the increased SP content decreases compressive strength of UHPC, especially at high RHA contents. Similar to the result in Figure 5.37b, a decrease in compressive strength of UHPC containing 20 vol.-% GGBS at the moderate SP dosages is observed in Figure 5.38b. The highest compressive strength comes from a ternary binder composed of cement, RHA and GGBS, and a low dosage of SP (Figure 5.37 and Figure 5.38).

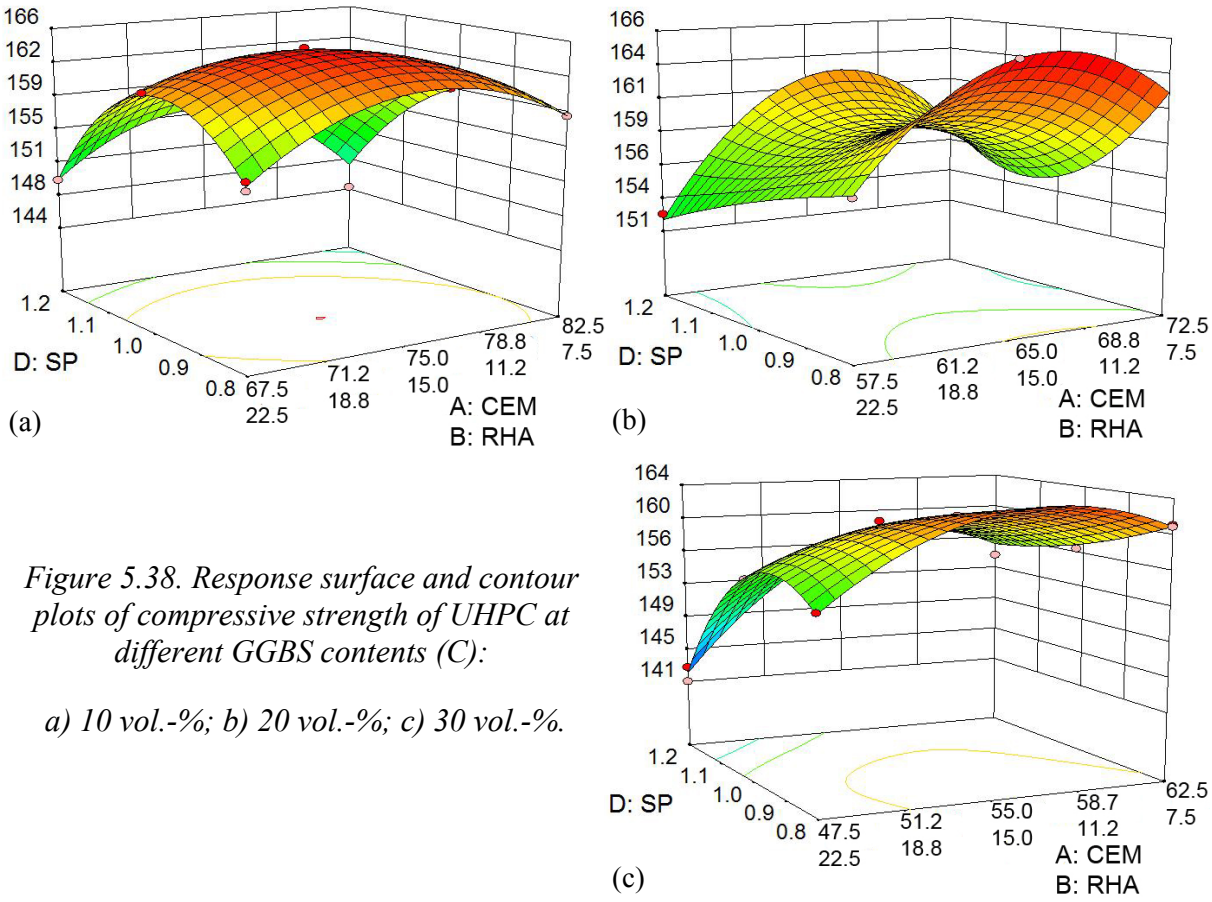

Figure 5.38. Response surface and contour plots of compressive strength of UHPC at different GGBS contents (C):

a) 10 vol.-%; b) 20 vol.-%; c) 30 vol.-%.

Optimization of mix proportions of UHPC containing RHA and GGBS

The optimization tool of the Design-Expert 8 software is conducted to find the optimal proportions of UHPC containing RHA and GGBS. The input criteria are shown in Table 5.7. The program gives some solutions. The best solution is chosen in terms of the highest compressive strength, low cement content and low SP dosage to produce UHPC more economically and environmentally (Table 5.7).

The results of the slump flow, compressive strength of the experimental mixture and Design-Expert's mixture in Table 5.7 are similar. Thus, UHPC with 15 vol.-% RHA and 20 vol.-% GGBS to partially replace cement, and 0.8% SP of cementitious materials is selected as the optimal mix proportions. The weight of materials for 1 m^3 concrete is given at UHPC-15%RHA-20%GGBS with W/F_v of 0.55 in Table 4.6.

Table 5.7. Experimental proportions versus optimized proportions

Material	Variable	Goal	Constrains	Unit	The mix proportions having the highest strength	
					Design-Expert	Experimental
Cement	A	In range	47.5-82.5	[vol.-%]	63.8	65
RHA	B		7.5-22.5		13.3	15
GGBS	C		10-30		22.9	20
SP	D		0.8-1.2	[wt.-%]	0.8	0.8
Slump flow		In range	295-351	[mm]	345	338
Comp. strength at 28d		Maximum	141-165.2	[MPa]	165.4	165.2

5.2.3. Discussion

The results of the compatibility between SP and UHPC containing RHA test clearly show that the effect of different SP on the flowability and compressive strength of the RHA-blended UHPC is varying significantly (Figure 5.27 and Figure 5.28). The different SP exhibits different water reduction efficiency, workability retention, air entraining and compressive strength development of concrete mixture. Selection of compatible superplasticizers for the designed cementitious materials is still a critical task. This challenge is enhanced in UHPC design which includes normally one or more mineral admixtures [91, 93]. Hence, the behavior of different SP on slump flow and compressive strength of UHPC containing for example RHA is very variable. When SP dosage is over the saturation dosage, the flowability of UHPC containing RHA or RHA and GGBS (Table 5.3 and Figure 5.36b, c) is offered even decreasing. The decreased workability of certain cement pastes was also observed at an over saturated dosage of SP in a previous study (i.e. over saturated dosage of SP induced longer flow time of cement paste in Marsh cone test) [215].

Adequate soluble alkali content in solution enhances the compatibility between SP and cement [90, 216]. The ICP results in Section 5.1.3 showed that RHA provides more alkali content for the CH solution than SF. Hence, the solution in the UHPC containing RHA possesses more adequate soluble alkali content than that in the UHPC containing SF. It may induce the better compatibility between SP and the low-alkali cement in the RHA-blended mixture compared with that in the SF-blended mixture. Hence, the slump flow of the RHA-blended mixture after mixing exceeds that of the SF-blended mixture at the same water and SP dosage (Figure 5.27). Moreover, because of the very small particles, SF tends to form agglomerates [217]. SF may not be dispersed well in cement matrix. The SF agglomerates decrease the micro-filler effect of SF and increases the water or/and SP demand of the cement paste and mortar containing SF (Figure 5.8 and Figure 5.9) or reduce the workability of the UHPC containing SF (Figure 5.27) compared to the RHA-blended mixtures. Thus, it is concluded that RHA and combination of RHA-GGBS improve the compatibility between SP and low-alkali cement, hence enhance workability of the mixtures.

With time of hydration, due to the adsorption of Ca^{2+} on particle surface, the surface charge of SF particles turns from negative to positive (Figure 5.25). To improve the dispersion of SF, addition of SP is crucial [91]. Hence, remixing the UHPC containing SF after a 15 minute pause increases the dispersion of SF. As a result, the increase in slump flow of the UHPC containing SF at 15 minutes after mixing is observed (Figure 5.27). It is known that GGBS adsorbs less SP than cement clinker. GGBS also releases a significant amount of K^+ and Na^+ ions into solution [93] which increases the compatibility between SP and the low-alkali cement. In this way, flowability of GGBS-blended mixture may be improved. GGBS with optimized particle size distribution may further improve the particle dispersion and packing density of the mixture containing SF as well. Thus, GGBS increases the slump flow of the UHPC containing SF (Figure 5.29).

The RHA-blended UHPC has a significantly higher slump flow value and slump life than that of the plain mixture (Ref) at the same water content and SP dosage (Figure 5.29). The effect

of RHA on workability of UHPC may be similar to GGBS (i.e. RHA with negative zeta potential in Figure 5.25 improves the cement particle dispersion and packing density of granular mixture), but it needs further detailed studies. On the other hand, the results of water and/or SP demand of RHA-modified cement paste or mortar at high w/b indicate that RHA clearly increases the water and/or SP demand of these mixtures (Figure 5.8 and Figure 5.9). This is obviously a side effect of the mesoporous structure of RHA. These results are consistent with those of many previous studies on concrete containing RHA with w/b more than 0.30 [33, 35, 36, 163, 165, 179]. Also, it was shown that the effect of high SSA and high water absorption of RHA on workability of mixture with increased w/b is more significant. This means that the mixtures containing RHA possess a higher water and/or SP demand at high w/b (Figure 5.8 and Figure 5.9) but a lower water and/or SP demand at w/b of about 0.22 (Figure 5.29) compared to the reference mixtures. The finer the RHA, the lower the SSA it has (Figure 5.3 and Table 5.1) and the higher the packing density of RHA-blended granular mixture [60]. Hence, increasing the fineness of RHA induces increased slump flow of UHPC (Figure 5.30), lower demand of water and/or SP of cement paste and mortar (Figure 5.8, Figure 5.9).

Besides the compatibility between SP and cementitious materials or the dispersion of materials, the role of packing density and hence excess water is also very important for workability of UHPC. Due to particle size, the packing density of the RHA-blended mixture is lower than that of the mixture containing SF [60]. Hence, the excess water content in the mixture containing SF is higher than that in the mixture containing RHA at the same W/F_v. Combining with the lubrication effect of spherical SF, the slump flow of the mixture containing SF is maintained when the W/F_v reduces from 0.55 to 0.50 and the SP dosage increases from 1.0% to 1.2%, respectively (Figure 5.29). Whereas, the excess water volume in the mixture containing RHA is lower. When the W/F_v of this mixture reduces (i.e. from 0.55 to 0.50), the frictional force between particles in the RHA-blended mixture increases significantly because of the mesoporous structure and irregular particle shape of RHA. Hence, the slump flow of the RHA-blended mixture strongly decreases when the W/F_v reduces from 0.55 to 0.50 and the SP dosage increases from 1.0% to 1.2% (Figure 5.29). It means that if w/b of mixture is below 0.20 (i.e. $W/F_v \leq 0.50$), the RHA-blended mixture requires significantly higher SP dosage than the SF-blended mixture to maintain the same slump flow. Results of Nguyen's investigations [58] also showed that RHA-blended UHPCs need significantly higher SP dosage to maintain the same slump flow as UHPC containing SF at w/b of 0.18. Additionally, the improvement of the mini-cone slump flow of UHPC containing RHA at $W/F_v = 0.50$ and 1% SP by GGBS (Figure 5.29) indicates that the effect of GGBS on packing density and hence on slump flow is more significant when UHPC containing RHA possesses a lack of excess water (i.e. $W/F_v = 0.50$). Figure 5.39 displays surface structure, morphology and size of particles of RHA, SF and GGBS which govern water, SP adsorption of pozzolan, packing density, and hence workability of UHPC. Thus, in this case, RHA possesses a drawback compared to SF and GGBS. For UHPC containing RHA, it can be concluded that w/b is more crucial to improve workability than SP dosage. To obtain a properly workable UHPC containing RHA with an acceptable SP dosage, w/b should not be below 0.20 (i.e. $W/F_v \geq 0.50$) in this study.

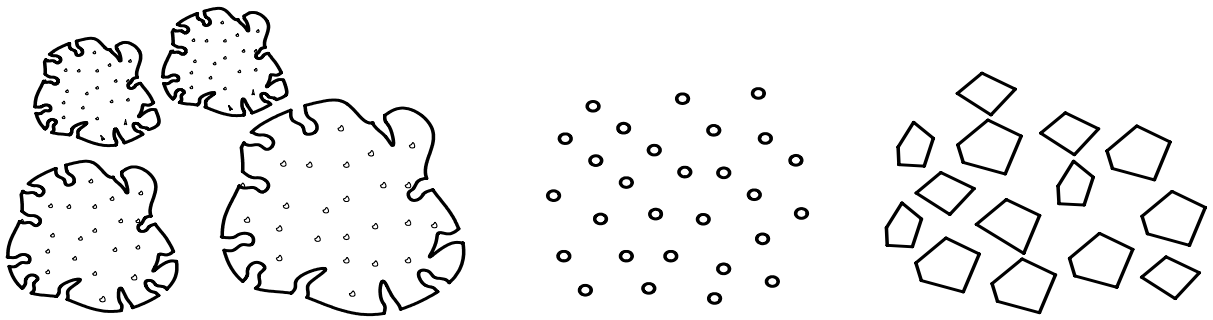

Figure 5.39. Surface structure, morphology and size of particle of different pozzolans.

By investigations in Section 5.1.2, it was assumed that compressive strength of the mortar containing RHA with different grinding periods depends not only on pozzolanic reactivity but also mainly on particle size and mesoporous structure of RHA. It was shown that compressive strength of mortars containing 10 wt.-% RHA (w/b = 0.484) is maximum for intermediate grinding period (with 45 min of grinding, RHA-45, Figure 5.9). For UHPC, it is known that compressive strength increases with increasing grinding period of RHA (Figure 5.30). Thus, it is concluded that RHA should be ground to a smaller mean particle size for UHPC production than for normal concrete or HPC. Furthermore, by comparing the enhancement of compressive strength, workability of UHPC by different fineness RHA (Figure 5.30), it can be assumed that significantly increasing grinding period of RHA is not necessary. RHA with mean particle size of 7.41 µm (120 min grinding) is suitable for UHPC production in terms of the technical and economical benefits.

Regarding the effects of RHA content and combination of RHA and GGBS on workability and compressive strength, there is an optimal RHA content which provides the highest workability and compressive strength of UHPCs with or without GGBS. The combination of RHA and GGBS enhances both workability and compressive strength compared with UHPC containing RHA (Figure 5.31 and from Figure 5.35 to Figure 5.38). The synergic effects of the combination of RHA, GGBS and SP on workability and compressive strength of UHPC are clearly interpreted through 3D response surface and contour plots of the combined mixture-process model produced by the Design-Expert 8 software (see Figure 5.35 to Figure 5.38).

5.2.4. Concluding remarks

Based on the investigations on compatibility between different SP and UHPC containing RHA, the effects of RHA ground for different periods of time, RHA content, and the combination of RHA, GGBS and SP on properties of UHPC, the conclusions can be summarized as follows:

- It is possible to use RHA to completely replace SF in producing UHPC. The compatibility between SP and UHPC is crucial to choose a suitable SP which helps UHPC to meet the specific requirements. Mineral admixtures have strong effect on the

compatibility between SP and UHPC. At W/F_v of 0.55 and 1% used SP, flowability of the RHA-blended mixture (with suitable fineness and content of RHA) after mixing exceeds that of the SF-blended mixture. Due to coarse particles, irregular particle shape of RHA, reducing the water content (i.e. $W/F_v \leq 0.50$) significantly decreases flowability of the RHA-blended mixture compared with that of the SF-blended mixture.

- When the dosage of the used SP is higher than the saturation dosage of the RHA-blended mixture, the slump flow slightly decreases, the air content increases, and hence compressive strength of the UHPC decreases. Thus, proper SP dosage is necessary for application.
- RHA clearly enhances the workability and flowability retention of UHPC compared with the plain cement mixture (Ref). The grinding period and content of RHA also influence the flowability and compressive strength of UHPC containing RHA. In terms of economical and technical aspects, 22.5 vol.-% RHA with mean particle size of 7.41µm (sample at 120 min grinding) for partial cement replacement is chosen to produce UHPC at W/F_v of 0.55 without SF in this study.
- The combination of RHA and GGBS improves both workability and compressive strength of UHPC containing RHA. It also reduces the saturation dosage of SP in the mixture. The use of 3D response surface and contour plots of the combined mixture-process model with Design-Expert 8 software is an appropriate method to understand the synergic effects of cement, RHA, GGBS and SP dosage on the workability and compressive strength of UHPC.
- When RHA and GGBS are used, the ternary binder composed of 65 vol.-% cement, 15 vol.-% RHA and 20 vol.-% GGBS combining with a dosage of 0.8% SP in solid weight referred to the amount of cementitious materials is the optimum mix proportions for the highest 28 d compressive strength of the sustainable UHPC under the normal treatment condition.

5.3. Impact of pozzolanic materials and treatment conditions on compressive strength and shrinkage of UHPC

Based on the results of the investigations in Section 5.2, UHPC compositions used in Section 5.3 and Section 5.4 are given in Table 5.8. The Vietnamese cement was used for U2Vn-22.5RHA. 1 vol.-% of steel fibers (a length of 9 mm and a diameter of 0.15 mm) was added to the mixture for producing prisms to measure compressive strength of UHPC. When fibers were used, volume of quartz sand was equally replaced by volume of fibers. UHPCs were treated under the three treatment conditions (20, 65, 90°C) to investigate the effect of pozzolanic materials and treatment conditions on properties of UHPC.

Table 5.8. Mix proportions of UHPC

UHPCs	Cement	Quartz Sand	Quartz Powder	RHA (SF)	GGBS	Total water	SP	w/b	W/F_v
	[kg/m^3]						[%]		
U1-22.5SF	780.8	1029.6	207.8	(162.9)	-	216.5	1.0	0.229	0.55
U1-22.5RHA				155.1				0.231	
U2-22.5SF	579.3			(162.9)	183.2		0.8	0.234	
U2-22.5RHA				155.1				0.236	
U2Vn-22.5RHA	573.9							0.237	
U2-15RHA	654.9			103.4				0.230	

5.3.1. Workability and compressive strength

5.3.1.1. Workability

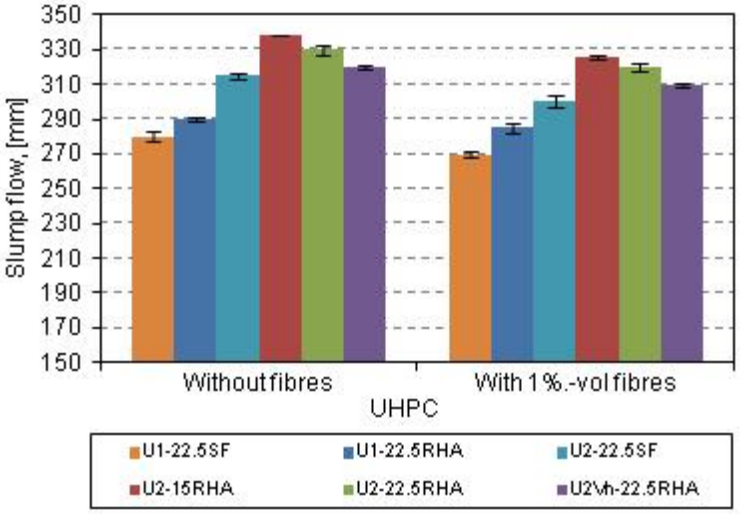

Figure 5.40. Flowability of UHPC.

As can be seen from results in Figure 5.40, the mini-cone slump flow values of all the UHPCs exceed 270 mm after mixing. When 1 vol.-% of steel fibers is used, it slightly decreases the flowability of the UHPCs. The workability of the RHA-blended mixture exceeds that of the respective SF-blended mixture. GGBS clearly enhances workability, mixing and casting properties of the UHPC containing RHA or SF. CEM-Vn induces a lower workability of UHPC than CEM-De.

5.3.1.2. Effect of RHA content on compressive strength of UHPC containing GGBS

Results of compressive strength of U2-15RHA and U2-22.5RHA in Figure 5.41 display that U2-15RHA possesses a higher compressive strength than U2-22.5RHA for normal treatment condition (20°C, Treatment 1) at the ages of 7 and 28 days. These results are in good agreement with the 28 d strength results of U2-15RHA and U2-22.5RHA without fibers in Section 5.2 (i.e. Run 13 and 22 in Table 5.4). Also, the results in Figure 5.41 show that the difference in compressive strength between these mixtures is insignificant in hydration period from 91 to 360 days. Compressive strength of both the mixtures strongly develops during the first 91 days but is much slower thereafter (Figure 5.41).

At increased temperatures (65 and 90°C), compressive strength of the samples is strongly accelerated and exceeds 190 MPa at the age of 7 days (Figure 5.42). The strength results of the 65°C treated samples are similar. For the 90°C treated samples, compressive strength of U2-22.5RHA is slightly lower than that of U2-15RHA from 28 days of hydration (Figure 5.42). Comparing to the strength of normally treated samples, there is no advantage of the

heat treatments for the long term compressive strength of the RHA-GGBS-blended UHPCs (Figure 5.41 and Figure 5.42).

5.3.1.3. Effect of pozzolans and treatment conditions on compressive strength

Compressive strength results of the UHPCs with different contents of RHA, SF and GGBS at different treatments are presented in Figure 5.43 to Figure 5.45. At 7 days of Treatment 1 (Figure 5.43), RHA enhances compressive strength of UHPCs compared to SF. Thereafter, the strength of U1-22.5SF and U1-22.5RHA is similar at the ages of 28 and 91 days. Comparing compressive strength of mixtures containing GGBS (U2-22.5SF and U2-22.5RHA), compressive strength of the RHA-GGBS-blended UHPC exceeds that of the SF-GGBS-blended UHPC during the first 91 days of hydration. But after even more extended hydration periods (i.e. 180 and 360 days), no significant variation in compressive strength between U2-22.5SF and U2-22.5RHA was measured. Also, results in Figure 5.43 clearly show that the addition of GGBS has a minor influence on compressive strength of the UHPC containing SF from 7 to 91 days of hydration. During hydration periods from 28 to 360 days, GGBS clearly improves compressive strength of the UHPC containing RHA (Figure 5.43).

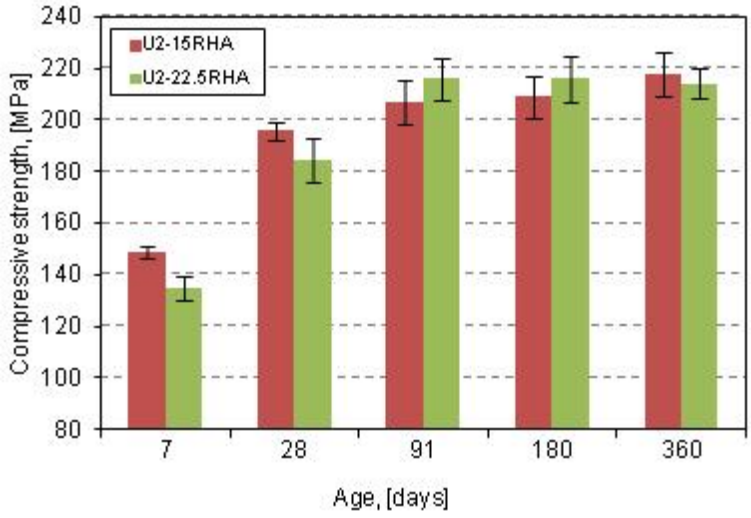

Figure 5.41. Effect of RHA contents on compressive strength of UHPC containing GGBS at normal treatment.

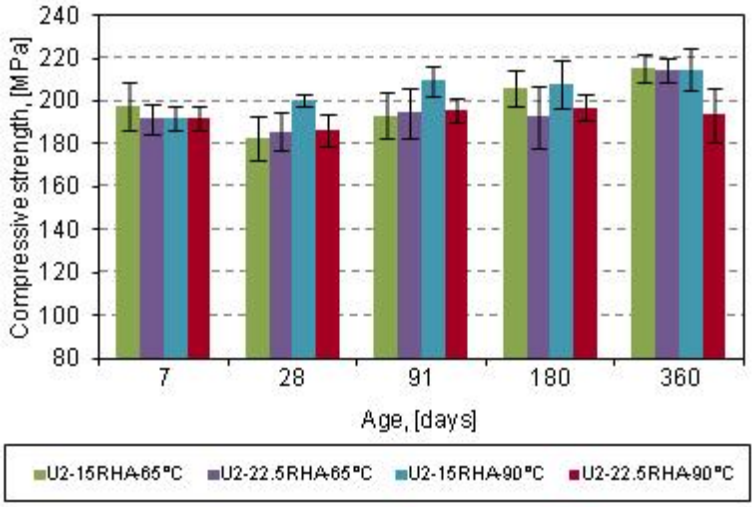

Figure 5.42. Effect of RHA contents and heat treatments on compressive strength of UHPC containing GGBS.

At elevated temperatures (65 and 90°C), the development of compressive strength of all the UHPCs is strongly accelerated (Figure 5.44 and Figure 5.45). After 7 days, compressive strength of all the investigated UHPCs obtains over 170 MPa. Generally, the documented increased compressive strength due to GGBS at the 20°C treatment was not detected in the heat treated UHPCs. At 65°C treatment, no variation in compressive strength between UHPCs containing RHA, respectively, SF, was measured at all the ages (Figure 5.44). At 90°C treatment, compressive strength of the heat treated U2-22.5SF exceeds that of the heat treated U2-22.5RHA after 180 and 360 days of hydration (Figure 5.45).

Comparing compressive strength of UHPC in dependence of the various treatment conditions, it can be observed that increasing the temperature generally increases 7 d compressive strength. After 360 days with the heat treatment at 90°C, U1-22.5RHA and U2-22.5RHA have lower strengths compared to U2-22.5SF (Figure 5.45) and do not exceed the strength of the UHPCs containing RHA at 20 and 65°C treatments (compare Figure 5.43, Figure 5.44 and Figure 5.45). These results indicate that the moderate temperature treatment (65°C) is suitable to increase 7 d compressive strength of UHPC. No significant long term compressive strength gain was documented for the investigated heat treated UHPCs.

5.3.1.4. Effect of cements and treatment conditions on compressive strength

Results in Figure 5.46 and Figure 5.47 show that at the age of 28 days, U2Vn-22.5RHA samples obtain compressive strength over 160 MPa. With the normally treated sample, compressive strength of U2Vn-22.5RHA exceeds 170 MPa at the age of 28 days and obtains 200 MPa after 360 days of hydration (Figure 5.46). These results indicate that UHPC can be produced from the available cement and RHA in Vietnam. Compressive strength of U2-22.5RHA exceeds that of U2Vn-22.5RHA at all the ages and

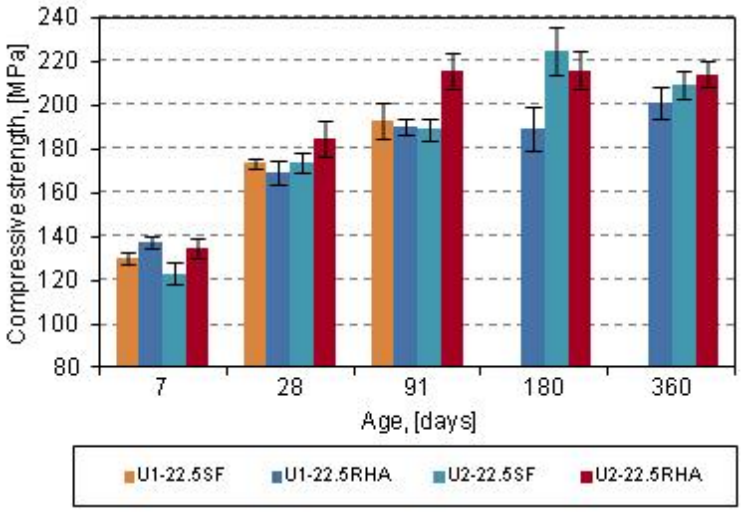

Figure 5.43. Effect of pozzolans on compressive strength at Treatment 1 (20°C).

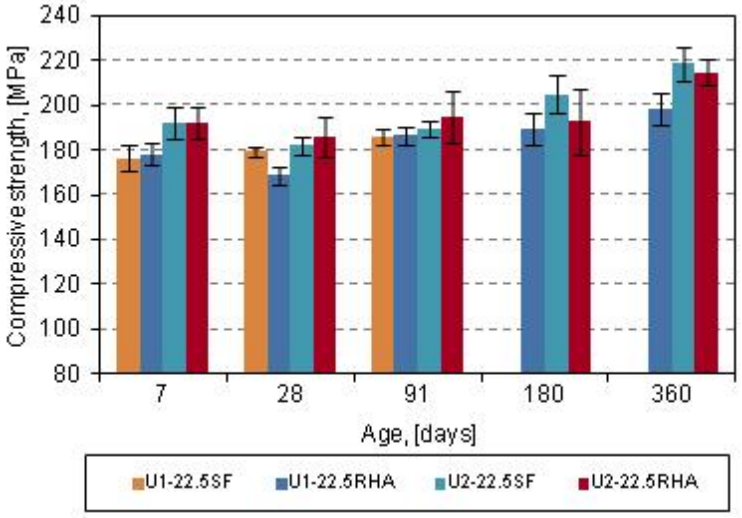

Figure 5.44. Effect of pozzolans on compressive strength at Treatment 2 (65°C).

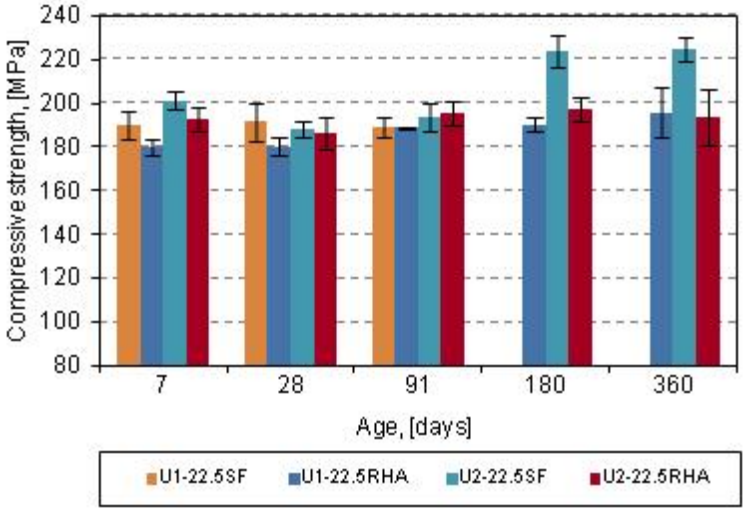

Figure 5.45. Effect of pozzolans on compressive strength at Treatment 3 (90°C).

treatment conditions. Similar to U2-22.5RHA, the long term compressive strength of the normally treated U2Vn-22.5RHA is higher than that of the heat treated samples (Figure 5.46 and Figure 5.47).

5.3.2. Shrinkage and internal relative humidity of UHPC

5.3.2.1. Autogenous shrinkage

The temperature and deformation of UHPCs were incessantly recorded as in Figure 5.48. It shows that the induction period of UHPCs is prolonged by the strong retarding effect of the high SP dosage. SF slightly accelerates the hydration of UHPC compared to RHA. GGBS does not substantially change the zeroed time (i.e. the time of highest temperature) of the mixture containing RHA.

Because the variation in temperature of the thin samples is small (i.e. about 1.5°C) and is almost the same among the different mixtures during hydration (Figure 5.48), the effect of the thermal dilatation to the value of autogenous shrinkage is ignored. The zero-timed autogenous shrinkage results given in Figure 5.49 indicate that the mixture containing SF exhibit the maximum autogenous shrinkage. RHA strongly mitigates autogenous shrinkage of UHPCs. GGBS partially replacing cement also reduces autogenous shrinkage of both UHPCs containing RHA and SF. During 28 days of

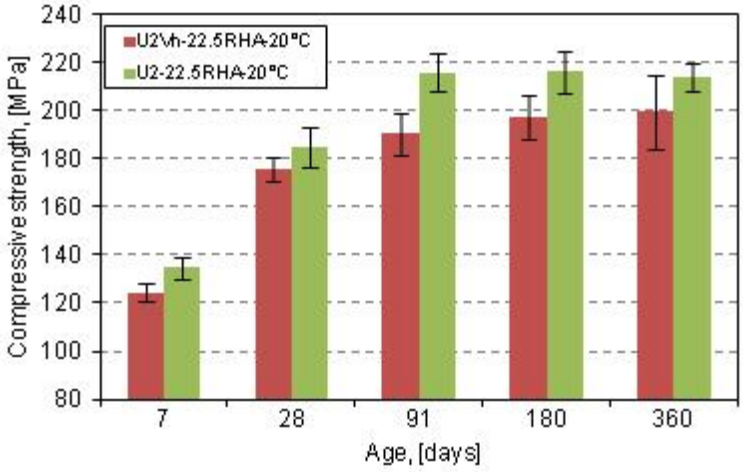

Figure 5.46. Effect of cements on compressive strength of UHPC at normal treatment.

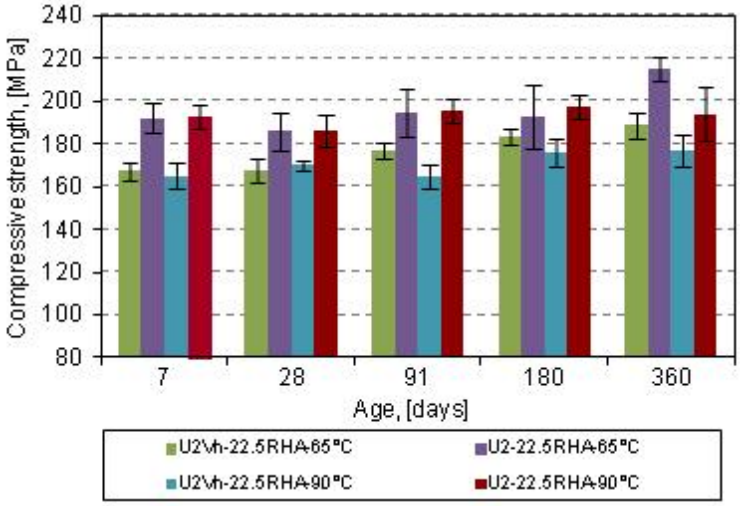

Figure 5.47. Effect of cements and heat treatments on compressive strength of UHPC.

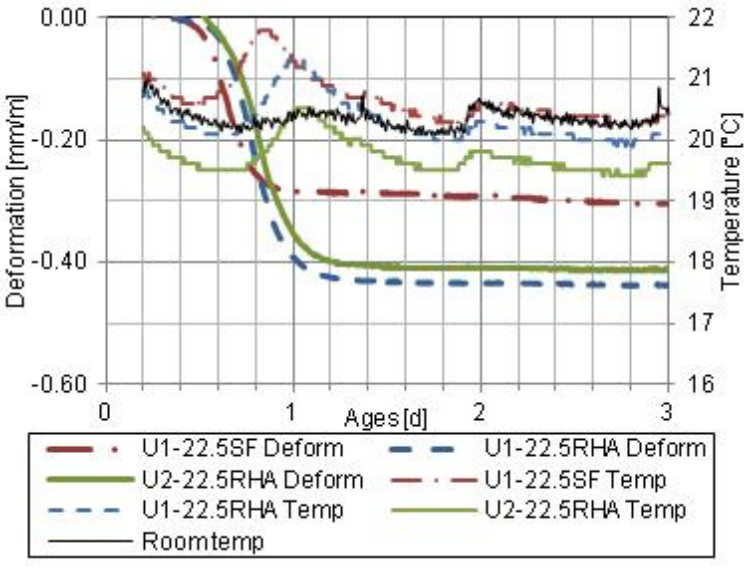

Figure 5.48. Measured deformation and temperature of UHPC during the first 3 days.

hydration, minor differences in autogenous shrinkage between the RHA-blended mixtures are observed. The lower the RHA content is in the mixture, the more the autogenous shrinkage it has. The variation of autogenous shrinkage in U2-15RHA and U2-22.5RHA seems to mainly occur at an early period of hydration (Figure 5.49).

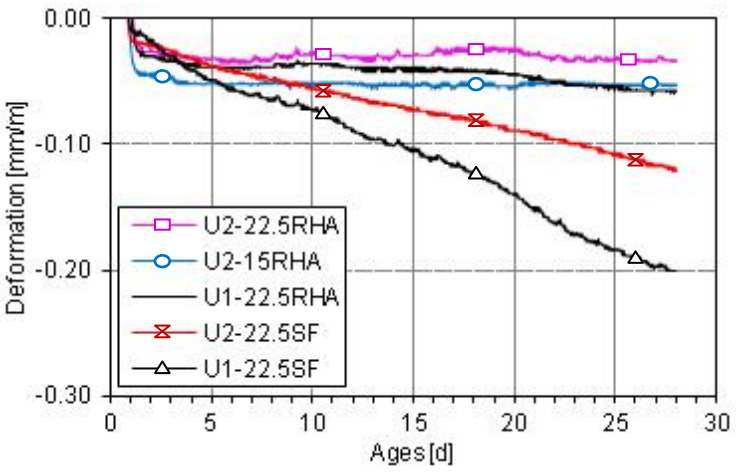

Figure 5.49. Zeroed deformation curves at the beginning of shrinkage measurement (i.e. from the highest temperature of hydration).

5.3.2.2. Autogenous and total shrinkage at different treatment conditions

The mean standard deviation of all the autogenous shrinkage measurements in Figure 5.50 and Figure 5.51 is 14.88 µm/m. The results in Figure 5.50 and Figure 5.51 reveal that the UHPCs containing SF possess significantly higher autogenous shrinkage compared to the UHPCs containing RHA at all treatment conditions (20, 65 and 90°C). The presence of GGBS decreases autogenous shrinkage of the SF-blended UHPC. Under the normal treatment, autogenous shrinkage of the RHA-blended UHPC is reduced by the addition of GGBS. A slightly increased autogenous shrinkage is measured in the heat treated UHPC containing RHA and GGBS (compare Figure 5.50 and Figure 5.51). In particular, autogenous shrinkage of U2-22.5RHA develops very slowly from 1 to 8 weeks at Treatment 1 (20°C). Thereafter, the development of autogenous shrinkage of the normally treated U2-22.5RHA is significant (Figure 5.51). During heat treatment, autogenous shrinkage of the UHPCs is strongly accelerated. Autogenous shrinkage of the 90°C treated sample is higher than that of the respective 65°C treated sample for all the UHPC mixtures (Figure 5.50 and Figure 5.51). After 48 hours of the heat treatments and 24-hour cooling, UHPCs exhibit almost no autogenous shrinkage. Apart from the 90°C treated U2-22.5RHA sample, autogenous shrinkage of all the normally treated samples exceeds that of the heat treated samples after 6 months. These results are consistent with those of the previous finding about the decreased autogenous shrinkage of UHPC mixtures containing RHA [60] or GGBS [82] and the non post-heated treatment shrinkage of UHPC containing SF [11, 105].

Figure 5.52 and Figure 5.53 display total shrinkage of the UHPCs at the different treatment conditions (20, 65 and 90°C) followed by storing at 20°C and 65% RH from 5th day of hydration. The mean standard deviation of all the total shrinkage measurements is 16.05 µm/m. The results show that total shrinkage of the UHPCs containing RHA is still lower than total shrinkage of the UHPCs containing SF at all the treatment conditions. The heat treatments significantly decrease total shrinkage of all the mixtures compared to the normal treatment. Comparing to autogenous shrinkage of respective UHPC in Figure 5.50 and Figure 5.51, it can be figured out that the RHA-modified samples possess a higher drying shrinkage than the SF-modified samples. The heat treatments strongly decrease drying

shrinkage of UHPCs, especially with the mixtures containing SF. This indicates that RHA strongly decreases autogenous shrinkage but increases drying shrinkage of UHPC compared to SF.

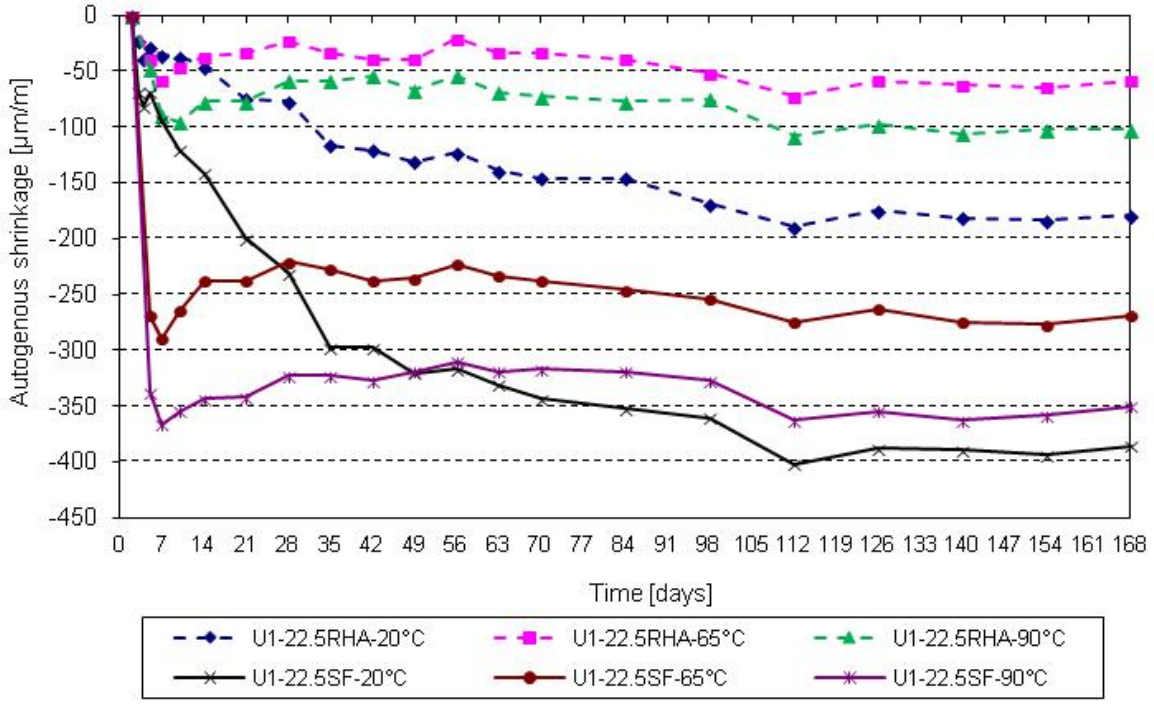

Figure 5.50. Autogenous shrinkage of UHPC containing RHA or SF at different treatment conditions.

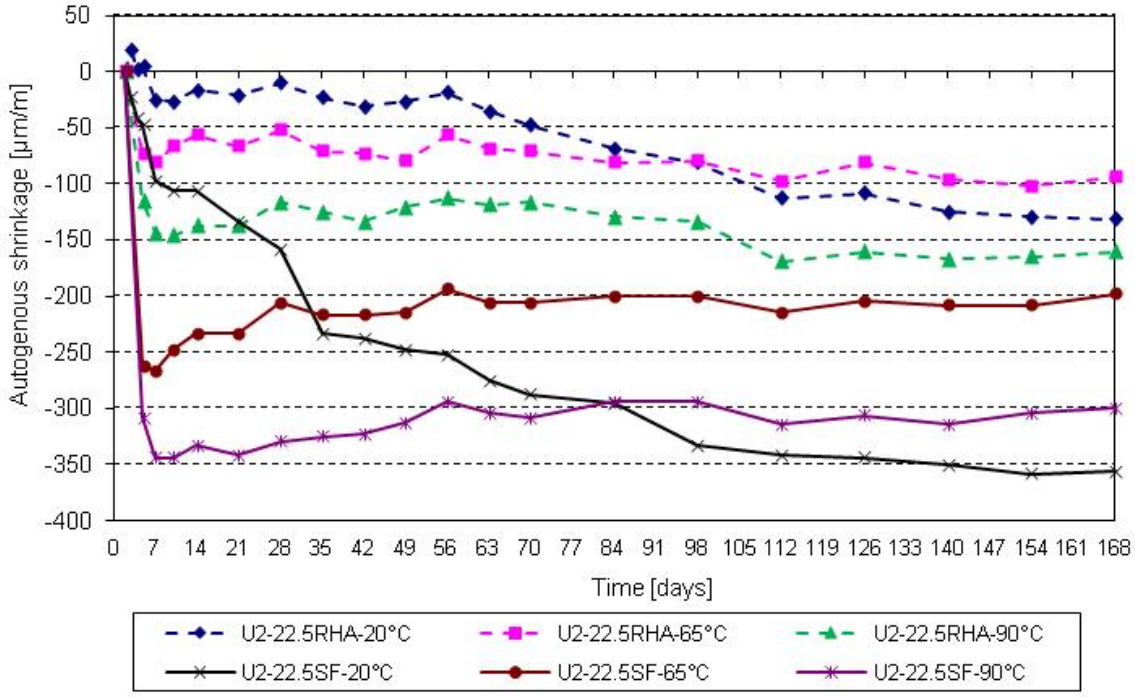

Figure 5.51. Autogenous shrinkage of UHPC containing GGBS and RHA or SF at different treatment conditions.

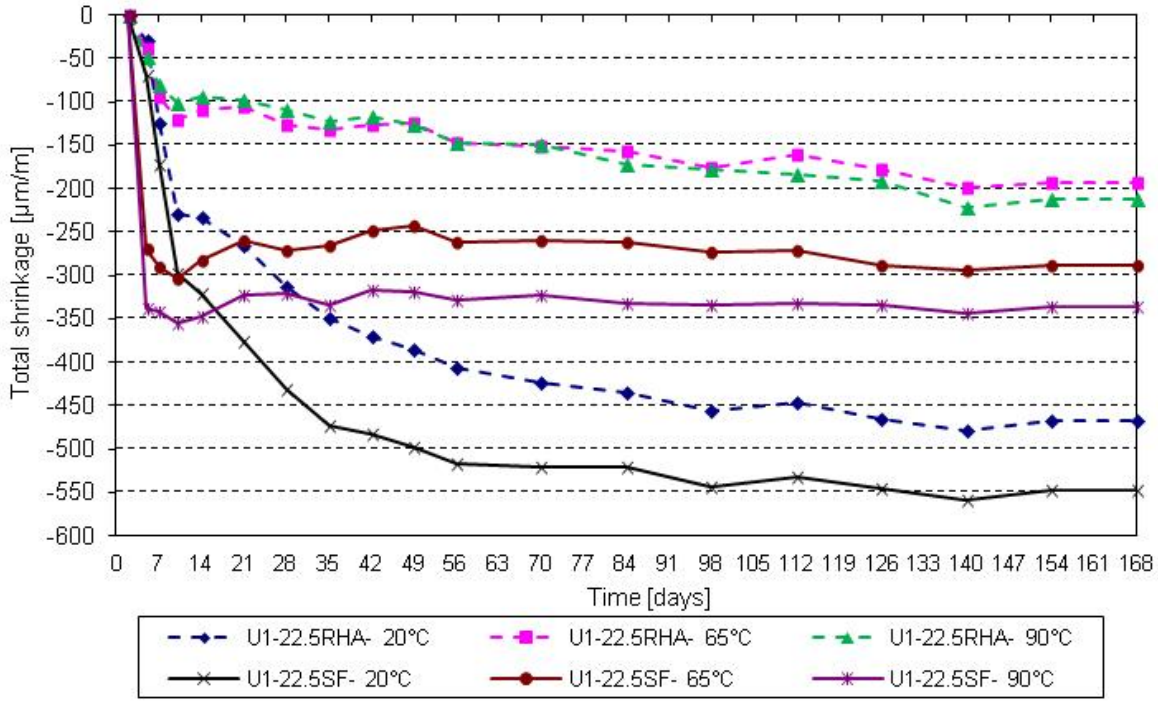

Figure 5.52. Total shrinkage of UHPC containing RHA or SF at different treatment conditions.

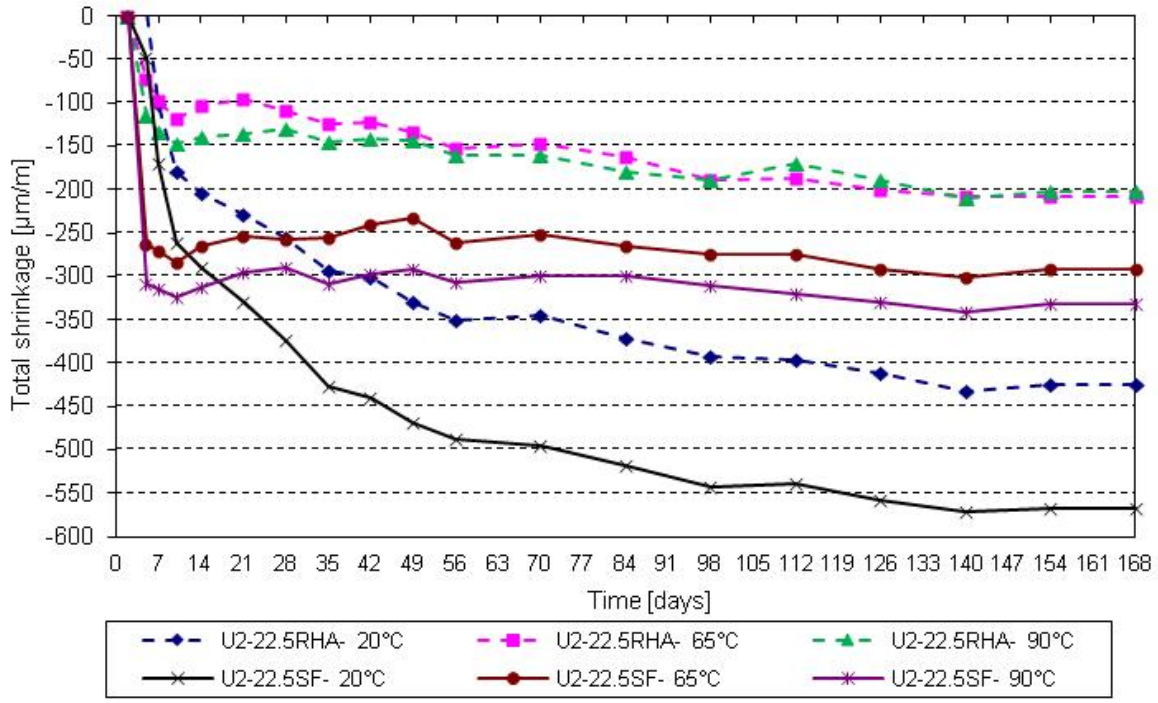

Figure 5.53. Total shrinkage of UHPC containing GGBS and RHA or SF at different treatment conditions.

5.3.2.3. Internal relative humidity

Internal relative humidity (RH) in hydrating UHPC samples was determined by RH sensors. The development of the internal RH in the sealed UHPC samples during hydration is given in Figure 5.54. Because of the accuracy of the RH sensor, the internal RH value in the UHPCs should be considered below 98%. As expected, the internal RH in U1-22.5SF starts below 98% after about 2 days of hydration and quickly drops during the first 10 days. Meanwhile,

the internal RH in U1-22.5RHA starts below 98% after about 10 days of hydration. Thereafter, the internal RH in both U1-22.5SF and U1-22.5RHA regularly decreases. The incorporation of GGBS and RHA or SF significantly prolongs the over 98% internal RH condition in the matrices. In particular, the internal RH condition in U2-22.5RHA is over 98% until about 4 weeks of hydration. After 28 days of hydration, the internal RH in U1-22.5SF and U2-22.5SF are similar. The internal RH reduction rates in the RHA-modified matrices are clearly lower than that in the SF-modified matrices (Figure 5.54).

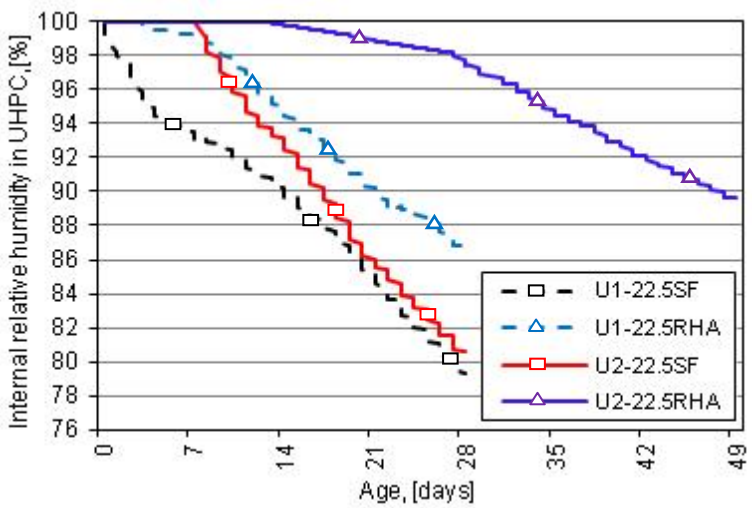

Figure 5.54. The internal RH of UHPC during hydration.

5.3.3. Discussion

5.3.3.1. Compressive strength

Based on the results of the experiments in Section 5.1, it can be seen that if cement is replaced by only 10 wt.-% (i.e. 14.6 vol.-%) of RHA, the RHA does not consume all portlandite formed in cement paste (Figure 5.10). At normal treatment condition (20°C), the pozzolanic reaction of RHA in cement paste (at w/b of 0.22) processes slowly. And the pozzolanic reactivity of RHA is accelerated and enhanced at high temperature treatment (Figure 5.10). The expected increased compressive strength development of U2-22.5RHA (22.5 vol.%) compared with that of U2-15RHA (15 vol.%) is observed at long hydration period under normal treatment condition (Figure 5.41). And after heat treatments, compressive strength of both U2-15RHA and U2-22.5RHA is similar, even at the age of 7 days (Figure 5.42). Therefore, the increased compressive of U2-22.5RHA compared with U2-15RHA can be a result from the additional pozzolanic reaction of increased RHA volume at long hydration periods of the normal treatment condition or at the heat treatments.

At 7 days of hydration under normal treatment, the portlandite (CH) content in the cement paste containing SF is almost similar at water binder ratio (w/b) of 0.22 (Figure 5.10a) or even lower at water binder ratio (w/b) of 0.18 [57, 60] compared with that of the paste containing RHA. In the meantime, the degree of cement hydration in SF-blended matrix exceeds that in RHA-blended matrix [57, 60]. However, after 7 days of hydration at normal treatment, compressive strength of the UHPCs containing RHA exceeds that of the UHPCs containing SF (Figure 5.43). It should be noted that the total water content (i.e. W/F_v) at the beginning in the mixtures is the same. The specific pore volume of RHA is 0.12 cm^3/g (RHA-120 in Table 5.2) and the content of RHA in U1-22.5RHA or U2-22.5RHA is 155.1 kg/m^3 (Table 5.8). Therefore, the water content absorbed by RHA is theoretically about 17.15 l/m^3. It leads to a decrease of the effective W/F_v from 0.55 to 0.51 in the mixtures containing RHA.

This indicates that the increased 7 d compressive strength of the RHA-modified UHPCs does not mainly result from the difference in the degree of cement and pozzolan hydration but from the water reduction and thus porosity reduction as a consequence of the mesoporous structure of RHA (i.e. water absorption).

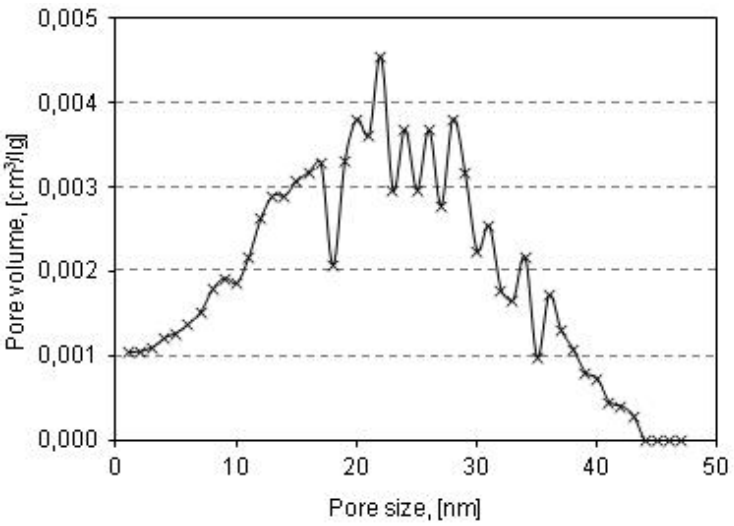

Figure 5.55. Pore size distribution of RHA-120.

In previous investigations, it was shown that increasing the treatment temperature induces decreased portlandite content for UHPC containing pozzolan (Figure 5.10). Hence, the increased compressive strength of the heat treated UHPC containing SF (Figure 5.44 and Figure 5.45) correlates well with the found increased degree of pozzolan hydration. These results are consistent with those of many previous studies on the effect of temperature treatment on compressive strength of UHPC containing SF [11, 94, 117]. However, for U2-22.5RHA and U2Vn-22.5RHA at extended periods of hydration, the reason for the decreased compressive strength of the high temperature treated samples compared to the normally treated samples (Figure 5.46 and Figure 5.47) is unclear. Hence, 48 h treatment at 65°C should be conducted for UHPC containing RHA to obtain high early-age (7d) compressive strength and economical UHPC.

5.3.3.2. RHA as an internal curing agent

The application of an ultra high resolution SEM (Nova NanoSEM 230, FEI) allowed us to show for the first time the mesoporous structure of ground RHA particles (Figure 5.4 to Figure 5.6) which before was just theoretically calculated from results of BET-SSA or BJH [141, 160, 161]. Additionally, with the very simple method to identify the water absorption capacity of RHA, this study also showed that the water absorption capacity of RHA correlates with the pore volume value measured by BJH and is significantly higher than that of SF (Table 5.2). As discussed, about 17.15 l/m^3 of water in the RHA-modified UHPCs will be theoretically absorbed by RHA. Furthermore, the pore size distribution in RHA particles derived from the BJH measurement is mainly from about 4 to 45 nm (Figure 5.55) and the mean pore size in RHA particles is approximately 30 nm. According to Kelvin's equation [218], this pore size range corresponds to the change of RH from about 76 to 98%. This means that when the internal RH in UHPC drops below 98%, the absorbed water in these pores will be released to compensate for self-desiccation during hydration. It postpones and slows the internal RH reduction in the RHA-modified matrices (Figure 5.54). Thus, RHA also plays as an internal curing agent to reduce the self-desiccation (Figure 5.54) and hence to mitigate autogenous shrinkage of UHPC (Figure 5.49, Figure 5.50 and Figure 5.51).

Furthermore, the partial replacement cement by the lower reactive GGBS induces the lower self-desiccation in the matrices containing RHA or SF, especially during early hydration period (Figure 5.54). Hence, GGBS reduces autogenous shrinkage of the UHPCs. The combination of GGBS and RHA results in a more significant positive effect on self-desiccation compared with the GGBS-SF-blended UHPC (Figure 5.54). As a result, a very low autogenous shrinkage of U2-22.5RHA under the normal treatment is observed during the hydration period between 1 and 8 weeks (Figure 5.51).

When super absorbent polymers (SAP) or pre-saturated lightweight aggregate (LWA) are used as an internal curing agent, the extra addition of water content for internal curing is normally about 0.03-0.05 g/g cement in UHPC [101, 111]. It is higher than the water volume absorbed by RHA (i.e. about 0.022 g/g cement in U1-22.5RHA and 0.03 g/g cement in U2-22.5RHA). It should be noted that the entrained water from SAP or LWA is considered as the additional water content. It will supply extra water to prevent self-desiccation of the matrix. Furthermore, SAP particles with a mean particle size of 200 µm and a maximum particle size up to 500 µm [111] as well as the volume reduction of SAP particles during hydration of cement matrix [20] are the weakest points in the UHPC matrix. Thus, the mixture with SAP possesses a higher volume of gel pores and total porosity, and hence a lower compressive strength in comparison to the reference mixture without internal curing agent [20, 111]. Also, the distribution of water reservoirs is an important parameter for eliminating autogenous shrinkage of extremely dense UHPC [101]. Hence, with the compressive strength, microstructure and distribution of water reservoir aspects, RHA is more appropriate for internal curing and pozzolanic reaction.

5.3.4. Concluding remarks

The following conclusions can be deduced from the results in this section:

- It is possible to use the cementitious materials available in Vietnam (i.e. cement and RHA) to produce sustainable UHPC.
- With the same water content (i.e. W/F_v = 0.55) and SP dosage, workability and compressive strength of the UHPCs containing RHA under the normal treatment are comparable with that of the mixtures containing SF. RHA strongly decreases autogenous shrinkage but increases drying shrinkage of UHPC compared to SF. The incorporation of RHA and GGBS improves workability, compressive strength and shrinkage of RHA-modified UHPC.
- The effect of the high temperature treatments on compressive strength of UHPC depends on the addition of RHA or SF. The long term compressive strength of the SF-GGBS-blended UHPC is increased at the higher temperature treatment. In contrast, the long term compressive strength of the heat treated RHA-GGBS-blended UHPC is decreased compared with the normally treated sample. In terms of the economical and technical aspects, 22.5 vol.-% RHA with a mean particle size of 7.41µm for cement replacement is also considered as the optimum RHA content to produce UHPC containing GGBS. And the 48 h treatment at 65°C is optimum for accelerating early (7 d) compressive strength.

- The high autogenous shrinkage in UHPCs containing SF is mainly caused by the high self-desiccation during hydration. RHA clearly plays as an internal curing agent. It significantly delays and slows down the decrease in the internal relative humidity in the UHPC matrix, and hence strongly mitigates autogenous shrinkage of the RHA-modified UHPC.
- RHA combines high pozzolanic reactivity and water adsorbing capacity. Thus, it is effective as both internal curing agent and pozzolanic admixture. Using RHA for UHPC production assures a homogeneous microstructure and a good distribution of water reservoirs in very dense UHPC.

5.4. Microstructure and durability of sustainable UHPC

5.4.1. Microstructure of UHPC

5.4.1.1. Portlandite content

Portlandite (CH) contents determined by DTA-TG for binder matrices of U2-22.5RHA and U2-22.5SF at the three treatment conditions (20, 65 and 90°C) in dependence with hydration time up to 360 days are presented in Figure 5.56, Figure 5.57 and Figure 5.58. The standard deviation (SD) of the DTA-TG results of one RHA-blended cement paste which was separately prepared five times (i.e. SD = 0.185% in Figure 5.10c) is indicated in Figure 5.56a (upper right corner). It can be seen that significant difference in CH content in binder matrix of UHPC is dependence of pozzolans, treatment conditions and periods of hydration.

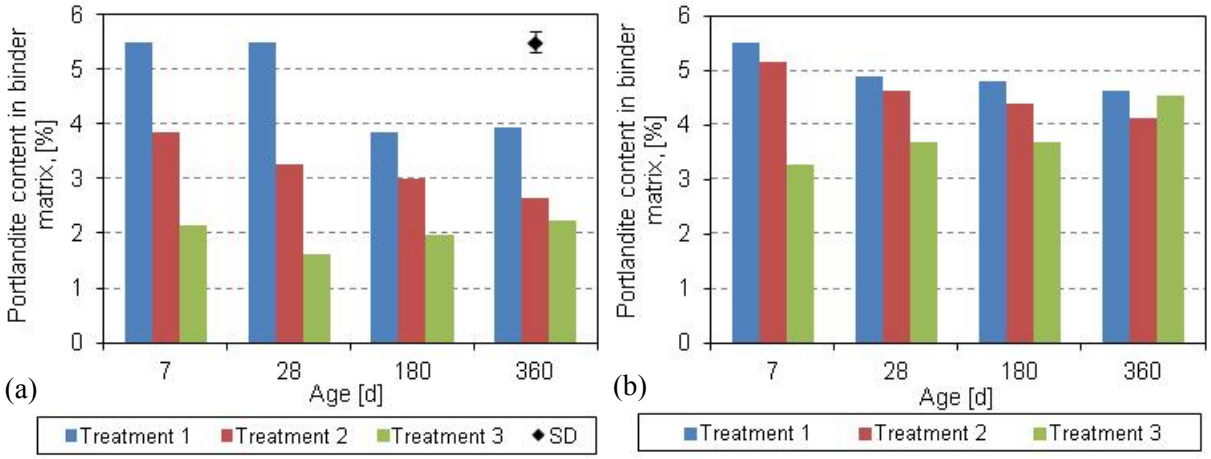

Figure 5.56. CH content in binder matrices of U2-22.5SF (a) and U2-22.5RHA (b) in dependence of treatment conditions and hydration periods. SD is the standard deviation of the results of five differently prepared samples from the RHA-blended paste in Figure 5.10c.

Results in Figure 5.56a indicate that increasing temperature generally results in decreased CH content of the SF-modified sample. For the normally treated sample (20°C, Treatment 1), the variation of the CH content between 7 and 28 days or 180 and 360 days of hydration is insignificant. For moderate temperature treatment (65°C, Treatment 2), the CH content regularly decreases in dependence of hydration time of the UHPC. The CH content in U2-22.5SF under the 90°C treatment strongly drops at the age of 7 days and is lowest after 28 days of hydration. At 28 days, the endothermic and derivative weight loss peaks at the

temperature range of 400-450°C of this sample slightly decrease (Figure 5.57). However, after 180 and 360 days for the 90°C treated sample, the peaks and hence CH content slightly increases with time of hydration (Figure 5.56a, Figure 5.57).

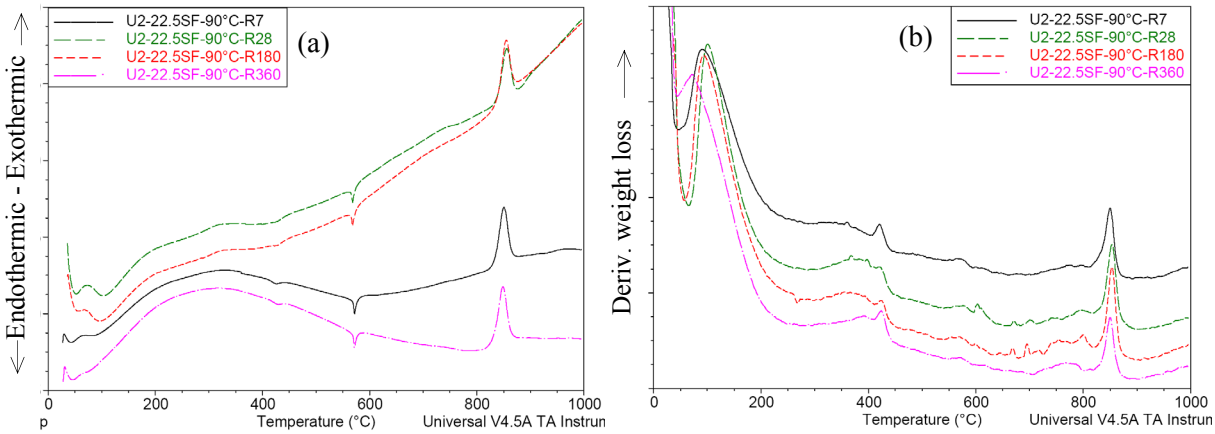

Figure 5.57. a) Heat flow (DTA) and b) derivative weight loss (DTG) of the 90°C treated U2-22.5SF.

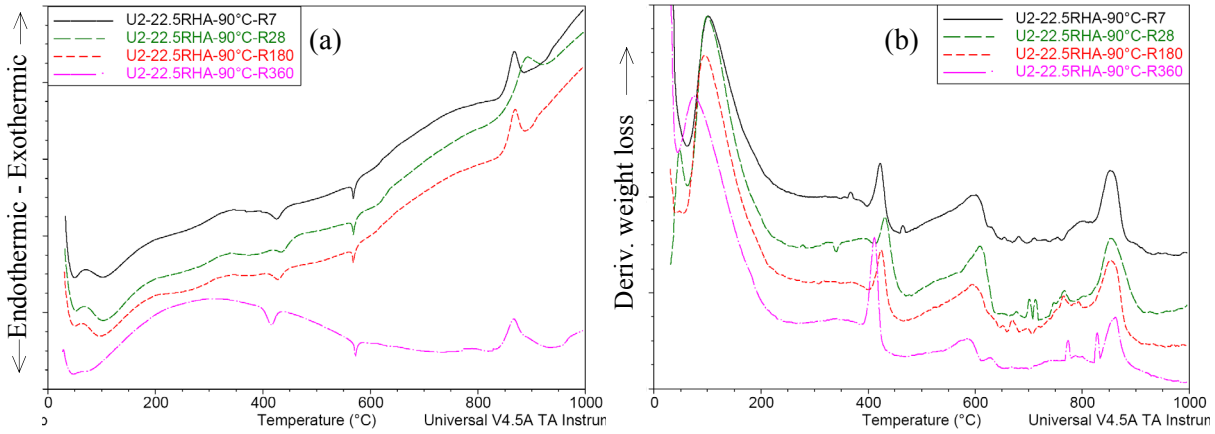

Figure 5.58. a) Heat flow (DTA) and b) derivative weight loss (DTG) of the 90°C treated U2-22.5RHA.

For U2-22.5RHA (Figure 5.56b), the results show that increasing temperature also decreases the CH content of the RHA-modified sample. After 360 days, the CH contents in the variously treated samples are seemly similar. During hydration, the CH content in the normally treated and the 65°C treated samples (Treatment 1 and Treatment 2) regularly decreases but increases in the 90°C treated sample (Figure 5.56b). The increase in the CH content of the 90°C treated sample during hydration is clearly observed by comparing the endothermic and derivative weight loss peaks at the temperature range of 400-450°C in Figure 5.58. The CH content in the RHA-modified samples always exceeds that of the SF-modified samples, especially at heat treatments or at the extended periods of hydration of the normal treatment (Figure 5.56a and b). This indicates a less pozzolanic reactivity of RHA compared to SF.

5.4.1.2. Porosity and water absorption coefficient

The pore size distribution and total porosity of UHPCs under the normal treatment condition (20°C, Treatment 1) measured by MIP are shown in Figure 5.59 and Table 5.9.

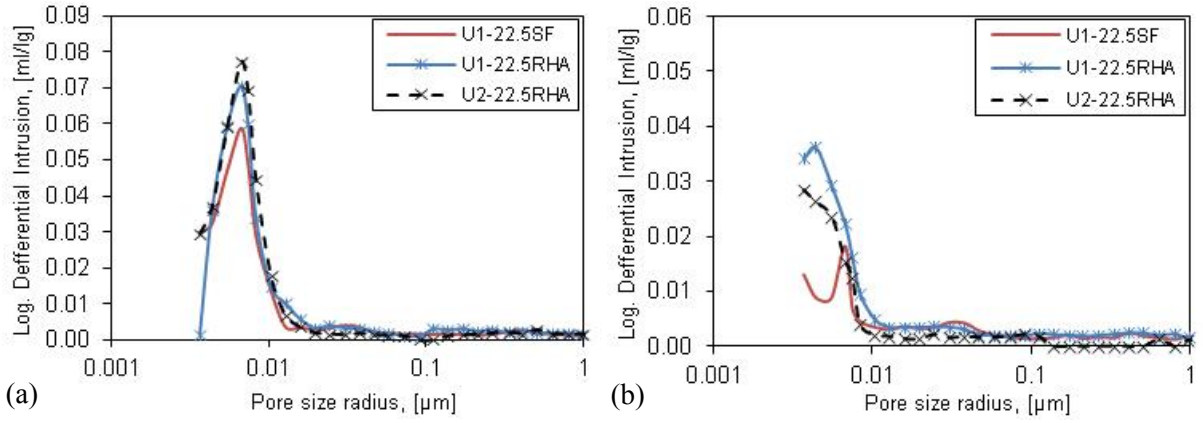

Figure 5.59. Pore size distribution of UHPC in dependence of pozzolans after normal treatment (20°C): a) 7 days; b) 28 days.

Table 5.9. Total MIP porosity of UHPC in dependence of pozzolans after 7 and 28 day normal treatment (20°C), [%]

Time of hydration	U1-22.5SF	U1-22.5RHA	U2-22.5RHA
7 days	7.42	7.34	8.30
28 days	4.13	5.43	3.91

The pore size distribution of the UHPCs at the age of 7 days shows clearly that the critical pore size radius in all the samples is about 0.007 µm. The pore size distribution in U1-22.5SF is better than that in U1-22.5RHA (Figure 5.59a). However, the total MIP porosity of U1-22.5SF slightly exceeds that of U1-22.5RHA (Table 5.9). GGBS decreases the density of UHPC containing RHA after 7 days of hydration (Figure 5.59a and Table 5.9). With increasing hydration time (28 days, Figure 5.59b and Table 5.9), the microstructure of UHPCs is clearly refined. The refining effect of SF is stronger than that of RHA in UHPC matrix. The density of the RHA-GGBS-blended UHPC is higher than that of the RHA-blended UHPC and SF-blended UHPC (Figure 5.59b and Table 5.9). The density of the UHPCs containing RHA at 28 days even exceeds that of an UHPC containing RHA at w/b of 0.18 investigated by Nguyen [60].

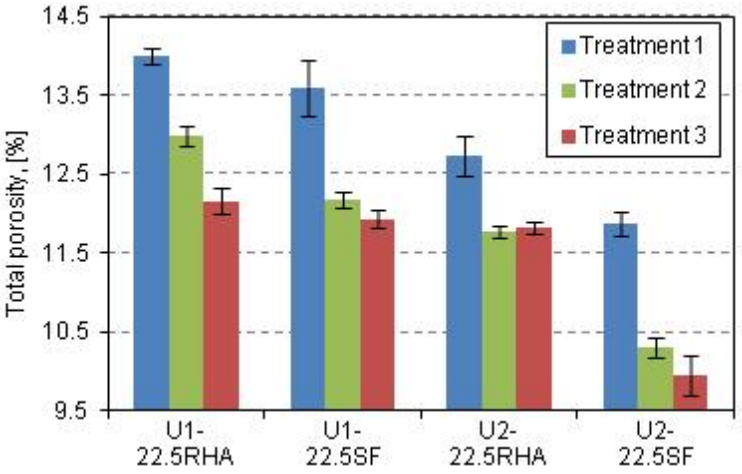

Figure 5.60. Effect of pozzolans and treatment conditions on total porosity.

Figure 5.60 displays results of total porosity calculated from bulk density and specific density of UHPCs under different treatment conditions at the age of 28 days. It can be seen that increasing temperature enhances the density of the UHPCs. The SF-modified samples possess higher density than the RHA-modified samples. The incorporation of GGBS and RHA or SF improves the microstructure of the UHPCs for all the treatment conditions (Figure 5.60). At

28 days, the total porosity results of the normally treated UHPCs in Figure 5.60 correlate well with the total MIP porosity results in Table 5.9.

Results of water absorption coefficient (W_{24}) of the UHPCs subjected to the different treatment conditions (Figure 5.61) show clearly that the SF-modified UHPCs perform a significantly lower water absorption compared to the RHA-modified UHPCs. The combination of GGBS and RHA or SF leads to a decrease in the water absorption. The water absorption coefficient of all investigated samples is decreased by increasing temperature of treatment (Figure 5.61).

5.4.1.3. Microstructure of UHPC containing RHA by SEM imaging

BSE-SEM image in Figure 5.62a shows that a large amount of unhydrated cement clinker remains after 28 days of hydration and RHA particles disperse well in the normally treated U1-22.5RHA. RHA particles are embedded very tightly into the cement matrix. The interfacial transition zone (ITZ) between RHA particle and the matrix is very dense (Figure 5.62b).

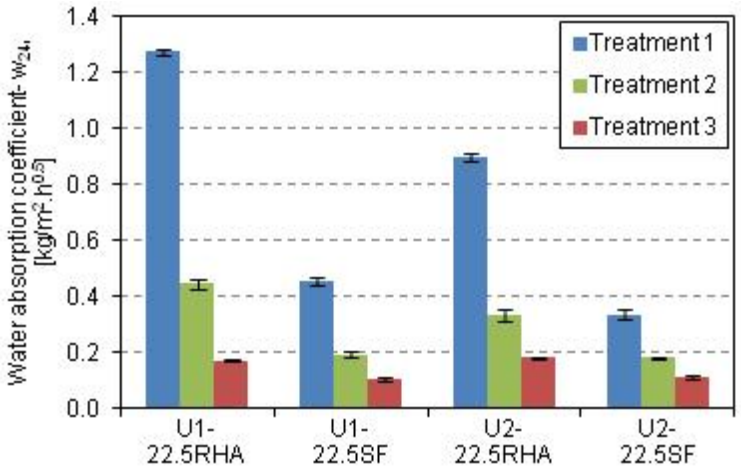

Figure 5.61. Effect of pozzolans and treatment conditions on water absorption coefficient (w_{24}).

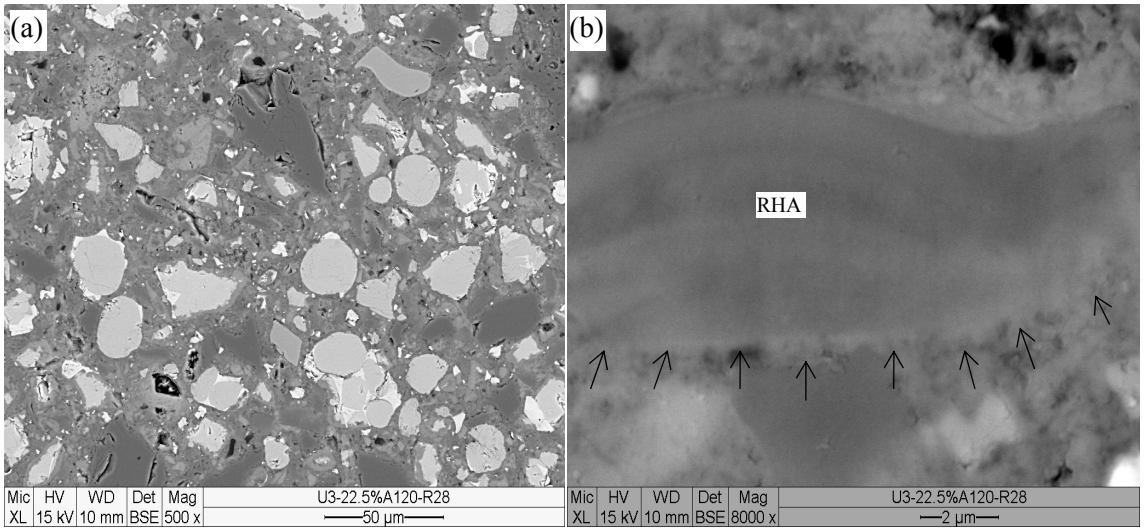

Figure 5.62. BSE-SEM images of polished section of the normally treated U1-22.5RHA at the age of 28 d: a) unhydrated cement clinker (light grey) and RHA particles (dark grey); b) unclear interfacial transition zone of RHA particle (arrows) showing a transition of calcium from matrix.

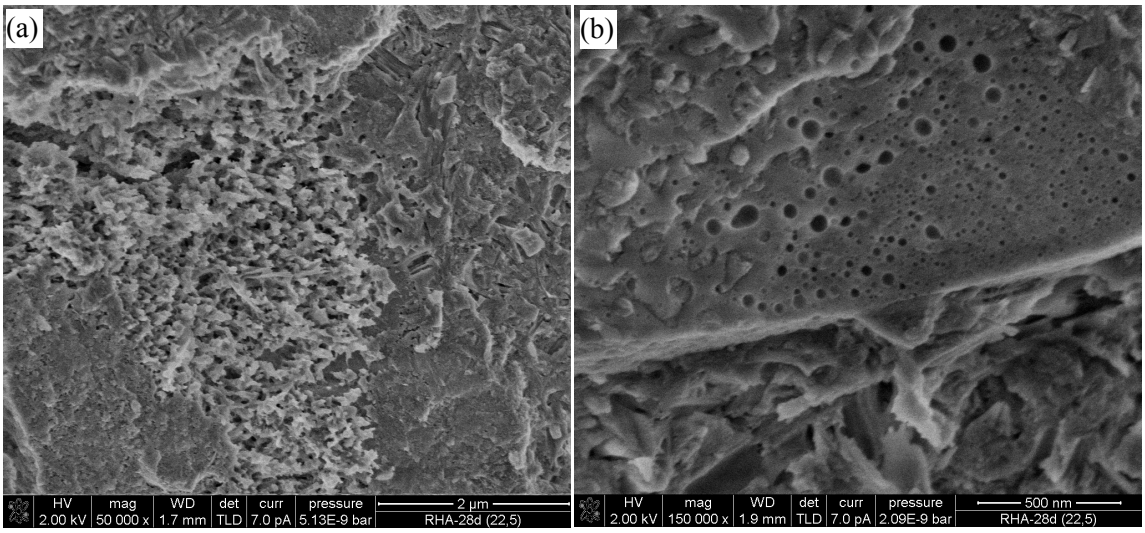

Figure 5.63. RHA particles in the normally treated U1-22.5RHA at the age of 28 d: a) dissolution structure on RHA particle; b) mesopores of RHA particle partially filled by hydration products.

Figure 5.63a displays that some RHA particles or some parts of RHA particle are strongly dissolved. However, some RHA particles or some parts of RHA particle still remain the initial shape with mesopores (Figure 5.63b). Comparing with the mesoporous structure of unhydrated RHA (Figure 5.6b), the mesopores of hydrated RHA particle in the UHPC are partially filled with hydration products after 28 days of hydration (Figure 5.63b). Combining this finding with the different gradient of grey values in RHA particle and the unclear ITZ on some parts of RHA particle (Figure 5.62b) indicates a continuous calcium transport from matrix into RHA. This is in good agreement with the findings in Figure 5.11.

5.4.2. Durability of UHPC

5.4.2.1. In NH_4NO_3 5M

Results in Figure 5.64 and Figure 5.65 display weight loss and corrosion depth of differently treated UHPCs (20, 65, 90°C) which were stored in NH_4NO_3 5M up to 12 weeks. The corrosion depth was measured by phenolphthalein and the digital microscopy (Figure 4.8). Generally, deterioration of the samples develops over time. Corrosion resistance to NH_4NO_3 5M of the SF-modified samples is better than the RHA-modified samples. For UHPCs containing SF, increased corrosion resistance is observed at high temperature of

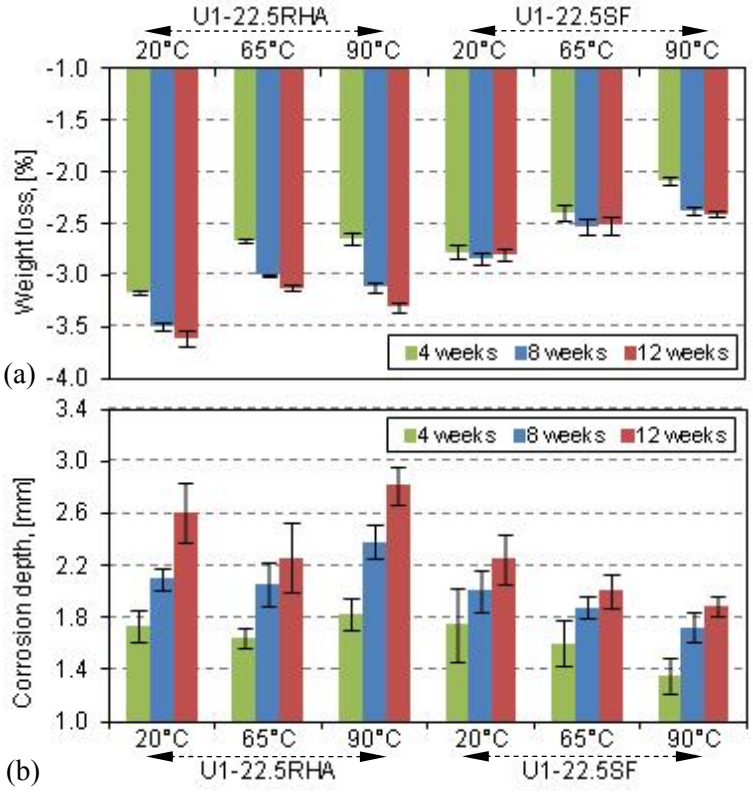

Figure 5.64. a) Weight loss and b) corrosion depth of differently treated UHPCs containing RHA or SF in dependence of periods in NH_4NO_3 5M.

treatment. GGBS slightly improves the corrosion resistance of the UHPC containing SF (Figure 5.64 and Figure 5.65). For UHPCs containing RHA, the highest corrosion resistance is obtained for the 65°C treated U1-22.5RHA. The corrosion depth of the 90°C treated U1-22.5RHA is increased compared to that of the 20°C treated sample (Figure 5.64b). The different treatment conditions do not significantly change the corrosion resistance of the RHA-GGBS-blended UHPC (U2-22.5RHA, Figure 5.65b). GGBS decreases the weight loss but slightly increases the corrosion depth of all the RHA-modified samples (Figure 5.64 and Figure 5.65).

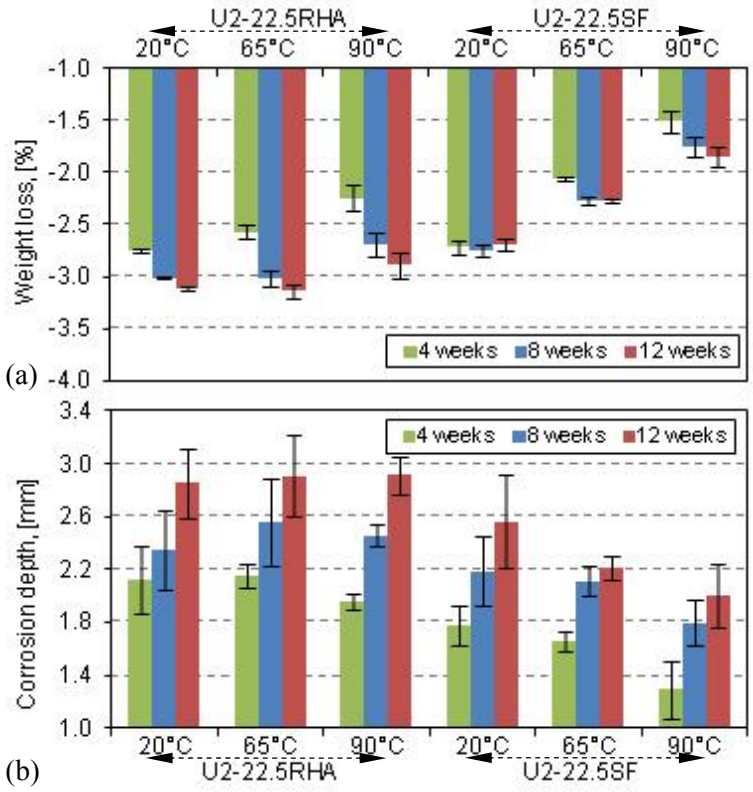

Figure 5.65. a) Weight loss and b) corrosion depth of differently treated UHPCs containing GGBS and RHA or SF in dependence of periods in NH_4NO_3 5M.

5.4.2.2. In H_2SO_4 pH 2.5

Results of weight change and expansion of differently treated UHPCs (20, 65, 90°C) stored for 36 weeks in H_2SO_4 at pH= 2.5 are given in Figure 5.66 to Figure 5.68. The mean standard deviation of all the weight change measurements is 0.03% and of all the length change measurements is 35.68 µm/m.

For the 20°C treated samples (at Treatment 1), the weight change results (Figure 5.66a) clearly show an increase in weight during the first two weeks of the storage. Thereafter, the weight of the SF-blended samples is almost constant up to 16 weeks. During the same period, there is a slight decrease in weight of the UHPCs containing RHA. From 16 to 36 weeks in the solution, the weight loss of all the samples is more significant. The SF-modified UHPCs have a lower weight loss than the RHA-modified UHPCs. The expansion results in Figure 5.66b reveal that the expansion of the samples is almost linear and has a high expansion rate during the first ten weeks. Thereafter, the expansion rate of the samples is slower. The SF-modified UHPCs possess a lower expansion than the RHA-modified UHPCs. GGBS enhances the durability (weight loss and expansion resistance) of the samples (Figure 5.66).

For the heat treated samples, the increase in weight of the samples during initial weeks is also observed. Apart from the 90°C treated U1-22.5RHA and the 90°C treated U1-22.5SF (Figure 5.66a), there is no significant difference in weight change of UHPC containing RHA, respectively, SF, for the same temperature treatment (Figure 5.67a and Figure 5.68a). Increasing temperature of treatment leads to an increase in the weight change but no

significant variation in expansion of the samples is found (compare Figure 5.67 and Figure 5.68). The expansion values of the heat treated samples slightly exceeds that of the normally treated samples (compare Figure 5.66b to Figure 5.67b and Figure 5.68b).

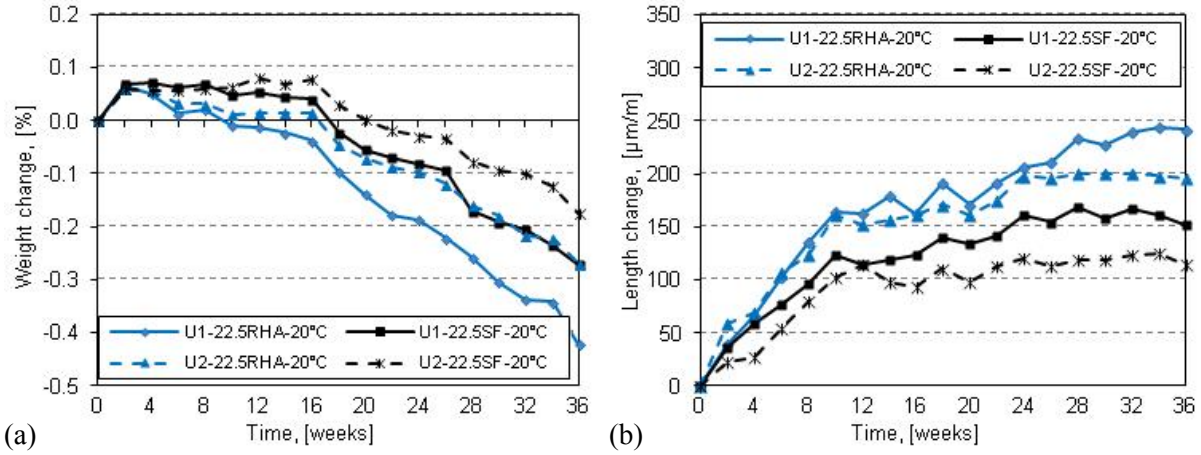

Figure 5.66. a) Weight change and b) expansion of UHPCs at the normal treatment in H_2SO_4 pH 2.5.

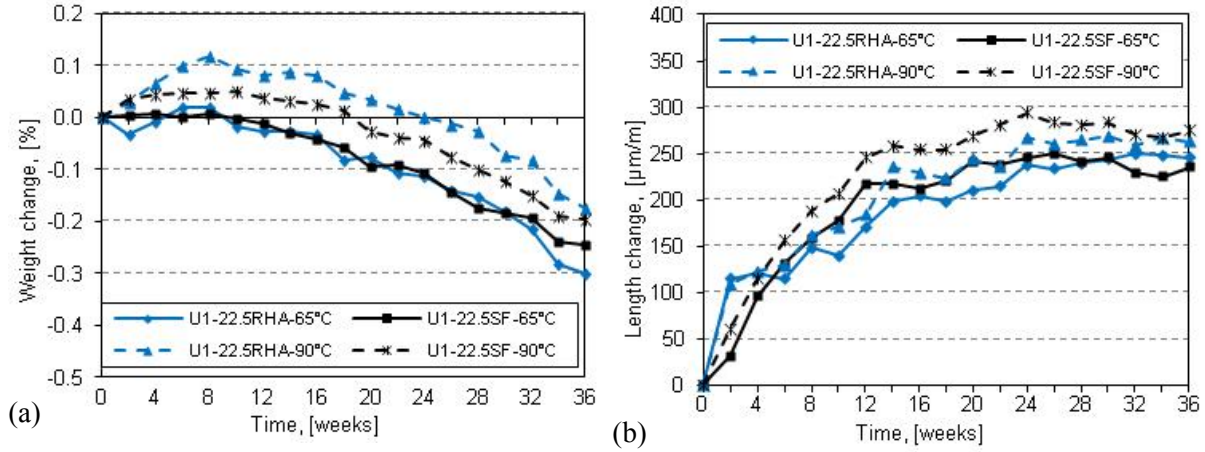

Figure 5.67. a) Weight change and b) expansion of U1-22.5RHA and U1-22.5SF at the different heat treatments in H_2SO_4 pH 2.5.

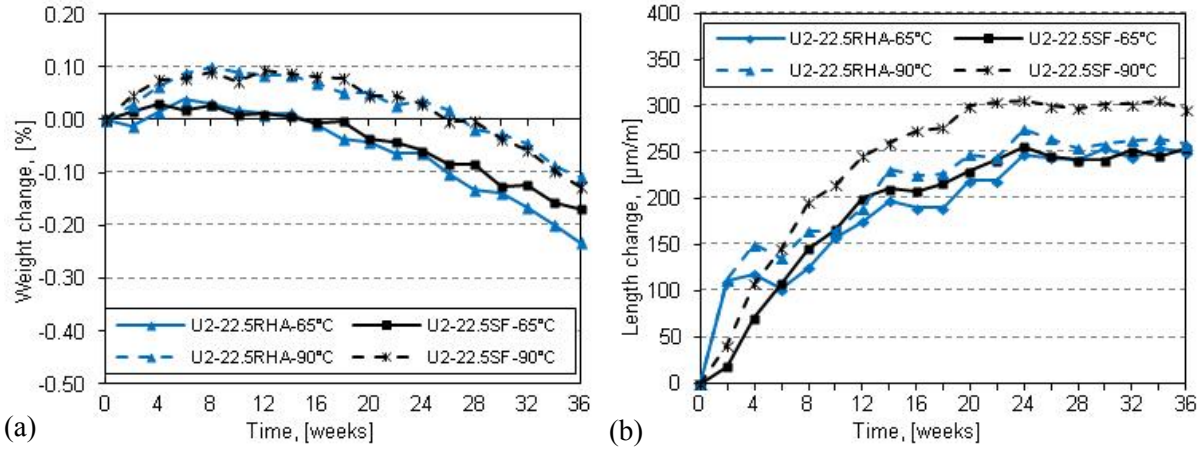

Figure 5.68. a) Weight change and b) expansion of U2-22.5RHA and U2-22.5SF at the different heat treatments in H_2SO_4 pH 2.5.

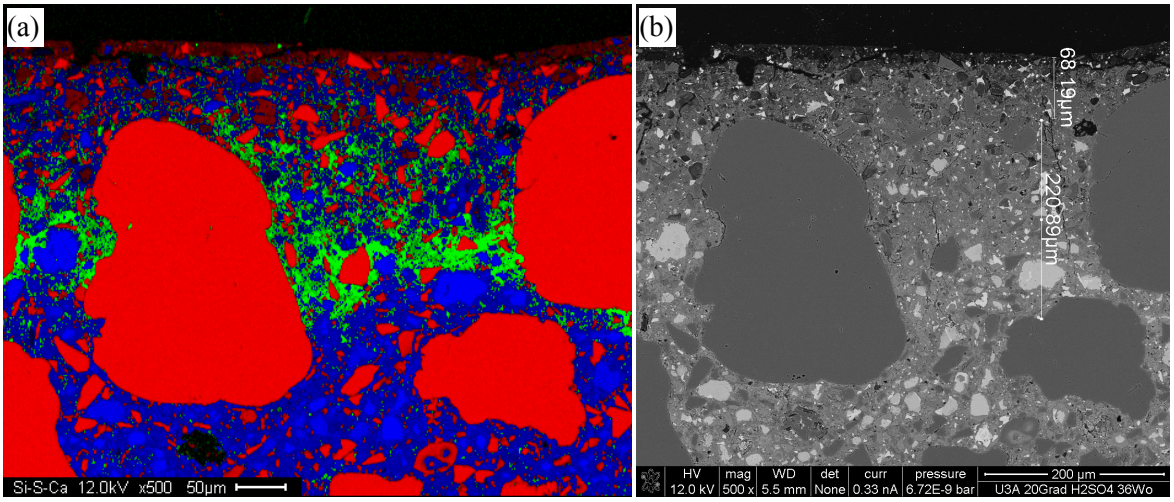

Figure 5.69. Deterioration of the normally treated U1-22.5RHA after 36 weeks in H_2SO_4 pH 2.5: a) EDX mapping showing Si in red, S in green, Ca in blue; b) BSE image with corrosion depth.

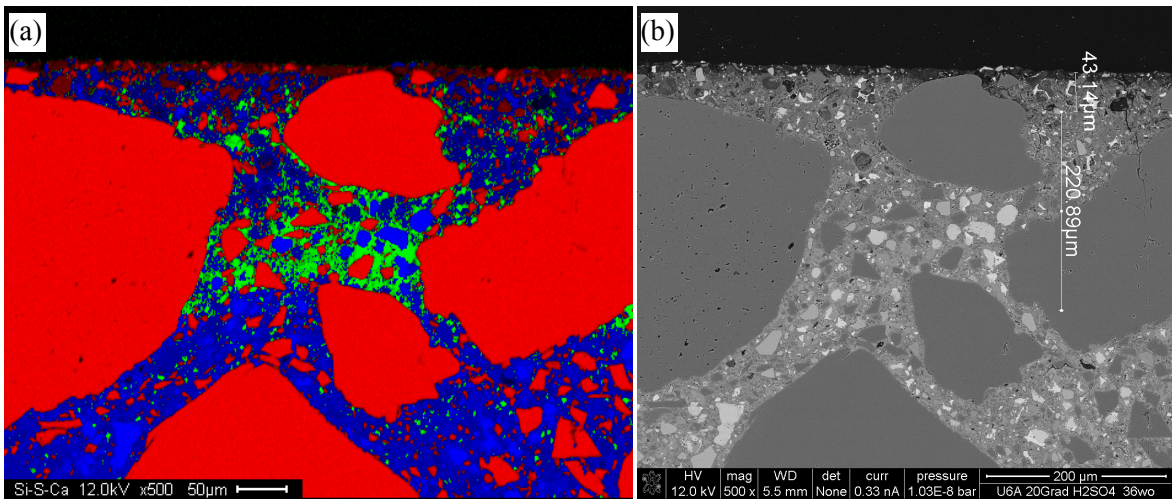

Figure 5.70. Deterioration of the normally treated U2-22.5RHA after 36 weeks in H_2SO_4 pH 2.5: a) EDX mapping showing Si in red, S in green, Ca in blue; b) BSE image with corrosion depth.

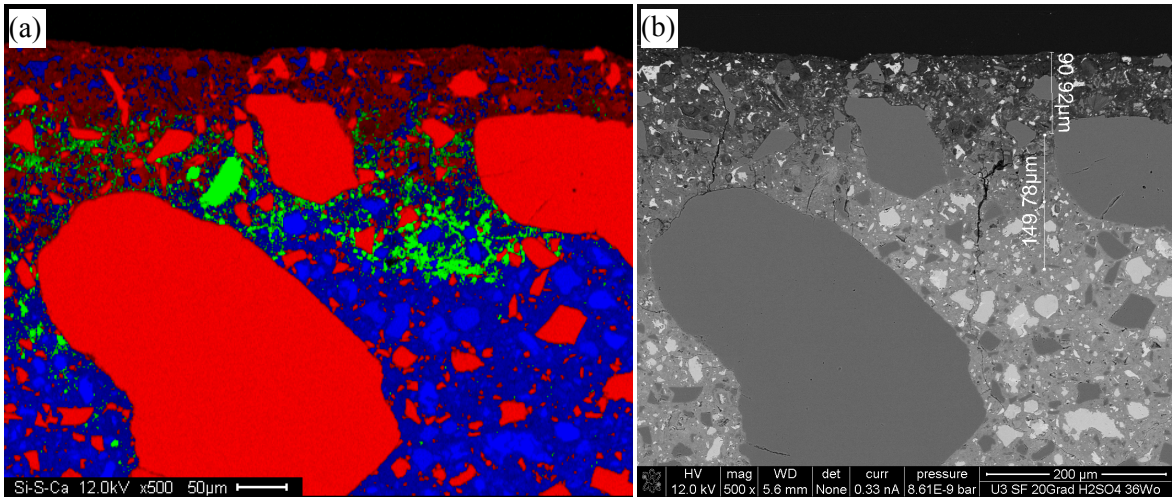

Figure 5.71. Deterioration of the normally treated U1-22.5SF after 36 weeks in H_2SO_4 pH 2.5: a) EDX mapping showing Si in red, S in green, Ca in blue; b) BSE image with corrosion depth.

Figure 5.69, Figure 5.70 and Figure 5.71 display energy dispersive X-ray (EDX) spectroscopy mappings and BSE images of the normally treated UHPCs after 36 weeks in H_2SO_4 pH 2.5. It can be seen that the ingress of sulfate from the solution into the different matrices is dependent on UHPC composition. The corrosion depths of SO_4^{2-} are about 290 µm in U1-22.5RHA (Figure 5.69), 265 µm in U2-22.5RHA (Figure 5.70) and 240 µm in U1-22.5SF (Figure 5.71). These results are consistent with the results of the weight change and expansion of the normally treated samples (Figure 5.66). It is assumed that the combination of RHA and GGBS improves the resistance of sulfuric acid attack of the RHA-blended UHPC at the normal treatment. The corrosion of SO_4^{2-} in the SF-blended UHPC is lower than that in the RHA-blended UHPC and RHA-GGBS-blended UHPC.

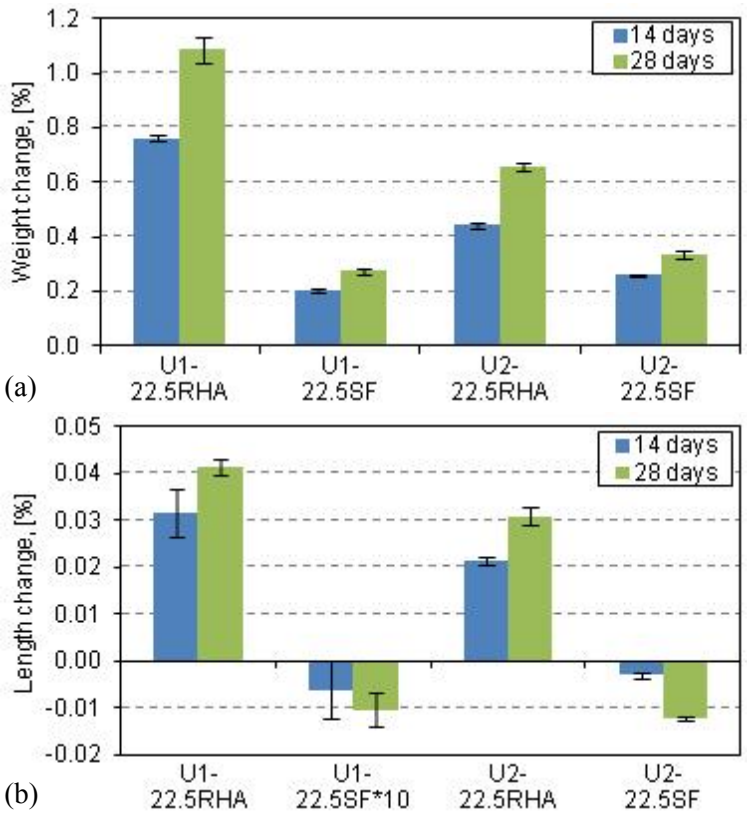

Figure 5.72. a) Weight and b) length change of 40 × 40 × 160 mm³ samples in the NaOH solution.

5.4.2.3. Alkali silica reaction (ASR)

Results of weight and length change of three 40 × 40 × 160 mm³ sized samples of the UHPCs after 14 and 28 days in NaOH 1M at 80°C are shown in Figure 5.72. The length change values of U1-22.5SF*10 in Figure 5.72b are given by multiplication of the experimental results to 10 times to make the results visible. It shows clearly that the longer the sample is in NaOH, the more the weight

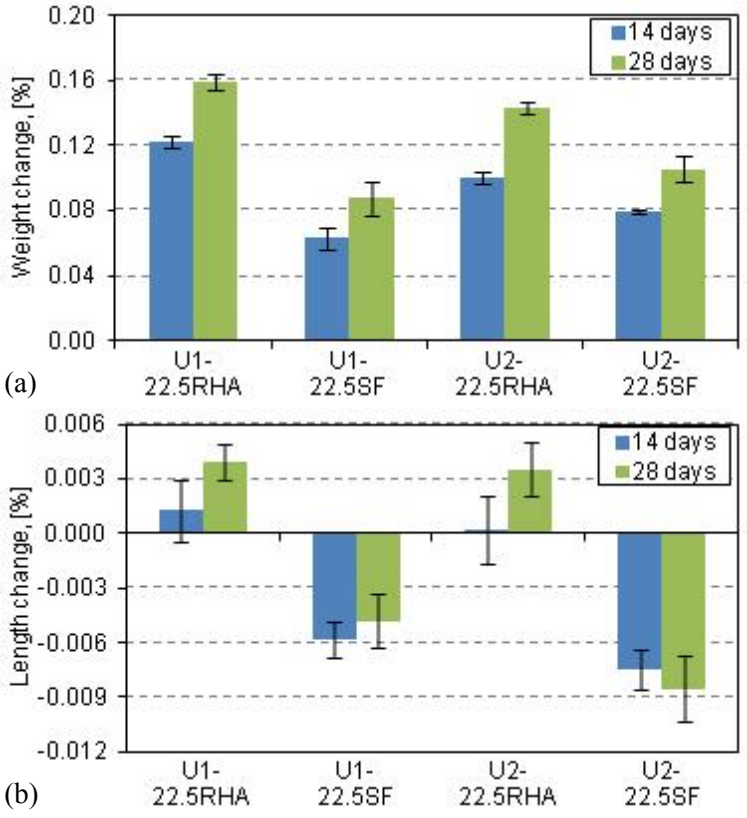

Figure 5.73. a) Weight and b) length change of 40 × 40 × 160 mm³ samples in water (replacing NaOH).

increases (Figure 5.72a) and the larger the length changes (Figure 5.72b). The RHA-modified UHPCs absorb more NaOH solution and show larger expansion than the SF-modified UHPCs. The samples containing SF are even shrunk (Figure 5.72b). GGBS clearly reduces the weight and length change of the RHA-modified sample (Figure 5.72).

Effect of autogenous shrinkage on length change value

It can be seen that weight change of the samples (40 × 40 × 160 mm^3) in water (Figure 5.73a) is consistent with that of the samples in NaOH 1M (Figure 5.72a). NaOH accelerates the liquid absorption and the expansion of the samples (compare Figure 5.72 and Figure 5.73). For the length change, after one day in water at 80°C the samples containing RHA slightly expanse during the next 28 days. Meanwhile, shrinkage is observed for the samples containing SF (Figure 5.73b). The length change values measured in water is subtracted from the length change values measured in the NaOH solution (Figure 5.74). Hence, the corrected length change values in Figure 5.74 present the absolute length change due to ASR in the NaOH solution. Obviously, the corrected length change of the RHA-blended UHPC samples is decreased. Except for U2-22.5SF after 28 days in the solution, the corrected length change of SF-modified UHPCs is now in the expansion range (Figure 5.74). From this finding, it can be concluded that the difference in autogenous shrinkage of different

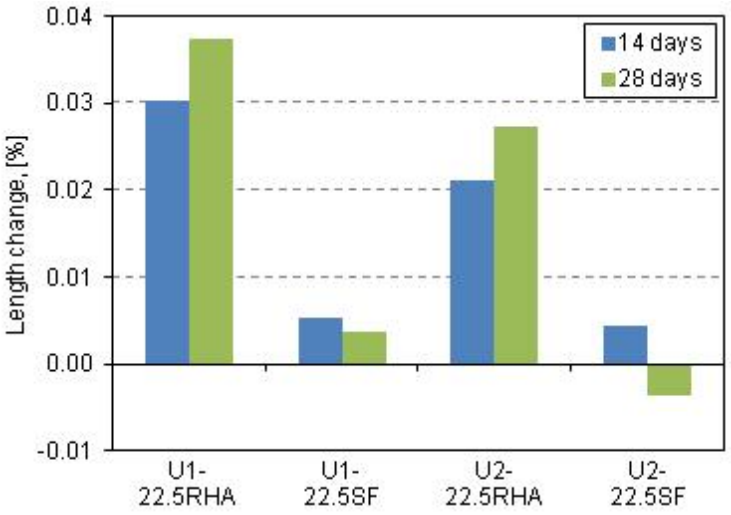

Figure 5.74. Corrected length change of 40× 40 × 160 mm^3 sized samples in the NaOH solution.

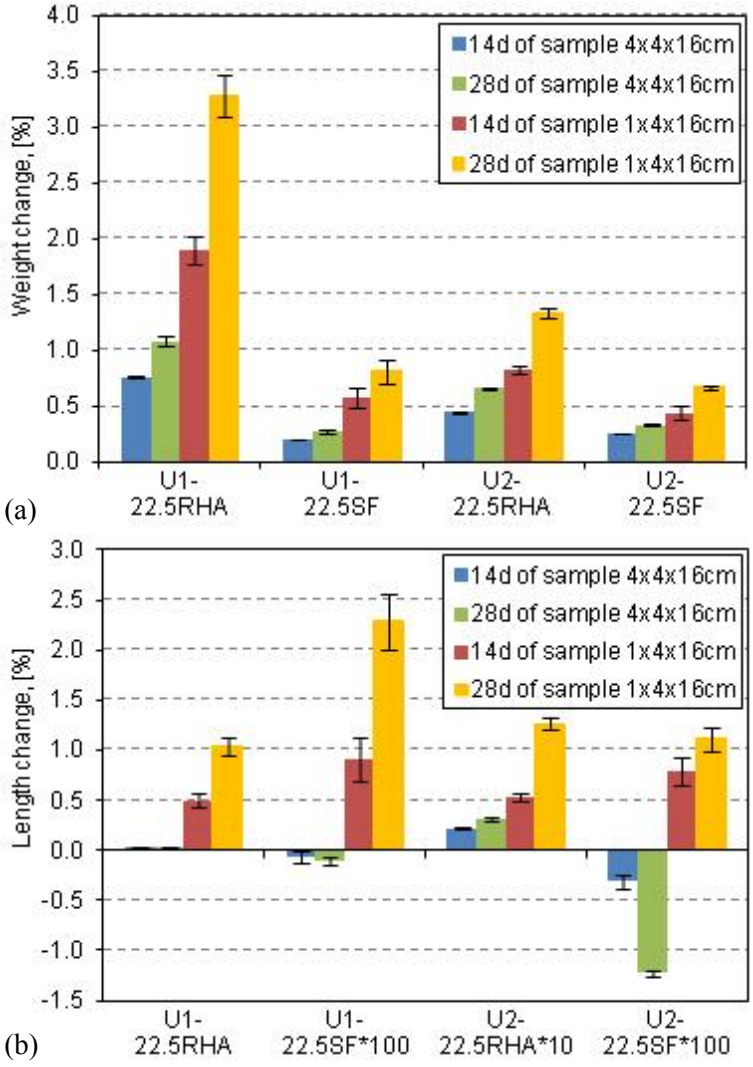

Figure 5.75. a) Weight and b) length change of different sized samples in the NaOH solution.

UHPCs should be take into account the final expansion results, as the indicator of deterioration degree of UHPCs.

Effect of sample dimension on weight and length change

Results of the weight and length change of 40 × 40 × 160 mm^3, respectively, 10 × 40 × 160 mm^3 sized samples during 28 days in the NaOH solution are shown in Figure 5.75. The length change values of U2-22.5RHA are magnified 10 times in Figure 5.75b (U2-22.5RHA*10). And the length change values of U1-22.5SF*100 and U2-22.5SF*100 in Figure 5.75b are the multiplication of the experimental results to 100 times.

As expected, the reduction of the cross sectional area of the samples increases the weight change (i.e. NaOH solution absorption, Figure 5.75a) and hence accelerates the expansion of all the samples (Figure 5.75b). Expansion of the small sized SF-modified samples is observed. In contrast, the larger sized SF-modified bars (40 × 40 × 160 mm^3) are shrunk (Figure 5.75b). The effects of hydration period in the NaOH solution and pozzolan addition on the deterioration of the UHPCs are more significant for specimens having smaller cross sectional area.

The variation in damage of U1-22.5RHA with the different sized samples is displayed at the Figure 5.76a and Figure 5.76b. The addition of GGBS clearly improves the durability of UHPC containing RHA in the NaOH solution (compare Figure 5.76b and Figure 5.76c). By means of SEM, it is observed that the alkali silica gel appears in pores below the surface of U1-22.5RHA (Figure 5.77). There are also some small cracks around the pore after 14 days in NaOH 1M at 80°C (Figure 5.77b).

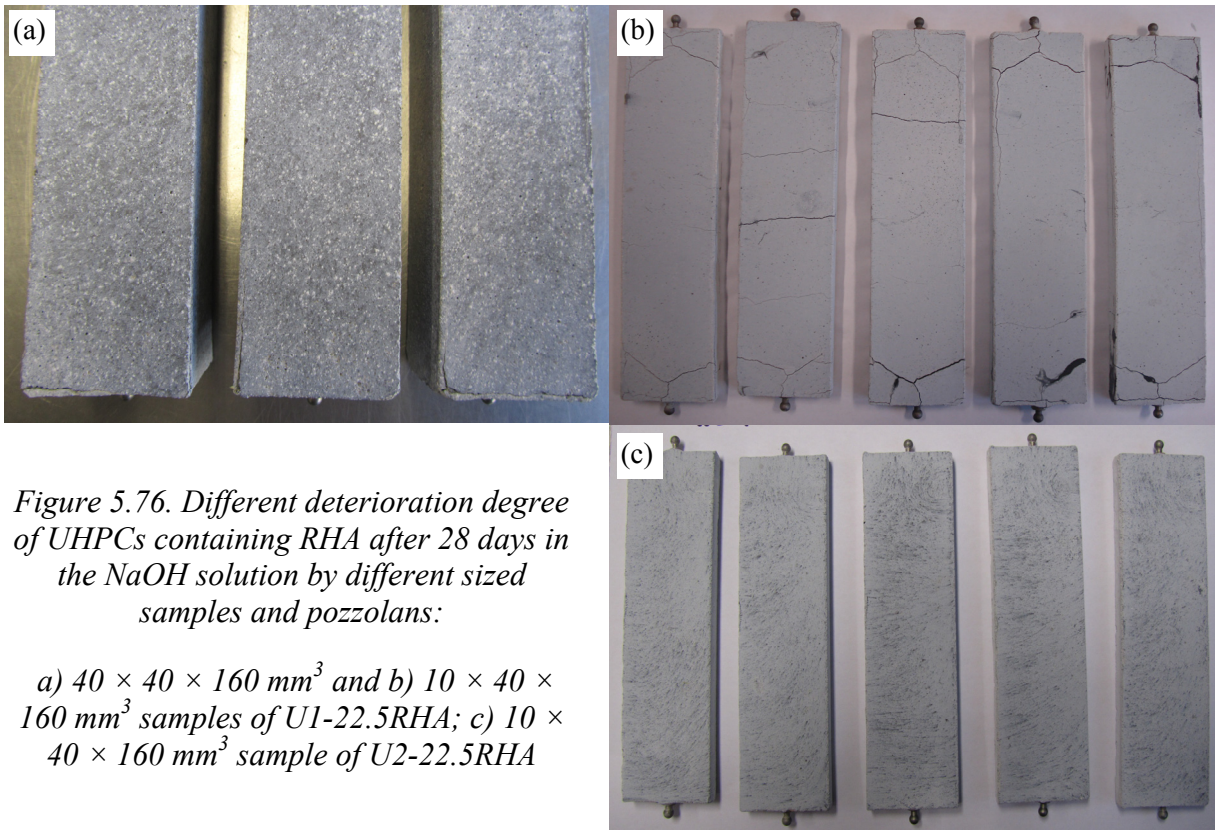

Figure 5.76. Different deterioration degree of UHPCs containing RHA after 28 days in the NaOH solution by different sized samples and pozzolans:

a) 40 × 40 × 160 mm^3 and b) 10 × 40 × 160 mm^3 samples of U1-22.5RHA; c) 10 × 40 × 160 mm^3 sample of U2-22.5RHA

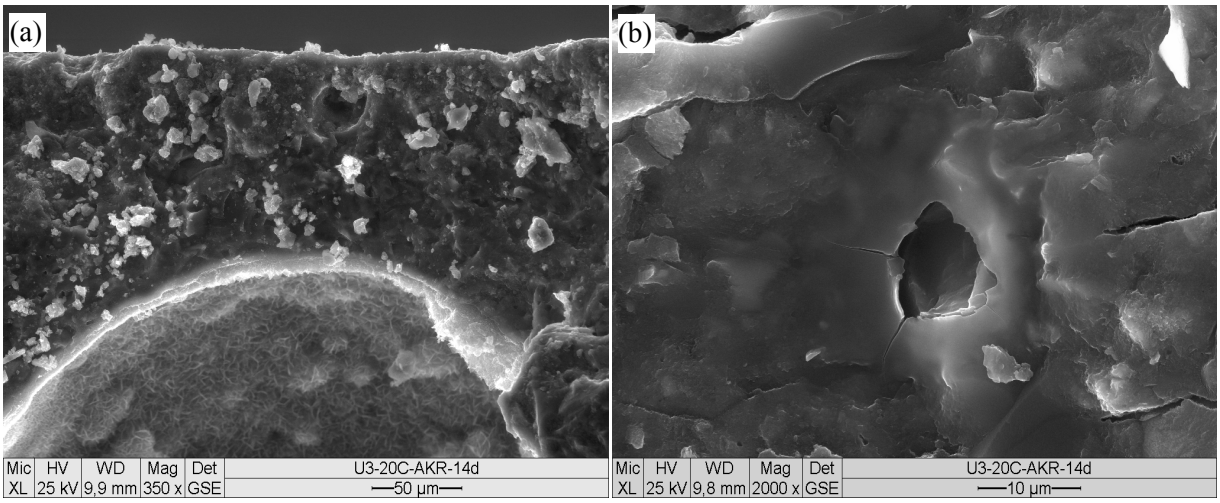

Figure 5.77. ASR in U1-22.5RHA after 14 days in the NaOH solution: a) alkali silica gel in pore below surface of sample; b) alkali silica reaction layer with cracks around a pore.

5.4.2.4. In cyclic climate storage (CCS)

Cyclic climate storage (CCS) test was conducted on 100 × 100 × 400 mm^3 sized samples (Treatment 1 and Treatment 2) at the age of 7 days. The length change results during the examination are shown in Figure 5.78 and Figure 5.79. Obviously, the expansion after the first cycle (21 days) is typical for concrete due to the water absorption [130]. The regular contractions of all the samples after the first cycle are observed during the test. SF and GGBS increase the contraction of the sample (Figure 5.78 and Figure 5.79). Apart from U1-22.5RHA, the heat treated samples have slightly increased contraction than the normally treated samples (compare Figure 5.78 and Figure 5.79). The length change values of all the samples are far below the limit value of 0.4 mm/m after 16 cycles (336 days). For comparison, a normal concrete [129] with CEM I 32.5 R, greywacke aggregates (reactive aggregate), quartz sand at water to cement ratio of 0.45 has been integrated into Figure 5.78. This indicates that the durability of the UHPCs is very high. There should be no concern about the ASR in the UHPCs containing RHA.

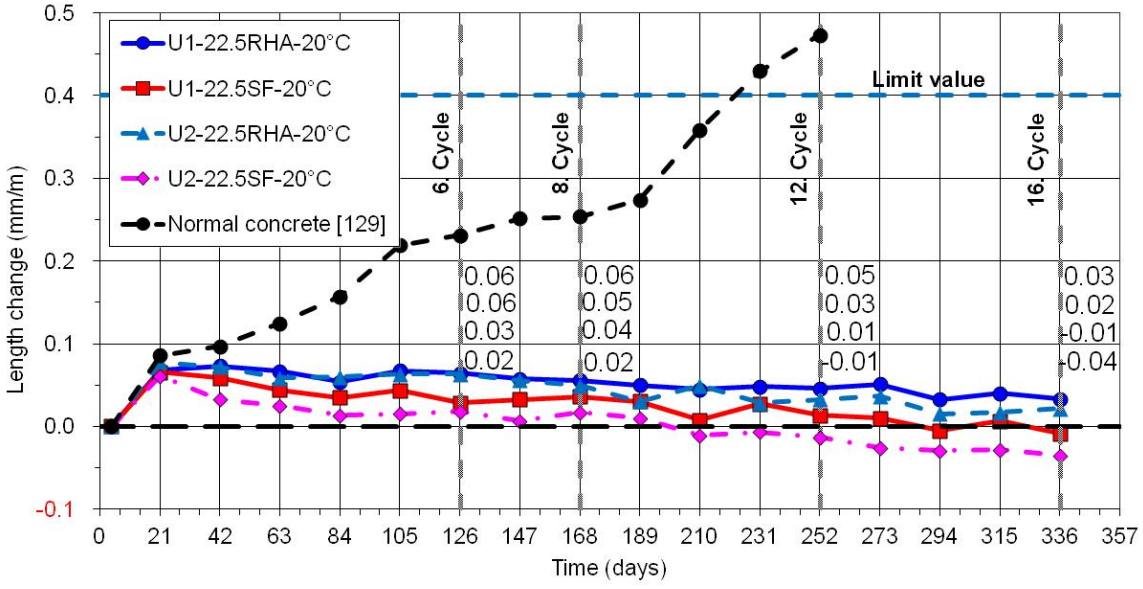

Figure 5.78. The length change of the normally treated UHPCs and a normal concrete [129] (with reactive aggregate) in CCS.

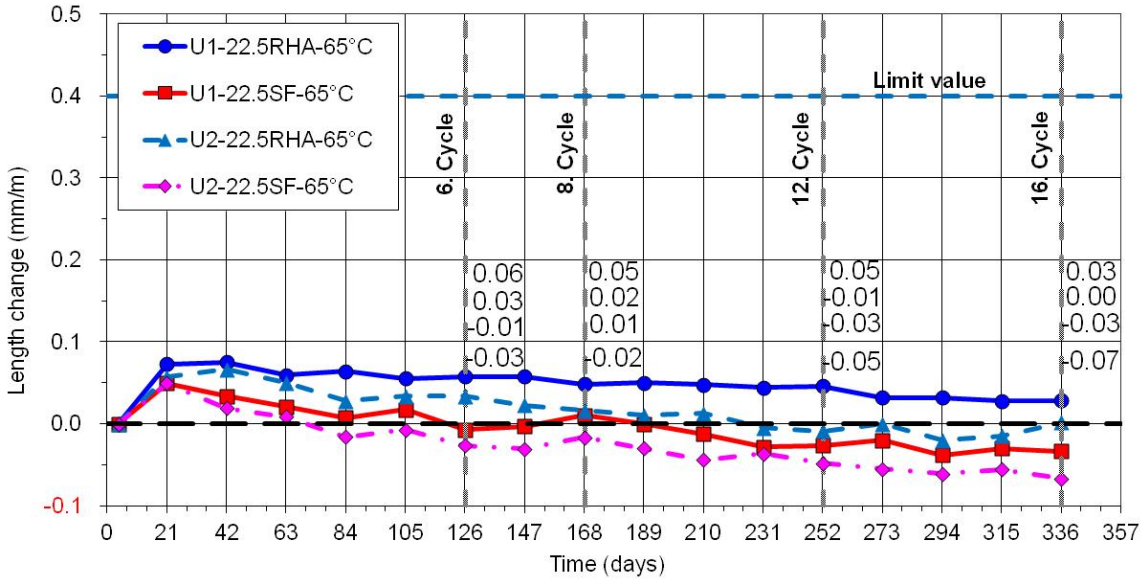

Figure 5.79. The length change of the 65°C treated UHPCs in CCS.

5.4.3. Discussion

At the normal treatment, the CH content in U2-22.5SF is nearly similar during the hydration periods between 7 and 28 days or 180 and 360 days (Figure 5.56a). After 28 days of hydration, the CH content in U2-22.5RHA does not significantly change as well (Figure 5.56b). The minor change in the CH content during 91 d hydration is also found in the normally treated RHA-blended, respectively, SF-blended pastes at w/b of 0.22 (Figure 5.10). At extended ages, the increased CH content is found in the heat treated samples containing RHA or SF for both w/b of 0.22 cement paste with 6 day treatment at 65°C (Figure 5.10c, d) and UHPC with 48 h treatment at 90°C (Figure 5.56). Meanwhile, the CH content in both U2-22.5SF and U2-22.5RHA with 48 h treatment at 65°C is regularly decreased (Figure 5.56). This confirms that the hydration of cement clinker and pozzolans (i.e. RHA or SF) in the very low water content matrices proceeds even up to 360 days. The CH content in the matrices is specified by how much CH is produced by the cement clinker hydration and is consumed by the pozzolanic reaction. It induces different CH contents in different matrices at different treatment conditions and hydration periods. The elevated temperature enhances the pozzolanic reactivity of the pozzolans.

It is known that RHA particle size is about 25 times bigger than SF particle size (Table 4.3 and Table 5.1). The packing density of a SF-modified UHPC is higher than that of RHA-modified UHPCs [60]. Furthermore, the combination of different fineness materials improves the packing density of mixture [115, 219]. Also, the combination of GGBS and SF, respectively, RHA, improves the workability and hence decreases the air content in vibrated mixture (Table 5.3, Figure 5.29 and Figure 5.35). Additionally, the pore refinement effect of SF in cement matrix is more significant than that of RHA which is observed in Figure 5.59 or in a previous study [60]. All of these factors induce the decreased total porosity and water absorption of SF-blended or GGBS-blended mixtures in Figure 5.60 and Figure 5.61. Increasing temperature enhances the pozzolanic reaction (Figure 5.10 and Figure 5.56). It improves the refinement of pore structure of concrete [98, 220] and thus decreases the total

porosity and water absorption of UHPC (Figure 5.60 and Figure 5.61). The variation in the water absorption of the UHPCs results in the different water evaporation, and hence the different drying shrinkage of the UHPCs (Figure 5.50 to Figure 5.53).

Generally, the results of durability of the UHPCs in the aggressive solutions (H_2SO_4, NH_4NO_3 and NaOH) show that the samples containing SF possess higher durability than the samples containing RHA. The combination of GGBS and RHA or SF improves the durability of the UHPCs containing RHA or SF. These results are in good agreement with the results of the effects of the pozzolans on the total porosity and water absorption coefficient of the UHPCs (Figure 5.60 and Figure 5.61). Hence, water absorption coefficient is considered as one of important parameters determining the aggressive agent resistance of UHPC. The enhanced microstructure characteristics of the UHPCs by the heat treatments are clear. However, the benefits of the heat treatments on long term compressive strength (in Section 5.3) and durability of the UHPCs are insignificant.

Furthermore, the investigation of the effect of autogenous shrinkage on the ASR expansion result (Figure 5.72 to Figure 5.74) indicates that autogenous shrinkage should be taken into account to discuss the length change values in durability tests. The long term autogenous shrinkage of the UHPCs containing RHA is significantly lower than that of the SF-modified UHPCs. Heat treatment ceases autogenous shrinkage of UHPC (Figure 5.50 and Figure 5.51). This may lead to the observed increased expansion of the normally treated UHPCs containing RHA compared to the normally treated UHPCs containing SF in the H_2SO_4 solution (Figure 5.66b). Also, expansion of the heat treated samples exceeds that of the normally treated samples in durability test (compare Figure 5.66b to Figure 5.67b and Figure 5.68b).

The standard ASR test methods [127, 203] reveals that expansion values less than 0.10% after 14 days in NaOH 1M at 80°C is considered to be innocuous. Values higher than 0.20% are indicative for potentially deleterious ASR. All the investigated UHPCs with $40 \times 40 \times 160$ mm^3 sized sample have the expansion values below the lower threshold (0.1%) after both of 14 and 28 days in the NaOH solution (Figure 5.72b). The contraction of a SF-modified UHPC was also observed in a previous investigation [122]. Additionally, the expansion of the UHPC samples in the CCS test is far below the limit value of 0.4 mm/m after 16 testing cycles (Figure 5.78 and Figure 5.79). Therefore, there should be no concern of ASR problems with the UHPCs containing RHA or SF.

According to the standard ASR test methods, the alkali content of cement has been found to have minor effect on expansion of the standard mortar at w/b of 0.47 because the high ingress of NaOH 1M into the standard mortar [127]. For UHPC, the water absorption of these UHPCs is very low and different (Figure 5.61). It was found that water and Na^+ ions from environment diffuse into the same sized samples differently (Figure 5.72a and Figure 5.73b). Furthermore, it is known that the size of sample in the American standard [127] is $25 \times 25 \times 285$ mm^3 which is different from $40 \times 40 \times 160$ mm^3 sized sample in the German standard [203]. The weight change of differently sized samples in Figure 5.75a unveils that reducing the cross sectional area (i.e. the concrete volume per unit length) results in an increased ingress level of aggressive agent (Na^+ ions) into the matrix. Hence, the length change value which indicates the deterioration of UHPC in the ASR test is strongly affected

by the level of Na^+ ions diffusing into the matrix. It relates to both the water absorption coefficient and the sample size in this accelerated test method with the external aggressive agent (Figure 5.75b).

As discussed, the hydration of cement clinker, RHA and SF proceeds up to 360 days even in the heat treated samples (Figure 5.56). The continuous hydration of cementitious materials in the UHPCs results in the decreased relative humidity (Figure 5.54), the increased autogenous shrinkage (Figure 5.49 to Figure 5.51) and the contraction of the samples (Figure 5.72b, Figure 5.73b, Figure 5.78 and Figure 5.79) during the examinations. The additional hydration of the cementitious materials compensates the minor microstructure deterioration of the UHPCs under the aggressive conditions.

5.4.4. Concluding remarks

Based on the investigations of the microstructure and durability of the UHPCs, the following conclusions can be drawn:

- Hydration of the cementitious materials in the extremely dense UHPCs proceeds up to 360 days even at the elevated temperature treatments.
- With super fine particles and high pozzolanic reactivity of SF, the microstructure characteristics of the SF-modified UHPCs are improved compared with that of the RHA-modified UHPCs. Durability of the RHA-blended UHPCs is high but not better than that of the SF-blended UHPCs. The permeability (water absorption) of UHPC should be considered as the important parameter which strongly affects the durability of UHPC in aggressive environment.
- The incorporation of GGBS and RHA or SF improves the microstructure characteristics and hence durability of UHPC.
- Heat treatments clearly enhance microstructure of UHPC. The effect of heat treatments on durability of UHPC seems insignificantly.
- Autogenous shrinkage of UHPCs containing RHA, respectively, SF, is distinctly different, i.e. SF induces a significantly increased autogenous shrinkage. Meanwhile, the expansion of the SF-blended samples in aggressive solution is normally lower than that of the RHA-blended samples. Hence, autogenous shrinkage should be considered for evaluation of final deformation results by length change value in durability test.
- There should be no concern about alkali silica reaction problem in the UHPC containing RHA, especially with GGBS combination. In terms of durability, RHA can be a good pozzolan to completely substitute SF in UHPC production.

6. Conclusions and Further Research

6.1. Conclusions

The investigations of this study showed clearly that properly burned RHA is a renewable mesoporous amorphous siliceous material with very high amorphous silica content and specific surface area. The collapse of the porous structure of RHA particles during grinding results in the decrease in pore volume, BET-SSA and water absorption capacity.

By studying the pozzolanic reactivity of SF and RHA samples ground for different periods of time in the cementitious systems and portlandite (CH) solution, it is found that C-S-H as products of the pozzolanic reaction can be observed after 6 hours of hydration in the CH-pozzolan suspension at 40°C. The pozzolanic reactivity of SF exceeds that of RHA indicated by CH consumption in both cement matrix and CH solution. The electrical conductivity reduction rate [mS/cm·min] of the CH-pozzolan suspension from 30 to 210 min is proposed as a quick criterion for proper comparison of the pozzolanic reactivity of differently adsorptive pozzolans, i.e. RHA and SF in this study. Increasing temperature increases the pozzolanic reactivity of RHA and SF.

However, in terms of enhancement of compressive strength of mortar or UHPC, the pozzolanic reactivity of RHA is comparable or even higher than that of SF. And there is no advantage of the heat treatment of UHPCs containing RHA for long term compressive strength. This indicates that the CH consumption capacity of RHA is not the most important parameter for the compressive strength development. Rather the microstructural effects of the mesoporous structure of RHA can be considered as the important strength determining parameter. Due to its mesoporous structure, RHA particles can absorb water. Thus, the effective w/b in cementitious matrix is reduced by the presence of RHA. Absorbed water allows Ca^{2+} ions to diffuse into internal parts of RHA particles. This is shown to be advantageous for enhancing pozzolanic reactivity of RHA. Also, a continuous hydration of cement and a long lasting pozzolanic reaction of RHA are assured by this adsorbed water, especially in UHPC matrix with the very low water content. And, the mesoporous RHA structure facilitates that the hydration products of the pozzolanic reaction intergrow intensely with the cement matrix. This induces the extremely dense interfacial transition zone of RHA particle in UHPC matrix.

The compatibility between SP and UHPC mixture is important to choose the suitable SP to produce a mixture with the highest flowability and compressive strength. The compatibility between SP and UHPC mixture is governed not only by the kinds of SP but also by the cement and mineral admixtures. Furthermore, at very low water content (i.e. $W/F_v = 0.55$), the packing density and dispersion effects of RHA are also important parameters to improve the workability and compressive strength of UHPC. It compensates the negative effects of high SSA, high water absorption of RHA on workability compared with the plain cement

mixture. Hence, the slump flow and flowability retention of the mixture containing RHA exceeds those of the plain cement mixture.

After mixing, mini-cone slump flow of UHPC containing RHA exceeds that of UHPC containing SF at $W/F_v = 0.55$. It is possible to maintain the workability of reduced water content mixture containing SF by increasing SP dosage due to very fine and perfect spherical particles of SF to improve the rheological properties of UHPC. Whereas, due to mesoporous, coarse particle and irregular particle shape of RHA, the workability of UHPC containing RHA strongly decreases when the excess water is insufficient. It needs a significantly high SP dosage to maintain the workability. Thus, $w/b \geq 0.20$ (i.e. $W/F_v \geq 0.50$) should be used for producing a properly workable UHPC containing RHA with an acceptable SP dosage in this study.

It is possible to produce sustainable UHPC without SF and with low cement content by using RHA and the combination of RHA and GGBS. With $W/F_v = 0.55$ and the same SP dosage, mini-cone slump flow of the mixtures containing RHA exceeds that of the mixtures containing SF after mixing. Compressive strength of the RHA-modified samples is comparable with that of the SF-modified samples under the normal treatment condition.

The combination of RHA and GGBS significantly improves flowability and compressive strength of UHPC. The synergic effects of RHA, GGBS and SP dosage on flowability and compressive strength have been clearly interpreted by 3D response surface and contour plots of the combined mixture-process model with the Design-Expert 8 software.

With high water absorption capacity, RHA particles become “micro water reservoirs” which disperse very well in matrix. They continuously supply water for the hydration of cementitious materials, for delaying the internal relative humidity reduction (i.e. self-desiccation) in UHPC. This induces the strong decrease of autogenous shrinkage of the RHA-blended mixtures compared with that of the SF-blended mixtures. Hence, RHA plays as an internal curing agent. Combining small particle size, good dispersion and high pozzolanic reactivity, RHA is appropriate for the autogenous shrinkage mitigation and microstructure improvement, especially in the extremely dense matrix of UHPC. As a result, RHA plays as both pozzolanic admixture and internal curing agent in cement matrix.

However, the UHPC containing RHA has a higher total porosity, water absorption coefficient and CH content. Hence, it possesses an increased drying shrinkage and slightly lower durability in aggressive solutions compared with those of the SF-modified sample. The incorporation of GGBS and RHA or SF improves the microstructure and durability of UHPC.

Heat treatment accelerates and enhances hydration of both cement clinker and RHA in matrix with very low w/b. It also improves the microstructure characteristics of UHPC. But the final compressive strength and durability of the heat treated samples containing RHA have no significant advantage. After 48 hours at 65°C or 90°C treatment, autogenous shrinkage of the RHA-modified mixtures almost ceases. Compressive strength, shrinkage and durability of the 65°C treated samples are slightly better than those of the 90°C treated samples. In terms of economical and technical aspects, the 65°C treatment instead of the 90°C treatment in 48 hours should be used for UHPC containing RHA for accelerating the early strength.

Finally, it can be concluded that reactive rice husk ash (RHA) can be a good pozzolanic admixture to completely substitute for SF in UHPC production in terms of both compressive strength and durability. As a result, sustainable UHPC can be produced by using RHA or combining RHA and GGBS. It is possible to use available cementitious materials (i.e. cement and RHA) in Vietnam to produce sustainable UHPC.

6.2. Further research

The findings from this thesis suggest a number of potential topics for future studies. Some open questions are pointed out as follows:

- In CH-pozzolan suspension, the Si concentration of RHA is higher than that of SF. But the reaction product precipitation and hence the pozzolanic reactivity of SF exceeds that of RHA. How is difference in mineral nature of silica between RHA and SF? How does the difference in nature of dissolved Si (i.e. Si-OH groups) effect on its pozzolanic reaction product precipitation and hence the pozzolanic reactivity in portlandite solution?
- Zeta potential of RHA and SF needs more detailed studies. What is the difference between their surface chemistry which affects superplasticizer adsorption and rheology of mineral-blended suspensions?
- The mini-cone slump flow of the UHPCs containing RHA is comparable or even higher than that of the UHPCs containing SF. However, the UHPCs containing RHA possess more difficult mixing and casting characteristics. What are the differences in the rheology between RHA-blended UHPC and SF-blended UHPC?
- The long term compressive strength and durability of the RHA-modified samples at the heat treatment conditions seems not better than that of the 20°C treated samples. Meanwhile, the microstructure (total porosity and CH content) of the RHA-modified mixtures are improved by the heat treatments. How does high temperature treatment affect the durability and long term compressive strength of UHPC containing RHA?
- With the different packing density and CH content, what is difference in the interfacial transition zone between matrix and aggregates or fibers of UHPC containing RHA or SF? How is different ductility (i.e. adhesive properties between fibers and matrix) between RHA-modified UHPC and SF-modified UHPC?
- How does RHA with high alkali content affect the degree of GGBS hydration in cement matrix of RHA-GGBS-blended UHPC?
- What are the effects of the differences in particle size and pore size distribution in particle between RHA and SAP on shrinkage, pore structure and other characteristics of UHPC?

References

1. Schmidt, M. and Fehling, E., Ultra-high-performance concrete: research, development and application in Europe, in The 7th International symposium on the utilization of high-strength- and high-performance-concrete, ACI Washington, 2005, pp. 51-78.
2. Schmidt, M. and Fehling, E., Die Gärtnerplatzbrücke in Kassel - Praktisches Ergebnis von 10 Jahren Forschung und Entwicklung auf dem Gebiet des Ultra-Hochfesten Betons an der Universität Kassel, Kassel University Press, 2007.
3. Rebentrost, M. and Wight, G., Experience and applications of ultra-high performance concrete in Asia, in Proceedings of the 2nd International Symposium on Ultra High Performance Concrete, Kassel, Germany, 2008, pp. 19-30.
4. Resplendino, J., State of the art of design and construction of UHPFRC structures in France, in Proceedings of Hipermat 2012- the 3rd International Symposium on UHPC and Nanotechnology for High Performance Construction Materials, Kassel, Germany, 2012, pp. 27-41.
5. Schmidt, M., Sustainable building with UHPC- Coordinated research program in Germany, in Proceedings of Hipermat 2012- the 3rd International Symposium on UHPC and Nanotechnology for High Performance Construction Materials, Kassel, Germany, 2012, pp. 17-25.
6. Richard, P. and Cheyrezy, M., Composition of reactive powder concretes, Cement and Concrete Research, 25(7) (1995) 1501-1511.
7. Blais, P.Y. and Couture, M., Precast, Prestressed Pedestrian Bridge- World's First Reactive Powder Concrete Structure, PCI Journal, (1999) 60-71.
8. Park, J.J., Kang, S.T., Koh, K.T., and Kim, S.W., Influence of the ingredients on the compressive strength of UHPC as a fundamental study to optimize the mixing proportion, in Proceedings of the 2nd International Symposium on Ultra High Performance Concrete, Kassel, Germany, 2008, pp. 105-112.
9. Graybeal, B.A., Characterization of the behaviour of Ultra-High Performance Concrete, PhD thesis, University of Maryland, USA, 2005.
10. Schmidt, M. and Teichmann, T., New development in Ultra-high performance concrete- non corrosive PVA-fibres and glueing of structural elements, in Proceedings of the 2rd fib congress- Section 13, Neapel, Italy, 2006, pp. 1-11.
11. Fehling, E., Schmidt, M., Teichmann, T., and Bunje, K., Entwicklung, Dauerhaftigkeit und Berechnung Ultrahochfester Beton (UHPC), Universität Kassel, 2005 (in German).
12. Resplendino, J., First recommendations for Ultra-High Performance Concretes and examples of application, in Proceedings of the 1st International Symposium on Ultra High Performance Concrete, Kassel, Germany, 2004, pp. 79-90.
13. Long, G., Wang, X., and Xie, Y., Very-high-performance concrete with ultrafine powders, Cement and Concrete Research, 32(4) (2002) 601-605.
14. De Larrard, F. and Sedran, T., Optimization of ultra-high-performance concrete by the use of a packing model, Cement and Concrete Research, 24(6) (1994) 997-1009.
15. Rougeau, P. and Borys, B., Ultra high performance concrete with ultrafine particles other than silica fume, in Proceedings of the 1st International Symposium on Ultra High Performance Concrete, Kassel, Germany, 2004, pp. 213-225.
16. Staquet, S., B. Espion, Early- age autogenous shrinkage of UHPC incorporating very fine fly ash or metakaolin in replacement of silica fume, in Proceedings of the 1st International Symposium on Ultra High Performance Concrete, Kassel, Germany, 2004, pp. 587-599.
17. YazIcI, H., The effect of curing conditions on compressive strength of ultra high strength concrete with high volume mineral admixtures, Building and Environment, 42(5) (2007) 2083-2089.

18. YazIcI, H., YardImcI, M.Y., AydIn, S., and Karabulut, A.S., Mechanical properties of reactive powder concrete containing mineral admixtures under different curing regimes, Construction and Building Materials, 23(3) (2009) 1223-1231.
19. Yunsheng, Z., Wei, S., Sifeng, L., Chujie, J., and Jianzhong, L., Preparation of C200 green reactive powder concrete and its static-dynamic behaviors, Cement and Concrete Composites, 30(9) (2008) 831-838.
20. Möser, B., Pfeifer, C., Gerlicher, T., Heinz, D., Mechtcherine, V., and Dudziak, L., Investigations on the workability and microstructure development of UHPC; Part 2: Influence of admixtures and curing on the microstructure of ultra-high strength concretes, Cement international, 8 (2010) 74-85.
21. YazIcI, H., Yigiter, H., Karabulut, A.S., and Baradan, B., Utilization of fly ash and ground granulated blast furnace slag as an alternative silica source in reactive powder concrete, Fuel, 87(12) (2008) 2401-2407.
22. Gerlicher, T., Heinz, D., and Urbonas, L., Effect of finely ground blast furnace slag on the properties of fresh and hardened UHPC, in Proceedings of the 2nd International Symposium on Ultra High Performance Concrete, Kassel, Germany, 2008, pp. 367-374.
23. Le, T.T., Soutsos, N.M., Millard, G.S., and Barnett, J.S., UHPFRC – Optimisation of Mix Proportions, in Proceedings of CONCRETE PLATFORM International Conference, Belfast, Northern Ireland, 2007, pp. 339-348.
24. Le, T.T., Ultra high performance fibre reinforced concrete paving flags, PhD Thesis, The University of Liverpool, England, 2008.
25. YazIcI, H., YardImcI, M.Y., Yigiter, H., AydIn, S., and Türkel, S., Mechanical properties of reactive powder concrete containing high volumes of ground granulated blast furnace slag, Cement and Concrete Composites, 32(8) (2010) 639-648.
26. Gerlicher, T., Leonhardt, S., Heinz, D., and Urbonas, L., Einfluss des Steinkohlenflugascheeinsatzes auf die Frisch- und Festbetoneigenschaften von ultrahochfestem Beton, in The 17th International Conference on Building materials (ibausil), Weimar, Germany, 2009, pp. (1)1091-(1)1098.
27. Gerlicher, T., Hilbig, H., and Heinz, D., Einfluss des Hüttensandmehleinsatzes auf den Hydratationsverlauf von ultrahochfestem Beton, in The 17th International Conference on Building materials (ibausil), Weimar, Germany, 2009, pp. (2)0593-(2)0598.
28. Tafraoui, A., Escadeillas, G., Lebaili, S., and Vidal, T., Metakaolin in the formulation of UHPC, Construction and Building Materials, 23(2) (2009) 669-674.
29. Nair, D.G., Fraaij, A., Klaassen, A.A.K., and Kentgens, A.P.M., A structural investigation relating to the pozzolanic activity of rice husk ashes, Cement and Concrete Research, 38(6) (2008) 861-869.
30. Chandrasekhar, S., Satyanarayana, K.G., Pramada, P.N., Raghavan, P., and Gupta, T.N., Review Processing, properties and applications of reactive silica from rice husk—an overview, Journal of Materials Science, 38(15) (2003) 3159-3168.
31. Chandrasekhar, S., Pramada, P.N., Raghavan, P., Satyanarayana, K.G., and Gupta, T.N., Microsilica from rice husk as a possible substitute for condensed silica fume for high performance concrete, Journal of Materials Science Letters, 21(16) (2002) 1245-1247.
32. Chandrasekhar, S., Pramada, P., and Majeed, J., Effect of calcination temperature and heating rate on the optical properties and reactivity of rice husk ash, Journal of Materials Science, 41(23) (2006) 7926-7933.
33. Salas, A., Delvasto, S., de Gutierrez, R.M., and Lange, D., Comparison of two processes for treating rice husk ash for use in high performance concrete, Cement and Concrete Research, 39(9) (2009) 773-778.
34. Feng, Q., Yamamichi, H., Shoya, M., and Sugita, S., Study on the pozzolanic properties of rice husk ash by hydrochloric acid pretreatment, Cement and Concrete Research, 34(3) (2004) 521-526.

35. Nehdi, M., Duquette, J., and El Damatty, A., Performance of rice husk ash produced using a new technology as a mineral admixture in concrete, Cement and Concrete Research, 33(8) (2003) 1203-1210.

36. Bui, D.D., Rice Husk Ash as a mineral admixture for high performance concrete, PhD thesis, Delft University, The Netherlands, 2001.

37. Ahmadi, M.A., Alidoust, O., Sadrinejad, I., and Nayeri, M., Development of mechanical properties of self compacting concrete containing rice husk ash, in Proceedings of world academy of science, engineering and technology, 2007, pp. 503-506.

38. Sousa Coutinho, J., The combined benefits of CPF and RHA in improving the durability of concrete structures, Cement and Concrete Composites, 25(1) (2003) 51-59.

39. Bui, D.D., Hu, J., and Stroeven, P., Particle size effect on the strength of rice husk ash blended gap-graded Portland cement concrete, Cement and Concrete Composites, 27(3) (2005) 357-366.

40. Qing-ge, F., Qing-yu, L., Qi-jun, Y., San-ying, Z., Lu-feng, Y., and Sugita, S., Concrete with highly active rice husk ash, Journal of Wuhan University of Technology--Materials Science Edition, 19(3) (2004) 74-77.

41. Saraswathy, V. and Song, H.-W., Corrosion performance of rice husk ash blended concrete, Construction and Building Materials, 21(8) (2007) 1779-1784.

42. Nehdi, M., Pardhan, M., and Koshowski, S., Durability of self-consolidating concrete incorporating high-volume replacement composite cements, Cement and Concrete Research, 34(11) (2004) 2103-2112.

43. Chindaprasirt, P., Rukzon, S., and Sirivivatnanon, V., Effect of carbon dioxide on chloride penetration and chloride ion diffusion coefficient of blended Portland cement mortar, Construction and Building Materials, 22(8) (2008) 1701-1707.

44. de Sensale, G.R., Ribeiro, A.B., and Gonçalves, A., Effects of RHA on autogenous shrinkage of Portland cement pastes, Cement and Concrete Composites, 30(10) (2008) 892-897.

45. Giaccio, G., de Sensale, G.R., and Zerbino, R., Failure mechanism of normal and high-strength concrete with rice-husk ash, Cement and Concrete Composites, 29(7) (2007) 566-574.

46. Isaia, G.C., Gastaldini, A.L.G., and Moraes, R., Physical and pozzolanic action of mineral additions on the mechanical strength of high-performance concrete, Cement and Concrete Composites, 25(1) (2003) 69-76.

47. Ganesan, K., Rajagopal, K., and Thangavel, K., Rice husk ash blended cement: Assessment of optimal level of replacement for strength and permeability properties of concrete, Construction and Building Materials, 22(8) (2008) 1675-1683.

48. Zhang, M.H., Lastra, R., and Malhotra, V.M., Rice-husk ash paste and concrete: Some aspects of hydration and the microstructure of the interfacial zone between the aggregate and paste, Cement and Concrete Research, 26(6) (1996) 963-977.

49. Habeeb, G.A., M.M. Fayyadh, Rice Husk Ash Concrete: the Effect of RHA Average Particle Size on Mechanical Properties and Drying Shrinkage, Australian Journal of Basic and Applied Sciences, 3(3) (2009) 1616-1622.

50. Rodríguez de Sensale, G., Strength development of concrete with rice-husk ash, Cement and Concrete Composites, 28(2) (2006) 158-160.

51. Chindaprasirt, P., Kanchanda, P., Sathonsaowaphak, A., and Cao, H.T., Sulfate resistance of blended cements containing fly ash and rice husk ash, Construction and Building Materials, 21(6) (2007) 1356-1361.

52. Chatveera, B. and Lertwattanaruk, P., Evaluation of sulfate resistance of cement mortars containing black rice husk ash, Journal of Environmental Management, 90(3) (2009) 1435-1441.

53. Cordeiro, G., Toledo Filho, R., and de Moraes Rego Fairbairn, E., Use of ultrafine rice husk ash with high-carbon content as pozzolan in high performance concrete, Materials and Structures, 42(7) (2009) 983-992.

54. Safiuddin, M., Development of self-consolidating high performance concrete incorporating rice husk ash, PhD Thesis, University of Waterloo, Canada, 2008.

55. Sampaio, J., J.S. Coutinho, and M.N. Sampaio, Portuguese's rice husk ash as a partial cement replacement, in Proceeding of the International Conference: Sustainable construction into the next Millennium: Environmentally friendly and innovative cement based materials, Joao Pessoa, Brasil, 2000, pp. 125-137.

56. Rizwan, S.A., High-performance mortars and concretes using secondary raw materials, PhD Thesis, Faculty of Maschinenbau, Verfahrens-und Energietechnik der Technischen Bergakademie Freiberg, Germany, 2006.

57. Nguyen, V.T., Ye, G., van Breugel, K., and Copuroglu, O., Hydration and microstructure of ultra high performance concrete incorporating rice husk ash, Cement and Concrete Research, 41(11) (2011) 1104-1111.

58. Nguyen, V.T., Ye, G., van Breugel, K., Fraaij, A.L.A., and Bui, D.D., The study of using rice husk ash to produce ultra high performance concrete, Construction and Building Materials, 25(4) (2011) 2030-2035.

59. Nguyen, V.T., Ye, G., Van Breugel, K., and Pham, H.H., Synergic effect of rice husk ash and silica fume on compressive strength of ultra high performace concrete, in The International RILEM Conference on Material Science- MATSCI, Aachen, Germany, 2010, pp. 255-263.

60. Nguyen, V.T., Rice husk ash as a mineral admixture for Ultra High Performance Concrete, PhD thesis, Delft University, The Netherlands, 2011.

61. Laskar, A.I. and Talukdar, S., Rheological behavior of high performance concrete with mineral admixtures and their blending, Construction and Building Materials, 22(12) (2008) 2345-2354.

62. FAOSTAT, Rice production, 2012, Available from: http://faostat.fao.org/site/567/DesktopDefault.aspx?PageID=567#ancor, [Accessed 15. February 2012].

63. Mehta, P.K., Rice husk ash - a unique supplementary cementing material, in Advances in Concrete Technology (2nd edition), CANMET, 1994, pp. 419-444.

64. Chindaprasirt, P. and Rukzon, S., Strength, porosity and corrosion resistance of ternary blend Portland cement, rice husk ash and fly ash mortar, Construction and Building Materials, 22(8) (2008) 1601-1606.

65. Chindaprasirt, P., Rukzon, S., and Sirivivatnanon, V., Resistance to chloride penetration of blended Portland cement mortar containing palm oil fuel ash, rice husk ash and fly ash, Construction and Building Materials, 22(5) (2008) 932-938.

66. Schmidt, M., Von der Nanotechnologie zum Ultra-Hochfesten Beton, in The 16th International Conference on Building materials (ibausil), Weimar, Germany, 2006, pp. (2)1405-(2)1416 (in German).

67. Shah, S.P., Recent Trends in the Science and Technology of Concrete, in Concrete Technology: New Trends, Industrial Applications- Proceedings of the International RILEM 26, E & FN Spon, 1995, pp. 1-18.

68. Guerrini, G.L., Applications of High-Performance Fiber-Reinforced Cement-Based Composites, Applied Composite Materials, 7(2) (2000) 195-207.

69. Dugat, J., Roux, N., and Bernier, G., Mechanical properties of reactive powder concretes, Materials and Structures, 29(4) (1996) 233-240.

70. Perry, V.H., Ductal® - A Revolutionary New Material for New Solutions, 2006, Available from: http://www.apegm.mb.ca/pdf/PD_Papers/ductal.pdf, [Accessed 08. November 2011].

71. Neville, A., Concrete: Neville's Insights and Issues, Thomas Telford Ltd, 2006.

72. Coppola, L., Cerulli, T., Troli, R., and Collepardi, M., The Influence of Materials on The Performance of Reactive Powder Concrete, in International Conference on High-Performance Concrete, and Performance and Quality of Concrete Structures, Florianopolis, Brazil, 1996, pp. 502-513.

73. Sakai, E., Aizawa, K., Nakamura, A., Kato, H., and Daimon, M., Influence of superplasticizers on the fluidity of cements with different amount of aluminate phase, in Proceedings of the 2nd International Symposium on Ultra High Performance Concrete, Kassel, Germany, 2008, pp. 85-92.

74. Müller, H.S. and Haist, M., New types of high performance concretes - Potentials for innovations in concrete constructions, in Innovative Materials and Techniques in Concrete Construction: ACES Workshop, (ed. Fardis, M.N.), Springer, 2012, p. 43-58.

75. Ma, J., Orgass, M., Dehn, F., Schmidt, D., and Tue, N.V., Comparative investigations on ultra-high performance concrete with and without coarse aggregates, in Proceedings of the 1st International Symposium on Ultra High Performance Concrete, Kassel, Germany, 2004, pp. 205-212.

76. Fardis, M.N., Innovative Materials and Techniques in Concrete Construction, Springer, 2011.

77. Chung, D.D.L., Review: Improving cement-based materials by using silica fume, Journal of Materials Science, 37(4) (2002) 673-682.

78. Gatty, L., Bonnamy, S., Feylessoufi, A., Clinard, C., Richard, P., and Van Damme, H., A transmission electron microscopy study of interfaces and matrix homogeneity in ultra-high-performance cement-based materials, Journal of Materials Science, 36(16) (2001) 4013-4026.

79. Chan, Y.-W. and Chu, S.-H., Effect of silica fume on steel fiber bond characteristics in reactive powder concrete, Cement and Concrete Research, 34(7) (2004) 1167-1172.

80. Papadakis, V.G., Experimental investigation and theoretical modeling of silica fume activity in concrete, Cement and Concrete Research, 29(1) (1999) 79-86.

81. Taylor, H.F.W., Cement chemistry, 2nd edition, Thomas Telford Ltd, 1997.

82. Schachinger, I., Schmidt, K., Heinz, D., and Schießl, P., Early-Age Cracking Risk and Relaxation by Restrained Autogenous Deformation of Ultra High Performance Concrete, in The 6th International Symposium on Utilization of High Strength/High Performance Concrete, Leipzig, Germany, 2002, pp. 1341-1354.

83. Nguyen, V.T., Ye, G., and van Breugel, K., Mitigation of early age shrinkage of Ultra High Performance Concrete by using Rice Husk Ash, in Proceedings of Hipermat 2012- 3rd International Symposium on Ultra-High Performance Concrete and Nanotechnology for High Performance Construction Materials, Kassel, Germany, 2012, pp. 341-348.

84. Yang, S.L., Millard, S.G., Soutsos, M.N., Barnett, S.J., and Le, T.T., Influence of aggregate and curing regime on the mechanical properties of ultra-high performance fibre reinforced concrete (UHPFRC), Construction and Building Materials, 23(6) (2009) 2291-2298.

85. Collepardi, S., Coppola, L., Troli, R., and Collepardi, M., Mechanical properties of modified reactive powder concrete, in Proceedings of the fifth CANMET/ACI international conference on superplasticizers and other chemical admixtures in concrete, Rome, Italy, ACI SP-173-1, 1997, pp. 1-21.

86. Boulet, D., Pleau, R., Rougeau, P., and Bodet, R., Flexural behaviour of ultra high-performance cementitious composites reinforced with different types of steel fibres, in Fifth International RILEM Symposium on Fibre-Reinforced Concrete (FRC), Lyon, France, 2000, pp. 759 - 768.

87. Hirschi, T. and Wombacher, F., Influence of different superplasticizers on UHPC, in Proceedings of the 2nd International Symposium on Ultra High Performance Concrete, Kassel, Germany, 2008, pp. 77-84.

88. Winnefeld, F., Becker, S., Pakusch, J., and Götz, T., Effects of the molecular architecture of comb-shaped superplasticizers on their performance in cementitious systems, Cement and Concrete Composites, 29(4) (2007) 251-262.

89. Terzijski, I., Compatibility of Components of High and Ultra High Performance Concrete, in Proceedings of the 1st International Symposium on Ultra High Performance Concrete, Kassel, Germany, 2004, pp. 175-186.

90. Jiang, S., Kim, B.-G., and Aïtcin, P.-C., Importance of adequate soluble alkali content to ensure cement/superplasticizer compatibility, Cement and Concrete Research, 29(1) (1999) 71-78.

91. Plank, J., Schroefl, C., Gruber, M., Lesti, M., and Sieber, R., Effectiveness of Polycarboxylate Superplasticizers in Ultra-High Strength Concrete: the Importance of PCE Compatibility with Microsilica, Journal of Advanced Concrete Technology, 7(1) (2009) 5-12.

92. Hommer, H., Interaction of polycarboxylate ether with silica fume, Journal of the European Ceramic Society, 29(10) (2009) 1847-1853.

93. Habbaba, A. and Plank, J., Interaction between Polycarboxylate Superplasticizers and Amorphous Ground Granulated Blast Furnace Slag, Journal of the American Ceramic Society, 93(9) (2010) 2857-2863.

94. Schachinger, I., Hilbig, H., and Stengel, T., Effect of temperature at an early age on the long-term strength development of UHPC, in Proceedings of the 2nd International Symposium on Ultra High Performance Concrete, Kassel, Germany, 2008, pp. 205-212.

95. Zanni, H., Cheyrezy, M., Maret, V., Philippot, S., and Nieto, P., Investigation of hydration and pozzolanic reaction in Reactive Powder Concrete (RPC) using 29Si NMR, Cement and Concrete Research, 26(1) (1996) 93-100.

96. Pfeifer, C., Moeser, B., Weber, C., and Stark, J., Investigations of the pozzolanic reaction of silica fume in Ultra-high performance concrete (UHPC), in The International RILEM Conference on Material Science- MATSCI, Aachen, Germany, 2010, pp. 287-298.

97. Feylessoufi, A., Crespin, M., Dion, P., Bergaya, F., Van Damme, H., and Richard, P., Controlled rate thermal treatment of reactive powder concretes, Advanced Cement Based Materials, 6(1) (1997) 21-27.

98. Cheyrezy, M., Maret, V., and Frouin, L., Microstructural analysis of RPC (Reactive Powder Concrete), Cement and Concrete Research, 25(7) (1995) 1491-1500.

99. Reda, M.M., Shrive, N.G., and Gillott, J.E., Microstructural investigation of innovative UHPC, Cement and Concrete Research, 29(3) (1999) 323-329.

100. Mehta, P.K. and Monteiro, P.J.M., Concrete- Microstructure, Properties, and Material, 3rd edition, McGraw-Hill, 2006.

101. Kovler, K. and Jensen, O.M., Internal curing of concrete. State-of-the-art Report of RILEM Technical Commite 196-ICC, RILEM Publications S.A.R.L., France, 2007.

102. Koh, K., Ryu, G., Kang, S., Park, J., and Kim, S., Shrinkage Properties of Ultra-High Performance Concrete (UHPC), Advanced Science Letters, 4(3) (2011) 948-952.

103. Habel, K., Charron, J.P., Denarie, E., and Bruhwiler, E., Autogenous deformations and viscoelasticity of UHPFRC in structures. Part I: experimental results, Magazine of Concrete Research, 58(3) (2006) 135–145.

104. Loukili, A., Khelidj, A., and Richard, P., Hydration kinetics, change of relative humidity, and autogenous shrinkage of ultra-high-strength concrete, Cement and Concrete Research, 29(4) (1999) 577-584.

105. Acker, P., Why Does Ultrahigh-Performance Concrete (UHPC) Exhibit Such Low Shrinkage and Such Low Creep?, ACI Materials Journal, SP 220-10(Special Publication) (2004) 141-154.

106. Ma, J., Dehn, F., and Koenig, G., Autogenous Shrinkage of Self-compacting Ultra-high Performance Concrete (UHPC), in Proceedings of the International Conference ICACS, Xuzhou, China, 2003, pp. 255-262.

107. Soliman, A., Early-age shrinkage of ultra high performance concrete: mitigation and compensation mechanisms, PhD Thesis, The university of Western Ontario, Canada, 2011.

108. Kim, S., Park, J., Yoo, D., and Yoon, Y., Shrinkage Behavior of Ultra High Performance Concrete at the Manufacturing Stage, in Proceedings of Hipermat 2012- 3rd International Symposium on Ultra-High Performance Concrete and Nanotechnology for High Performance Construction Materials, Kassel, Germany, 2012, pp. 317-324.

109. Wang, F., Zhou, Y., Peng, B., Liu, Z., and Hu, S., Autogenous Shrinkage of Concrete with Super-Absorbent Polymer, ACI Materials Journal, 106(2) (2009) 123-127.

110. Mechtcherine, V., Dudziak, L., and Hempel, S., Mitigating early age shrinkage of Ultra-High Performance Concrete by using Super Absorbent Polymers (SAP), in Proceedings of the 8th International Conference on Creep, Shrinkage and Durability Mechanics of Concrete and Concrete Structures, London, Taylor & Francis, 2008, pp. 847-853.

111. Dudziak, L. and Mechtcherine, V., Mitigation of volume changes of Ultra-high performance concrete (UHPC) by using Super Absorbent Polymers, in Proceedings of the 2nd International Symposium on Ultra High Performance Concrete, Kassel, Germany, 2008, pp. 425-432.

112. Orgass, M. and Klug, Y., Fibre Reiforced Ultra-high Strength Concretes, in Proceedings of the 1st International Symposium on Ultra High Performance Concrete, Kassel, Germany, 2004, pp. 637-647.

113. Acker, P. and Behloul, M., Ductal Technology: A Large Spectrum of Properties, A Wide Range of Applications, in Proceedings of the 1st International Symposium on Ultra High Performance Concrete, Kassel, Germany, 2004, pp. 11-23.

114. Möser, B. and Pfeifer, C., Microstructure and Durability of Ultra-High Performance Concrete, in Proceedings of the 2nd International Symposium on Ultra High Performance Concrete, Kassel, Germany, 2008, pp. 417-424.

115. Droll, K., Influence of additions on ultra high performance concretes – grain size optimisation, in Proceedings of the 1st International Symposium on Ultra High Performance Concrete, Kassel, Germany, 2004, pp. 285-301.

116. Teichmann, T. and Schmidt, M., Influence of the packing density of fine particles on structure, strength and durability of UHPC, in Proceedings of the 1st International Symposium on Ultra High Performance Concrete, Kassel, Germany, 2004, pp. 313-323.

117. Heinz, D. and Ludwig, H.-M., Heat Treatment and the Risk of DEF Delayed Ettringite Formation in UHPC, in Proceedings of the 1st International Symposium on Ultra High Performance Concrete, Kassel, Germany, 2004, pp. 717-730.

118. Scheydt, J.C. and Müller, H.S., Microstructure of Ultra High Performance Concrete (UHPC) and its Impact on Durability, in Proceedings of Hipermat 2012- 3rd International Symposium on Ultra-High Performance Concrete and Nanotechnology for High Performance Construction Materials, Kassel, Germany, 2012, pp. 349-356.

119. Franke, L., Deckelmann, G., and Schmidt, H., Behavior of ultra high performance concrete with respect to chemical attack, in The 17th International Conference on Building materials (ibausil), Weimar, Germany, 2009, pp. (1)1099-(1)1104.

120. Franke, L. and Deckelmann, G., Behavior of ultra high performance concrete with respect to chemical attack, in Proceedings of the 2nd International Symposium on Ultra High Performance Concrete, Kassel, Germany, 2008, pp. 453-460.

121. Bonneau, O., Lachemi, M., Dallaire, E., Dugat, J., and Aitcin, P.-C., Mechanical Properties and Durability of Two Industrial Reactive Powder Concretes, ACI Materials Journal, 94(4) (1997) 286-290.

122. Graybeal, B. and Tanesi, J., Durability of an Ultrahigh-Performance Concrete, Journal of Materials in Civil Engineering, 19(10) (2007) 848-854.

123. Lee, M.-G., Wang, Y.-C., and Chiu, C.-T., The study for bend strength and bond durability of reactive powder concrete, Journal of ASTM International, 2(7) (2005).

124. Lee, M.-G., Wang, Y.-C., and Chiu, C.-T., A preliminary study of reactive powder concrete as a new repair material, Construction and Building Materials, 21(1) (2007) 182-189.

125. Palecki, S. and Setzer, M.J., Ultra-high-performance concrete under frost and de-icing salt attack, in Proceedings of the 2nd International Symposium on Ultra High Performance Concrete, Kassel, Germany, 2008, pp. 443-451.

126. Thomas, M., Green, B., O'Neal, E., Perry, V., Hayman, S., and Hossack, A., Marine Performance of UHPC at Treat Island, in Proceedings of Hipermat 2012- 3rd International

Symposium on Ultra-High Performance Concrete and Nanotechnology for High Performance Construction Materials, Kassel, Germany, 2012, pp. 365-370.

127. ASTM C1260-01: Standard test method for potential alkali reactivity of aggregates (mortar-bar method), American Society for Testing and Materials, Philadelphia, USA. 2001.

128. Stark, J., Freyburg, E., Seyfarth, K., and Giebson, C., AKR – Prüfverfahren zur Beurteilung von Gesteinskörnungen und projektspezifischen Betonen, 2006.

129. Giebson, C. and Stark, J., Assessing the Durability of Concrete Regarding ASR, in Proceedings of the 7th CANMET/ACI International Conference on Durability of Concrete, Montreal, Canada, American Concrete Institute SP-234, 2006, pp. 225 – 238.

130. Giebson, C., Seyfarth, K., and Stark, J., Effectiveness of ground granulated blast furnace slag in preventing deleterious ASR in concretes exposed to alkali-containing deicer solutions, in The International RILEM Conference on Material Science- MATSCI, Aachen, Germany, 2010, pp. 221-230.

131. Muthadhi, A.A., R. Kothandaraman, S., Rice Husk Ash - Properties and its Uses: A Review, Journal of the Institution of Engineers. India. Civil Engineering Division, 88 (2007) 50-56.

132. Mansaray, K.G. and Ghaly, A.E., Physical and Thermochemical Properties of Rice Husk, Energy Sources, Part A: Recovery, Utilization, and Environmental Effects, 19 (1997) 989-1004.

133. Prasad, C.S., Maiti, K.N., and Venugopal, R., Effect of rice husk ash in whiteware compositions, Ceramics International, 27(6) (2001) 629-635.

134. Kapur, P., Singh, R., and Srinivasan, J., Tube-in-Basket burner for rice husk. I: Properties of husk as a fuel and basic design considerations, Sadhana, 7(4) (1984) 291-300.

135. Park, B.-D., Wi, S.G., Lee, K.H., Singh, A.P., Yoon, T.-H., and Kim, Y.S., Characterization of anatomical features and silica distribution in rice husk using microscopic and micro-analytical techniques, Biomass and Bioenergy, 25(3) (2003) 319-327.

136. Kamiya, K., Oka, A., Nasu, H., and Hashimoto, T., Comparative Study of Structure of Silica Gels from Different Sources, Journal of Sol-Gel Science and Technology, 19(1) (2000) 495-499.

137. Chaudhary, D.S. and Jollands, M.C., Characterization of rice hull ash, Journal of Applied Polymer Science, 93(1) (2004) 1-8.

138. Omatola, K.M. and Onojah, A.D., Elemental analysis of rice husk ash using X – ray fluorescence technique, International Journal of Physical Sciences, 4(4) (2009) 189-193.

139. Malhotra, V.M., Fly Ash, Slag, Silica Fume, and Rice Husk Ash in Concrete: A Review, Concrete International, 15(4) (1993) 23-28.

140. Chumee, J., Grisdanurak, N., Neramittagapong, S., and Wittayakun, J., Characterization of AlMCM-41 synthesized with rice husk silica and utilization as supports for platinumiron catalysts, Brazilian Journal of Chemical Engineering, 26 (2009) 367-373.

141. Srivastava, V.C., Mall, I.D., and Mishra, I.M., Characterization of mesoporous rice husk ash (RHA) and adsorption kinetics of metal ions from aqueous solution onto RHA, Journal of Hazardous Materials, 134(1-3) (2006) 257-267.

142. Chatterjee, M. and Naskar, M.K., Sol-gel synthesis of lithium aluminum silicate powders: The effect of silica source, Ceramics International, 32(6) (2006) 623-632.

143. Bondioli, F., Andreola, F., Barbieri, L., Manfredini, T., and Ferrari, A.M., Effect of rice husk ash (RHA) in the synthesis of $(Pr,Zr)SiO_4$ ceramic pigment, Journal of the European Ceramic Society, 27(12) (2007) 3483-3488.

144. Foletto, E.L., Gratieri, E., Oliveira, L.H.d., and Jahn, S.L., Conversion of rice hull ash into soluble sodium silicate, Materials Research, 9 (2006) 335-338.

145. Sun, L. and Gong, K., Silicon-Based Materials from Rice Husks and Their Applications, Industrial & Engineering Chemistry Research, 40(25) (2001) 5861-5877.

146. Loiha, S., Prayoonpokarach, S., Songsiriritthigun, P., and Wittayakun, J., Synthesis of zeolite beta with pretreated rice husk silica and its transformation to ZSM-12, Materials Chemistry and Physics, 115(2-3) (2009) 637-640.

147. Kalapathy, U., Proctor, A., and Shultz, J., A simple method for production of pure silica from rice hull ash, Bioresource Technology, 73(3) (2000) 257-262.

148. Kalapathy, U., Proctor, A., and Shultz, J., An improved method for production of silica from rice hull ash, Bioresource Technology, 85(3) (2002) 285-289.

149. Rozainee, M., Ngo, S.P., Salema, A.A., and Tan, K.G., Fluidized bed combustion of rice husk to produce amorphous siliceous ash, Energy for Sustainable Development, 12(1) (2008) 33-42.

150. Sugita, S., Method of producing active rice husk ash, Patent number 5329867, 7-1994.

151. Umeda, J. and Kondoh, K., High-purity amorphous silica originated in rice husks via carboxylic acid leaching process, Journal of Materials Science, 43(22) (2008) 7084-7090.

152. Chandrasekhar, S., Pramada, P., and Praveen, L., Effect of organic acid treatment on the properties of rice husk silica, Journal of Materials Science, 40(24) (2005) 6535-6544.

153. Liou, T.-H., Preparation and characterization of nano-structured silica from rice husk, Materials Science and Engineering A, 364(1-2) (2004) 313-323.

154. Krishnarao, R.V., Subrahmanyam, J., and Jagadish Kumar, T., Studies on the formation of black particles in rice husk silica ash, Journal of the European Ceramic Society, 21(1) (2001) 99-104.

155. Wansom, S., Janjaturaphan, S., and Sinthupinyo, S., Pozzolanic Activity of Rice Husk Ash: Comparison of Various Electrical Methods, Journal of Metals, Materials and Minerals, 19(2) (2009) 1-7.

156. Chaudhary, D, S., Jollands, and M, C., Characterization of rice hull ash, 93, Wiley, New York, NY, ETATS-UNIS, 2004.

157. Muthadhi, A. and Kothandaraman, S., Optimum production conditions for reactive rice husk ash, Materials and Structures, 43(9) (2010) 1303-1315.

158. James, J. and Rao, M.S., Reactivity of rice husk ash, Cement and Concrete Research, 16 (1986) 296-302.

159. James, J. and Rao, M.S., Silica from rice husk through thermal decomposition, Thermochimica Acta, 97(0) (1986) 329-336.

160. Feng, Q., Sugita, S., Shoya, M., and Yamamichi, H., Reply to the discussion by Ayhan Demirbas of the paper "Study on the pozzolanic properties of rice husk ash by hydrochloric acid pretreatment", Cement and Concrete Research, 35(5) (2005) 1018-1019.

161. Genieva, S., Turmanova, S., Dimitrova, A., and Vlaev, L., Characterization of rice husks and the products of its thermal degradation in air or nitrogen atmosphere, Journal of Thermal Analysis and Calorimetry, 93(2) (2008) 387-396.

162. Real, C., Alcalá, M.D., and Criado, J.M., Preparation of Silica from Rice Husks, Journal of the American Ceramic Society, 79(8) (1996) 2012-2016.

163. Sugita, S., Shoya, M., and Tokuda, H., Evaluation of Pozzolanic Activity of Rice Husk Ash, in Proceedings of the 4th CANMET/ACI International Conference on Fly ash, Silica Fume, Slag and Natural Pozzolans in Concrete, Istanbul, Turkey, 1992, pp. 495-512.

164. Yu, Q., Sawayama, K., Sugita, S., Shoya, M., and Isojima, Y., The reaction between rice husk ash and $Ca(OH)_2$ solution and the nature of its product, Cement and Concrete Research, 29(1) (1999) 37-43.

165. Feng, Q., Lin, Q., Yu, Q., Zhao, S., Yang, L., and Sugita, S., Concrete with highly active rice husk ash, Journal of Wuhan university of technology, 19(3) (2004) 74-77.

166. Mehta, P.K., Siliceous ashes and hydraulic cements prepared therefrom, Patent number 4105459, 8-1978.

167. Payá, J., Monzó, J., Borrachero, M.V., Mellado, A., and Ordoñez, L.M., Determination of amorphous silica in rice husk ash by a rapid analytical method, Cement and Concrete Research, 31(2) (2001) 227-231.

168. James, J. and Subba Rao, M., Reaction product of lime and silica from rice husk ash, Cement and Concrete Research, 16(1) (1986) 67-73.

169. Khangaonkar, P.R., Rahmat, A., and Jolly Kutty, K.G., Kinetic study of the hydrothermal reaction between lime and rice-husk-ash silica, Cement and Concrete Research, 22(4) (1992) 577-588.

170. Luxán, M.P., Madruga, F., and Saavedra, J., Rapid evaluation of pozzolanic activity of natural products by conductivity measurement, Cement and Concrete Research, 19(1) (1989) 63-68.

171. Payá, J., Borrachero, M.V., Monzó, J., Peris-Mora, E., and Amahjour, F., Enhanced conductivity measurement techniques for evaluation of fly ash pozzolanic activity, Cement and Concrete Research, 31(1) (2001) 41-49.

172. Cizer, O., Van Balen, K., Van Gemert, D., and Elsen, J., Carbonation and hydration of mortars with calcium hydroxide and calcium silicate binders, in International Conference on Sustainable Construction Materials and Technologies, Coventry, UK, 11-13 June 2007.

173. da Silva Rêgo, J.H.; Nepomuceno, A.A.; Hasparyk, N.P., and Vieira, F.L., Assessment of the pozzolanic reaction of crystalline and amorphous rice husk ashes (RHA), in Proceedings of the International RILEM conference on the use of recycled materials in buildings and structures, Barcelona, Spain, 2004, pp. 715-723.

174. Gava, G.P. and Prudencio Jr, L.R., Pozzolanic activity tests as a measure of pozzolans' performance Part 1, Magazine of Concrete Research, 59(10) (2007) 729-734.

175. Gava, G.P. and Prudêncio Jr, L.R., Pozzolanic activity tests as a measure of pozzolans' performance. Part 2, Magazine of Concrete Research, 59(10) (2007) 735-741.

176. ASTM C1240-05: Standard Specification for Silica Fume Used in Cementitious Mixtures, American Society for Testing and Materials, Philadelphia, USA. 2005.

177. El-Dakroury, A. and Gasser, M.S., Rice husk ash (RHA) as cement admixture for immobilization of liquid radioactive waste at different temperatures, Journal of Nuclear Materials, 381(3) (2008) 271-277.

178. Rostovsky, I., Barovsky, N., and Uzunov, I., Rice husk ash-Active mineral addition to cement based composites, in Proceedings of the 12th International Conference MTCM'2009, Varna, Bulgaria, 2009, pp. 110-115.

179. Zhang, M.-H. and Malhotra, V.M., High-performance concrete incorporating rice husk ash as a supplementary cementing material, ACI- Materials Journal, 93(6) (1996) 629-636.

180. Feng, Q., Yamamichi, H., Shoya, M., and Sugita, S., Efficiency of highly active rice husk ash on the high-strength concrete, in Proceedings of the 11th International Congress on the Chemistry of Cement (ICCC), Durban South Africa, 2003, pp. 816-822.

181. Yamamichi, H., Feng, Q., and Sugita, S., Some Properties of Concrete with Highly Active Rice Husk Ash, in Proceedings of the 6th CANMET/ACI International conference on Durability of Concrete, SP-212, 2003, pp. 891-905.

182. Wada, I., Kawano, T., Kawakami, M., and Maeda, N., Effect of Highly Reactive Rice Husk Ash on Durability of Concrete and Mortar, in Proceedings of the 5th CANMET/ACI International conference on Durability of Concrete, Barcelona, Spain, 2000, pp. 205-222.

183. Gastaldini, A.L.G., Isaia, G.C., Hoppe, T.F., Missau, F., and Saciloto, A.P., Influence of the use of rice husk ash on the electrical resistivity of concrete: A technical and economic feasibility study, Construction and Building Materials, 23(11) (2009) 3411-3419.

184. Gastaldini, A.L.G., Isaia, G.C., Gomes, N.S., and Sperb, J.E.K., Chloride penetration and carbonation in concrete with rice husk ash and chemical activators, Cement and Concrete Composites, 29(3) (2007) 176-180.

185. Mehta, P.K. and Folliard, K.J., Rice husk ash - a unique supplementary cementing material: Durability aspects, in Proceedings of the 2nd CANMET/ACI International Symposium, ACI SP 154-28, Nevada, USA, 1995, pp. 531-541.

186. Hasparyk, N.P., Monteiro, P.J.M., and Carasek, H., Effect of Silica Fume and Rice Husk Ash on Alkali-Silica Reaction, ACI Materials Journal, 97(4) (2000) 486-492.

187. Ramezanianpour, A.A., Zarrabi, K., and Mahdikhani, M., Mitigation of alkali aggregate reaction of concrete incorporation rice husk ash (RHA), in Proceedings of The 13rd ICAAR, Trondheim, 2008, pp. 1091-1102.

188. Oner, A. and Akyuz, S., An experimental study on optimum usage of GGBS for the compressive strength of concrete, Cement and Concrete Composites, 29(6) (2007) 505-514.

189. Makrides-Saravanos, E., Engineering properties of high performance concrete containing large volume of class C fly ash, PhD Thesis, University of Saskatchewan, Canada, 1996.

190. Meryman, H., Concrete for a Warming World, 2007.

191. Lange, F., Moertel, H., and Rudert, V., Dense packing of cement pastes and resulting consequences on mortar properties, Cement and Concrete Research, 27(10) (1997) 1481-1488.

192. Rodríguez-de-Sensale, G., Strength development of concrete with rice-husk ash, Cement and Concrete Composites, 28(2) (2006) 158-160.

193. Young, J.F., Humidity control in the laboratory using salt solutions—a review, Journal of Applied Chemistry, 17(9) (1967) 241-245.

194. Klimesch, D.S. and Ray, A., Use of the second-derivative differential thermal curve in the evaluation of cement-quartz pastes with metakaolin addition autoclaved at 180°C, Thermochimica Acta, 307(2) (1997) 167-176.

195. Ramachandran, V.S., Paroli, R.M., Beaudoin, J.J., and Delgado, A.H., Handbook of thermal analysis of construction materials, Noyes Publications, 2002.

196. Johnson, S.B., Franks, G.V., Scales, P.J., Boger, D.V., and Healy, T.W., Surface chemistry-rheology relationships in concentrated mineral suspensions, International Journal of Mineral Processing, 58(1-4) (2000) 267-304.

197. Myers, R.H., Montgomery, D.C., and Anderson-Cook, C.M., Response surface methodology: process and product optimization using designed experiments, Third Edition, Wiley, 2009.

198. Anderson-Cook, C.M., Goldfarb, H.B., Borror, C.M., Montgomery, D.C., Canter, K.G., and Twist, J.N., Mixture and mixture–process variable experiments for pharmaceutical applications, Pharmaceutical Statistics, 3(4) (2004) 247-260.

199. Duineveld, C.A.A., Smilde, A.K., and Doornbos, D.A., Comparison of experimental designs combining process and mixture variables: Part I. Design construction and theoretical evaluation, Chemometrics and Intelligent Laboratory Systems, 19(3) (1993) 295-308.

200. Jensen, O.M. and Hansen, P.F., Autogenous deformation and RH-change in perspective, Cement and Concrete Research, 31(12) (2001) 1859-1865.

201. Eppers, S. and Müller, C., Autogenous shrinkage strain of ultra high performance concrete, in Proceedings of the 2nd International Symposium on Ultra High Performance Concrete, Kassel, Germany, 2008, pp. 433-441.

202. DIN EN ISO 15148:2003-03: Hygrothermal Performance of Building Materials and Products - Determination of Water Absorption Coefficient by Partial Immersion.

203. Vorbeugende Maßnahmen gegen schädigende Alkalireaktion im Beton (Alkali-Richtlinie), Deutscher Ausschuss für Stahlbeton, Draft, Beuth Verlag, Berlin, 2007.

204. Seyfarth, K. and Stark, J., Performance Testing Method for Durability of Concrete using Climate Simulation, in Proceedings of the 7th CANMET/ACI International Conference on Durability of Concrete, Montreal, Canada, 2006, pp. 305-326.

205. IUPAC, Manual of symbols and terminology for physicochemical quantities and units, Commission on Colloid and Surface Chemistry including Catalysis, Wageningen, The Netherlands, 2001.

206. Zdravkov, B., Čermák, J., Šefara, M., and Janků, J., Pore classification in the characterization of porous materials: A perspective, Central European Journal of Chemistry, 5(2) (2007) 385-395.

207. Rouquerol, F., Rouquerol, J., and Sing, K., Adsorption by Powders and Porous Solids: Principles, Methodology and Applications, ACADEMIC PRESS, 1999.

208. Sowoidnich, T. and Rößler, C., The influence of superplasticizers on the dissolution of C_3S, in Proceedings of the 9th CANMET/ACI international conference on superplasticizers and other chemical admixtures in concrete, Seville, Spain, 2009, pp. 335-346.

209. Ramachandran, A.R. and Grutzeck, M.W., Effect of pH on the Hydration of Tricalcium Silicate, Journal of the American Ceramic Society, 76(1) (1993) 72-80.

210. Suzuki, K., Nishikawa, T., Ikenaga, H., and Ito, S., Effect of NaCl or NaOH on the formation of C---S---H, Cement and Concrete Research, 16(3) (1986) 333-340.

211. Hiemstra, T. and Riemsdijk, W.H.v., Multiple activated complex dissolution of metal (hydr)oxides: a thermodynamic approach applied to quartz, Journal of Colloid and Interface Science, 136 (1990) 132–150.

212. Koutsoukos, P.G., Kofina, A.N., and Kanellopoulou, D.G., Solubility of salts in water: Key issue for crystal growth and dissolution processes, Pure and Applied Chemistry, 79(5) (2007) 825-850.

213. de Meer, S., Spiers, C.J., and Peach, C.J., Pressure solution creep in gypsum: Evidence for precipitation reaction control, Physics and Chemistry of The Earth, 22(1-2) (1997) 33-37.

214. Anderson, M.J. and Whitcomb, P.J., Designing Experiments that Combine Mixture Components with Process Factors, Chemical Engineering Progress, 12 (2000) 1-9.

215. Hallal, A., Kadri, E.H., Ezziane, K., Kadri, A., and Khelafi, H., Combined effect of mineral admixtures with superplasticizers on the fluidity of the blended cement paste, Construction and Building Materials, 24(8) (2010) 1418-1423.

216. Kim, B., Jiang, S., and Aïtcin, P., Slump improvement mechanism of alkalies in PNS superplasticized cement pastes, Materials and Structures, 33(6) (2000) 363-369.

217. Mitchell, D.R.G., Hinczak, I., and Day, R.A., Interaction of silica fume with calcium hydroxide solutions and hydrated cement pastes, Cement and Concrete Research, 28(11) (1998) 1571-1584.

218. Lura, P., Jensen, O.M., and van Breugel, K., Autogenous shrinkage in high-performance cement paste: An evaluation of basic mechanisms, Cement and Concrete Research, 33(2) (2003) 223-232.

219. Gong, J.-q., Xiao, H.-n., Huang, Z.-y., Li, J.-s., Cao, R.-k., and Mao, D., Effects of packing density of micropowders on the compressive strength of cement pastes, Key Engineering Materials, 353 - 358 (2007) 1394-1397.

220. Shaheen, Ehab, Shrive, and Nigel, G., Optimization of mechanical properties and durability of reactive powder concrete, ACI Materials Journal, 103(6) (2006) 444-451.

Erklärung (German Declaration)

Ich erkläre, dass ich die vorliegende Arbeit selbständig und nur unter Verwendung der angegebenen Quellen und Hilfsmittel angefertigt habe.

Weimar, 01.12.2012

Viet-Thien-An Van

List of Publications

Conferences:

1. ***Van, V-T-A.***, Ludwig, H-M., Study on pozzolanic reactivity of rice husk ash in cement system. In: Workshop on Performance-based Specifications for Concrete. Leipzig, Germany, 2011. p. 70-79.
2. ***Van, V-T-A.***, Ludwig, H-M., Using rice husk ash and ground granulated blast-furnace slag to replace silica fume in UHPC. In: Workshop on Performance-based Specifications for Concrete. Leipzig, Germany, 2011. p. 80-89.
3. ***Van, V-T-A.***, Ludwig, H-M., Proportioning Optimization of UHPC Containing Rice Husk Ash and Ground Granulated Blast-furnace Slag, in Proceedings of Hipermat 2012- 3rd International Symposium on Ultra-High Performance Concrete and Nanotechnology for High Performance Construction Materials, Kassel, Germany, 2012, pp. 197-205.
4. ***Van, V.-T.-A.***, Rößler, C., Bui, D.-D., and Ludwig, H.-M., Impact of pozzolanic materials and heat treatments on properties of ultra-high performance concrete, in The 18th International Conference on Building materials (ibausil), Weimar, Germany, 9-2012, pp. (2)0529-(2)0537.
5. ***Van, V.-T.-A.***, Rößler, C., Bui, D.-D., and Ludwig, H.-M., Rice Husk Ash in Sustainable Ultra-High Performance Concrete, in The international conference on sustainable built environment for now and the future, Hanoi, Vietnam, 3-2013, pp. 221-228.

Journals:

1. ***Van, V.-T.-A.***, Rößler, C., Bui, D.D., and Ludwig, H.-M., Mesoporous structure and pozzolanic reactivity of rice husk ash in cementitious system, Construction and Building Materials, 43(0) (2013) 208-216.
2. ***Van, V.-T.-A.***, Rößler, C., Bui, D.D., and Ludwig, H.-M., Mesoporous structure and pozzolanic reactivity of rice husk ash in portlandite solution, Cement and Concrete Research, (2013), Current status: Decision in process.

Curriculum Vitae

Name:	Viet-Thien-An Van (Văn Viết Thiên Ân)
Date of birth:	February 15th, 1976
Place of birth:	Quang Tri, Vietnam
Email:	Thien.An-Weimar@daad-alumni.de

1994 – 1999	Undergraduate thesis of Civil Engineering at Department of Building Materials Technology- National University of Civil Engineering, Hanoi, Vietnam
1999 – 2000	Center for Tropical Building Materials at National University of Civil Engineering, Hanoi, Vietnam
2000 – present	Lecturer at Department of Building Materials Technology - National University of Civil Engineering, Hanoi, Vietnam
2001 – 2004	Master of science thesis at Department of Building Materials Technology - National University of Civil Engineering, Hanoi, Vietnam
2008 – present	Doctoral thesis at F.A. Finger- Institute for Building Materials Science (FIB)- Bauhaus University Weimar, Germany

Weimar, 01.12.2012